https://ntrs.nasa.gov/search.jsp?R=19730001303 2020-03-23T09:43:19+00:00Z

General Disclaimer

One or more of the Following Statements may affect this Document

- This document has been reproduced from the best copy furnished by the organizational source. It is being released in the interest of making available as much information as possible.
- This document may contain data, which exceeds the sheet parameters. It was furnished in this condition by the organizational source and is the best copy available.
- This document may contain tone-on-tone or color graphs, charts and/or pictures, which have been reproduced in black and white.
- This document is paginated as submitted by the original source.
- Portions of this document are not fully legible due to the historical nature of some of the material. However, it is the best reproduction available from the original submission.

Produced by the NASA Center for Aerospace Information (CASI)

NASA TECHNICAL MEMORANDUM

NASA TM X-62,174

NASA TM X-62,174

(NASA-TM-X-62174) LONGITUDINAL AERODYNAMIC CHARACTERISTICS OF A LARGE SCALE MODEL WITH A SWEPT WING AND AUGMENTED JET FLAP IN GROUND EFFECT M.D. Falarski, et al (NASA) Oct. 1972 131 p CSCL 01B G3/02

N73-10030

Unclas 45820

LONGITUDINAL AERODYNAMIC CHARACTERISTICS OF A LARGE-SCALE MODEL WITH A SWEPT WING AND AUGMENTED JET-FLAP IN GROUND EFFECT

Michael D. Falarski and David G. Koenig

Ames Research Center
and
U.S. Army Air Mobility R&D Laboratory
Moffett Field, Calif. 94035

RECEIVED NOV 1972 NASA STI FACILITY INPUT BRANCH

October 1972

PRECEDING PAGE BLANK NOT FILMED

NOTATION

A	thrust augmentation ratio of jet augmentor, J_A/J_I
b	wing span, m (ft)
BLC	boundary layer control
c	chord, m (ft)
$\bar{c}$	mean aerodynamic chord, m (ft)
C_D	drag coefficient, $\frac{\text{drag}}{qS}$
C_{D_m}	total momentum drag coefficient, $\frac{\text{momentum drag}}{qS}$
$C_{J_{AI}}$	isentropic augmentor jet force coefficient, $\frac{\text{isentropic force}}{qS}$
$C_{J_{aI}}$	isentropic aileron BLC coefficient, $\frac{\text{isentropic BLC force}}{qS}$
C_{J_I}	total isentropic thrust coefficient, $C_{J_{AI}} + C_{J_{aI}}$
C_L	lift coefficient, $\frac{\text{lift}}{qS}$
C_m	pitching-moment coefficient, $\frac{\text{pitching moment}}{qS\bar{c}}$
C_T	underwing engine total thrust coefficient, $\frac{\text{thrust}}{qS}$
$C_{T_{JP}}$	augmentor turbocompressor jet pipe thrust coefficient, $\frac{\text{thrust}}{qS}$
h	distance from ground to wing chord plane, m (ft)
h/c	ratio of distance from ground to mean aerodynamic chord at $\alpha = 0°$
i_t	horizontal tail incidence, positive with trailing edge down, deg
J_A	augmentor jet force at q = 0, N/m^2 (psf)
J_I	isentropic jet force at q = 0, N/m^2 (psf)
PTAUG	total pressure of primary air measured inside wind duct, cm Hg (in Hg)

q	free-stream dynamic pressure, N/m^2 (psf)
S	wing area, sq m (sq ft)
T.S.	thrust split between augmentor and underwing engines (67:33 means 67 percent of total thrust is in the wing and 33 percent is in the underwing engines)
t	airfoil thickness, m (ft)
x	chordwise station, m (ft)
y	airfoil ordinate, m (ft)
Z	distance between moment center and line of action of thrust, m (ft)
α, AL	model angle of attack, deg
δ_a	aileron deflection, positive with trailing edge down, deg
δ_e	elevator deflection, positive with trailing edge down, deg
δ_f	augmentor flap deflection measured with respect to diffuser mid-line, positive with trailing edge down, deg (see figure 4(a))
δ_{ID}	augmentor intake door deflection, positive with leading edge down, deg (see figure 4(a))
δ_{JP}	deflection of augmentor turbocompressor jet pipes relative to fuselage datum plane, deg
δ_{TH}	angle of thrust deflection of J-85 underwing engines, deg
θ	augmentor jet angle relative to wing chord plane, deg

SUBSCRIPTS

a	aileron
A	augmentor
f	flap
I	isentropic
JP	augmentor turbocompressor jet pipes
L	left
R	right
s	slat
u	uncorrected
u/w	underwing
V	Viper
w	wing

LONGITUDINAL AERODYNAMIC CHARACTERISTICS OF A LARGE-SCALE MODEL WITH A SWEPT WING AND AUGMENTED JET-FLAP IN GROUND EFFECT

Michael D. Falarski and David G. Koenig

Ames Research Center

and

U.S. Army Air Mobility R&D Laboratory

SUMMARY

This report presents the data of a wind tunnel investigation of the in-ground-effect longitudinal aerodynamic characteristics of a large-scale swept augmentor wing model in the Ames 40- by 80-Foot Wind Tunnel. The investigation was conducted at three ground heights; h/c = 2.01, 1.61, and 1.34. The induced effect of underwing nacelles was studied with two powered nacelle configurations. One configuration used four JT-15D turbofans while the other used two J-85 turbojet engines. Two conical nozzles on each J-85 were used to deflect the thrust at angles from 0° to 120°. Tests were also performed without nacelles to allow comparison with previous data taken out of ground effect.

INTRODUCTION

The augmentor wing concept is being studied as one means of attaining STOL performance in turbofan powered aircraft. Wind tunnel tests of a large-scale unswept augmentor wing model are reported in reference 1 and 2. An initial investigation of a swept augmentor wing model was reported in reference 3. The aerodynamics of the swept model were subsequently investigated more extensively and these results, which include the lateral stability and control characteristics, were reported in reference 4.

This report presents the results of a wind tunnel investigation of the longitudinal aerodynamic characteristics of the swept augmentor wing model in ground effect. The study was performed at ground heights of h/c = 2.01, 1.61, and 1.34. The ground effects of two different underwing nacelle configurations were documented: (1) four JT-15D turbofan nacelles, and (2) two J-85 turbojet engines with the exhaust being deflected through twin conical nozzles. The model was also tested without nacelles to allow comparison with the results out of ground effect (references 3 and 4).

This research program was undertaken in cooperation with the Defense Research Board of Canada and DeHavilland Aircraft of Canada, Ltd.

MODEL AND APPARATUS

Basic Model

The model is shown installed in the wind tunnel in figure 1. Figure 1(a) shows the model with no underwing engines at a ground height of 1.34 h/c. Figure 1(b) shows the model at a ground height of 2.01 h/c with the four JT-15D nacelles mounted on the wing. Figure 1(c) shows the model with the two J-85 turbojet engines installed. The basic geometric details of the model are shown in figure 2, and the model reference dimensions and airfoil coordinates are listed in Tables I to III. The wing planform and leading-edge geometry are presented in figures 2(c) and 2(d).

The air for the augmentor and aileron BLC systems was supplied by a pump consisting of a J-85 coupled pneumatically to two turbocompressors, which were modified Viper engines. A diagram of the compressor system is presented in figure 2(e).

The horizontal tail planform geometry is described in figure 3(a) and Table II. The tail was equipped with the leading-edge slat shown in figure 3(b). The slotted, double-hinged elevator is shown in figure 3(c). When the tail was installed it was set at an incidence of -8.7° and the elevator was set at zero.

Augmentor Flap

The geometry of the augmentor flap cross section is shown in figure 4(a). The augmentor is an ejector system consisting of a trailing-edge primary nozzle (figure 4(b)) through which the compressed air is delivered, a (lower) flap, a (upper) shroud, and an intake door. The secondary air is entrained from the wing upper surface, the slot between the intake door and shroud, and the tertiary gap between the wing lower surface and flap. The mixed jet is ejected downward between the flap and the shroud. The diffusion angle for this report and reference 4 is 4°50'; for the investigation of reference 3, it was 6°37'. The intake door was set at its optimum position for each flap angle.

The ducting for the primary air and aileron BLC is shown in figures 4(c) and 4(d). Figure 4(d) shows the variation of duct diameter with wing span which was designed to maintain a duct Mach number of .36.

Aileron BLC

The geometry of the aileron BLC is shown in figure 5. The system was fed through an extension of the augmentor primary air duct and therefore was coupled with the augmentor output. Airflow to the aileron was 5% of the total turbocompressor airflow. The ailerons were deflected symmetrically to 30° unless otherwise specified.

Underwing Nacelles

JT-15D turbofan engines.- Four JT-15D turbofan nacelles were mounted under the wing for a series of tests at ground heights of 2.01 h/c and 1.34 h/c. The geometry of the engine installation is shown in figures 2(a) and 6. This engine has a bypass ratio of 3 and a pressure ratio of 1.45.

J-85 turbojet engines.- The starboard J-85 underwing engine is shown in figure 7. The exhaust was split and ducted through two conical nozzles, one on each side of the engine. The nozzles were rotated from 0° (aligned with freestream) to 120° (30° forward of vertical). The geometry details of the nacelle installation are presented in figures 7(b) and 7(c).

TESTS

The test procedure consisted primarily of varying angle of attack at constant augmentor and underwing engine thrust coefficients. The angle of attack range varied from -4° to 8° at h/c = 1.34 to -6° to 18° at h/c = 2.01. The augmentor thrust coefficient was varied from 0 to 1.5. The operating parameters varied with underwing engine installation. The dynamic pressure, augmentor total pressure and underwing engine thrust levels for each configuration are tabulated below:

Underwing Engines Removed

C_{J_I} Nominal	q N/m^2 (psf)	PTAUG cm(in) of Hg
1.6	191.5 (4.0)	61 (24)
1.2	244 (5.1)	↓ ↓
.9	335 (7.0)	↓ ↓
.4	684 (14.3)	↓ ↓
.2	↓ ↓	23.9 (9)
0	445 (9.3)	0 (0)

JT-15D Underwing Engines

C_{J_I} Nominal	q N/m^2 (psf)	PTAUG cm(in) of Hg	Thrust/Engine N(lb) 67/33 T.S.	Thrust/Engine N(lb) 40/60 T.S.
1.6	192 (4.0)	61 (24)	778 (175)	2335 (525)
1.2	244 (5.1)	↓ ↓	↓ ↓	↓ ↓
0.9	335 (7.0)	↓ ↓	↓ ↓	↓ ↓
0.4	684 (14.3)	↓ ↓	↓ ↓	↓ ↓
0.2	↓ ↓	23.9 (9)	↓ ↓	↓ ↓
0	445 (9.3)	0	0	0

J-85 Underwing Engines

C_{J_I} Nominal	q N/m^2 (psf)	PTAUG cm(in) of Hg	Thrust/Engine N(lb)
50/50 T.S.			
1.2	173 (3.6)	40.7 (16)	2225 (500)
.9	240 (5.0)	↓ ↓	↓ ↓
.4	493 (10.3)	↓ ↓	↓ ↓
.2	684 (14.3)	23.9 (9)	1335 (300)
30/70 T.S.			
1.2	139 (2.9)	30.5 (12)	4050 (910)
.9	191.5 (4.0)	↓ ↓	↓ ↓
.4	388 (8.1)	↓ ↓	↓ ↓
.2	684 (14.3)	23.9 (9)	3115 (700)

DATA REDUCTION

For all force and moment data, the effects of compressor residual jet thrust, and the intake momentum drag of the fuselage mounted J-85, Viper compressors, and underwing engines, have been subtracted from the measured values. The reactive forces and moment created by the thrust of the underwing engines have also been removed from the measured data. The corrections made for thrust and ram drag are as follows:

$$C_L = C_{L_u} - C_{T_{JP}} \sin(\alpha - \delta_{JP}) - C_T \sin(\delta_{TH} + \alpha)$$

$$C_D = C_{D_u} - C_{D_{m\ J\text{-}85}} - C_{D_{m\ Viper}} + C_{T_{JP}} \cos(\alpha - \delta_{JP}) + C_T \cos(\delta_{TH} + \alpha) - C_{D_{m\ u/w}}$$

$$C_m = C_{m_u} - C_{T_{JP}} \frac{Z_{J\text{-}85}}{\bar{c}} - C_T \frac{Z_{u/w}}{\bar{c}}$$

The forces and moments are referred to the stability axes. The moment center used for data computation was located longitudinally at $0.25\bar{c}$ and vertically $0.20\bar{c}$ below the wing chord datum. The data were not corrected for wind tunnel wall effects.

Values of C_{J_I} were computed on the basis of the measured mass flow and total pressure in the duct prior to discharge.

DATA PRESENTATION

The aerodynamic data are presented in three sections. The first section, figures 8 to 17, is the data without underwing engines. The second section, figures 18 to 23, is the results with the JT-15D nacelles mounted under the wing. The third section, figures 24 to 39, presents the data with the underwing J-85 engines. A summary of the data is presented at the end of each section.

An index to the aerodynamic data figures is presented in Table IV. Table V presents a run-by-run index of the wind tunnel investigation.

REFERENCES

1. Koenig, David G., Corsiglia, Victor R., and Morelli, Joseph P.: Aerodynamic Characteristics of a Large Scale Model with an Unswept Wing and Augmented Jet Flap. NASA TN D-4610, 1968.

2. Cook, Anthony M., and Aiken, Thomas N.: Low Speed Aerodynamic Characteristics of a Large Scale STOL Transport Model with an Augmented Jet Flap. NASA TM X-62,017, 1971.

3. Falarski, Michael D., and Koenig, David G.: Aerodynamic Characteristics of a Large Scale Model with a Swept Wing and Augmented Jet Flap. NASA TM X-62,029, 1971.

4. Falarski, Michael D., and Koenig, David G.: Longitudinal and Lateral Stability and Control Characteristics of a Large-Scale Model with a Swept Wing and Augmented Jet Flap. NASA TM X-62,145, 1972.

TABLE I. - WING REFERENCE DIMENSIONS

Wing area, sq m (sq ft)	21.36(230.0)
Aspect ratio	8.0
Span, m (ft)	13.08(42.895)
Taper ratio	0.30
Sweep at ¼ chord, deg	27.5
Airfoil section	RAE 104
Root chord, m (ft)	2.515(8.25)
Tip chord, m (ft)	0.755(2.475)
Root thickness, percent	12½
Tip thickness, percent	10½
Augmentor span limits, Inner, m (ft) (percent)	1.111(3.645)(12.34)
Augmentor span limits, Outer, m (ft) (percent)	4.575(15.01)(70.0)
Wing area spanned by one augmentor, sq m (sq ft)	6.75(72.62)
Wing area spanned by one aileron, sq m (sq ft)	1.997(21.50)
Wing area spanned by fuselage, sq m (sq ft)	3.88(41.77)
Flap hinge axis, percent chord	68.543
Aileron hinge axis, percent chord	68.0
Incidence, camber, twist	0
Mean aerodynamic chord, m (ft)	1.793(5.880)

NOTE: All chords are measured in streamwise direction.

TABLE II. - TAIL REFERENCE DIMENSIONS

Horizontal Tail

Gross area, sq m (sq ft)	5.58(60.0)
Aspect ratio	4.5
Span, m (ft)	5.005(16.432)
Taper ratio	0.40
Sweep at ¼ chord, deg	25
Airfoil section	RAE 104 with modified l.e.
Thickness/chord ratio, percent	10
Root chord, m (ft)	1.591(5.22)
Tip chord, m (ft)	0.635(2.082)
Elevator hinge axis	see figure 3(c)
Elevator travel, deg	±30
Tailplane incidence, deg	±12
Tailplane arm, m (ft)	6.804(22.32)
Tailplane volume coefficient	0.990
Mean aerodynamic chord, m (ft)	1.114(3.654)

Vertical Fin

Fin arm, m (ft)	5.361(17.603)
Fin volume coefficient	0.07476

TABLE III. - COORDINATES OF R.A.E. 104 AIRFOIL (t/c max. = .10)

x/c	y/c(100)	x/c	y/c(100)
0	0	0.35	4.9300
0.001	0.3441	0.35	4.9488
0.002	0.4863	0.38	4.9775
0.003	0.5953	0.4	4.9946
0.004	0.6870	0.42	5.0000
0.005	0.7676	0.44	4.9937
0.006	0.8404	0.45	4.9862
0.007	0.9072	0.46	4.9756
0.0075	0.9387	0.48	4.9454
0.008	0.9692	0.5	4.9027
0.009	1.0274	0.52	4.8468
0.01	1.0824	0.54	4.7769
0.012	1.1842	0.55	4.7363
0.0125	1.2083	0.56	4.6917
0.014	1.2776	0.58	4.5802
0.016	1.3642	0.6	4.4650
0.018	1.4452	0.62	4.3113
0.02	1.5215	0.64	4.1370
0.025	1.6960	0.65	4.0438
0.03	1.8522	0.66	3.9473
0.035	1.9945	0.68	3.7452
0.04	2.1256	0.7	3.5331
0.05	2.3617	0.72	3.3128
0.06	2.5709	0.74	3.0861
0.07	2.7592	0.75	2.9708
0.075	2.8468	0.76	2.8545
0.08	2.9307	0.78	2.6103
0.09	3.0881	0.8	2.3819
0.1	3.2336	0.82	2.1437
0.12	3.4945	0.84	1.9055
0.14	3.7222	0.85	1.7864
0.15	3.8254	0.86	1.6673
0.16	3.9224	0.88	1.4202
0.18	4.0992	0.9	1.1910
0.2	4.2556	0.92	0.9528
0.22	4.3936	0.925	0.8932
0.24	4.5149	0.94	0.7146
0.25	4.5697	0.95	0.5955
0.26	4.6208	0.96	0.4764
0.28	4.7124	0.975	0.2977
0.3	4.7905	0.98	0.2382
0.32	4.8556	0.9875	0.1489
0.34	4.9082	1.0	0

TABLE IV.- INDEX TO DATA FIGURES.

FIGURE	EFFECT	h/c	δ_f, deg	TAIL	U/W ENG	T.S.	REMARKS
8a	C_{J_I}	2.04	40	OFF	OFF	—	
b	↓	↓	↓	ON	↓	↓	
9a	↓	↓	70	OFF	↓	↓	
b	↓	↓	↓	ON	↓	↓	
10	↓	1.61	30	OFF	↓	↓	
11a	↓	↓	40	OFF	↓	↓	
b	↓	↓	↓	ON	↓	↓	
12a	↓	↓	70	OFF	↓	↓	
b	↓	↓	↓	ON	↓	↓	
13	↓	1.34	30	OFF	↓	↓	
14a	↓	↓	40	OFF	↓	↓	
b	↓	↓	↓	ON	↓	↓	
15	↓	↓	60	OFF	↓	↓	
16a	↓	↓	70	OFF	↓	↓	
b	↓	↓	↓	ON	↓	↓	
17a	h/c	~	40	OFF	↓	↓	
b	↓	~	70	↓	↓	↓	
18a	C_{J_I}	2.04	40	OFF	JT-15	40:60	
b	↓	↓	↓	↓	↓	67:33	
c	T.S.	↓	↓	↓	↓	~	C_{J_I}=1.18
d	C_{J_I}	↓	↓	ON	↓	40:60	
e	↓	↓	↓	↓	↓	67:33	
19a	↓	↓	70	↓	↓	40:60	
b	↓	↓	↓	↓	↓	67:33	
c	T.S.	↓	↓	↓	↓	~	C_{J_I}=1.18
20a	C_{J_I}	1.34	40	OFF	↓	40:60	
b	↓	↓	↓	↓	↓	67:33	
c	T.S.	↓	↓	↓	↓	~	C_{J_I}=1.18
d	C_{J_I}	↓	↓	ON	↓	40:60	
e	↓	↓	↓	↓	↓	67:33	
21a	↓	↓	70	OFF	↓	40:60	
b	↓	↓	↓	↓	↓	67:33	
c	T.S.	↓	↓	↓	↓	~	C_{J_I}=1.18
d	↓	↓	↓	ON	↓	40:60	
e	↓	↓	↓	↓	↓	67:33	
22a	h/c	~	40	OFF	↓	40:60	
b	↓	↓	↓	↓	↓	67:33	
c	T.S.	2.04	↓	↓	↓	~	
d	↓	1.34	↓	↓	↓	↓	
23a	h/c	~	70	ON	↓	40:60	
b	↓	~	↓	↓	↓	67:33	
c	T.S.	1.34	↓	↓	↓	~	

TABLE IV. - INDEX TO DATA FIGURES CONTINUED.

FIGURE	EFFECT	h/c	δ_f, deg	TAIL	I/W ENG	T.S.	REMARKS
24a	C_{JI}	2.04	40	OFF	J-85	50:50	$\delta_{TH}=0$
b	↓					30:70	
c	T.S.			↓		~	: $C_{JI}=1.2$
d	C_{JI}			ON.		30:70	↓
25a						50:50	$\delta_{TH}=30$
b	↓					30:70	
c	T.S.		↓	↓		~	↓ : $C_{JI}=1.2$
26a	C_{JI}		70	OFF		50:50	$\delta_{TH}=60$
b	↓					30:70	
c	T.S.			↓		~	: $C_{JI}=.85$
d	C_{JI}			ON		30:70	↓
27a				OFF		50:50	$\delta_{TH}=90$
b	↓					30:70	
c	T.S.			↓		~	: $C_{JI}=.85$
d	C_{JI}			ON		50:50	
e				↓		30:70	↓
28a				OFF		50:50	$\delta_{TH}=120$
b	↓					30:70	
c	T.S.			↓		~	: $C_{JI}=.85$
d	C_{JI}			ON		50:50	
e	↓			↓		30:70	↓
29a	δ_{TH}			OFF		50:50	$C_{JI}=.42$
b	↓	↓	↓			↓	$C_{JI}=.85$
30a	C_{JI}	1.61	40			50:50	$\delta_{TH}=0$
b	↓					30:70	
c	T.S.					~	↓ : $C_{JI}=1.2$
31a	C_{JI}					50:50	$\delta_{TH}=30$
b	↓					30:70	
c	T.S.		↓			~	↓ : $C_{JI}=1.2$
32a	C_{JI}		70			50:50	$\delta_{TH}=60$
b	↓					30:70	
c	T.S.					~	↓ : $C_{JI}=.85$
33a	C_{JI}					50:50	$\delta_{TH}=90$
b	↓					30:70	
c	T.S.	↓	↓			~	↓ : $C_{JI}=.85$
34a	C_{JI}	1.34	40			30:70	$\delta_{TH}=0°$
b	T.S			↓		~	: $C_{JI}=1.2$
c	C_{JI}			ON		30:70	↓
35a	C_{JI}					30:70	$\delta_{TH}=30$
b	T.S.			↓		~	: $C_{JI}=1.2$
c	C_{JI}	↓	↓	ON	↓	30:70	↓

TABLE IV. - INDEX TO DATA FIGURES CONCLUDED

FIGURE	EFFECT	h/c	δ_f, deg	TAIL	L/W ENG	T.S.	REMARKS
36a	C_{JI}	1.34	70	OFF	J-85	50:50	$\delta_{TH}=60$
b	↓	↓	↓	↓	↓	30:70	↓
c	T.S.					~	: $C_{JI}=.85$
d	C_{JI}			ON		30:70	
37	↓			OFF		50:50	$\delta_{TH}=90$
38a	h/c	~	40	↓		50:50	$\delta_{TH}=0$
b	↓	↓	↓			30:70	↓
c						↓	$\delta_{TH}=30$
39a			70			50:50	$\delta_{TH}=60$
b			↓			30:70	↓
c						50:50	$\delta_{TH}=90$
d	δ_{TH}	2.04				50:50	~

TABLE V. - RUN INDEX

RUN	h/c	δ_f	HORIZ. TAIL	U/W ENGINE	T.S.	THRUST ENG.	C_{J_I}	q, psf	PTAIL	REMARKS	FIGURE
1	2.04	30	ON	JT-15	–	~	∞			JT-15 THRUST CALIBRATION	–
2		↓			↓	↓				" " "	–
3		40			67:33	175	1.62				18e
4							1.20				
5							.89				
6							.44				
7					↓	↓	.27				↓
8					40:60	525	1.58				18d
9							1.17				
10							.87				
11							.43				
12		↓			↓	↓	.27				↓
13		70			40.60	525	1.59				19a
14							1.20				
15							.88				
16					↓	↓	.44				↓
17					67:33	175	1.60				19b
18							1.25				
19							.89				
20					↓	↓	.44				
21		↓	↓		~	~	~			$\alpha = 14°$	↓
22		40	OFF		40:60	525	1.58				18a
23							1.23				
24							.90				
25					↓	↓	.44				↓
26					67:33	175	.44				18b
27							1.58				
28							1.27				
29	↓				↓	↓	.89				↓
30	1.34				40:60	525	1.59				20a
31							1.21				
32							.89				
33	↓	↓	↓	↓	↓	↓	.44				↓

TABLE V. - RUN INDEX

RUN	h/c	δ_f	HORIZ. TAIL	U/W ENGINE	T.S.	THRUST/ENG.	C_{J_I}	q, psf	PTAUG	REMARKS	FIGURE
34	1.34	40	OFF	JT-15	67:33	175	.44				20b
35							.90				
36							1.21				
37					100:0	0	1.22				
38					0:0	0	0				
39		70			40:60	525	1.53				21a
40							1.53			$\alpha = -4, -2$	
41							1.19				
42							.87				
43							.43				
44					67:33	175	.43				21b
45							.88				
46							1.19				
47							1.54				
48					100:0	0	1.22				
49					0:0	0	0				
50			ON		40:60	525	1.58				21d
51							1.20				
52							.88				
53							.43				
54					67:33	175	.43				21e
55							.89				
56							1.20				
57							1.53				
58					100:0	0	1.20				
59					0:0	0	0				
60		40			40:60	525	1.56				20d
61							1.18				
62							.89				
63							.43				
64					67:33	175	.43				20e
65							.89				
66							1.21				

TABLE V. - RUN INDEX

RUN	h/c	δ_f	HORIZ. TAIL	U/W ENGINE	T.S.	THRUST ENG.	C_{J_I}	q, psf	PTAUG	REMARKS	FIGURE
67	1.34	40	ON	JT-15	40:60	175	1.56				20e
68					100:0	0	1.21				
69					0:0	0	0				
70				OFF	—	—	1.52				14b
71							1.17				
72							.87				
73							.42				
74							.18		9		
75							0				
76		70					1.54				16b
77							1.18				
78							.86				
79							.42				
80							.18				
81							0				
82			OFF				1.54				16a
83							1.16				
84							.86				
85							.42				
86							.19				
87							0				
88		40					1.55				14a
89							1.21				
90							.89				
91							.43				
92							.19				
93							0				
94		30					1.51				13
95							1.18				
96							.88				
97							.43				
98							.19				
99							0				

TABLE V. - RUN INDEX

RUN	h/c	δ_f	HORIZ. TAIL	U/W ENGINE	T.S.	THRUST/ENG.	C_{J_I}	q, psf	PTAUG	REMARKS	FIGURE
100	1.34	60	OFF	OFF	—	—	0				15
101							1.48				
102							1.16				
103							.86				
104							.43				
105							.19				
106	1.61	70					1.49				12a
107							1.17				
108							.89				
109							.43				
110							.19				
111							0				
112		40					1.54				11a
113							1.16				
114							.86				
115							.42				
116							.18				
117		30					1.54				10
118							1.19				
119							.87				
120							.43				
121							.18				
122							0				
123		40	ON				1.51				11b
124							1.16				
125							.19				
126							.43				
127							0				
128		70					1.53				12b
129							1.19				
130							.18				
131							.43				
132							0				

TABLE V. - RUN INDEX

RUN	h/c	δ_f	HORIZ. TAIL	U/W ENGINE	T.S.	THRUST ENG.	C_{JI}	q, psf	PTAUG	δ_{TH}	REMARKS	FIGURE
133	204	70	ON	OFF	–	–	1.49			–		9b
134							1.15					
135							.85					
136							.19					
137							.43					
138		↓					0					↓
139		40					1.52					8b
140							1.19					
141							.87					
142							.43					
143							.19					
144			↓				0					↓
145			OFF				1.48					8a
146							1.16					
147							.87					
148							.42					
149							.19					
150		↓					0					↓
151		70					0					9a
152							1.52					
153							1.19					
154							.87					
155							.43					↓
156		↓		↓	↓	↓	.19			↓		
157		40		J-85	0:~	~	0			0	ENGINE THRUST CALIBRATION	–
158					30:70	700	1					
159					50:50		.43					24a
160							.88					↓ 24c
161						↓						
162					↓	700						
163					–	~					ENGINE THRUST CALIB.	
164					50:50	700	1.53					24a
165	↓	↓	↓	↓	↓	↓	1.16			↓		24a

TABLE V.- RUN INDEX

RUN	h/c	δ_f	HORIZ. TAIL	U/W ENGINE	T.S.	THRUST ENG.	C_{J_I}	q, psf	PTAUG	δ_{TH}	REMARKS	FIGURE
166	2.04	40	OFF	J-85	30:70	1167	1.14			0		24b
167							.83					
168					↓	↓	.42					↓
169					50:50	300	.19					24a
170		↓			0:0	0	0			↓		↓
171		70			0:~	~	-			60	THRUST CALIBRATION	
172					50:50	700	1.18					26a
173							.88					
174						↓	.43					
175					↓	300	.19					
176					0:0	0	0					↓
177					30:70	1167	1.17					26b
178						700	.84					
179					↓	910	.19			↓		↓
180					0:~	~				90	THRUST CALIBRATION	
181					50:50	300	.19					27a
182						500	.42					
183							.83					
184					↓	↓	1.10					↓
185					30:70	700	.18					27b
186					0:0	0	0					
187					30:70	910	.79					
188					↓	↓	.41			↓		↓
189					0:~	~				120	THRUST CALIBRATION	
190					0:~	~					"	
191					50:50	300	.19					28a
192						500	.42					
193					↓	↓	.83					↓
194					50:70	700	.19					28b
195					↓	910	.41					
196					0:0	0	0					
197			↓		100:0	0	.41					↓
198	↓	↓	ON	↓	50:50	300	.19			↓		28d

TABLE V.- RUN INDEX

RUN	h/c	δ_f	HORIZ. TAIL	U/W ENGINE	T.S.	THRUST ENG.	C_{JI}	q, psf	PTAUG	S_{TH}	REMARKS	FIGURE
199	2.04	70	ON	J-85	50:50	500	.42			120		28d
200					↓	↓	.85					↓
201					30:70	700	.19					28e
202					↓	910	.41					
203					100:0	0	.42			↓		↓
204					0:~	~				90	THRUST CALIBRATION	
205					50:50	300	.19					27d
206						500	.42					
207							.84					
208					↓	↓	1.15					
209					0:0	0	0					↓
210					30:70	700	.18					27e
211						910	.40					
212					↓	910	.79			↓		↓
213					0:~	~				60	THRUST CALIBRATION	
214					30:70	910	1.12					26d
215							.81					
216						↓	.40					
217					↓	700	.19					
218		↓			0:0	0	0			↓		↓
219		40			0:~	~				0	THRUST CALIBRATION	
220					100:0	0					STATIC AUGMENTATION	
221					30:70	910	1.17					24d
222					↓	↓	.81					↓
223					~	~	~					
224					30:70	910	.41					24d
225						700	.19					
226					100:0	0	.81					
227					0:0	0	0			↓		↓
228					0:~	~				30	THRUST CALIBRATION	
229					30:70	700	.18					25b
230						910	.42					
231	↓	↓	↓	↓	↓	↓	.82			↓		↓

TABLE V. - RUN INDEX

RUN	h/c	δ_f	HORIZ. TAIL	U/W ENGINE	T.S.	THRUST ENG.	C_{J_I}	q, psf	PTAUG	δ_{TH}	REMARKS	FIGURE
232	2.04	40	ON	J-85	30:70	910	1.15			30		25b
233					100:0	0	.82					
234					50:50	500	1.15					25a
235							.84					
236					0:0	0	0					
237	1.34				30:70	910	1.12					35c
238							.81					
239							.41					
240						700	.19					
241					0:0	0	0					
242					30:70	910	1.12			0		34c
243							.81					
244							.41					
245						700	.18					
246					0:0	0	0					
247		70			30:70	700	.18			60		36d
248						910	.41					
249							.79					
250							1.14					
251					0:0	0	0					
252			OFF		50:50	300	.19					36a
253					30:70	700	.19					36b
254					50:50	500	43					36a
255					30:70	910	.42					36b
256					50:50	500	.87					36a
257					30:70	910	.85					36b
258					50:50	500	1.19					36a
259					0:0	0	0					36a
260		40			30:70	910	1.15			0		34a
261							.82					
262							.41					
263						700	.19					
264					0:0	0	0					

TABLE V. - RUN INDEX

RUN	h/c	δ_f	HORIZ. TAIL	U/W ENGINE	T.S.	THRUST / ENG.	C_{JI}	q, psf	PTAVG	δ_{TH}	REMARKS	FIGURE
265	1.34	40	OFF	J-85	30:70	910	1.16			30		35a
266							.84					
267						↓	.41					
268					↓	700	.19					
269		↓			0:0	0	0			↓		↓
270		70			50:50	300	.19			90		37
271					50:50	500	.42					
272					↓	↓	.87					
273	↓				0:0	0	0					↓
274	161				50:50	300	.19					33a
275					30:70	700	.19					33b
276					50:50	500	.42					33a
277					30:70	910	.41					33b
278					50:50	500	84					33a
279					0:0	0	0			↓		33a
280					50:50	300	.18			60		32a
281					30:70	700	.19					32b
282					50:50	500	42					32a
283					30:70	910	.42					32b
284					50:50	500	.86					32a
285					30:70	910	.84					32b
286					50:50	500	1.17					32a
287					30:70	910	1.16					32b
288		↓			0:0	0	0			↓		32a
289		40			30:70	700	.19			30		31b
290					50:50	500	.43					31a
291					30:70	910	.42					31b
292					50:50	500	.86					31a
293					30:70	910	.85					31b
294					50:50	500	1.17					31a
295					30:70	910						
296					0:0	0				↓		↓
297	↓	↓	↓	↓	30:70	700	.19			0		30b

TABLE V. - RUN INDEX

RUN	h/c	δ_f	HORIZ. TAIL	U/W ENGINE	T.S.	THRUST / ENG.	C_{J_I}	q, psf	PTAIL	δ_{TH}	REMARKS	FIGURE
298	1.61	40	OFF	J-85	30:70	910	.42			0		30b
299	↓	↓	↓	↓	50:50	500	.86			↓		30a
300	↓	↓	↓	↓	30:70	910	1.17			↓		30b
301	↓	↓	↓	↓	50:50	500	1.18			↓		30a
302	↓	↓	↓	↓	100:0	0	1.19			↓		↓
303	↓	↓	↓	↓	30:70	910	1.17			↓		30b
304	↓	↓	↓	↓	0:0	0	0			↓		30a

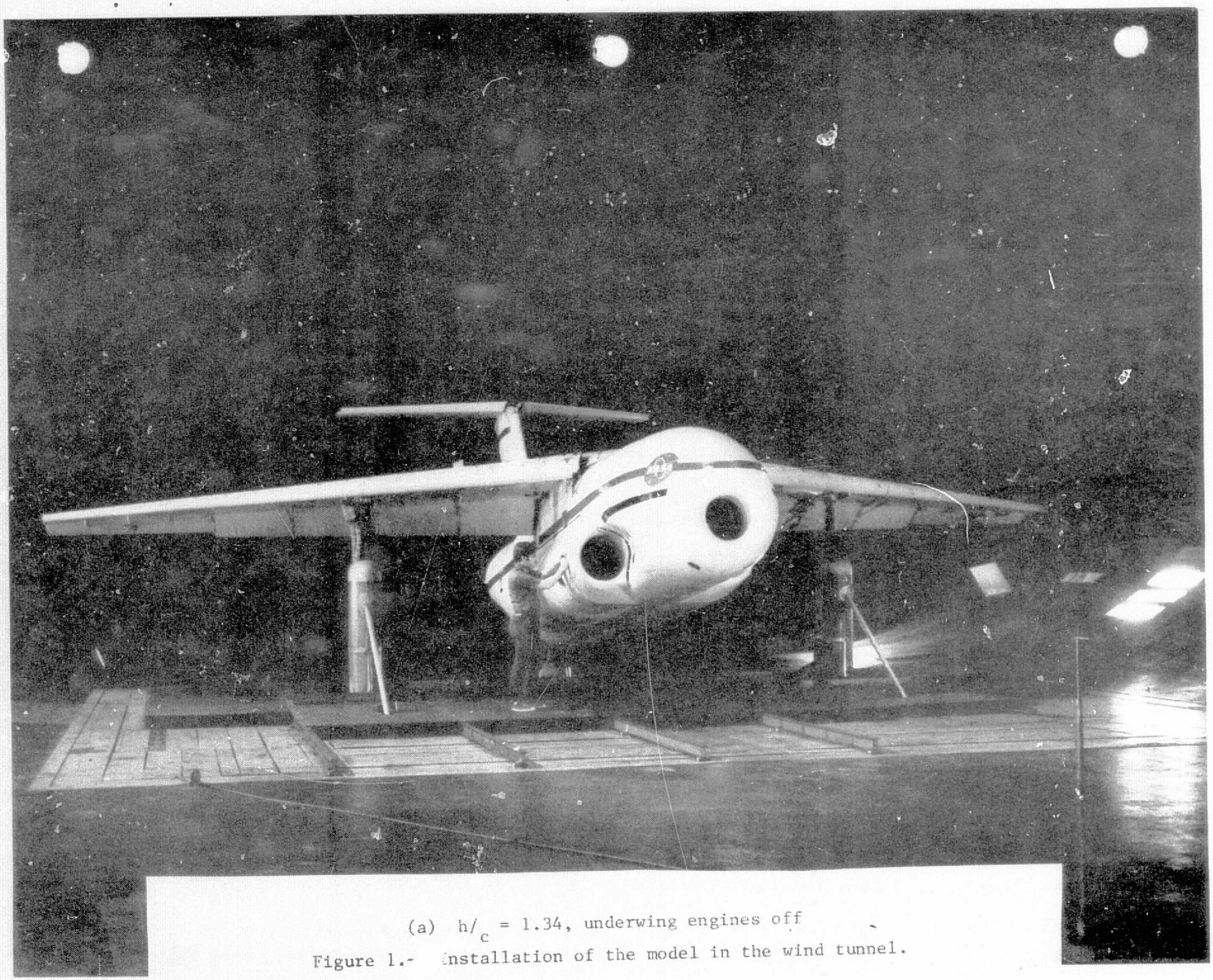

(a) $h/_c = 1.34$, underwing engines off

Figure 1.- Installation of the model in the wind tunnel.

(b) $h/_c$ = 2.01, JT-15 underwing engines

Figure 1.- Continued.

(c) $h/_c$ = 1.34, J-85 underwing engines

Figure 1.- Concluded.

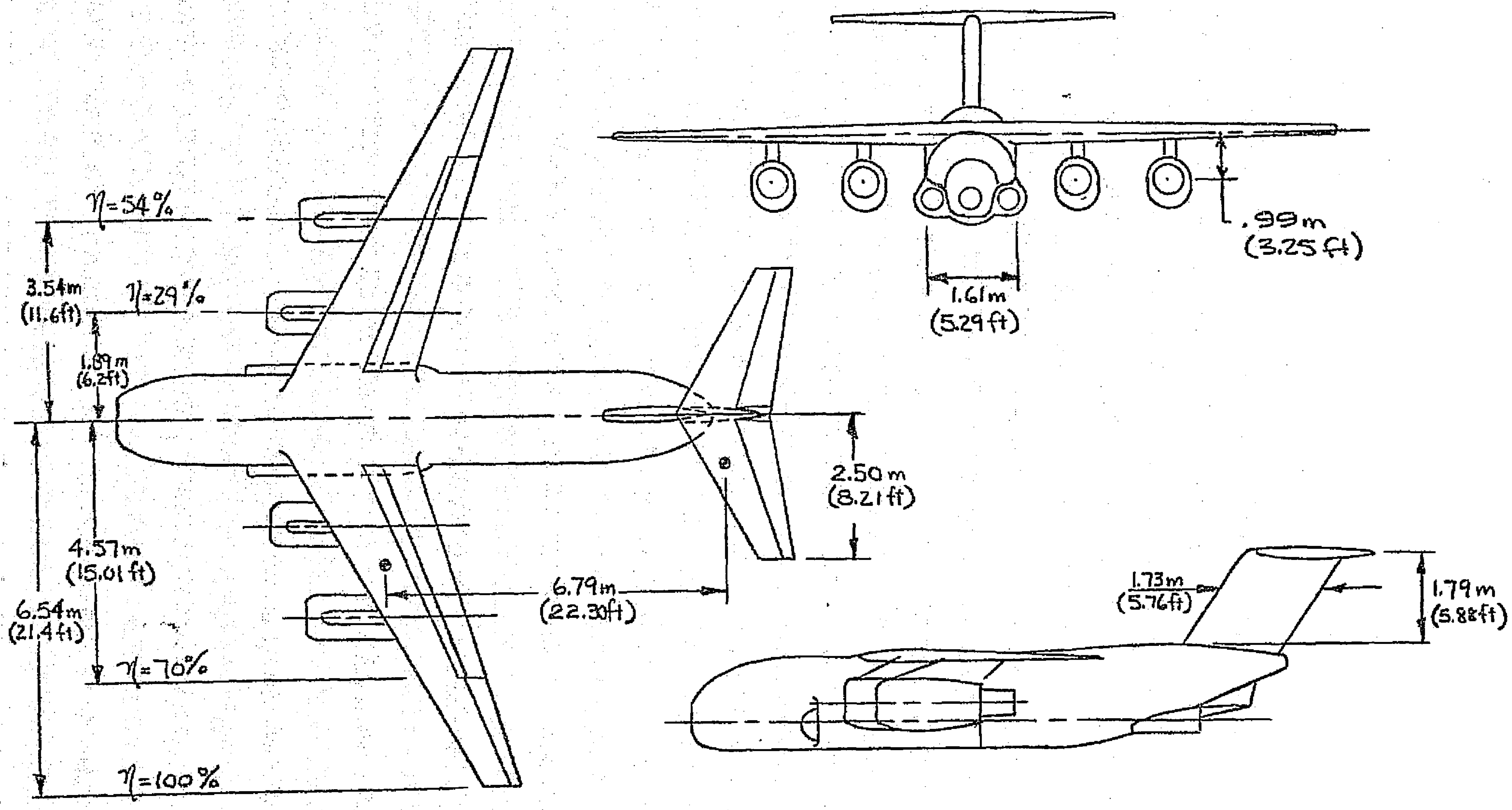

(a) model with JT-15 underwing engines

Figure 2.- Swept augmentor wing basic geometry.

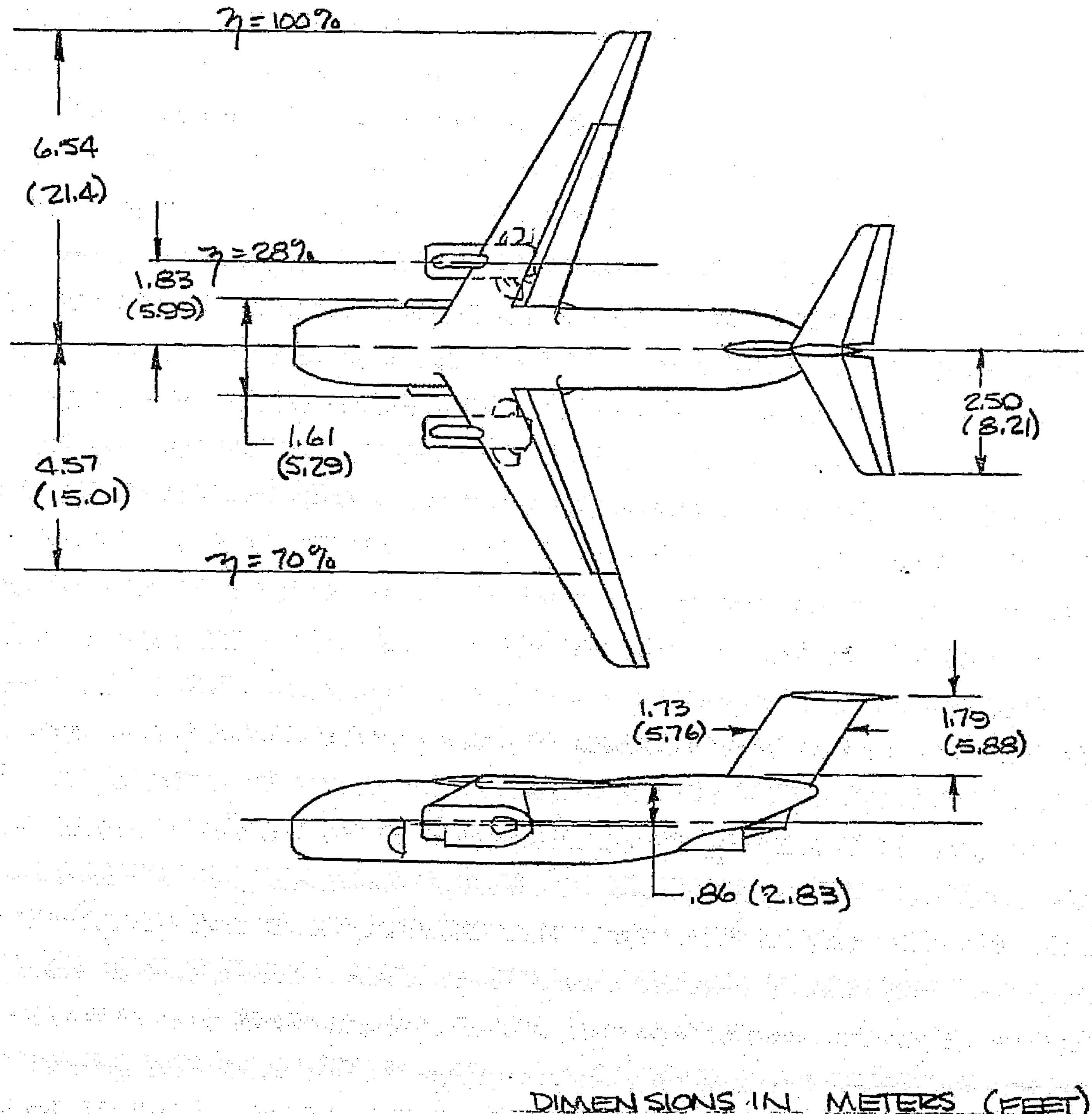

(b) model with J-85 underwing engines

Figure 2.- Continued.

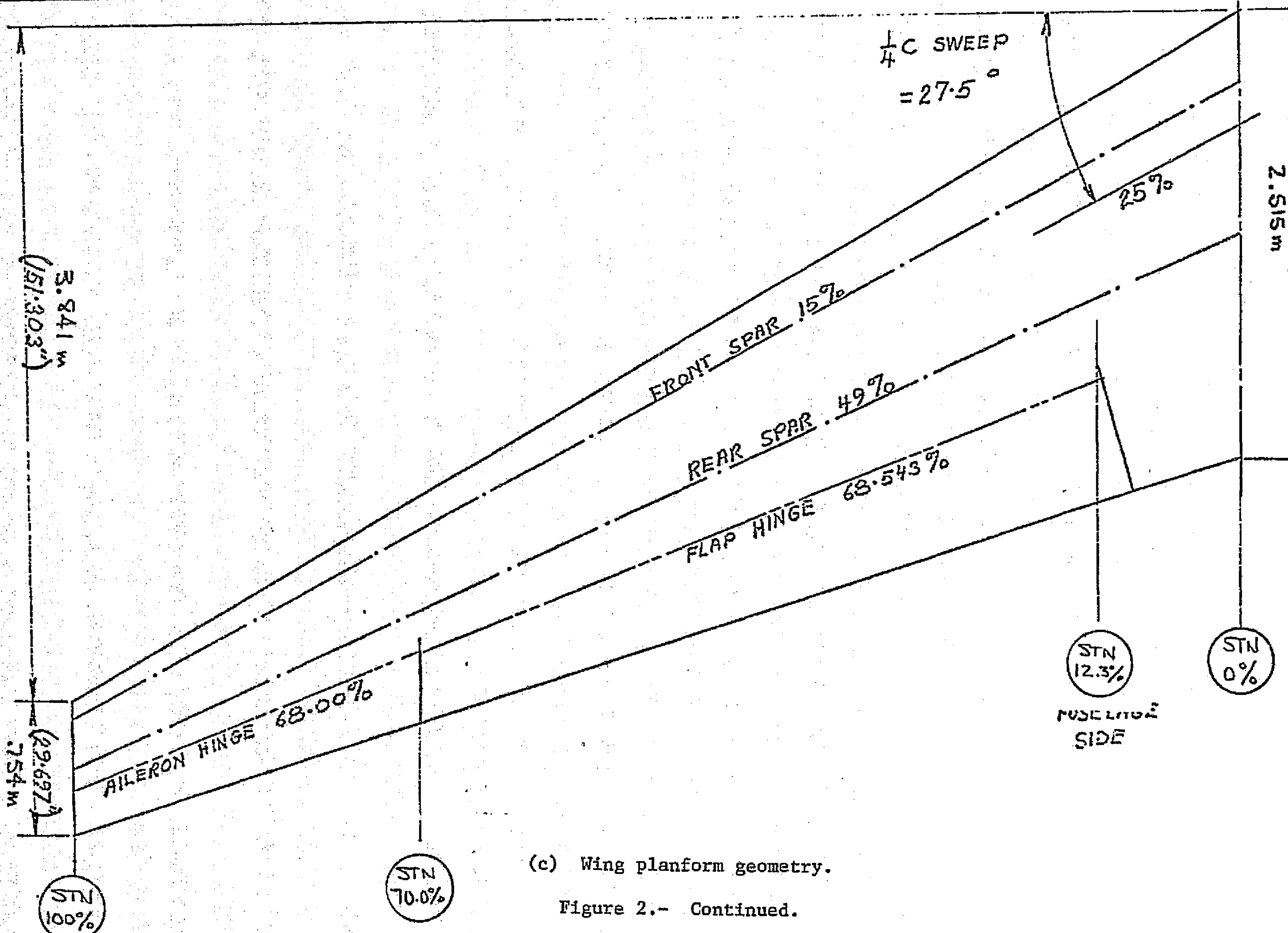

(c) Wing planform geometry.

Figure 2.- Continued.

SLAT CO-ORDINATES	
x/c_s	y/c_s Upper
0.025	0.0667
0.05	0.1000
0.10	0.1520
0.15	0.1843
0.20	0.2088
0.25	0.2255
0.30	0.2375
0.40	0.2500
0.50	0.2476
0.60	0.2265
0.70	0.1941
0.80	0.1431
0.90	0.0794
1.00	0.0000
L/E RADIUS = 9.314% c_s	

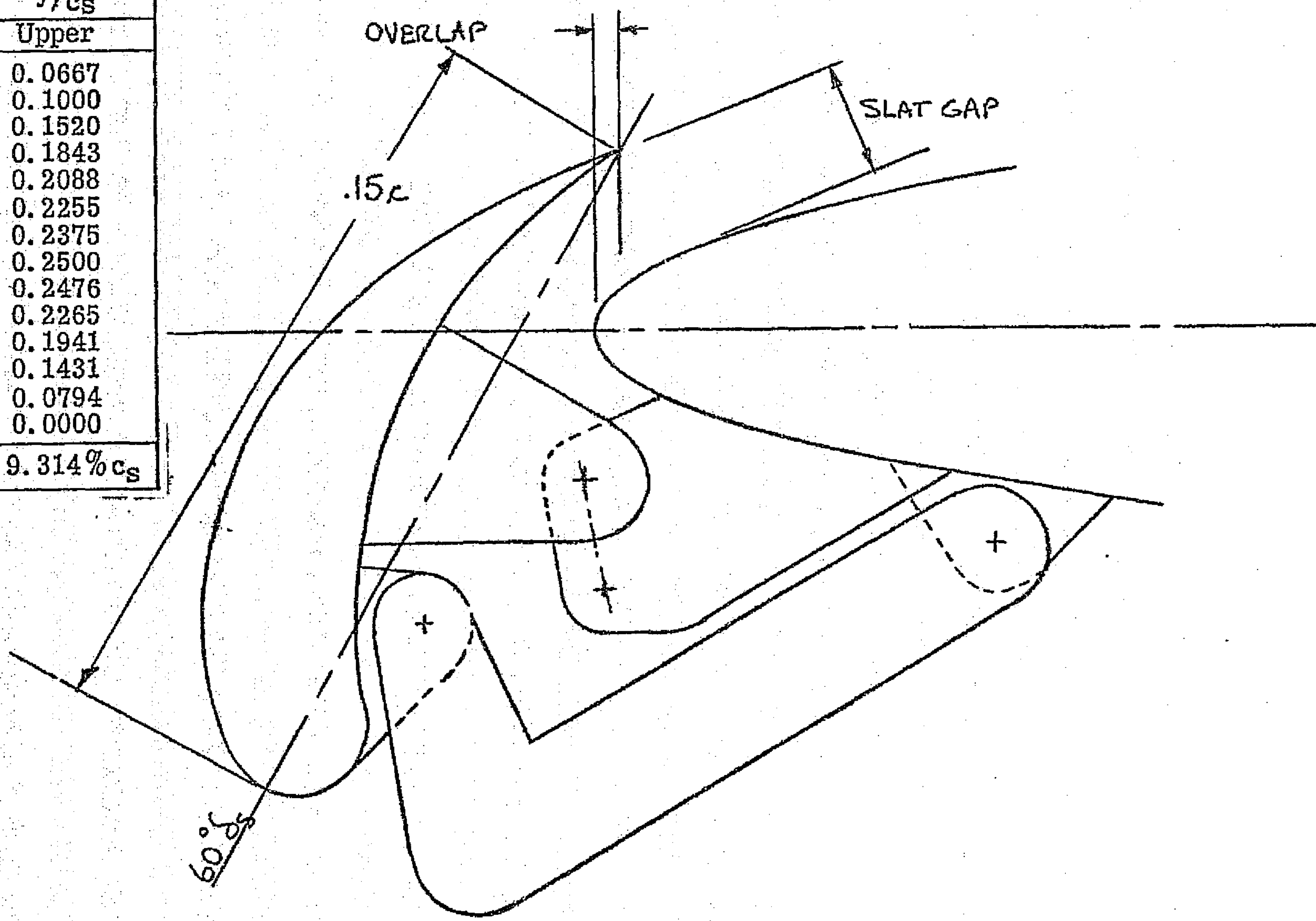

(d) wing leading-edge slat

Figure 2.- Continued.

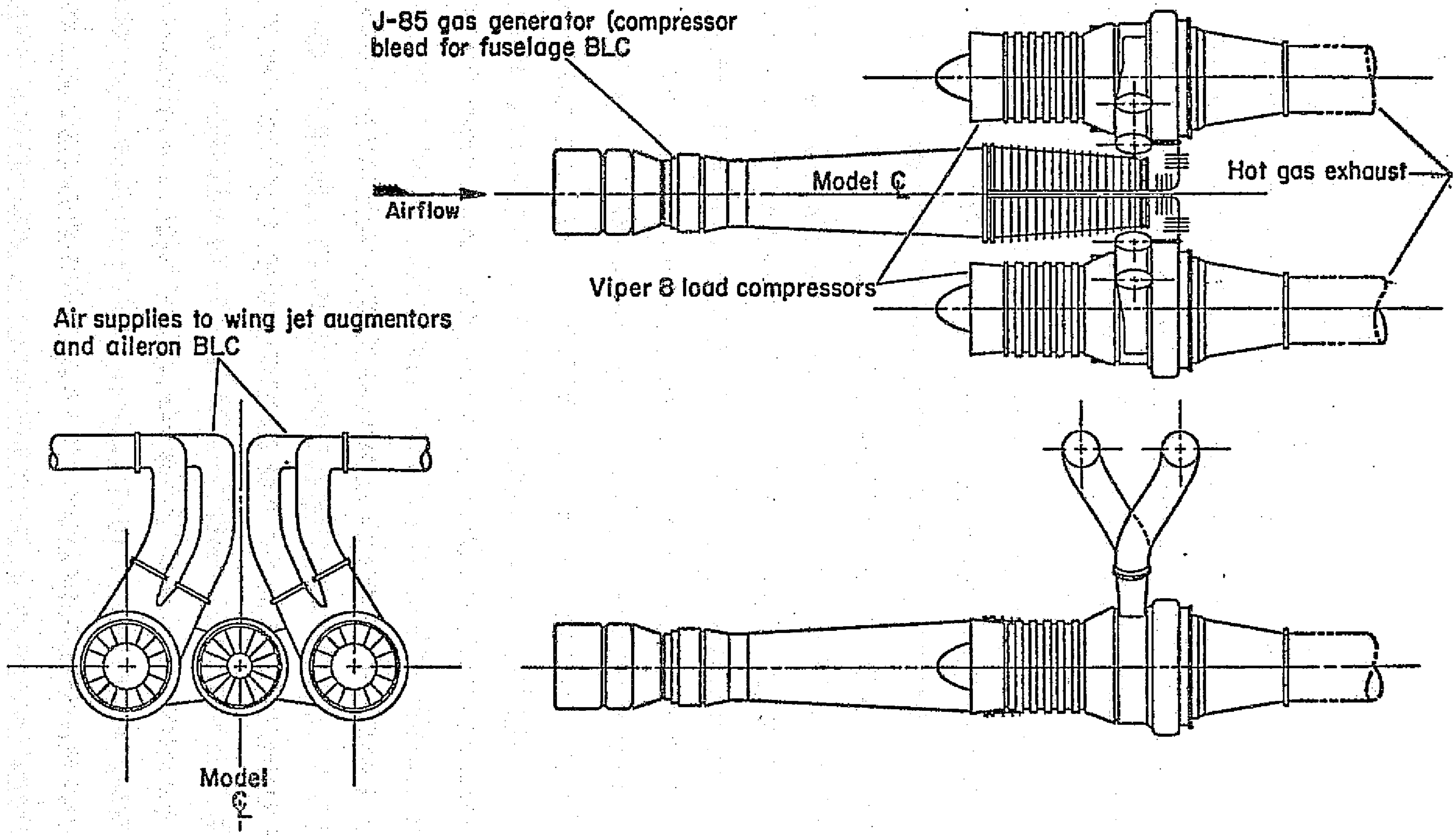

(e) augmentor air compressor system

Figure 2.- Concluded.

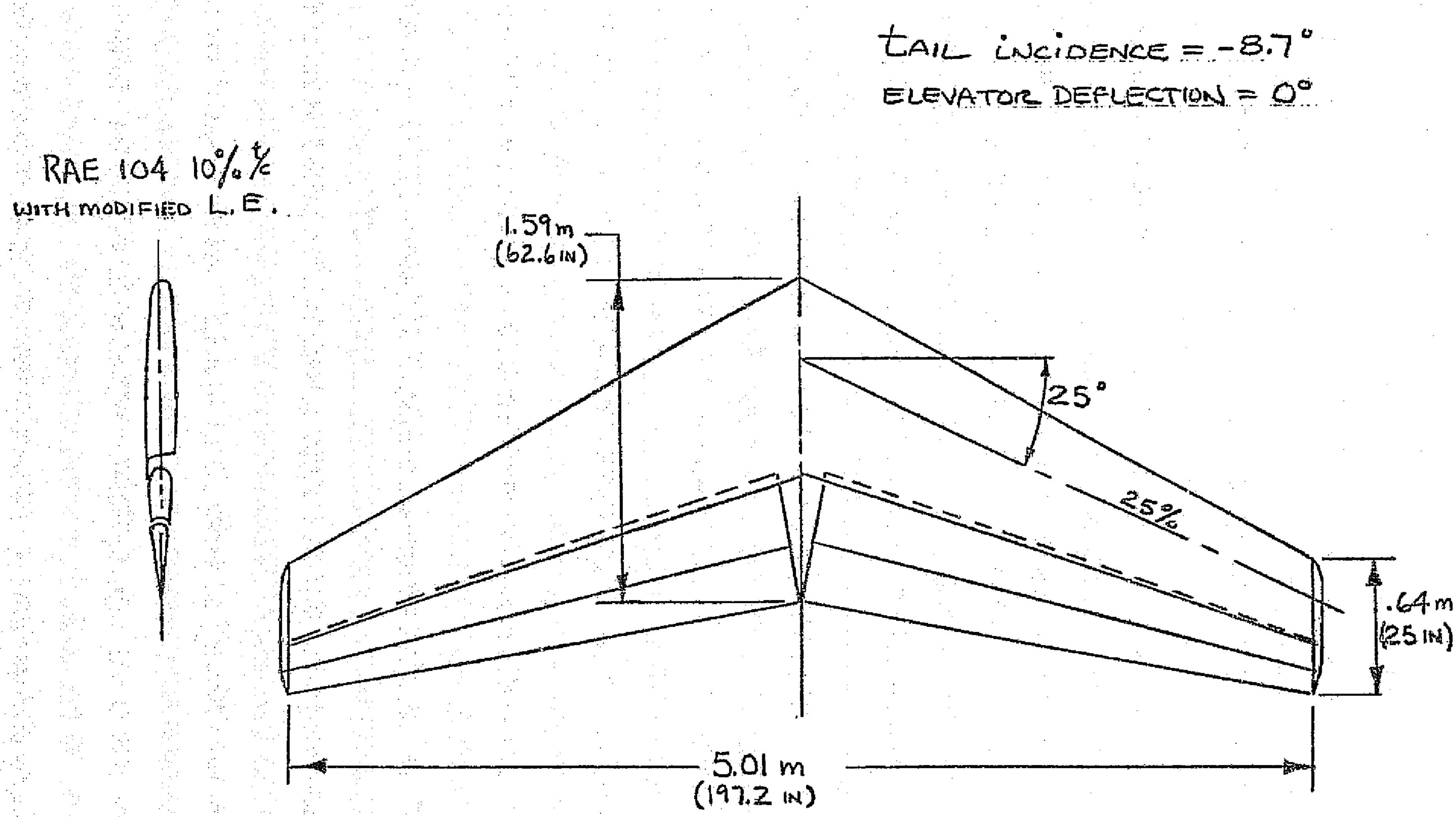

(a) planform geometry

Figure 3.- Horizontal tail geometry.

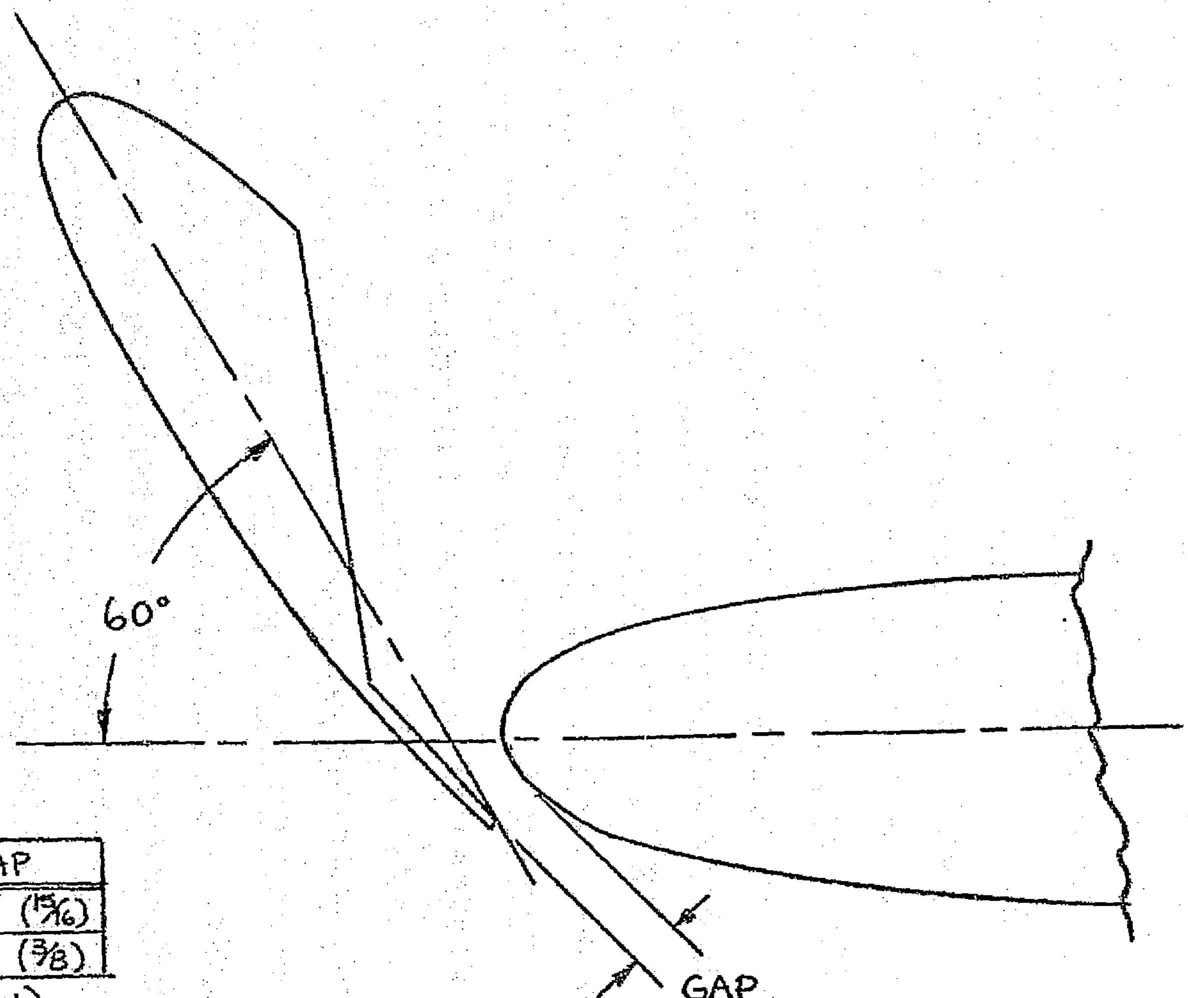

	CHORD	GAP
ROOT	20.3 (8)	2.4 (15/16)
TIP	10.2 (4)	1.0 (3/8)

DIMENSIONS IN CM (IN)

(b) leading-edge slat

Figure 3.- Continued.

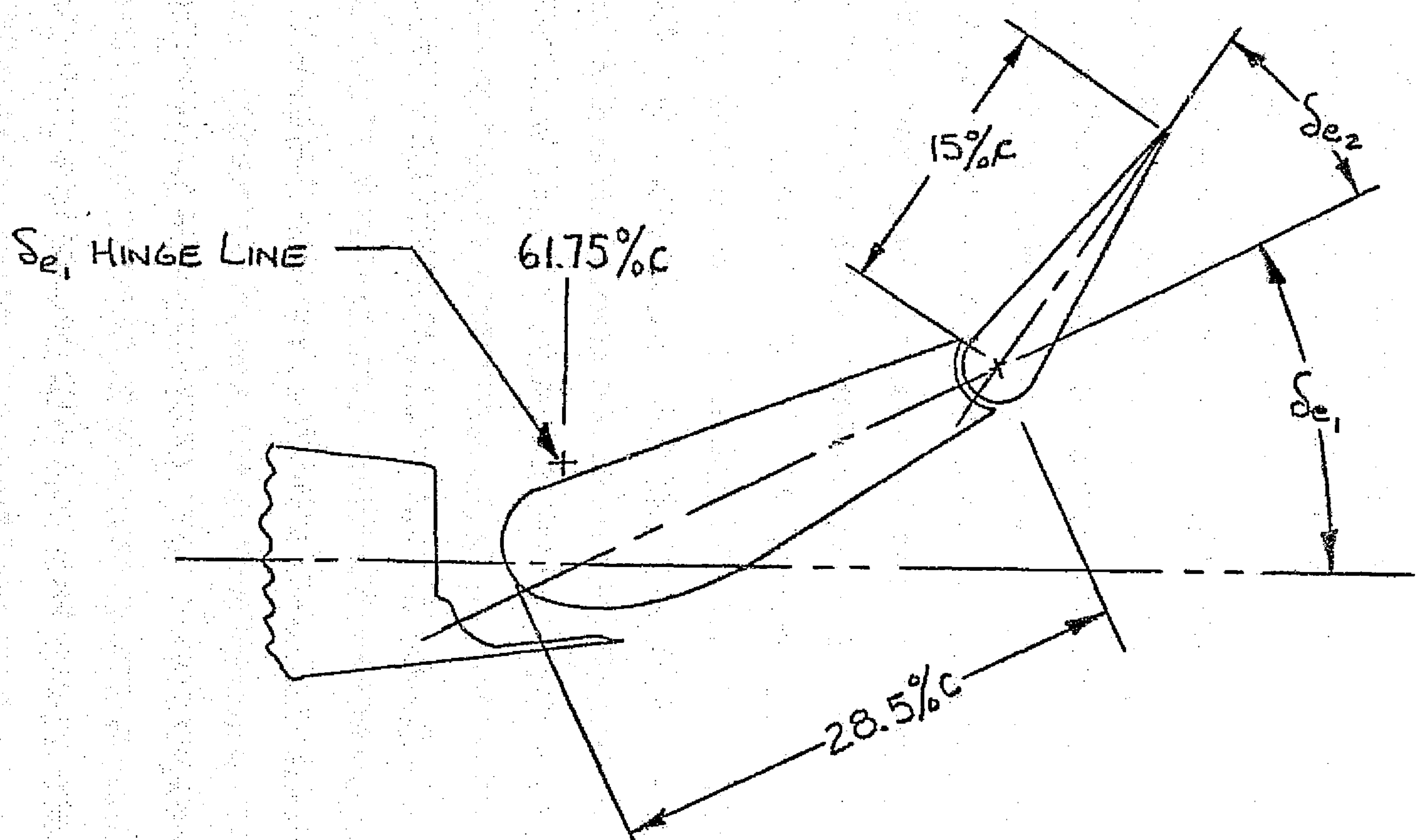

(c) slotted, double-hinged elevator

Figure 3.- Concluded.

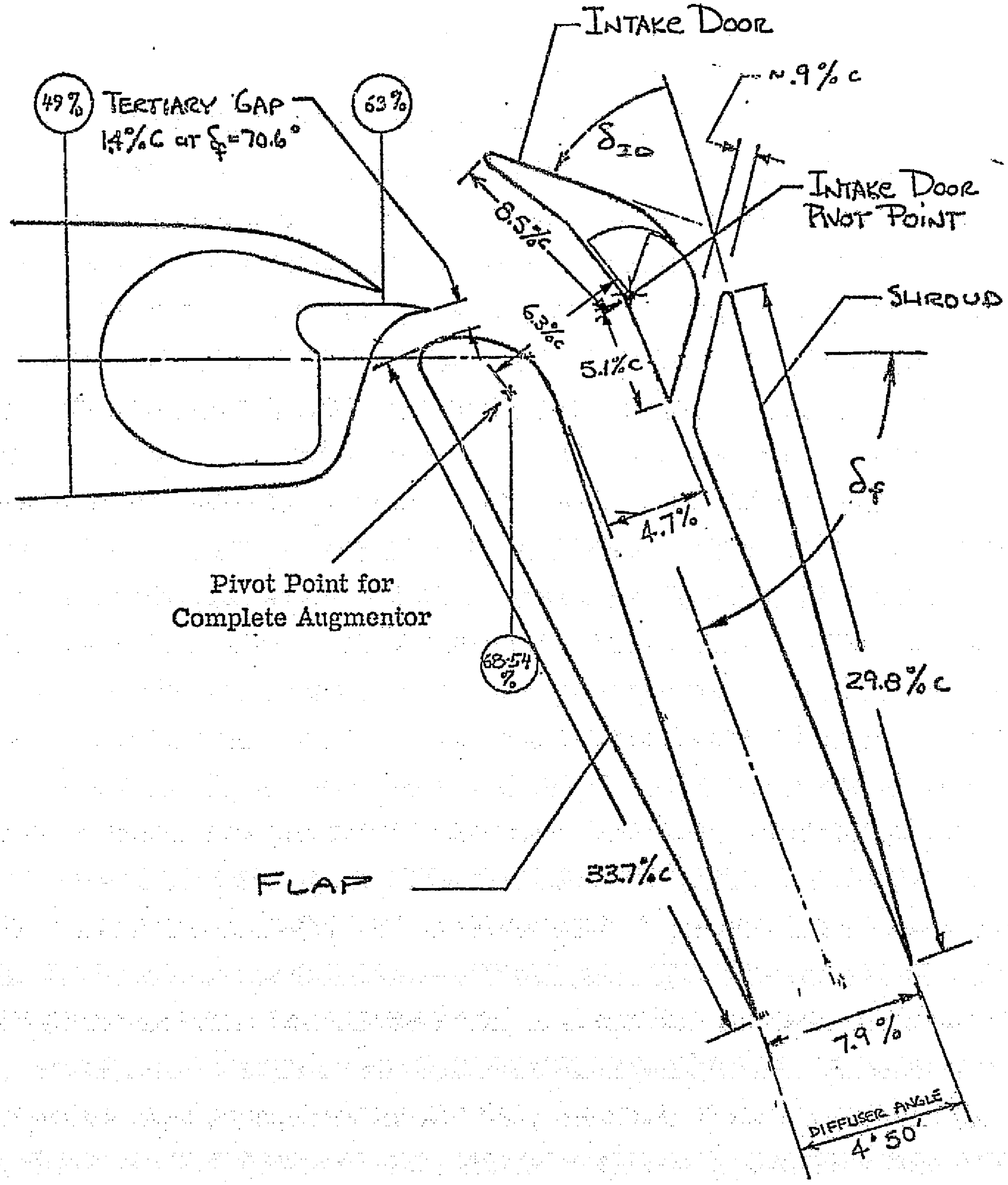

(a) basic geometry

Figure 4.- Augmentor geometry.

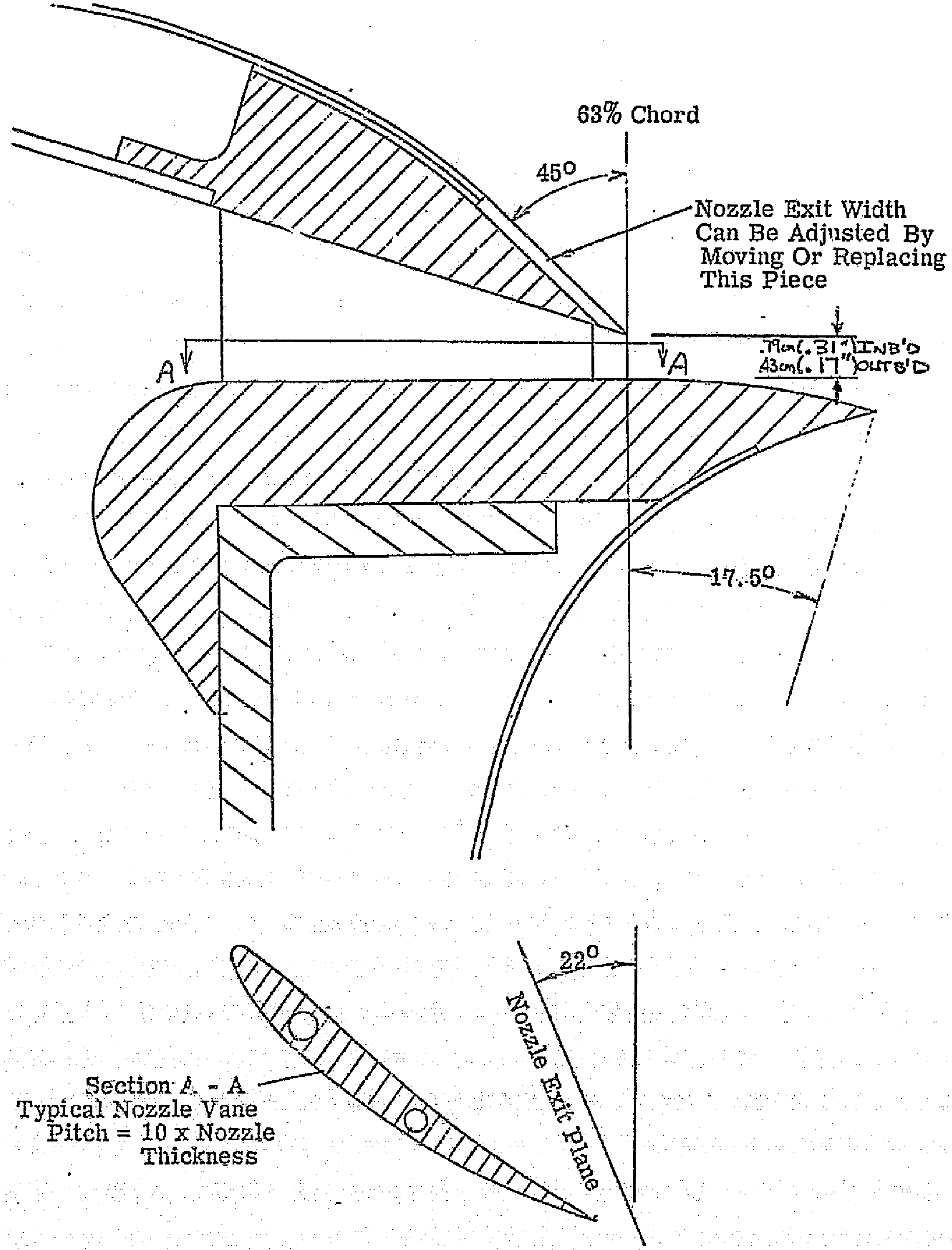

(b) primary nozzle geometry

Figure 4.- Continued.

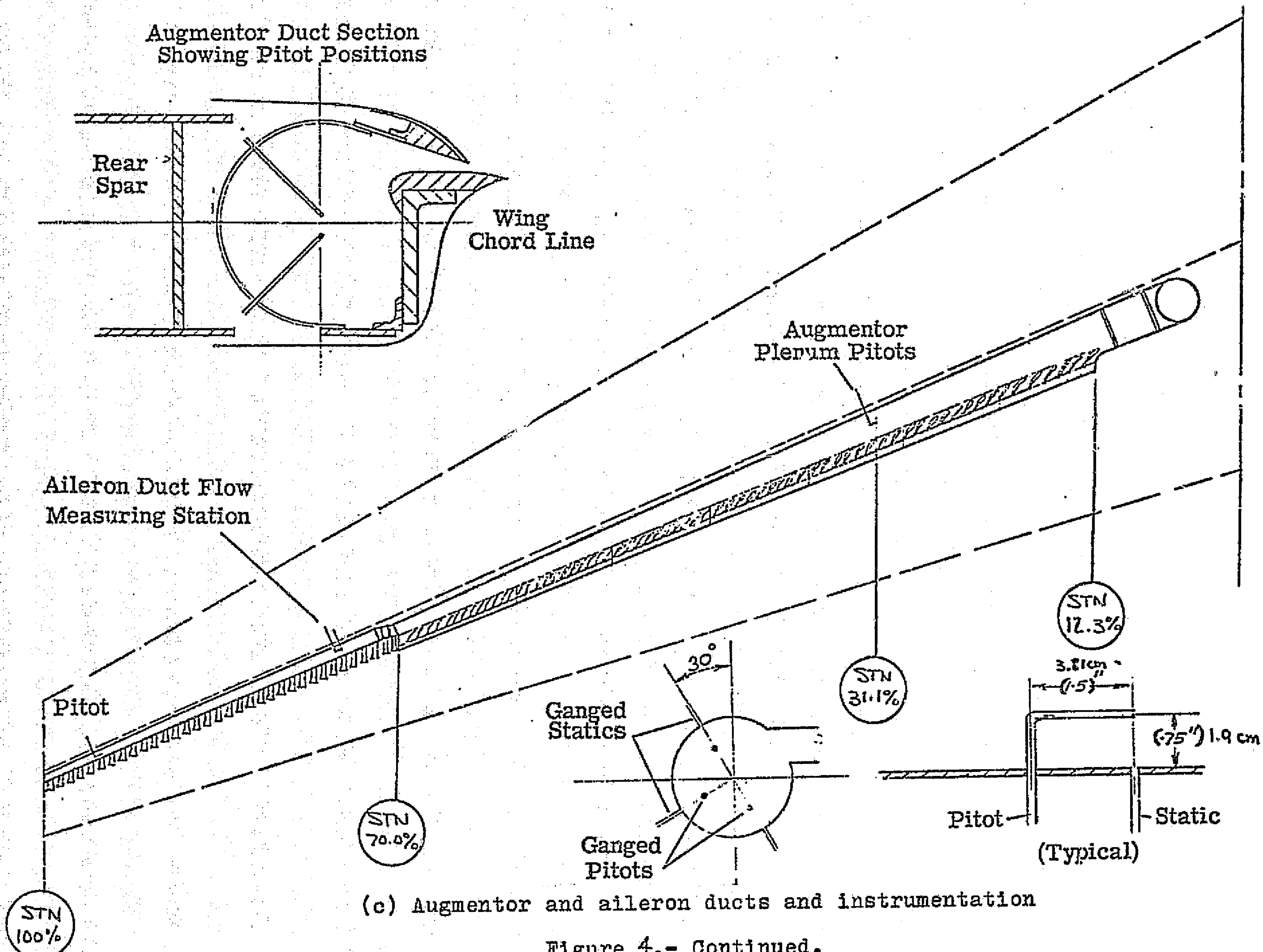

(c) Augmentor and aileron ducts and instrumentation

Figure 4.- Continued.

REPRODUCIBILITY OF THE ORIGINAL PAGE IS POOR.

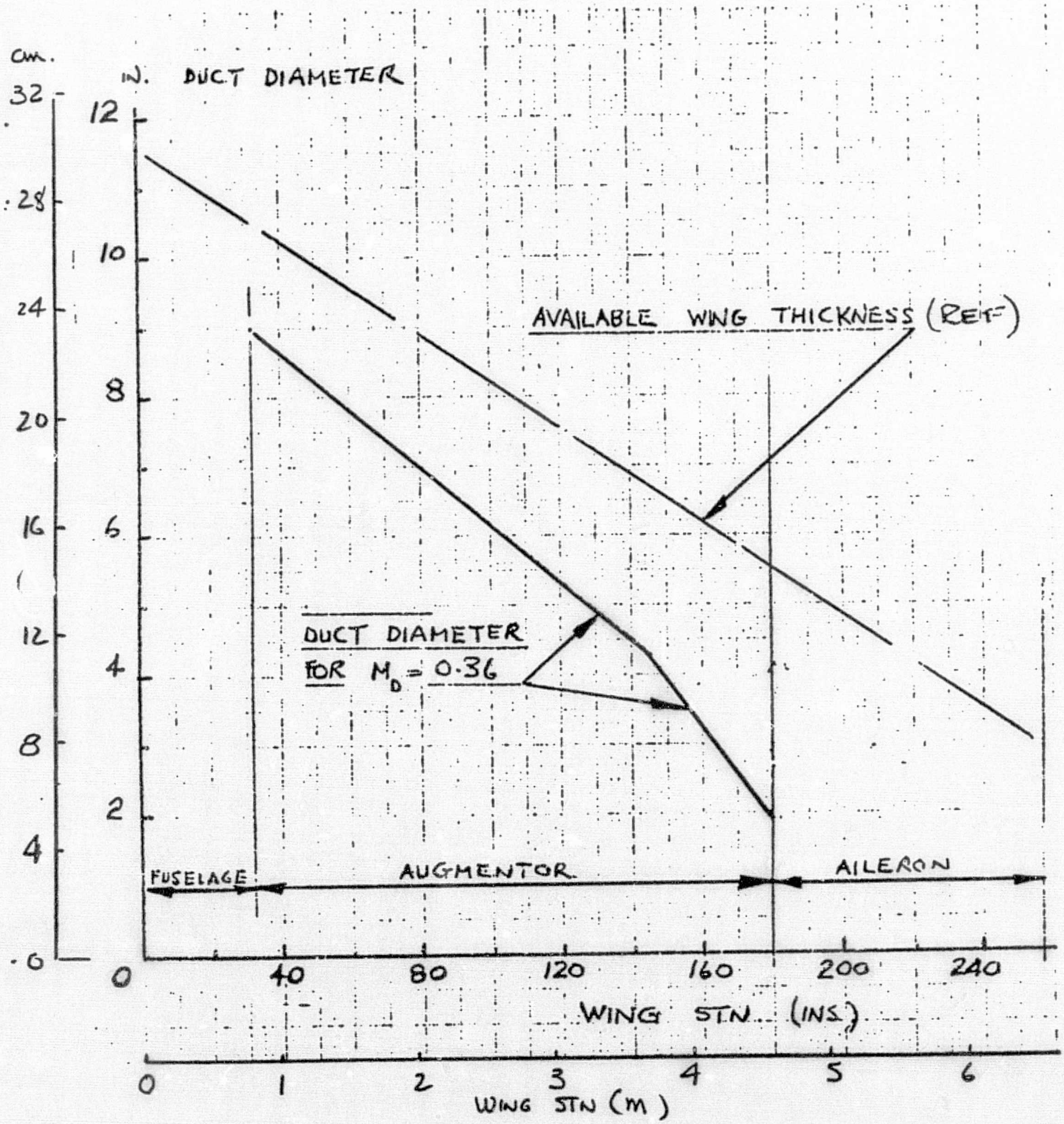

(d) augmentor duct diameter as a function of wing span

Figure 4.- Concluded.

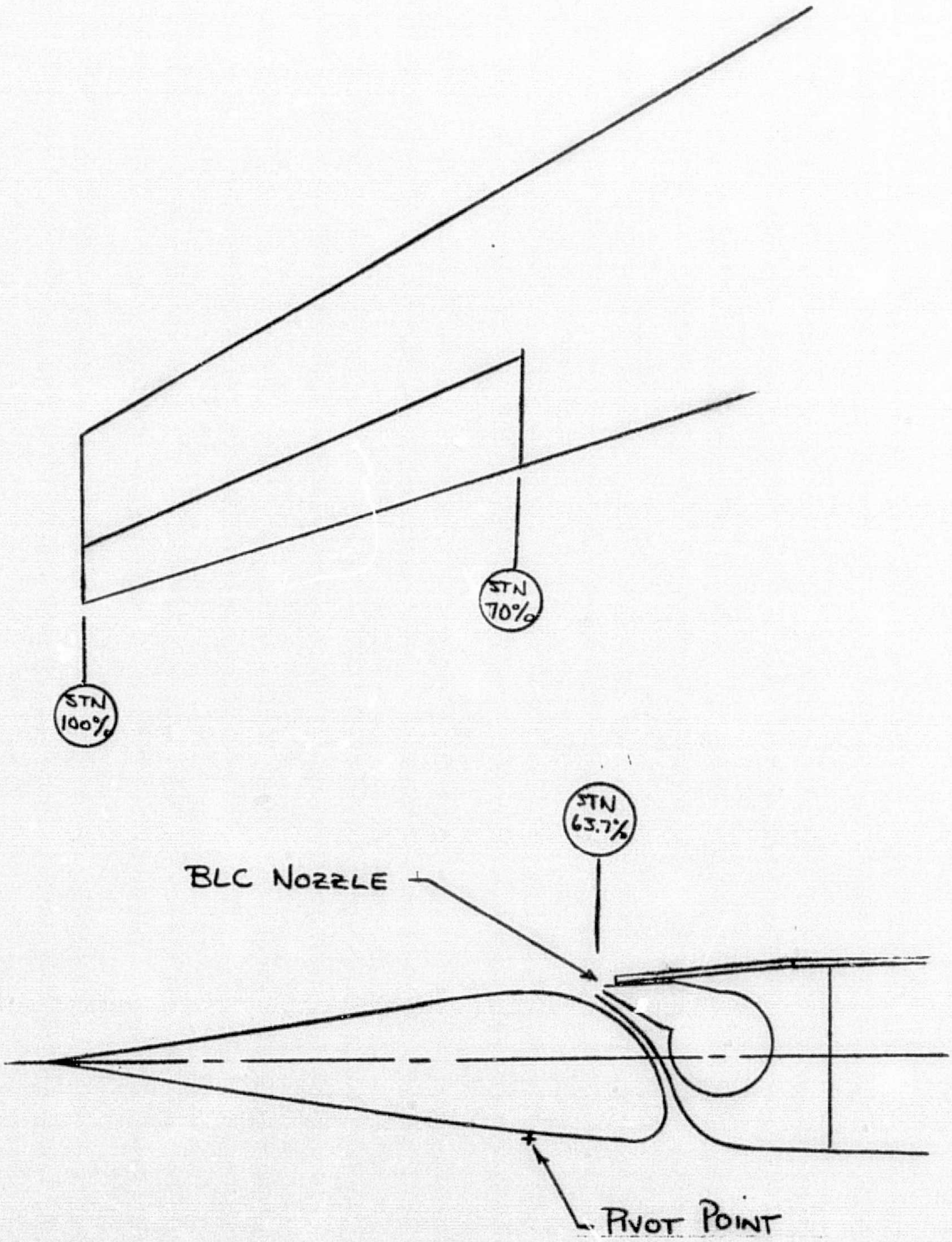

Figure 5.- Geometry of the aileron BLC

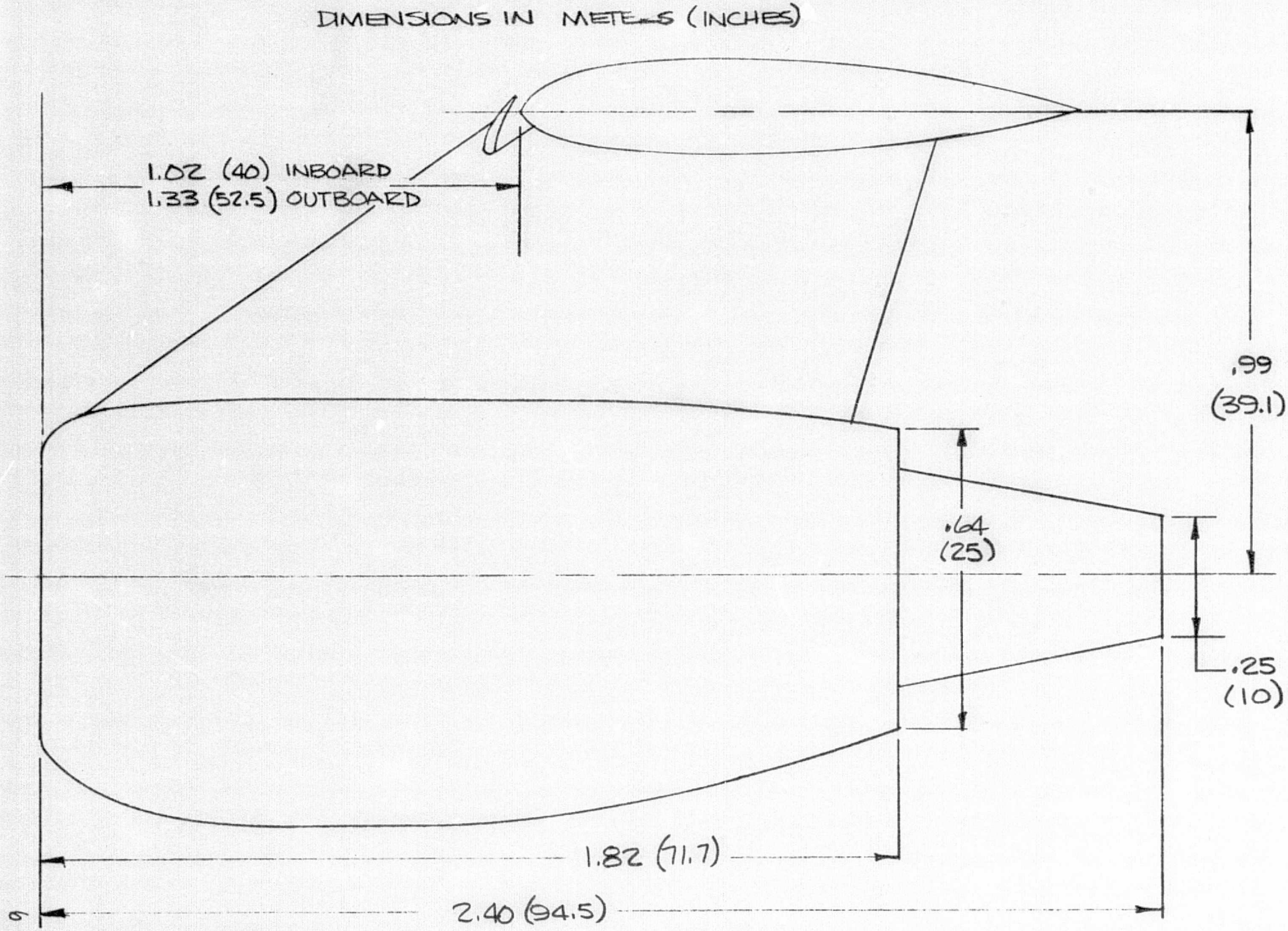

Figure 6.- JT-15 underwing engine installation

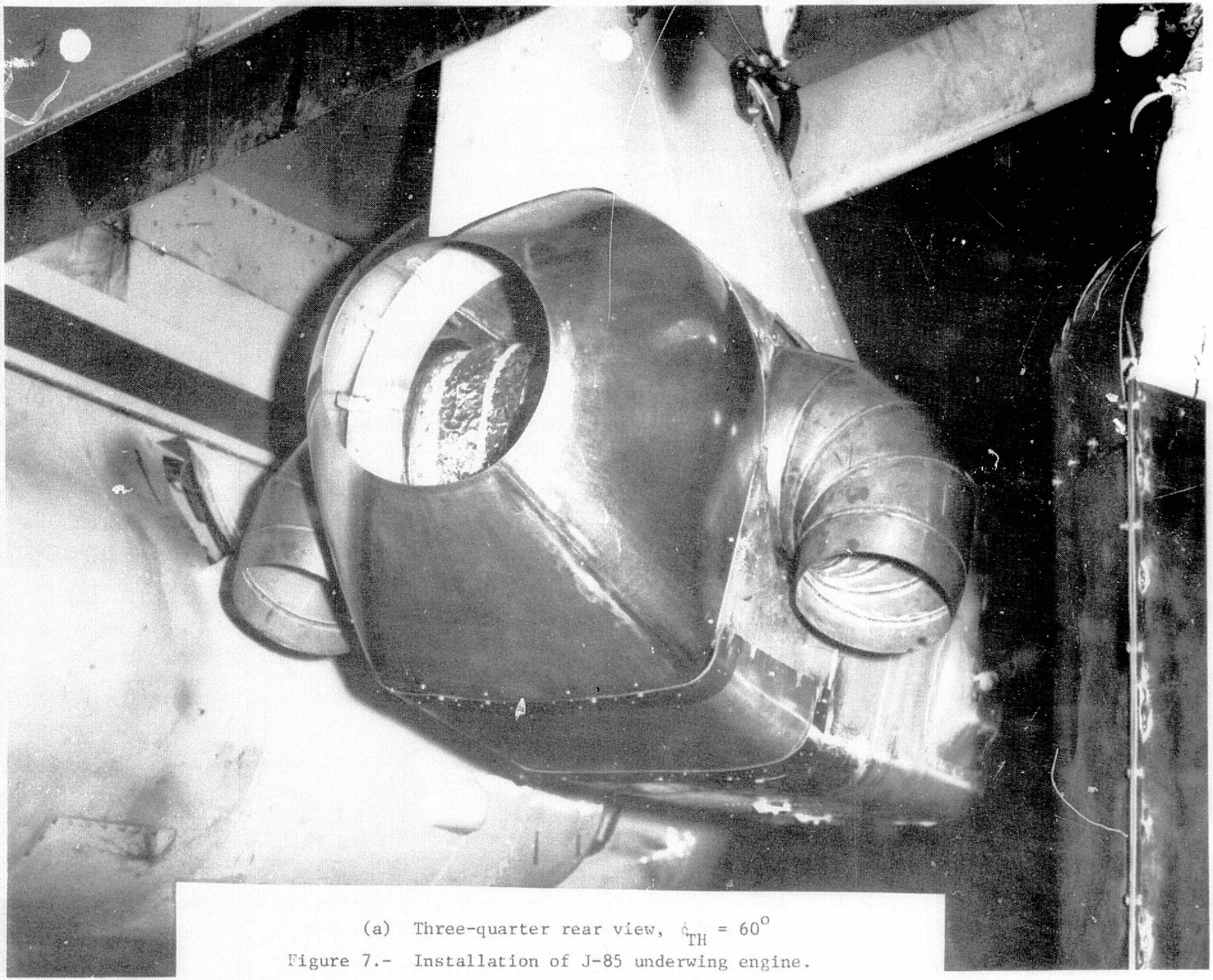

(a) Three-quarter rear view, $\phi_{TH} = 60^{\circ}$

Figure 7.- Installation of J-85 underwing engine.

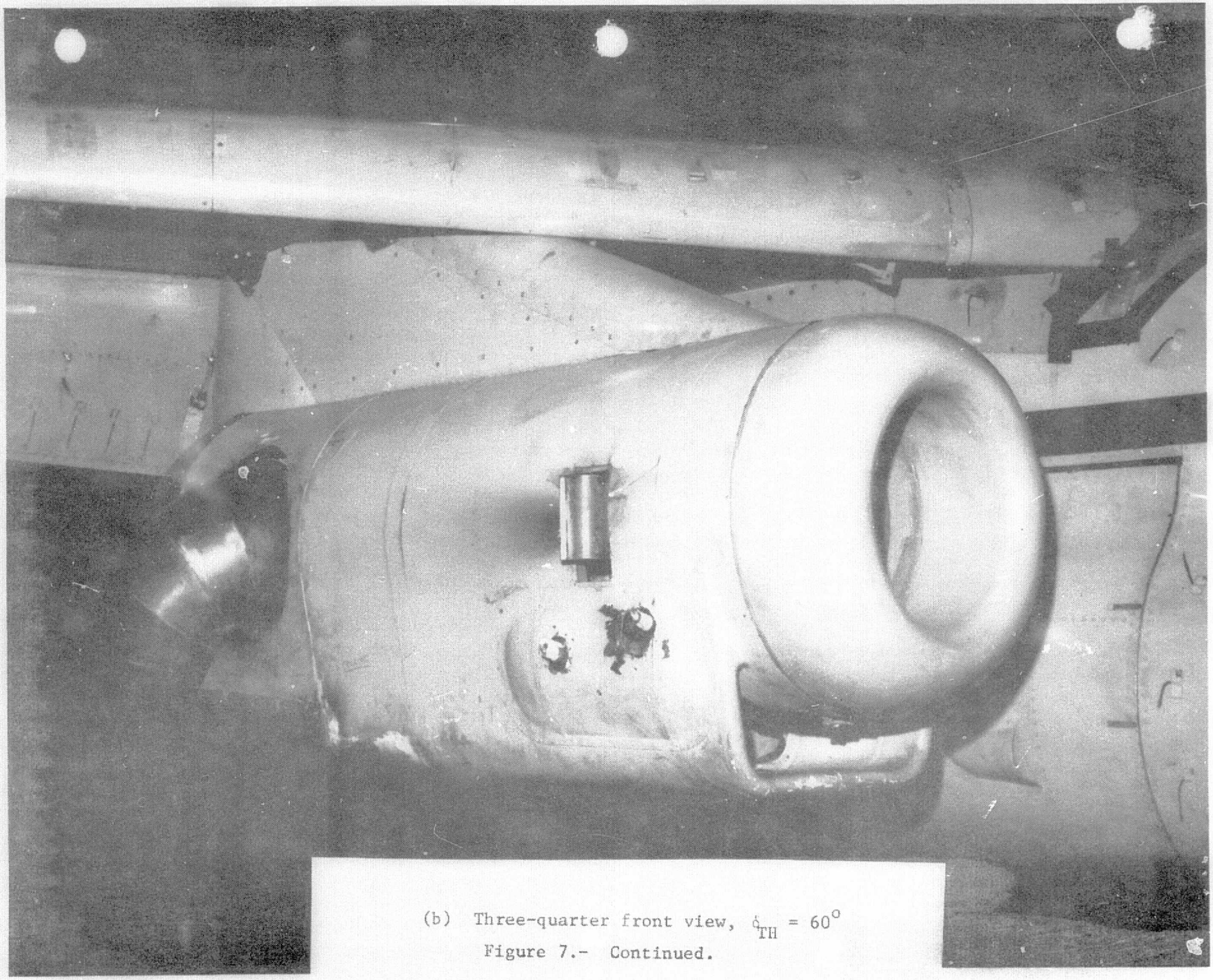

(b) Three-quarter front view, $\delta_{TH} = 60^{\circ}$

Figure 7.- Continued.

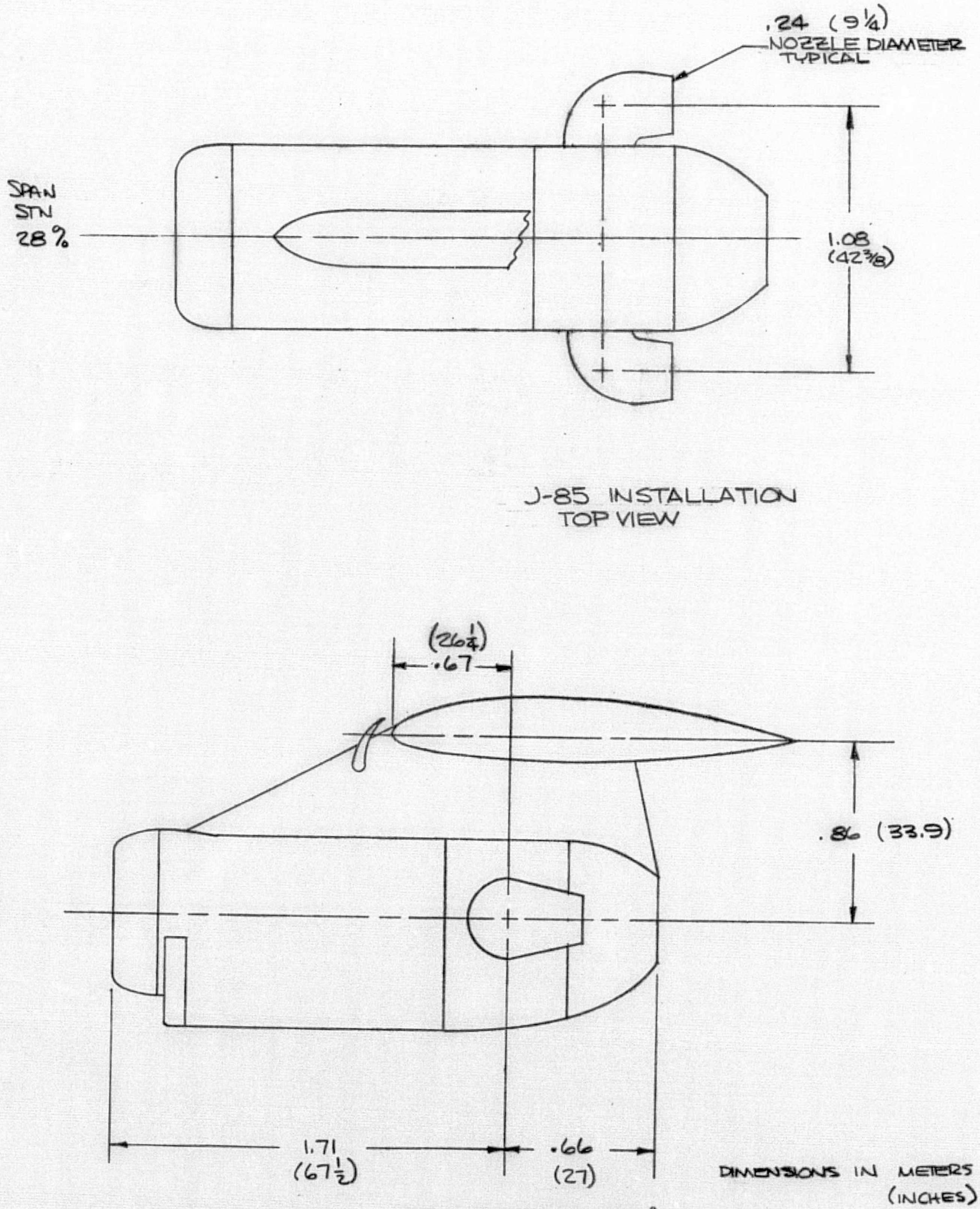

(c) basic geometry of engine, $\delta_{TH} = 0^{\circ}$

Figure 7.- Concluded.

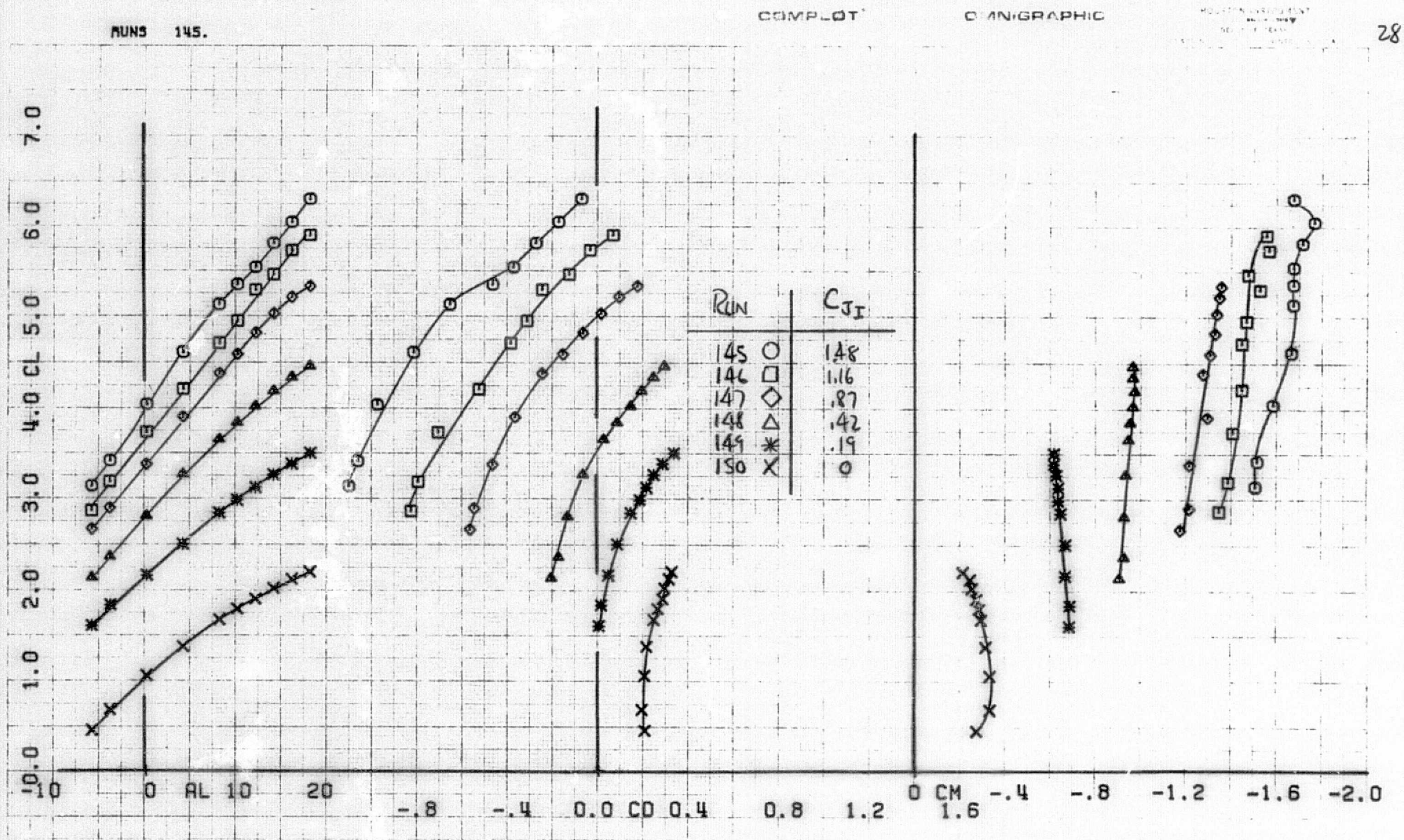

(a) tail off

Figure 8.- Longitudinal aerodynamic characteristics with no underwing engines; h/c = 2.01, $\delta_f = 40^\circ$.

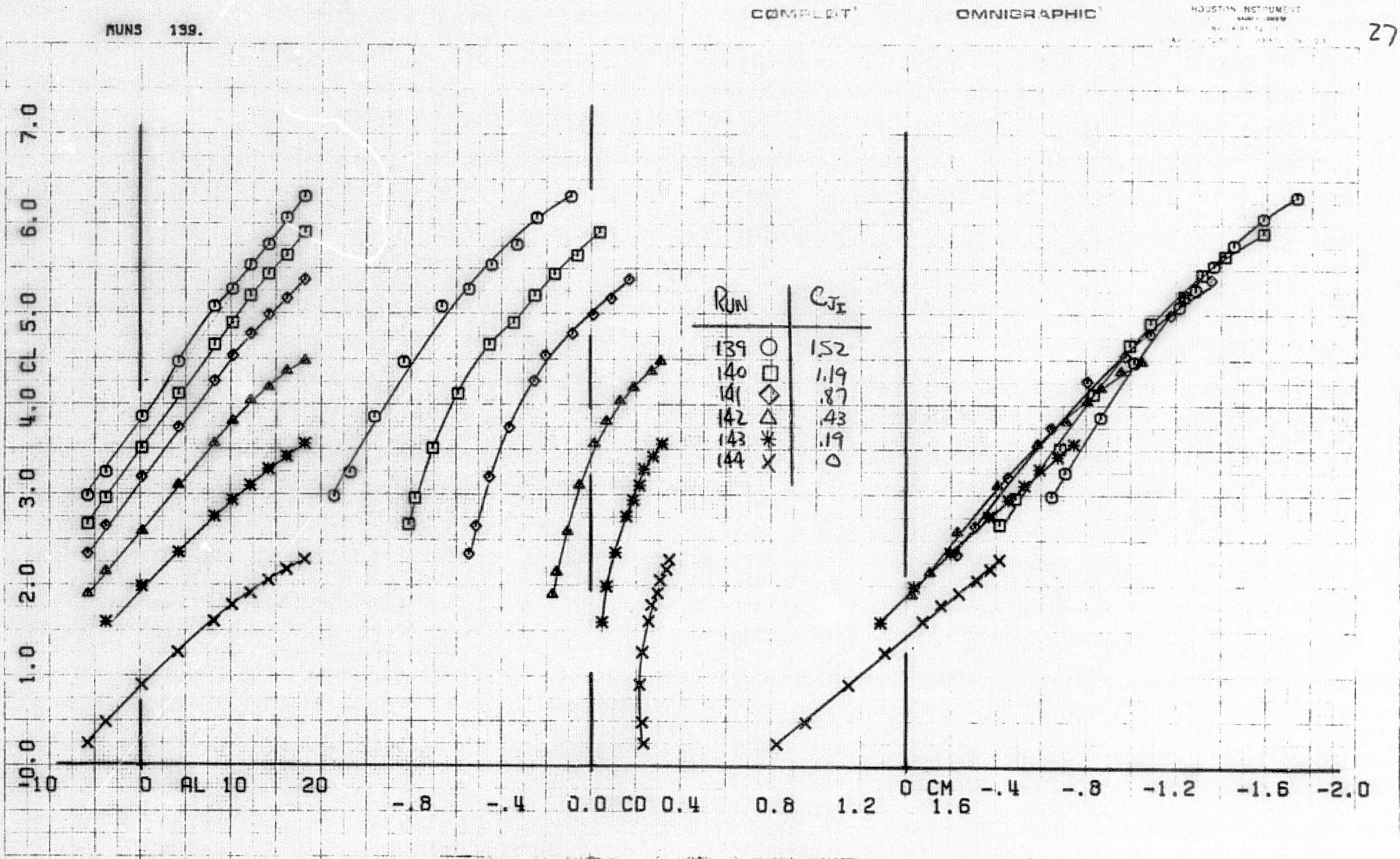

(b) tail on

Figure 8.- Concluded.

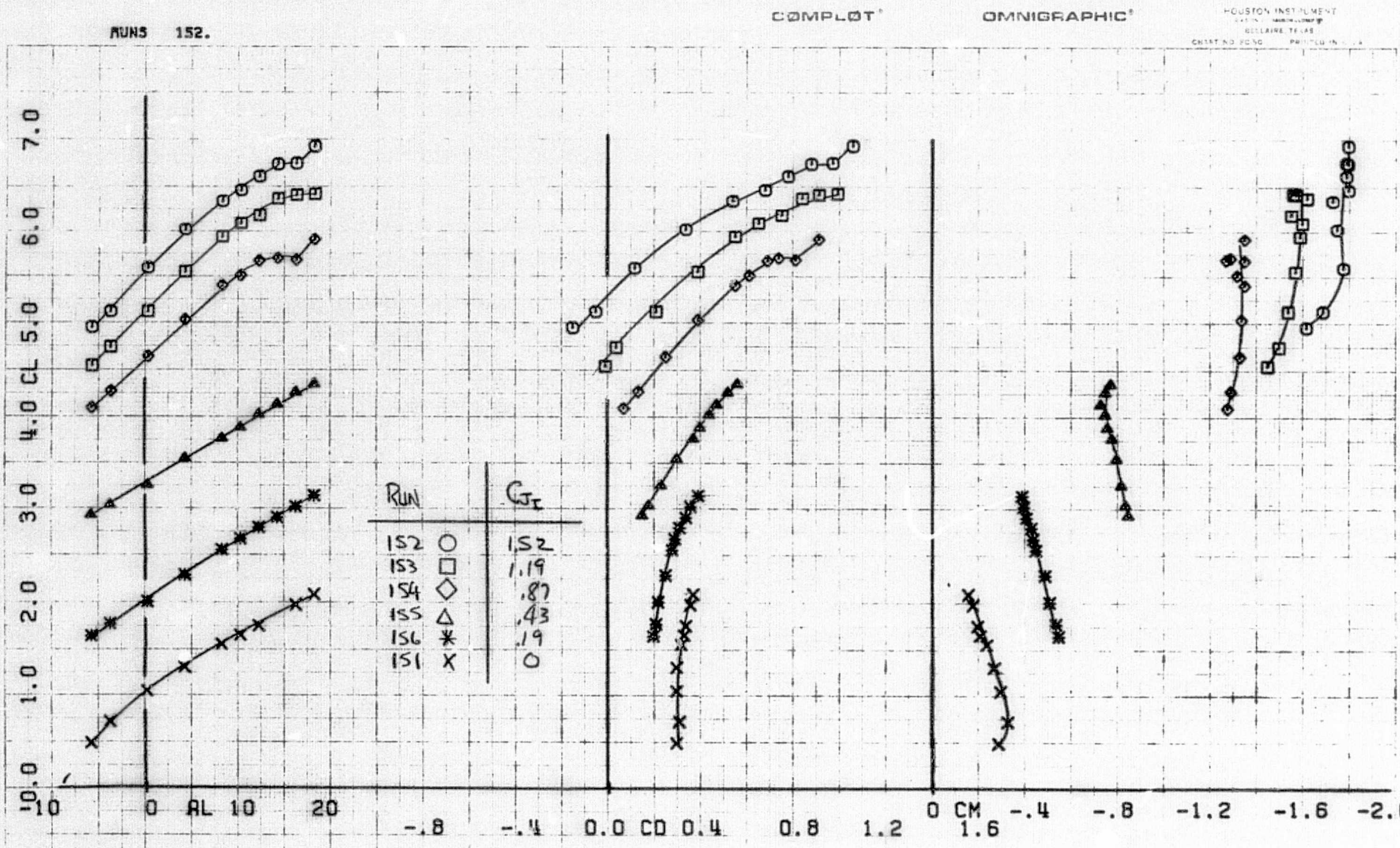

(a) tail off

Figure 9.- Longitudinal aerodynamic characteristics with no underwing engines; h/c = 2.01, $\delta_f = 70^\circ$.

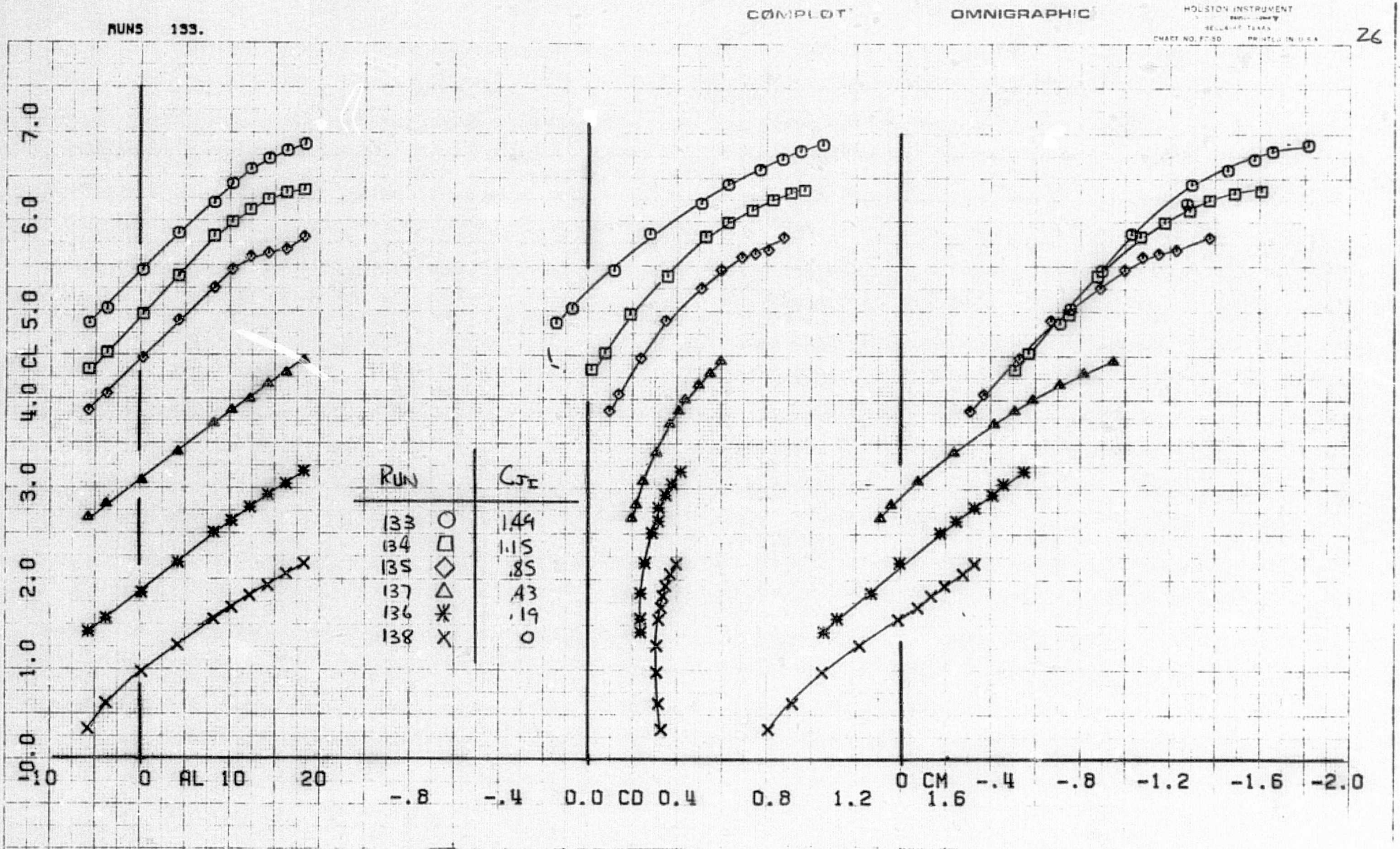

(b) tail on

Figure 9.- Concluded.

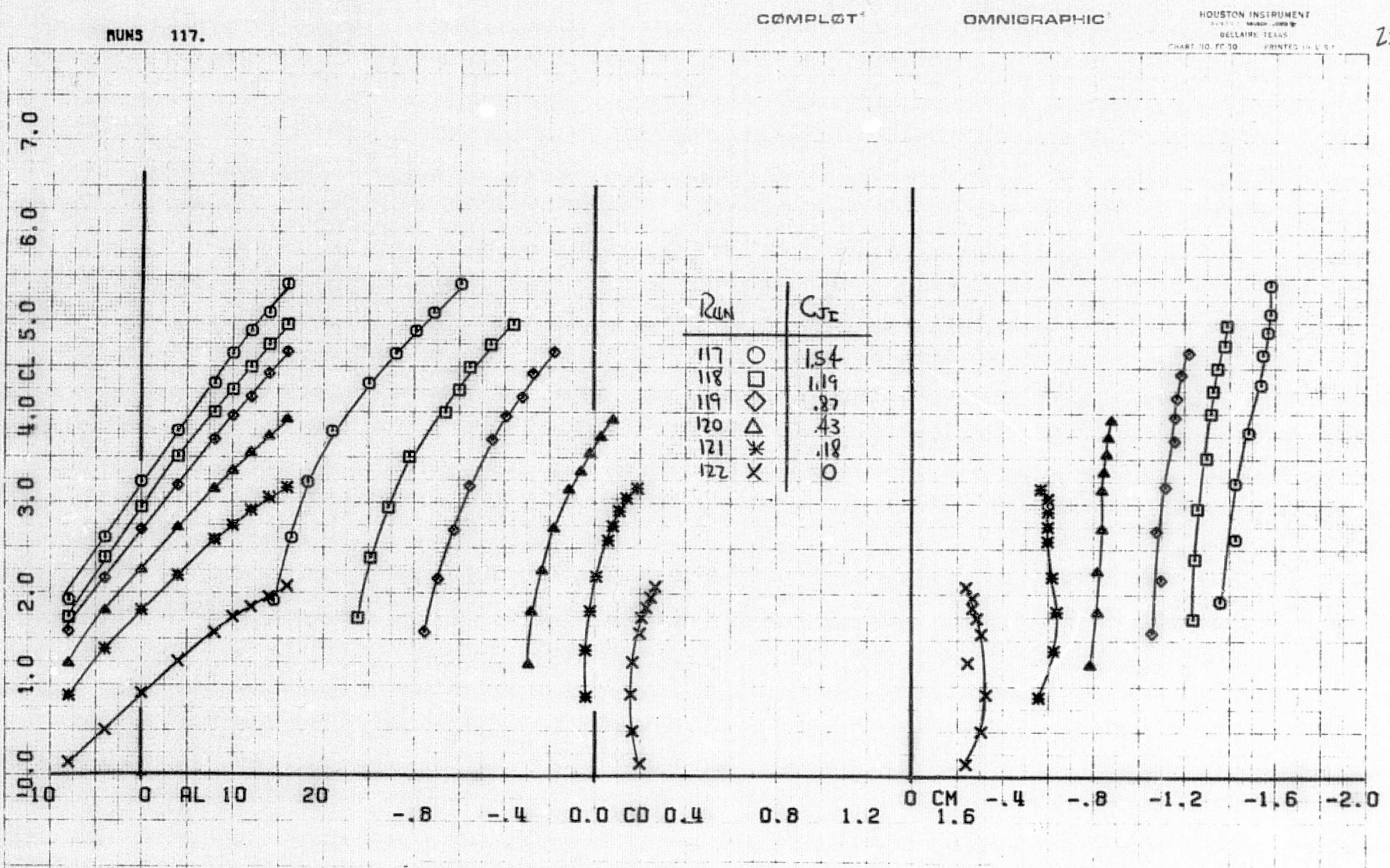

Figure 10.- Longitudinal aerodynamic characteristics with no underwing engines; h/c = 1.61, δ_f = 30°, tail off.

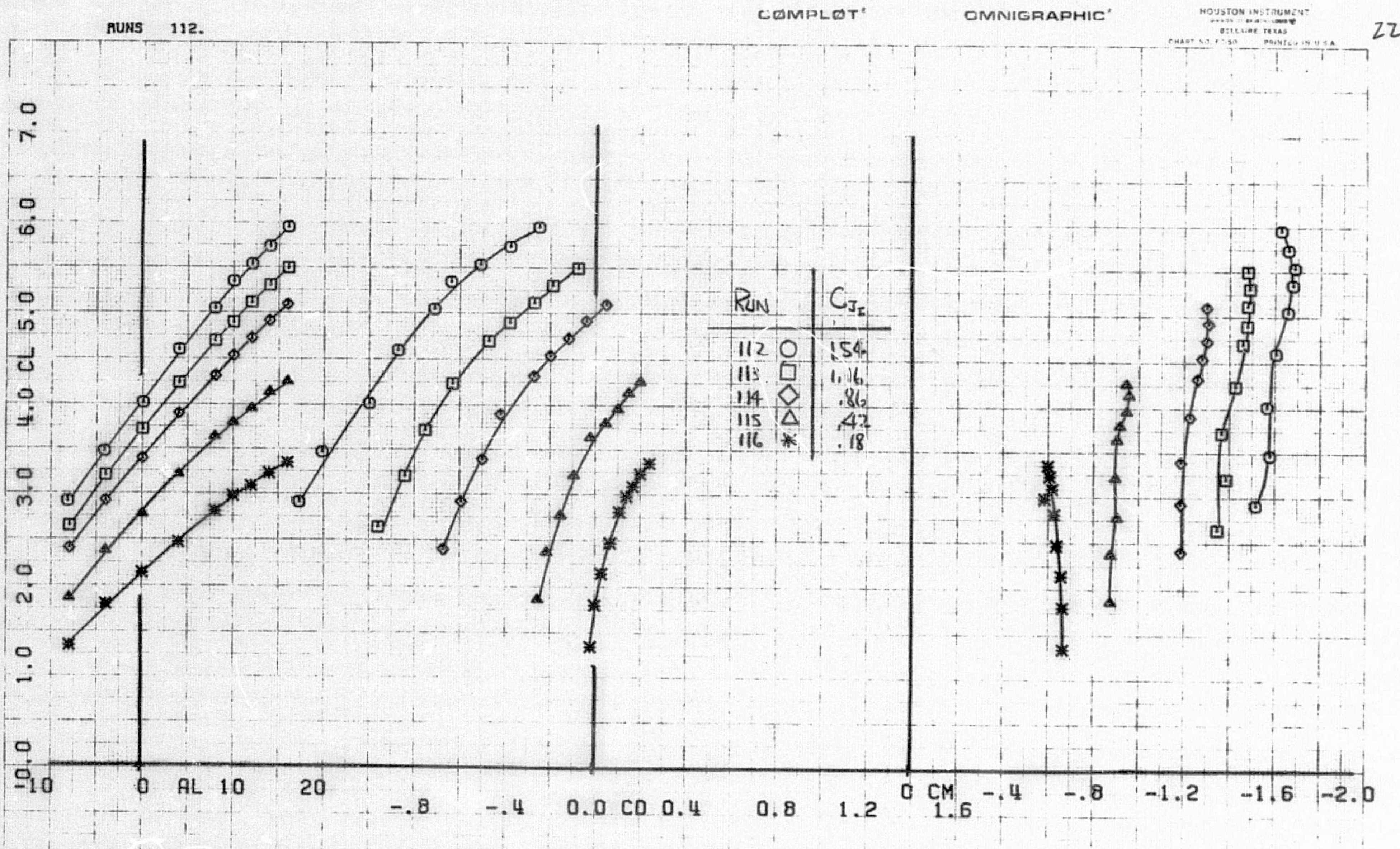

(a) tail off

Figure 11.- Longitudinal aerodynamic characteristics with no underwing engine; h/c = 1.61, δ_f = 40°.

11a

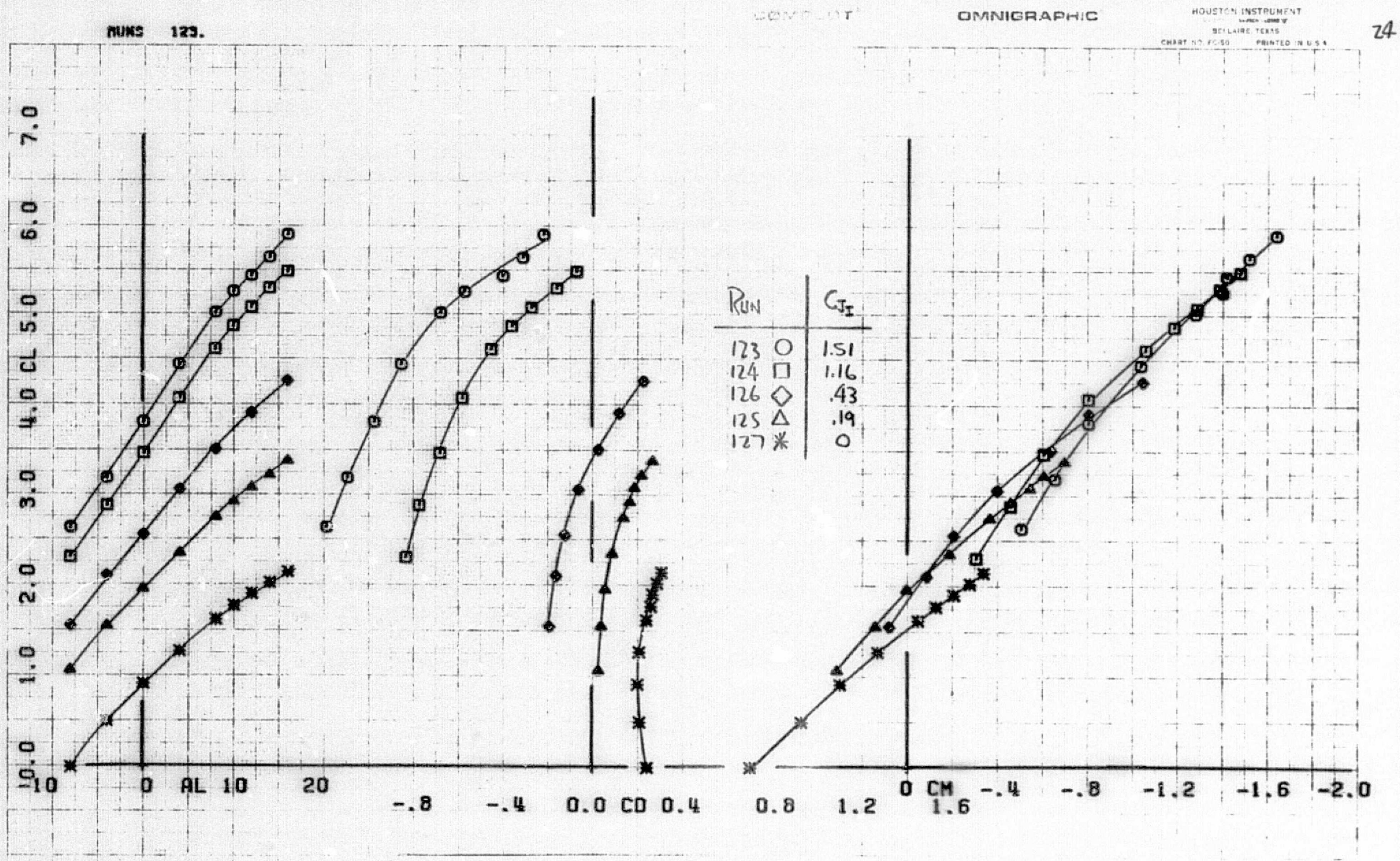

(b) tail on

Figure 11.- Concluded.

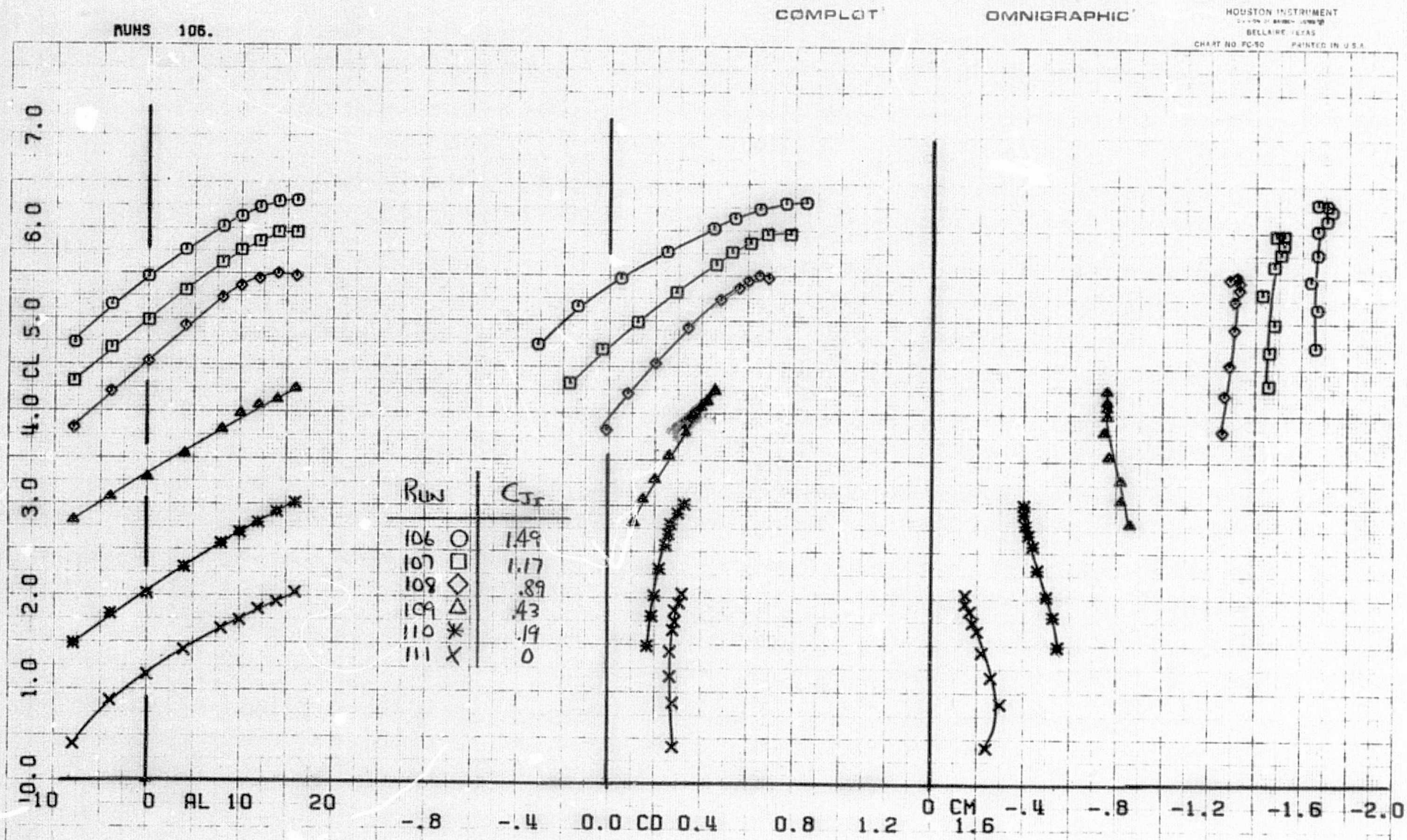

(a) tail off

Figure 12.- Longitudinal aerodynamic characteristics with no underwing engine; $h/c = 1.61$, $\delta_f = 70^o$.

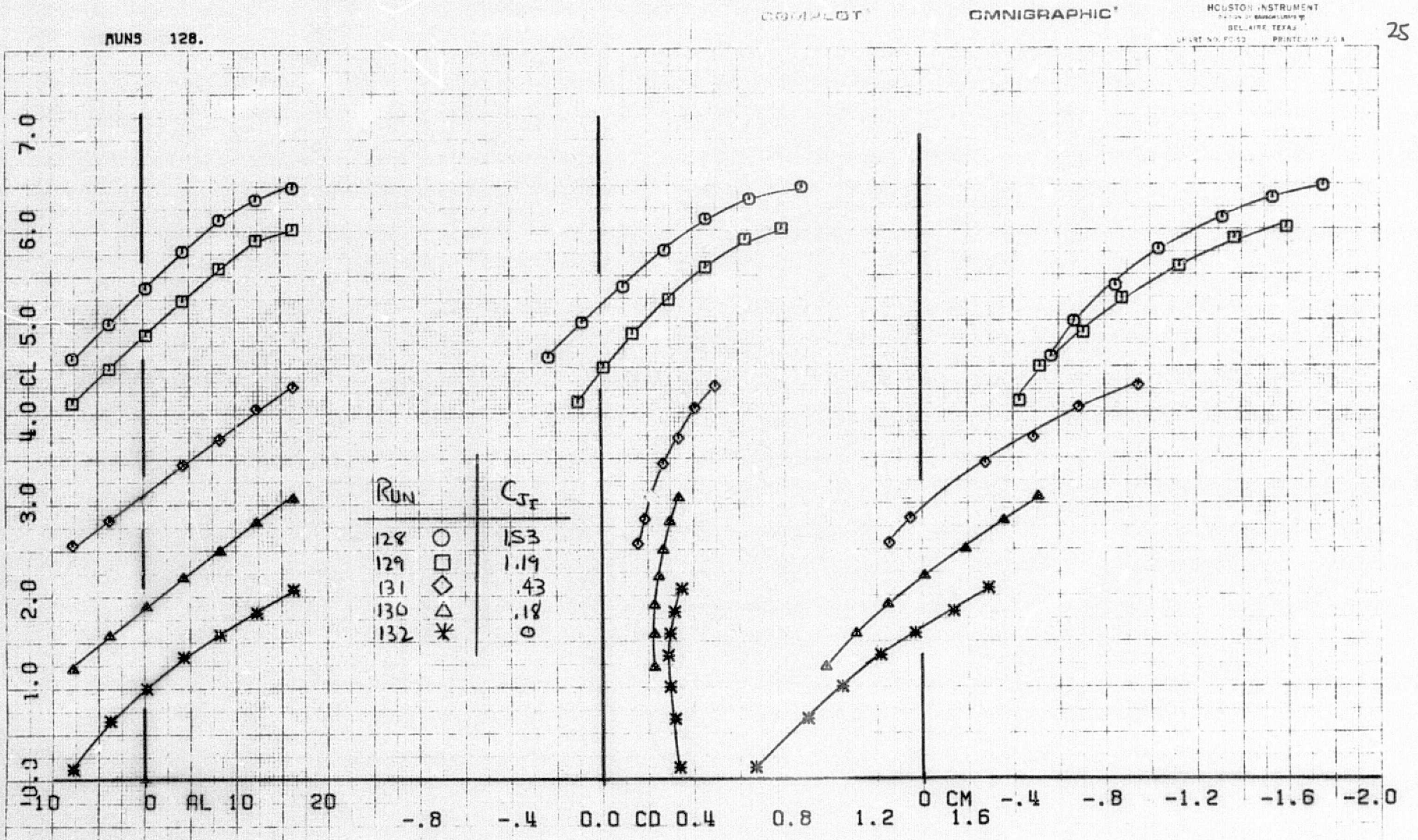

(b) tail on

Figure 12.- Concluded.

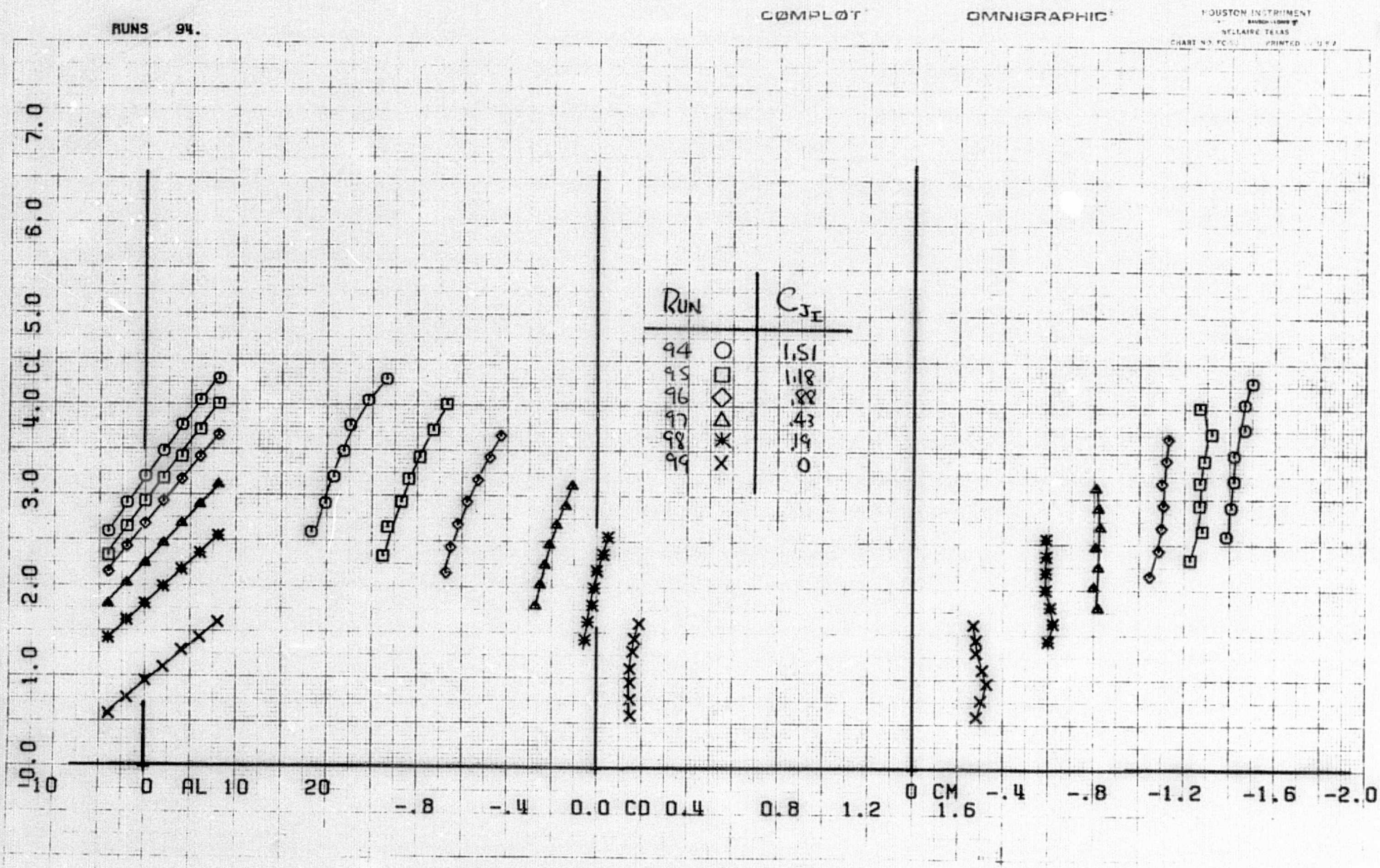

Figure 13.- Longitudinal aerodynamic characteristics with no underwing engine; h/c = 1.34, $\delta_f = 30^o$, tail off.

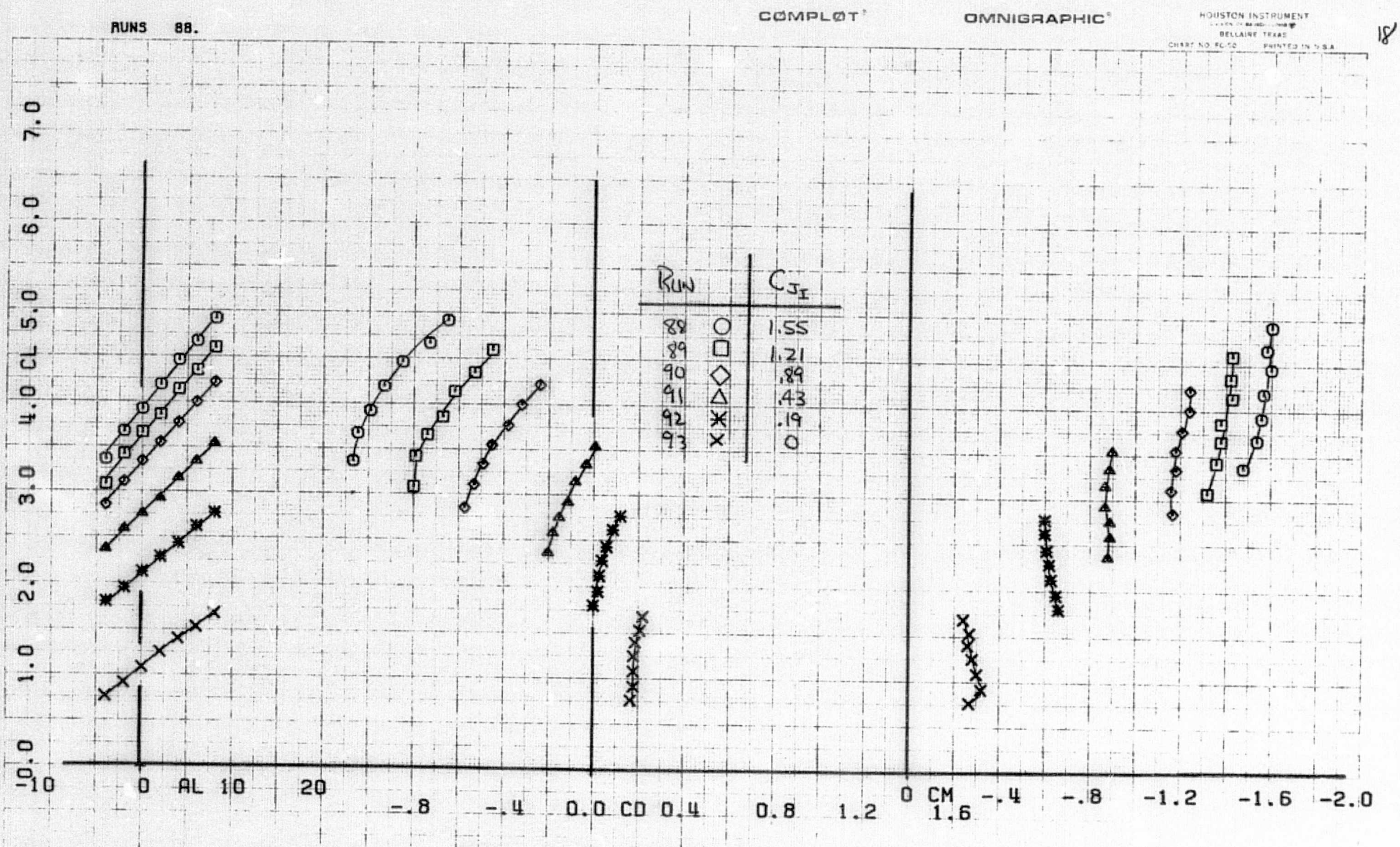

(a) tail off

Figure 14.- Longitudinal aerodynamic characteristics with no underwing engine; h/c = 1.34, $\delta_f = 40^{\circ}$.

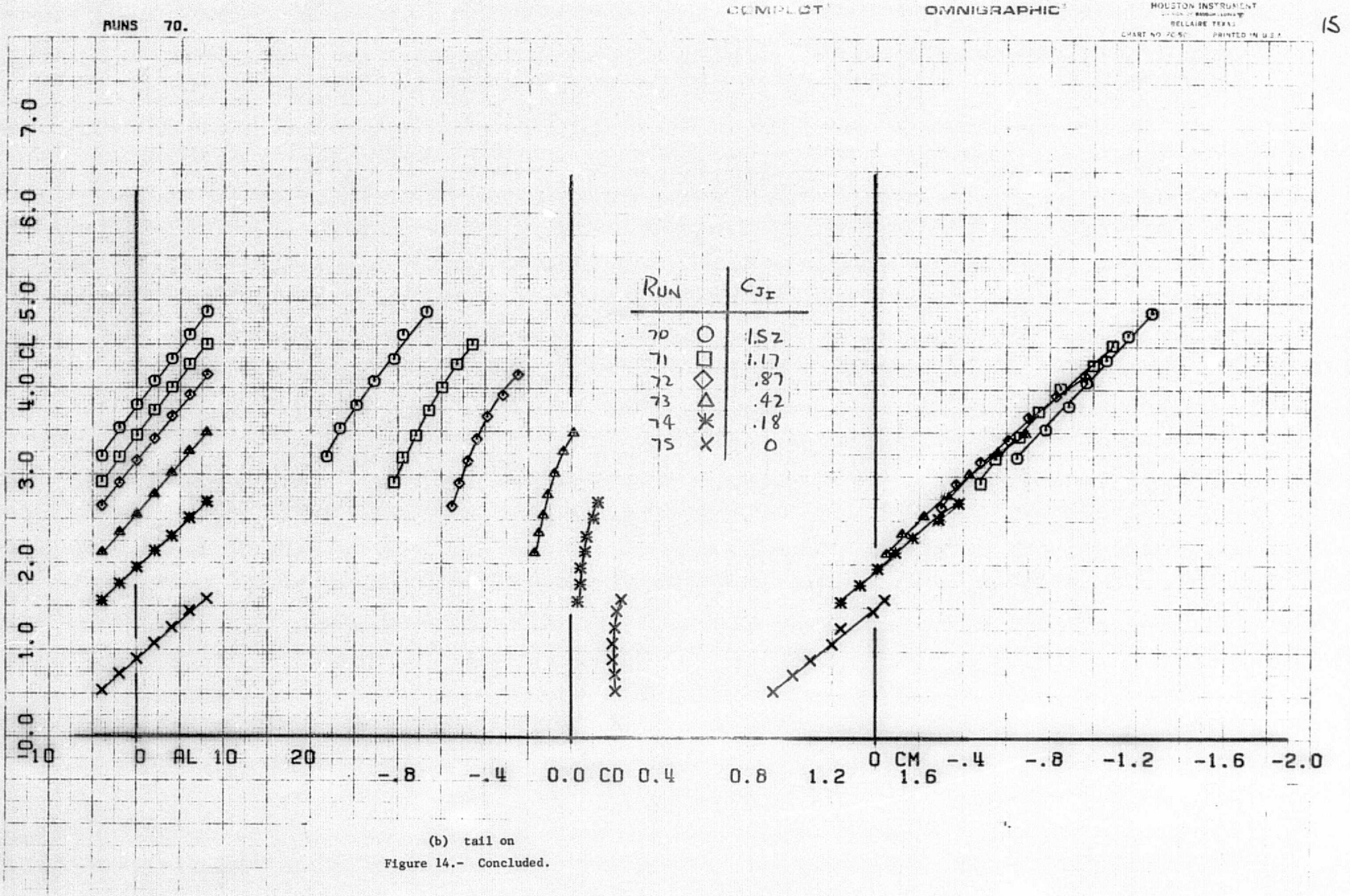

(b) tail on

Figure 14.- Concluded.

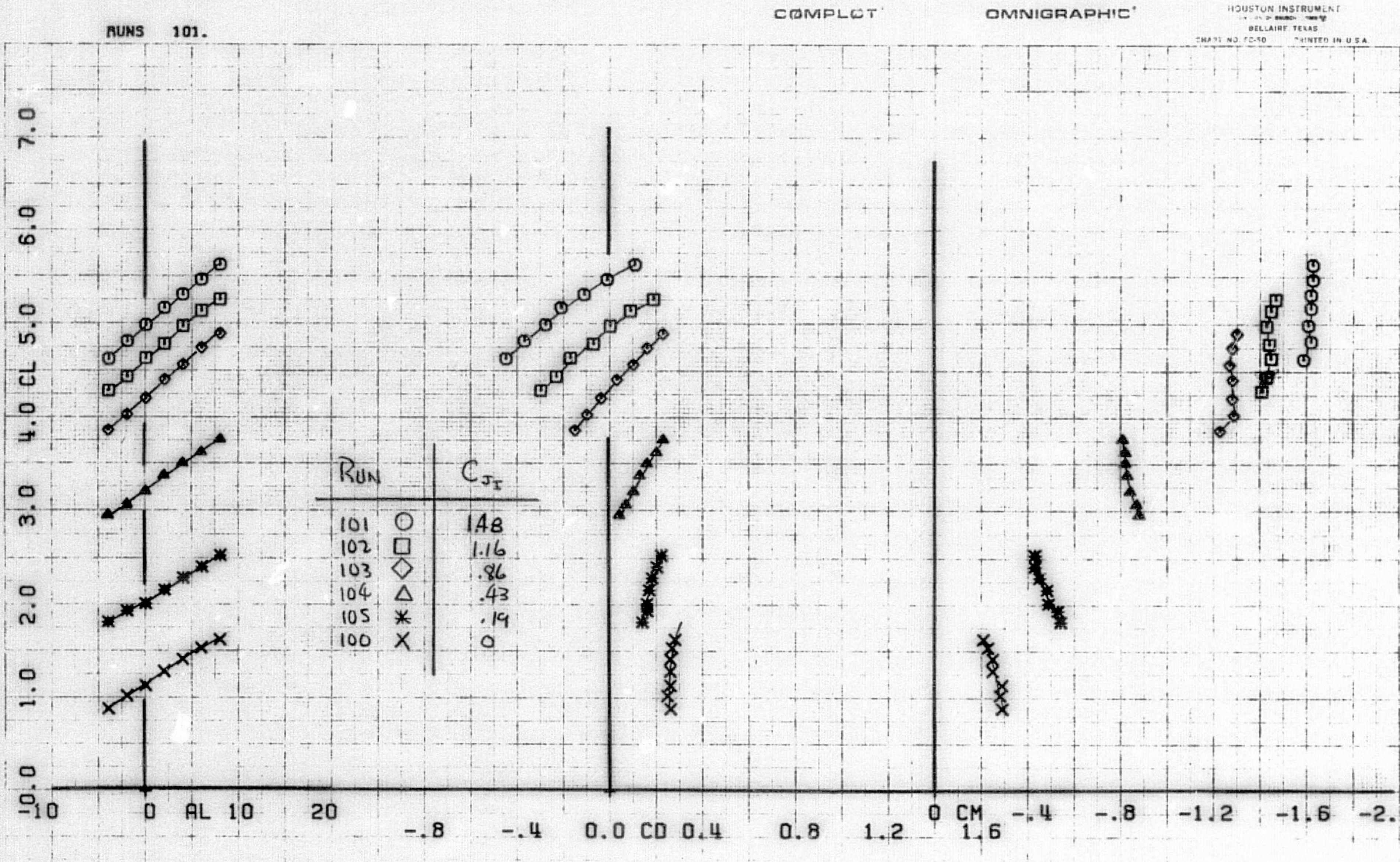

Figure 15.- Longitudinal aerodynamic characteristics with no underwing engine; h/c = 1.34, $\delta_f = 60^\circ$, tail off.

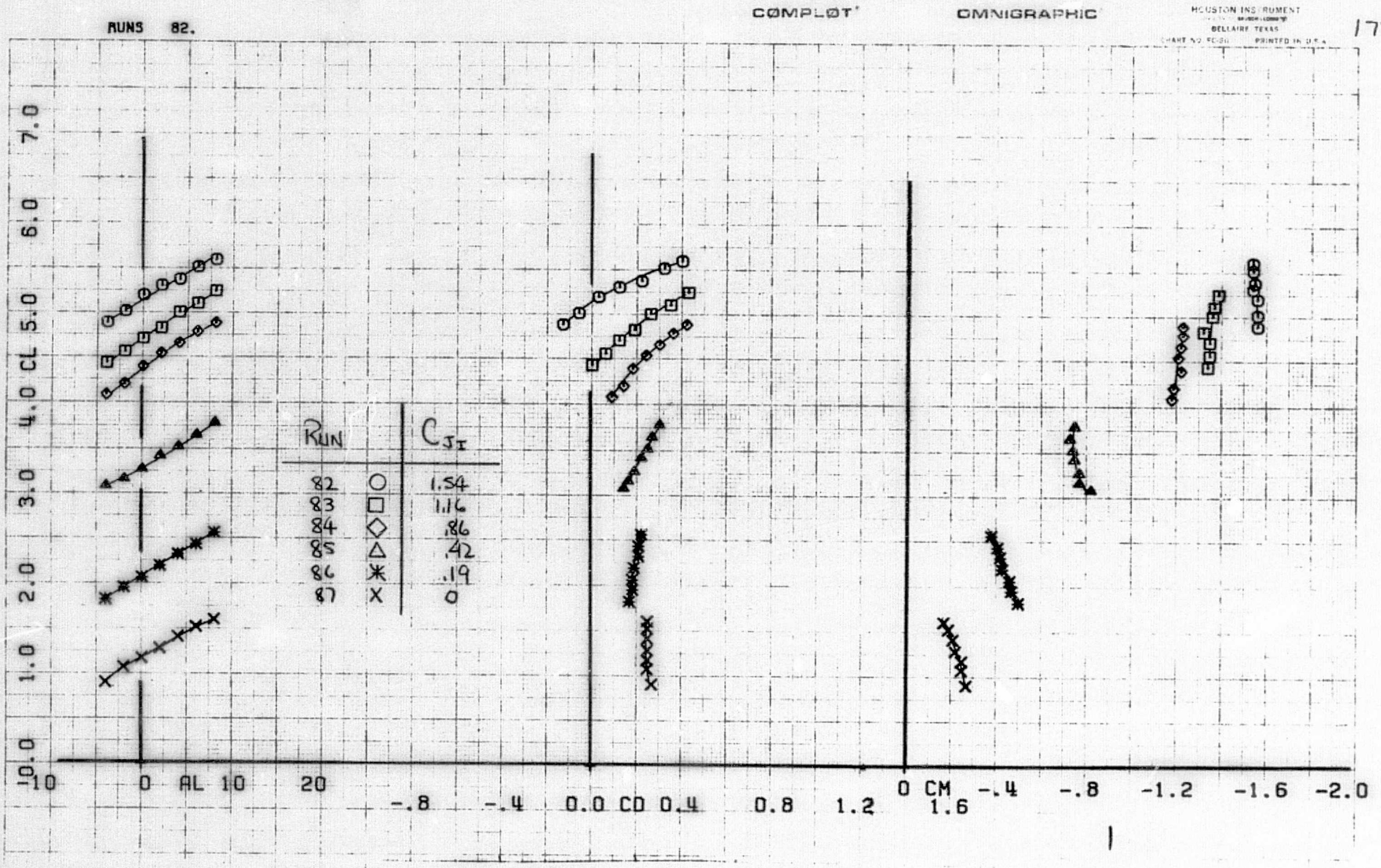

(a) tail off

Figure 16.- Longitudinal aerodynamic characteristics with no underwing engine; h/c = 1.34, $\delta_f = 70^{\circ}$.

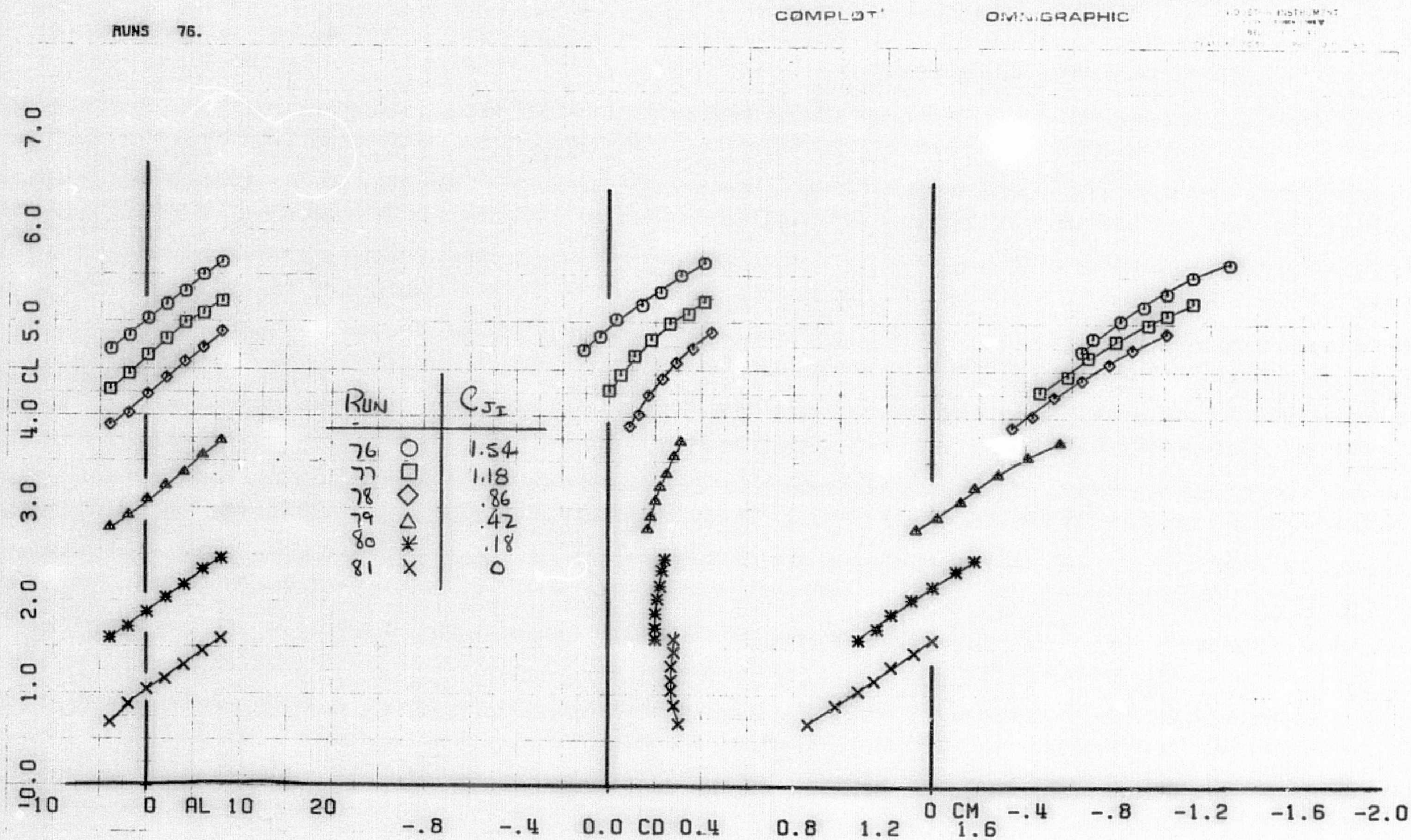

(b) tail on

Figure 16.- Concluded.

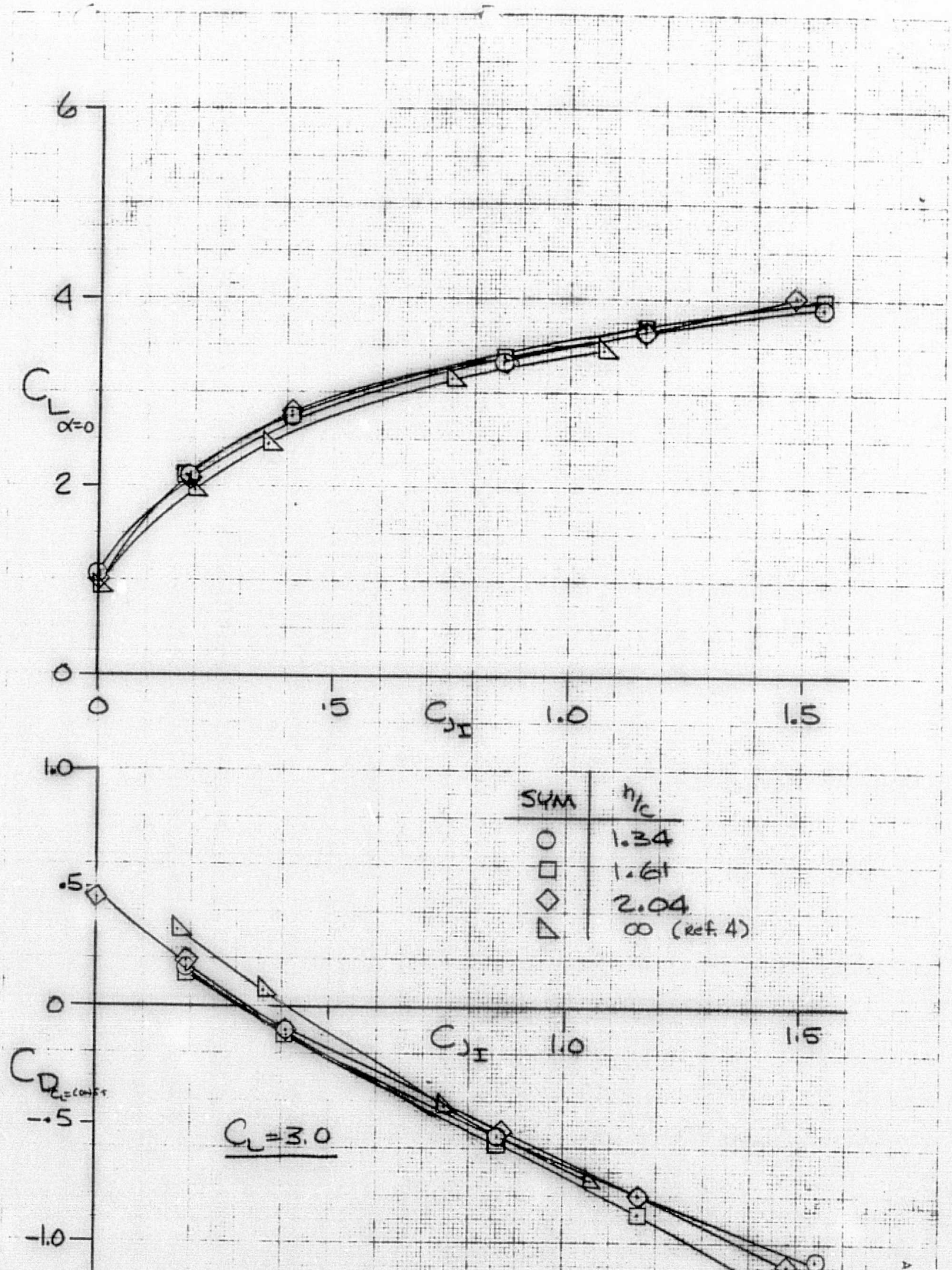

(a) $\delta_f = 40°$.

Figure 17.- Effect of height on the longitudinal aerodynamic characteristics with no underwing engine.

NASA
AMES RESEARCH CENTER

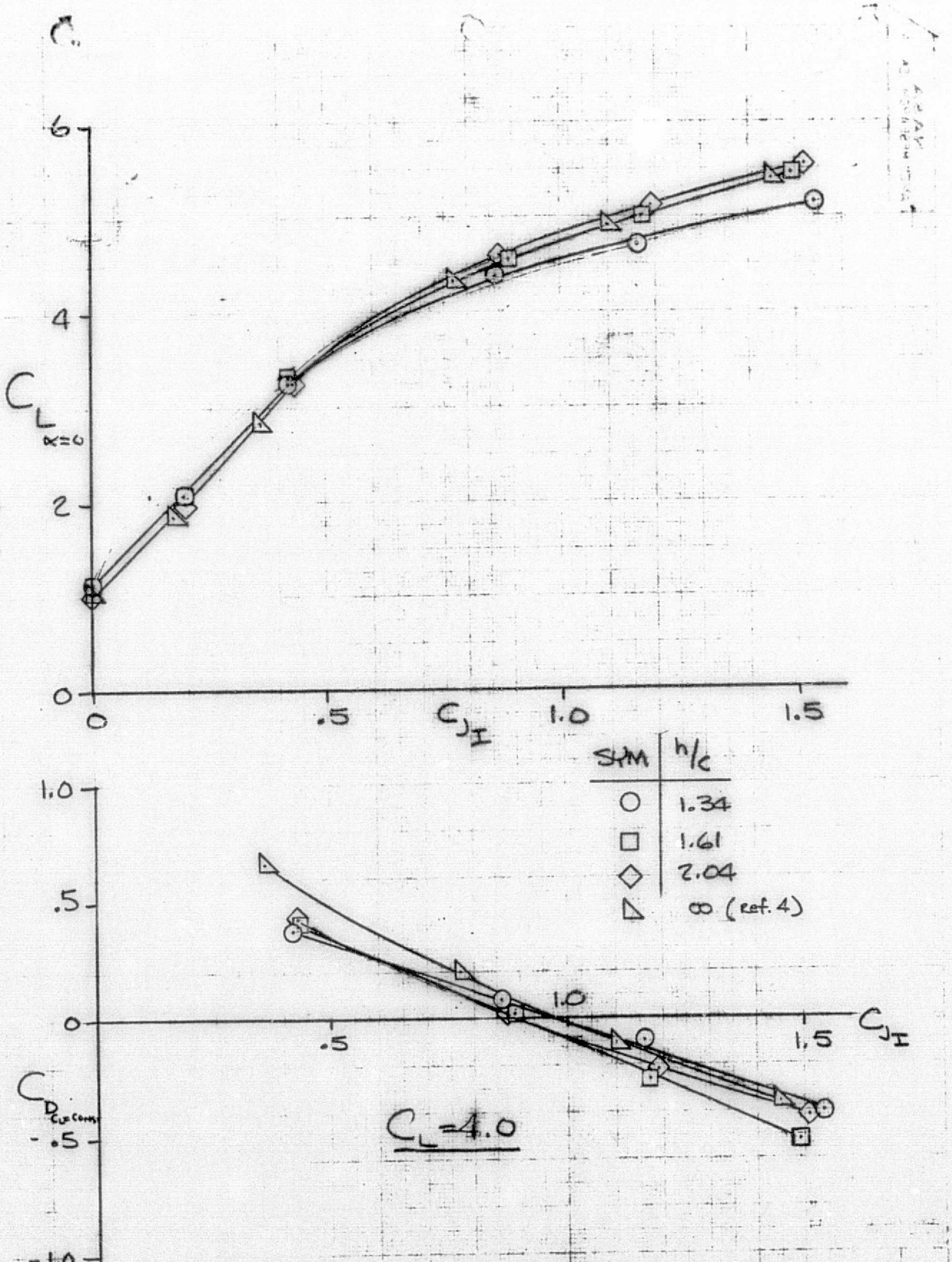

(b) $\delta_f = 70^\circ$.

Figure 17.- Concluded.

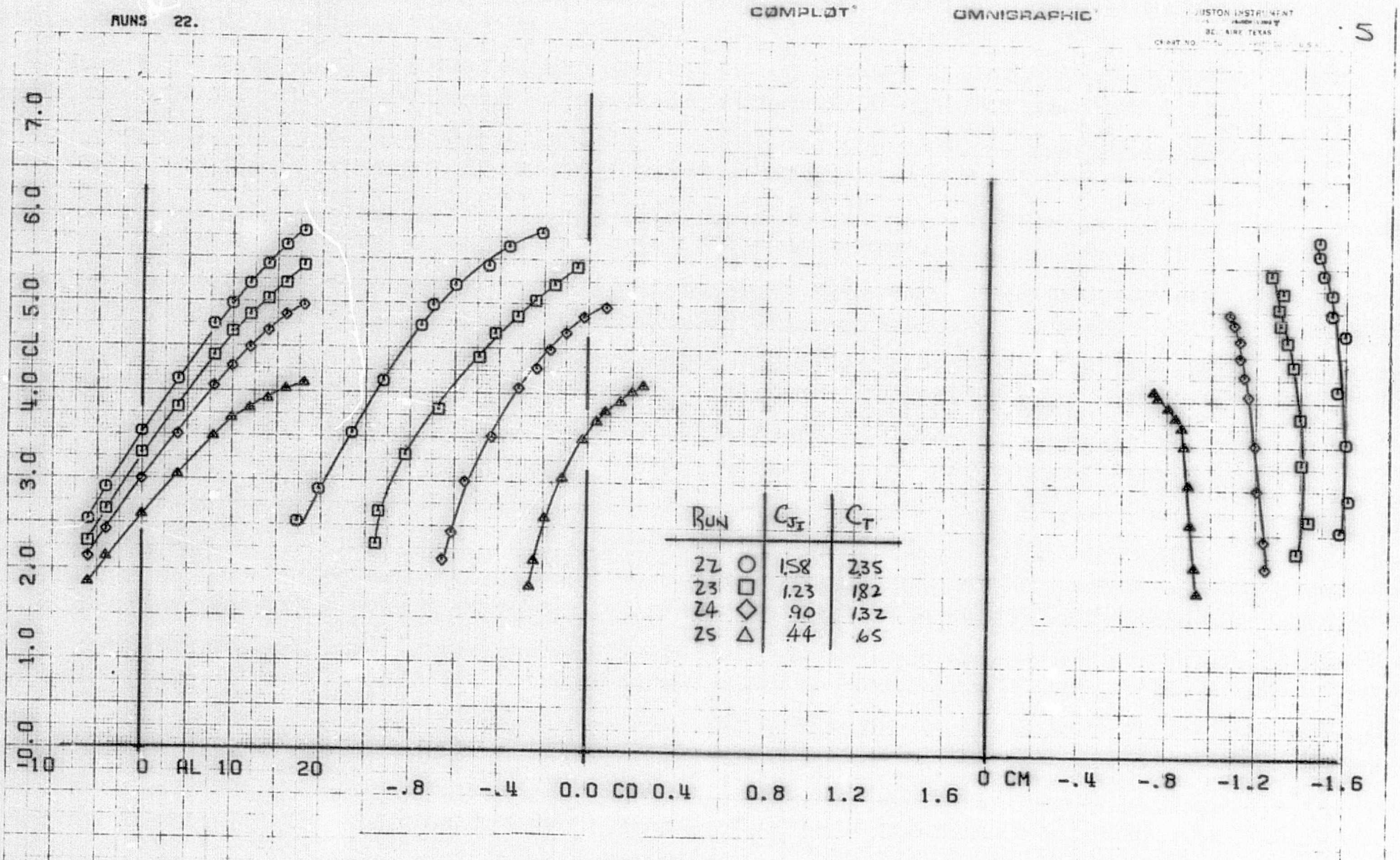

(a) T. S. = 40:60, tail off.

Figure 18.- Longitudinal aerodynamic characteristics with four JT-15 underwing engines; h/c = 2.04, $\delta_f = 40°$.

18a

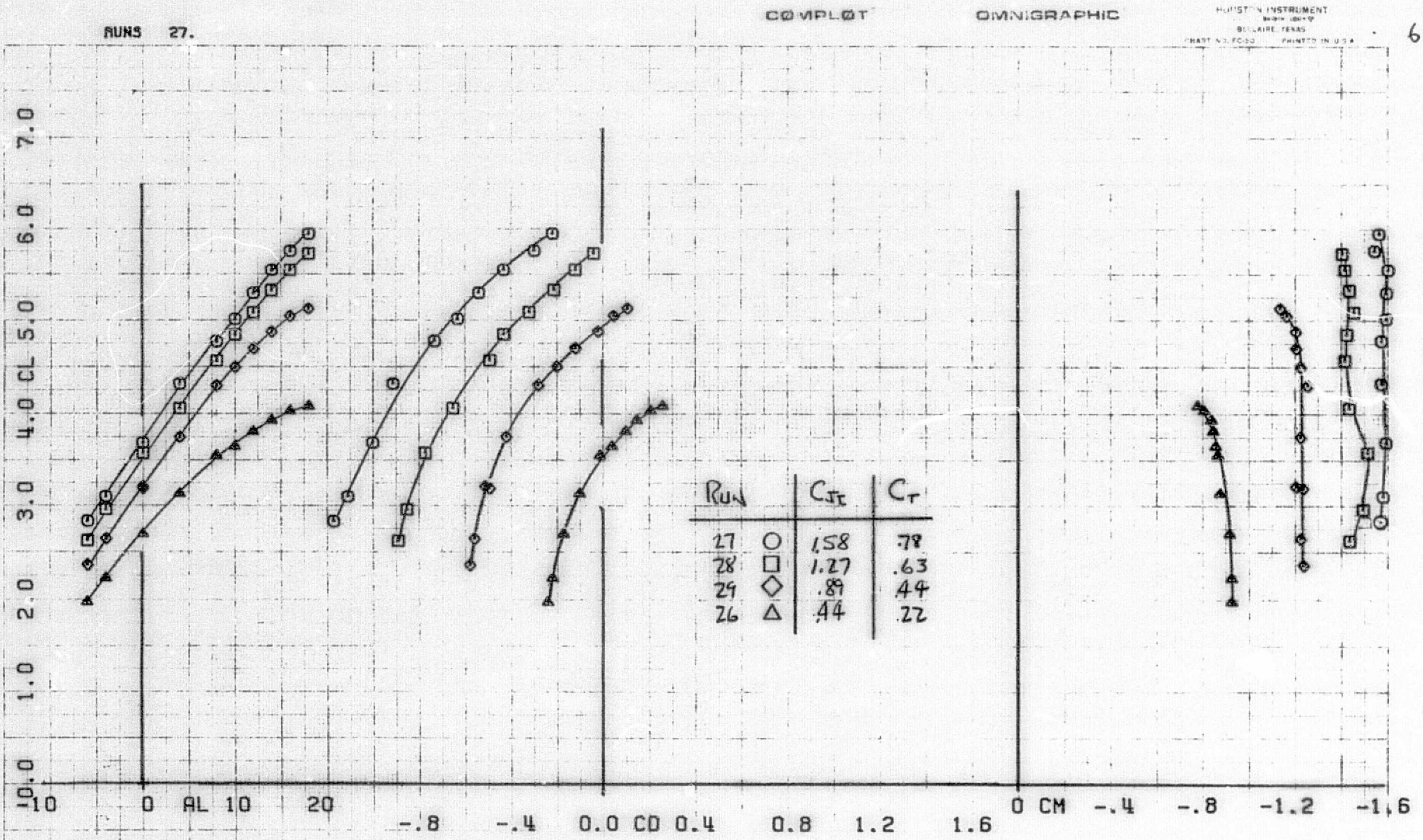

(b) T. S. = 67:33, tail off

Figure 18.- Continued.

18b

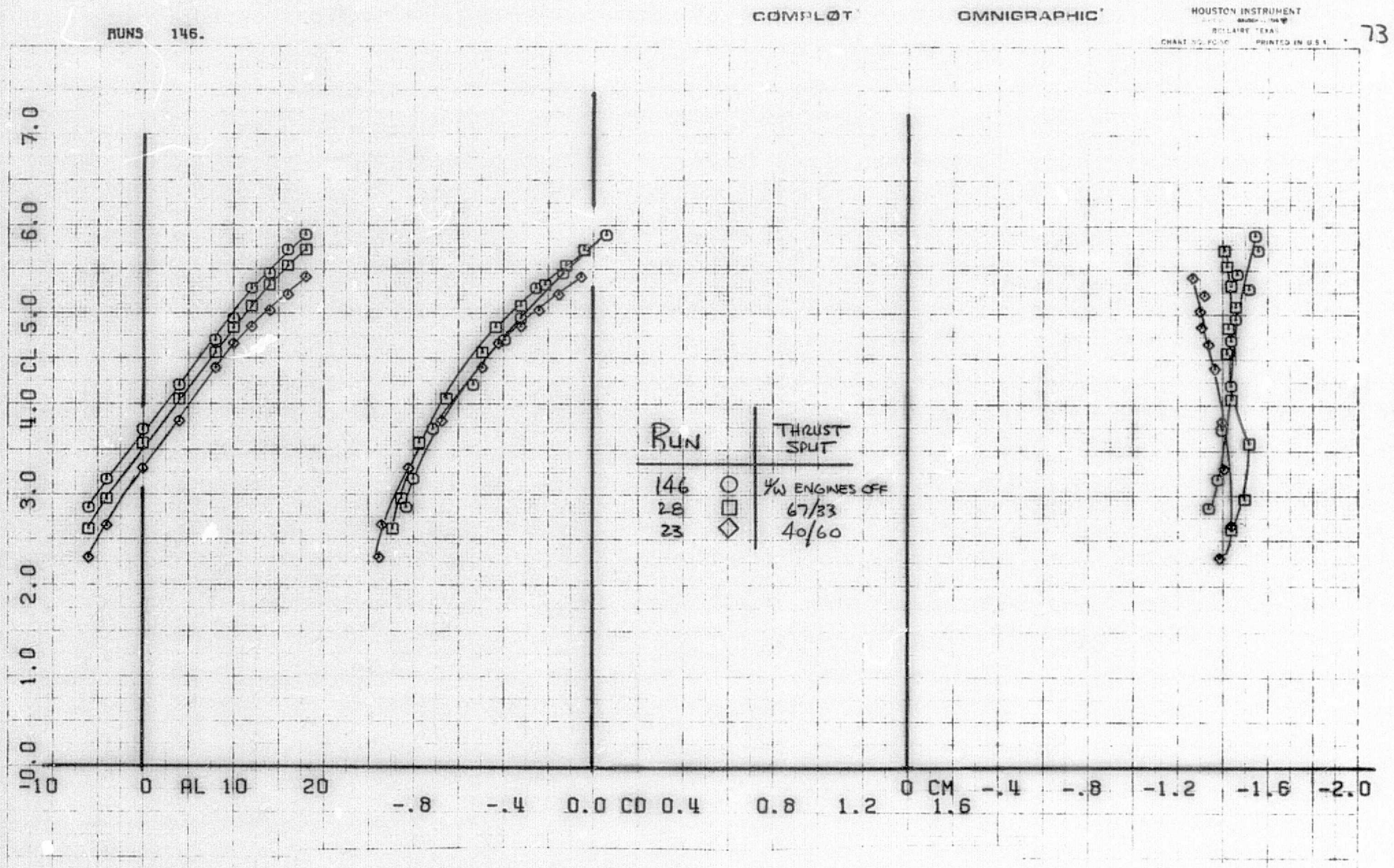

(c) Effect of T. S., C_{J_I} = 1.18, tail off

Figure 18.- Continued.

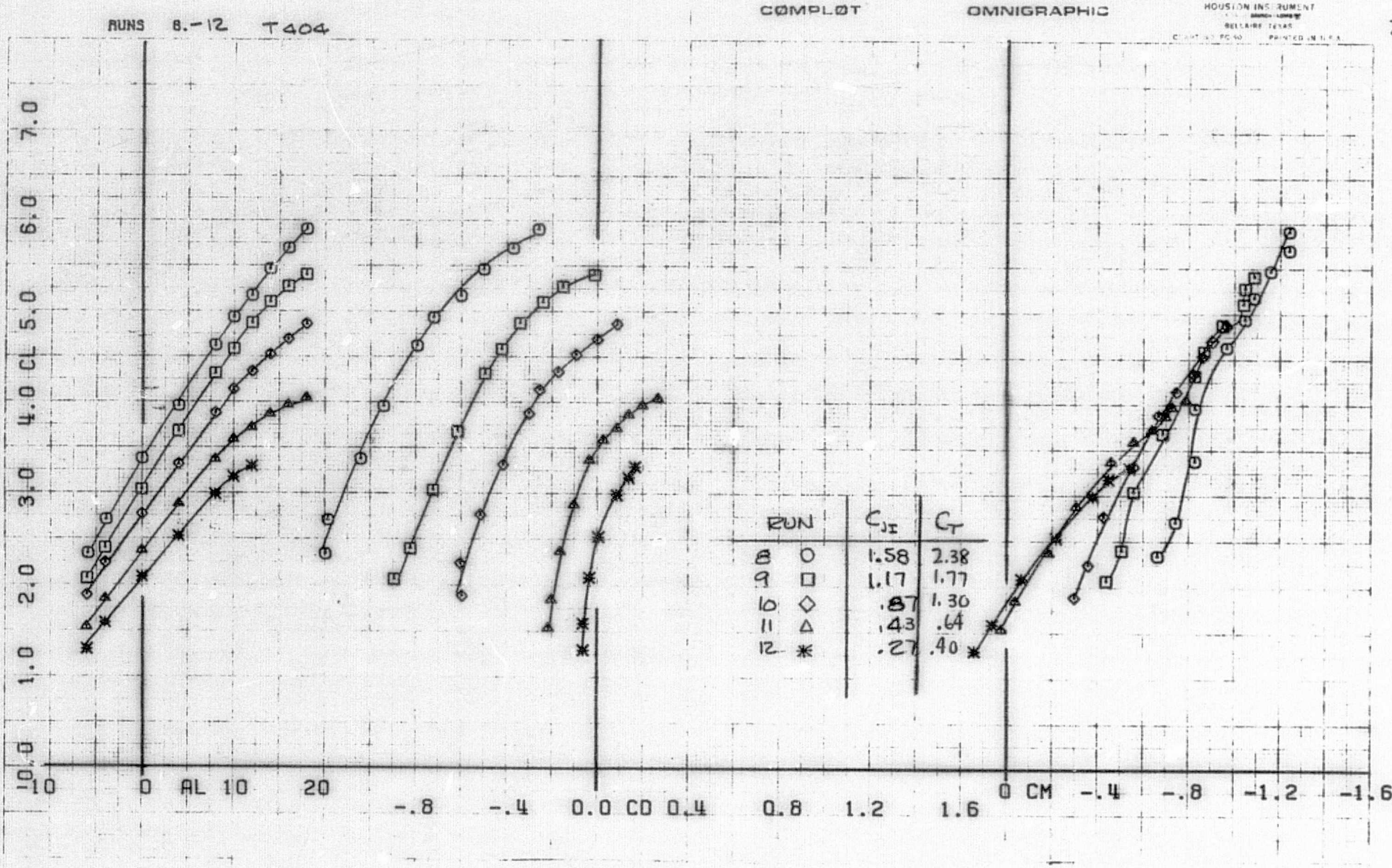

(d) T. S. = 40:60, tail on

Figure 18.- Continued.

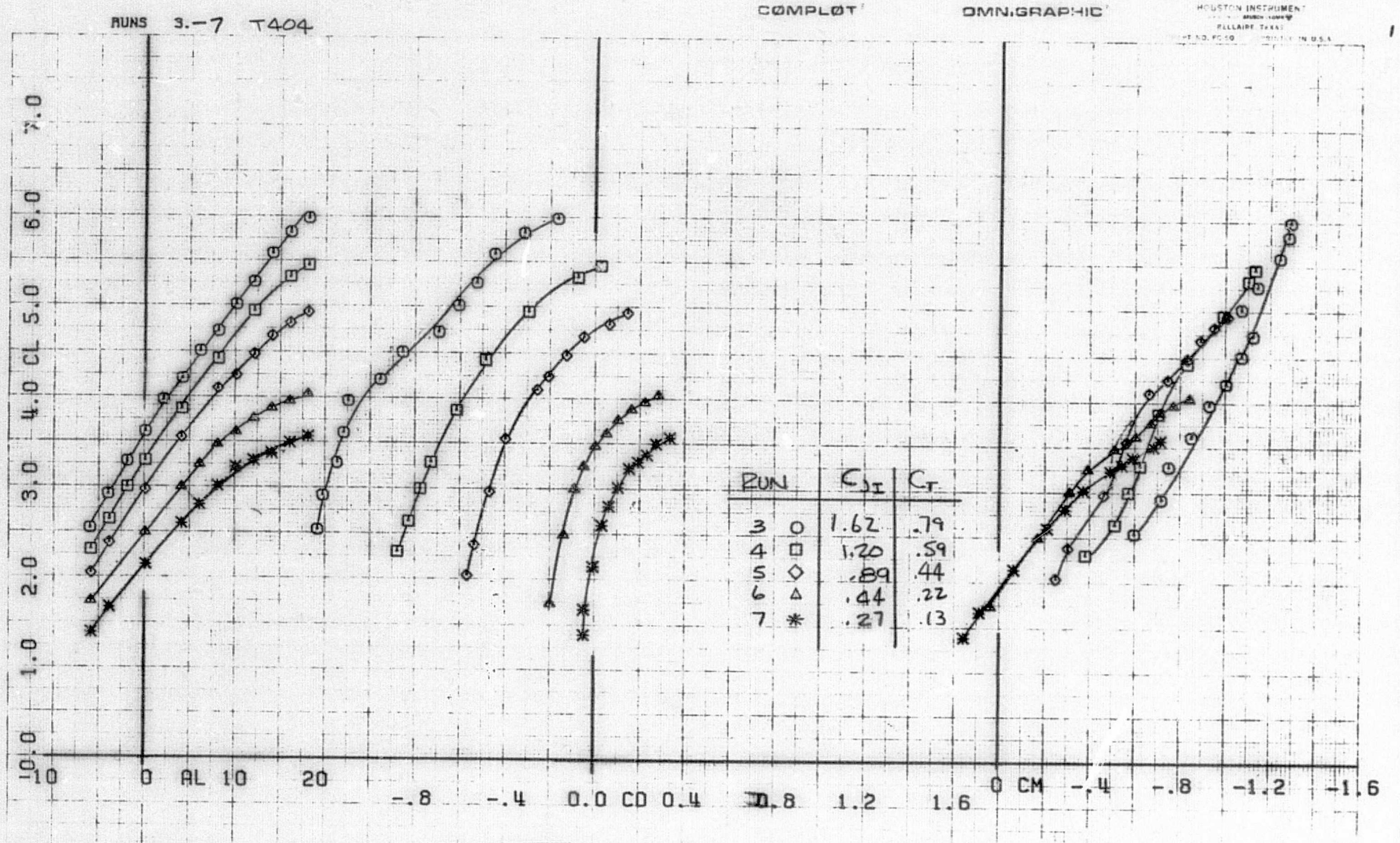

(e) T. S. = 67:33, tail on

Figure 18.- Concluded.

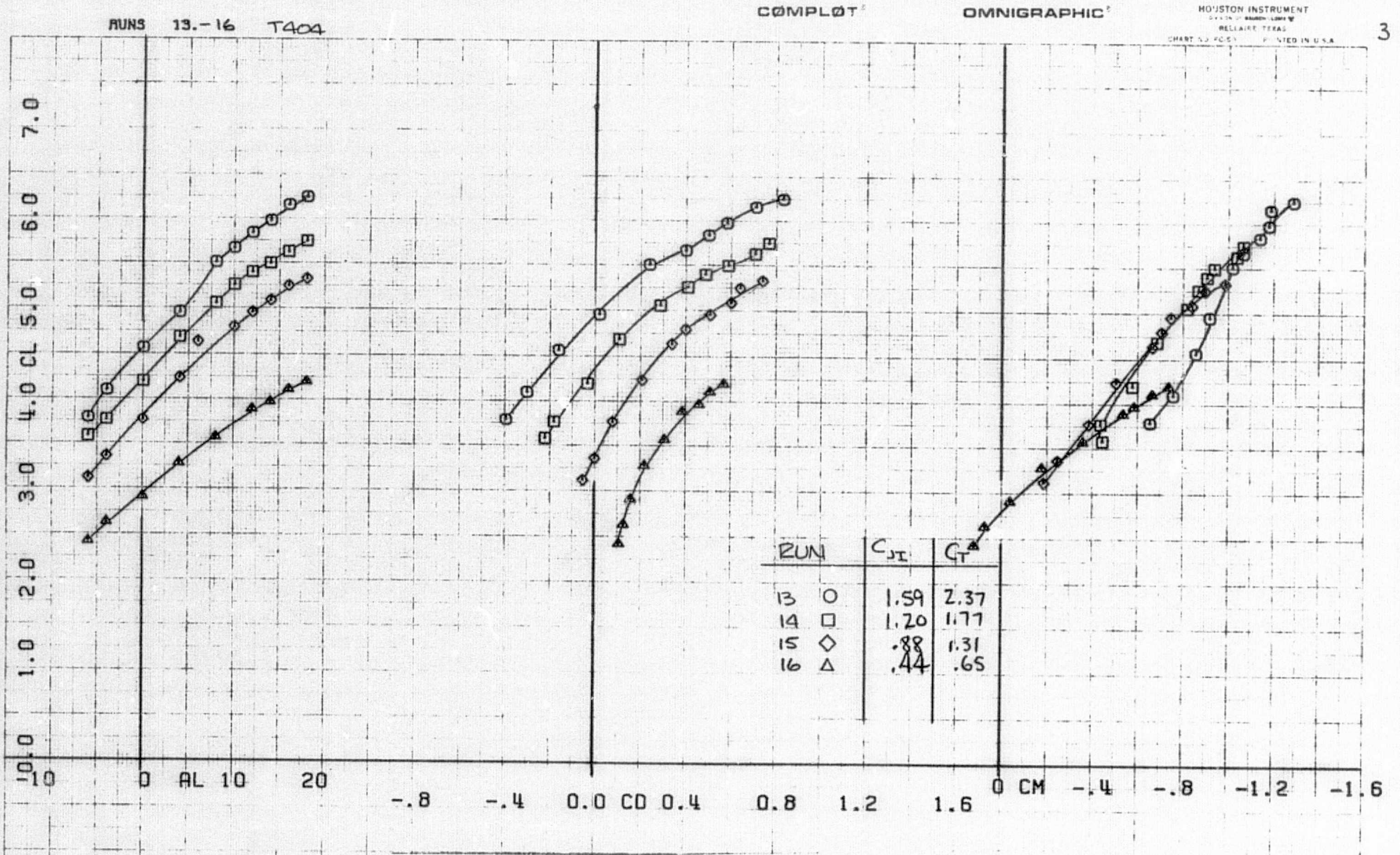

(a) T. S. = 40:60

Figure 19.- Longitudinal aerodynamic characteristics with four JT-15 underwing engines; h/c= 2.04, δ_f = 70°, tail on.

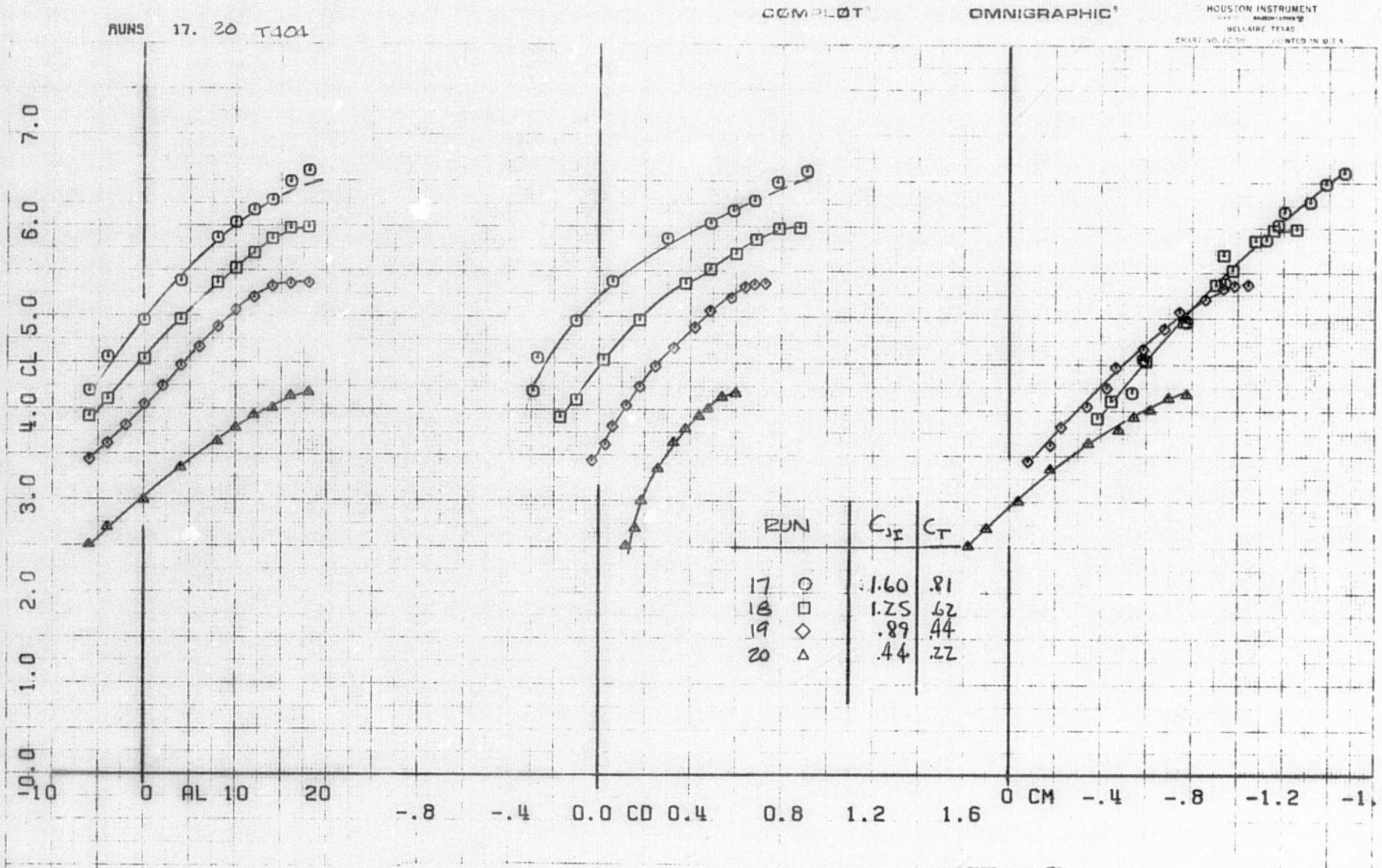

(b) T. S. = 67:33

Figure 19.- Continued.

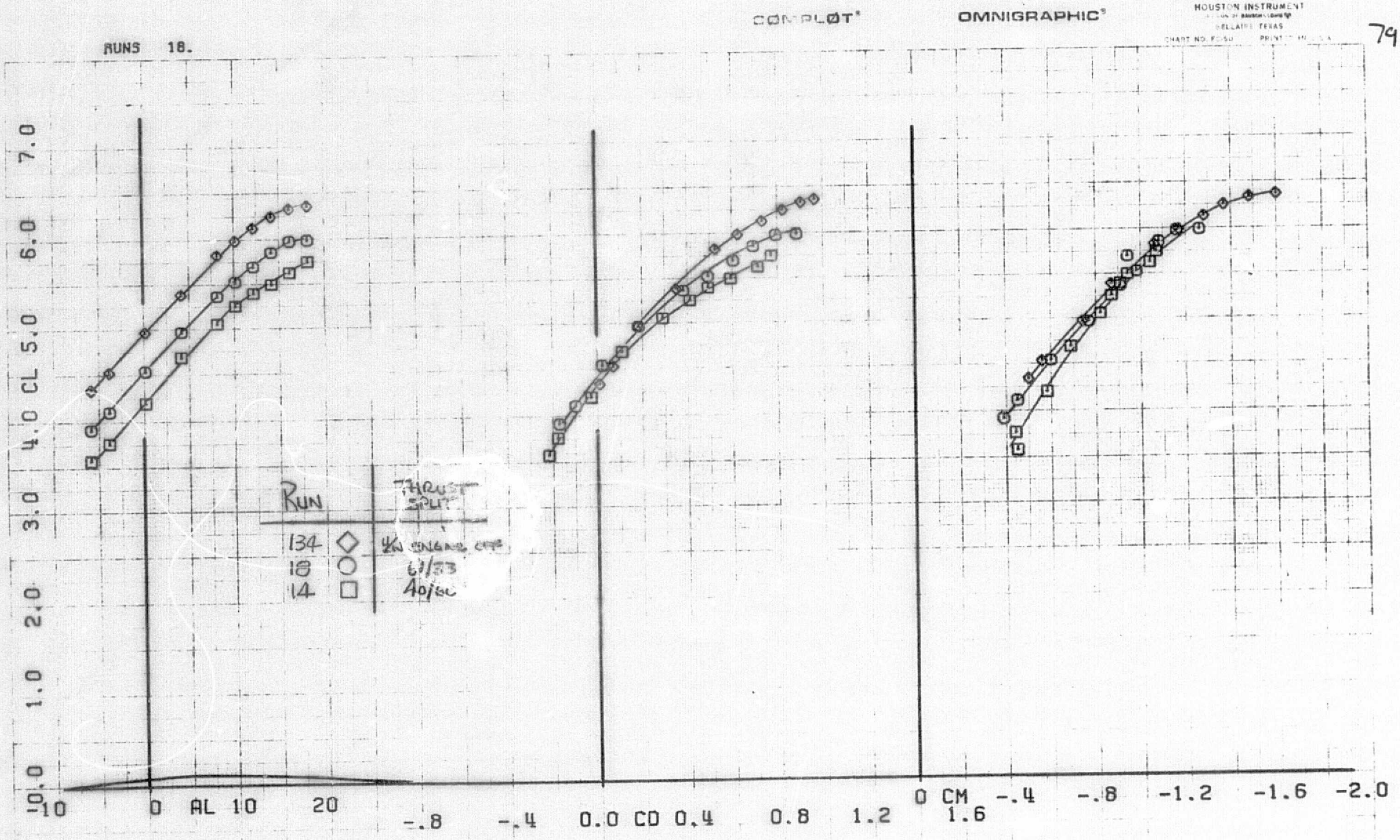

(c) Effect of T. S., C_{J_I} = 1.18

Figure 19.- Concluded.

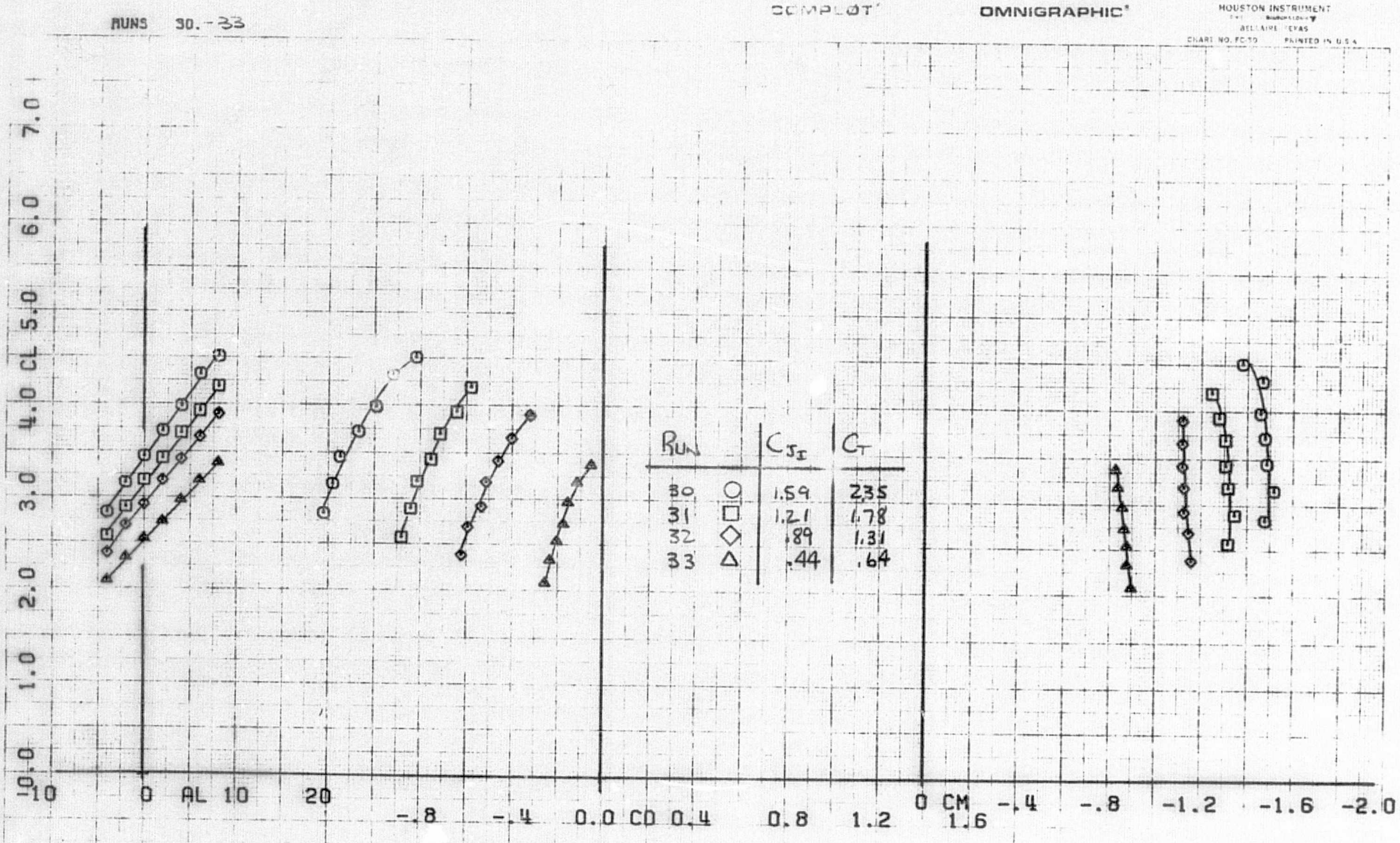

(a) T. S. = 40:60, tail off

Figure 20.- Longitudinal aerodynamic characteristics with four JT-15 underwing engines; h/c = 1.34, $\delta_f = 40^{\circ}$.

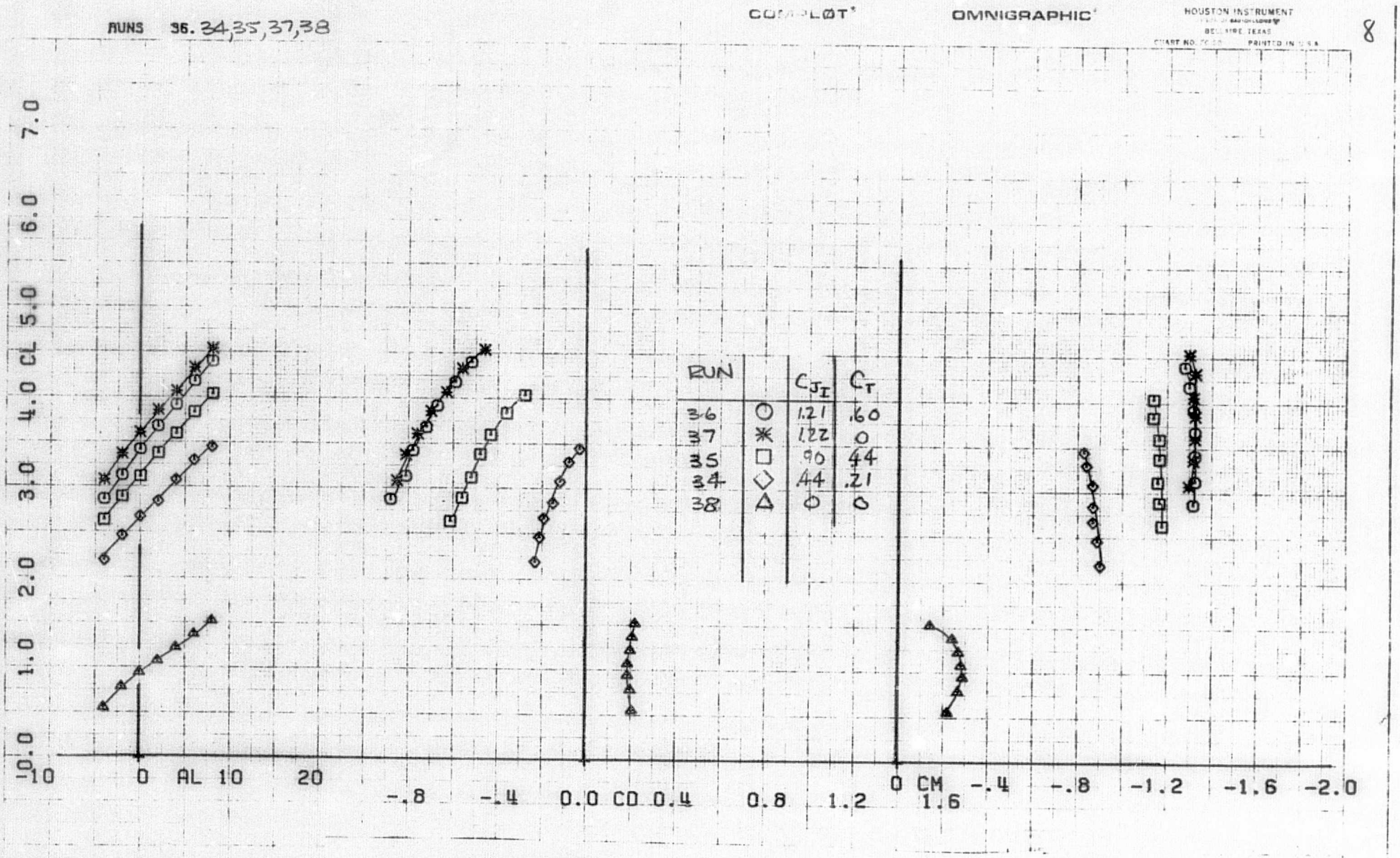

(b) T. S. = 67:33, tail off

Figure 20.- Continued.

206

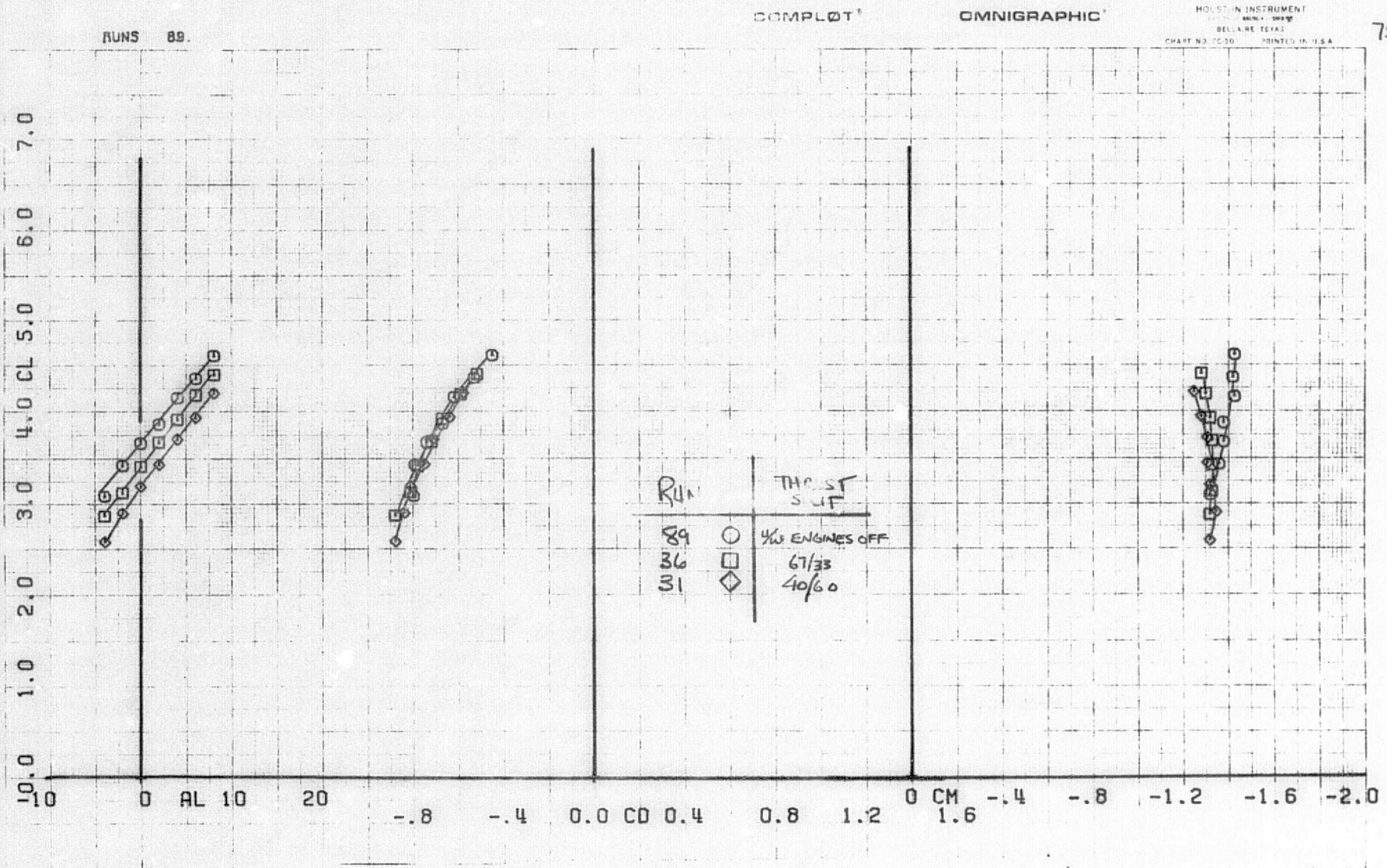

(c) Effect of T. S., C_{J_I} = 1.18, tail off

Figure 20.- Continued.

20c

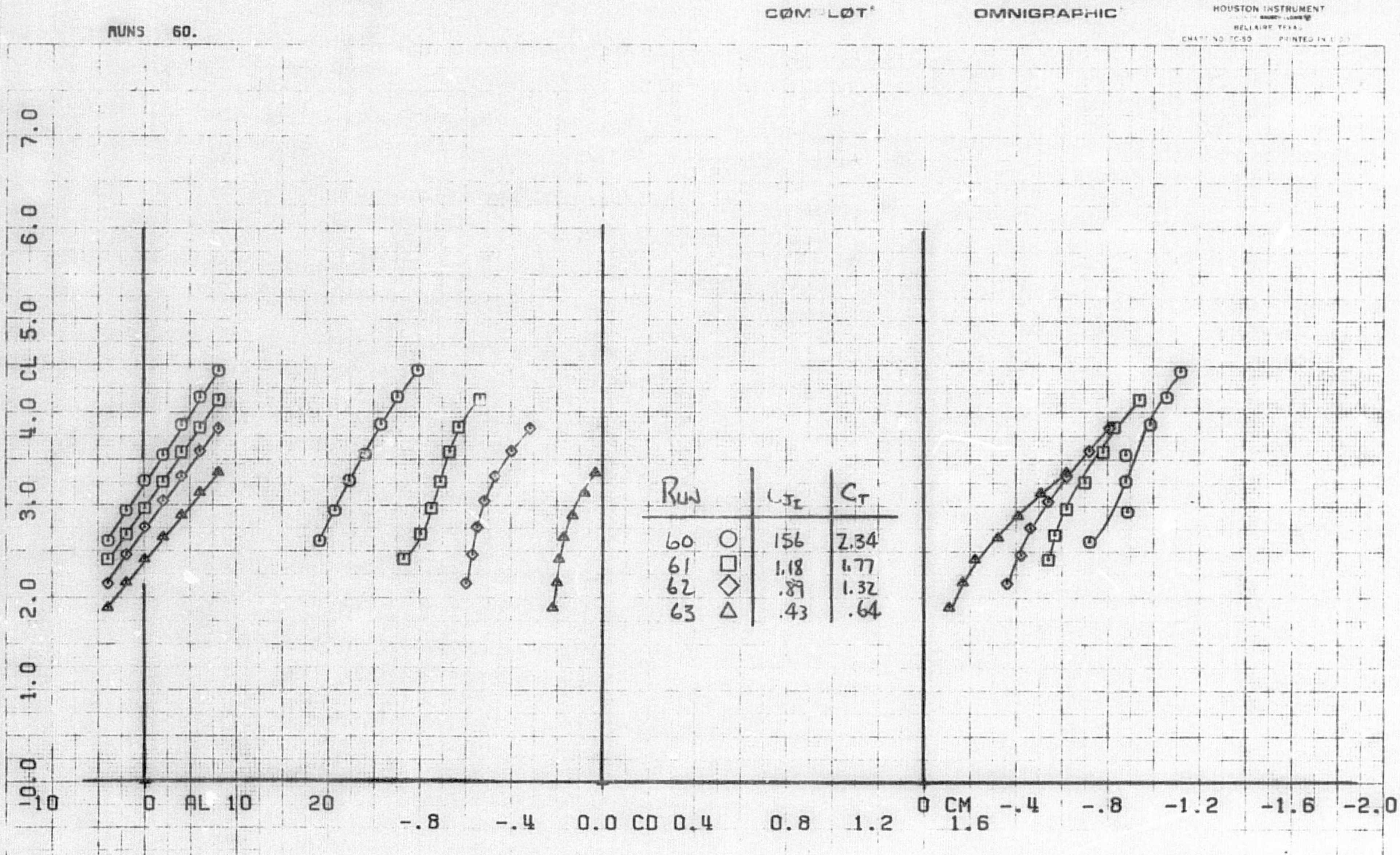

(d) T. S. = 40:60, tail on

Figure 20.- Continued.

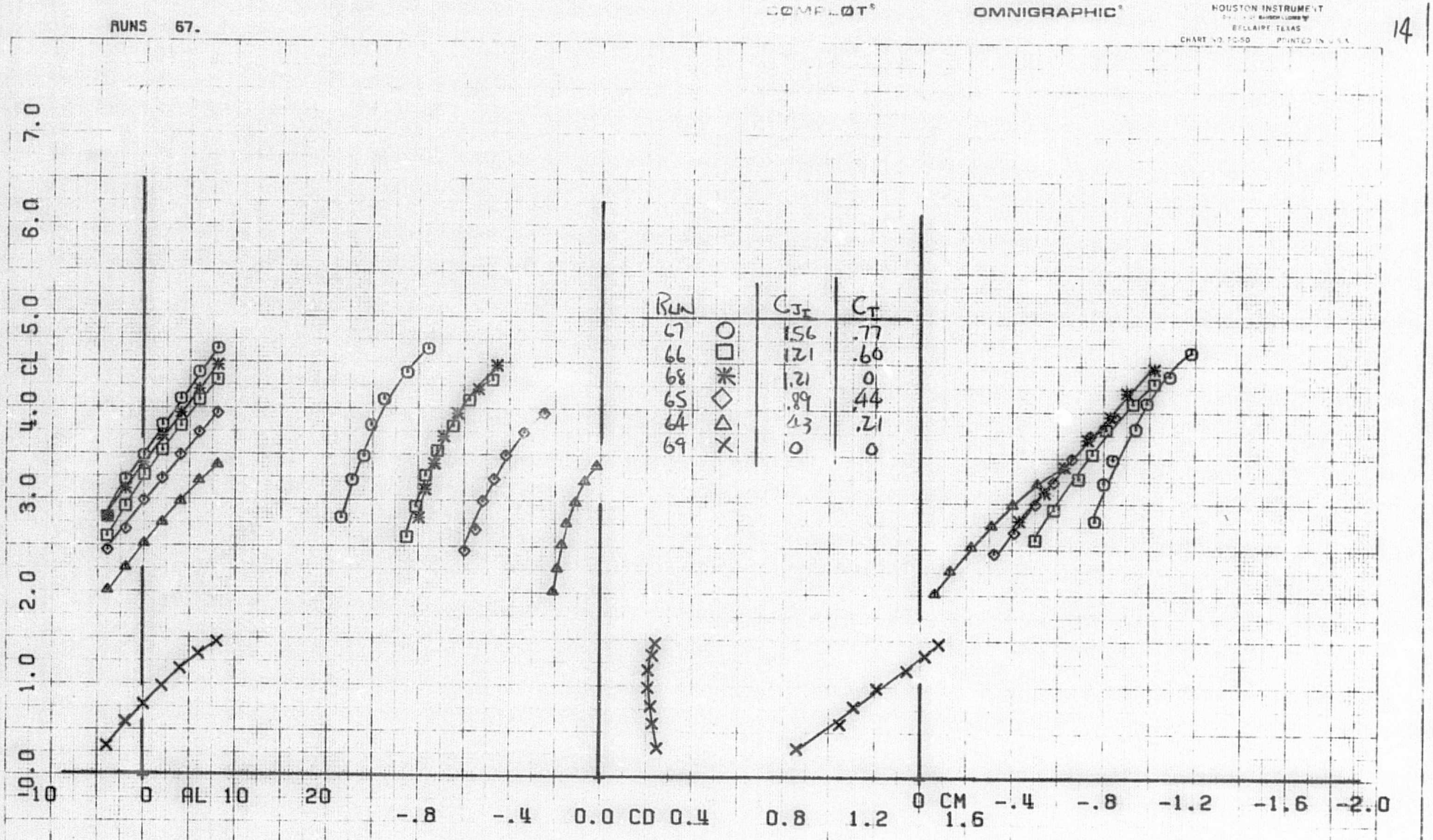

(e) T. S. = 67:33, tail on

Figure 20.- Concluded.

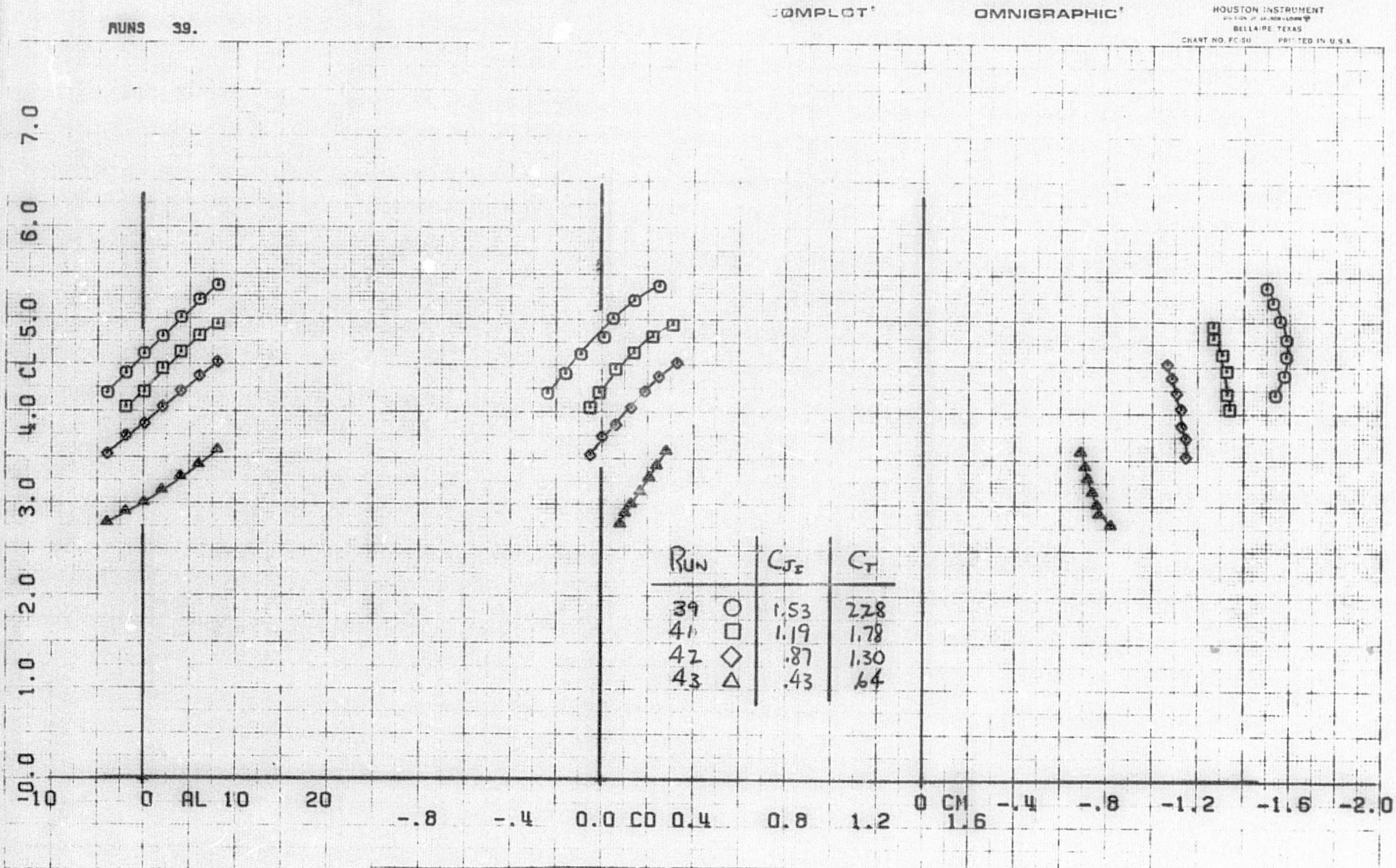

(a) T. S. = 40:60, tail off

Figure 21.- Longitudinal aerodynamic characteristics with four JT-15 underwing engines; h/c = 1.34, δ_f = 70°.

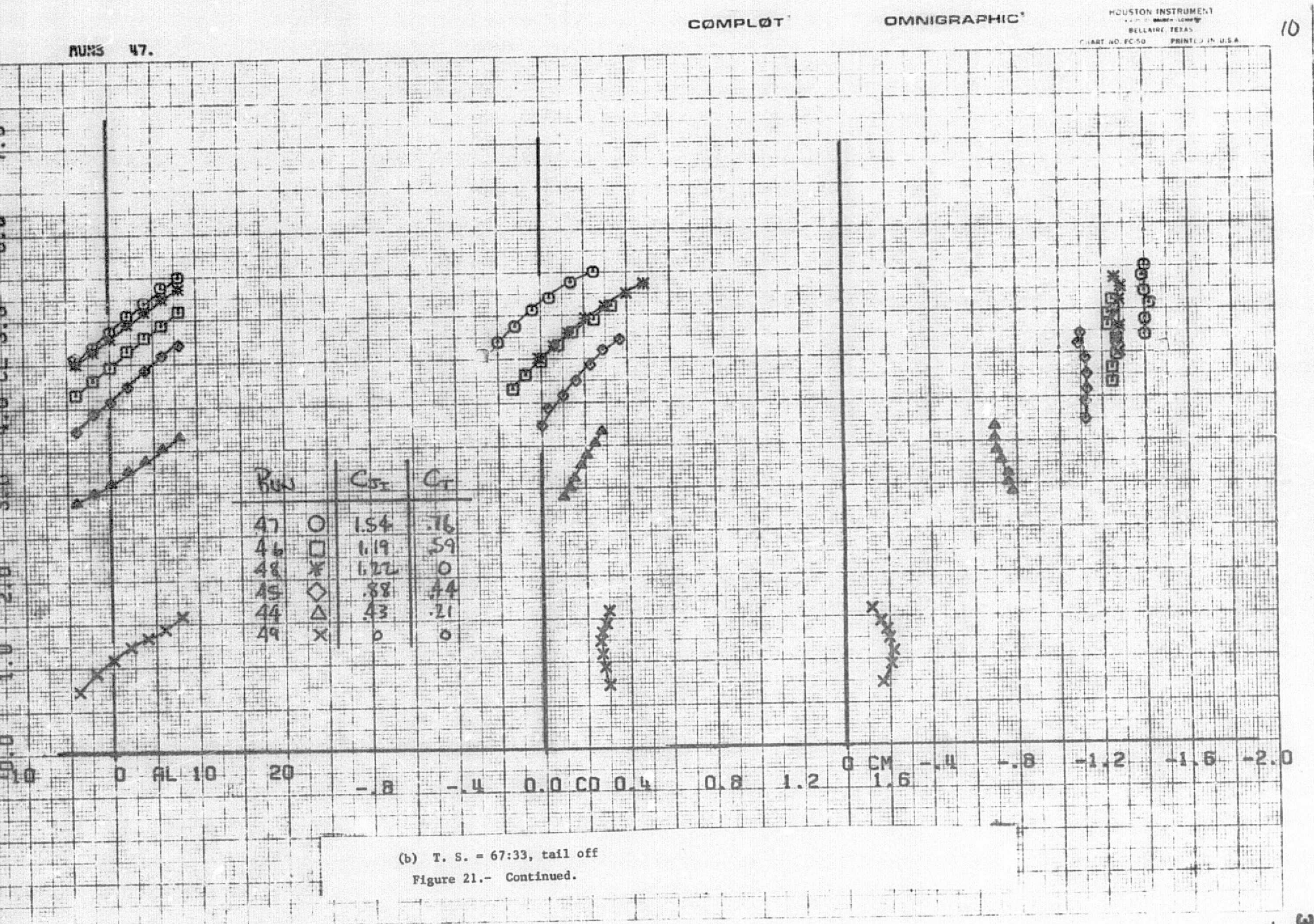

(b) T. S. = 67:33, tail off

Figure 21.- Continued.

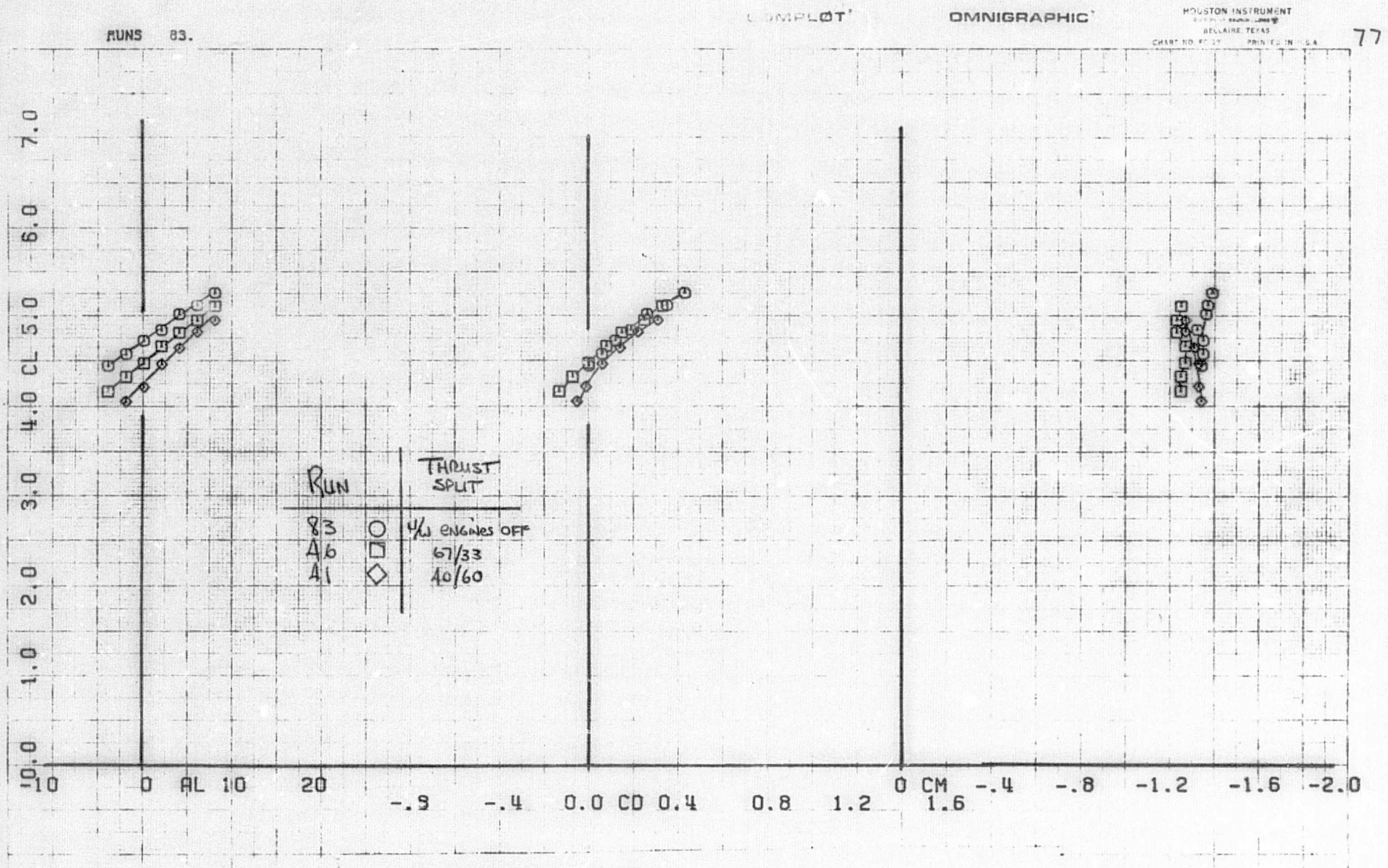

(c) Effect of T. S., tail off

Figure 21.- Continued.

21c

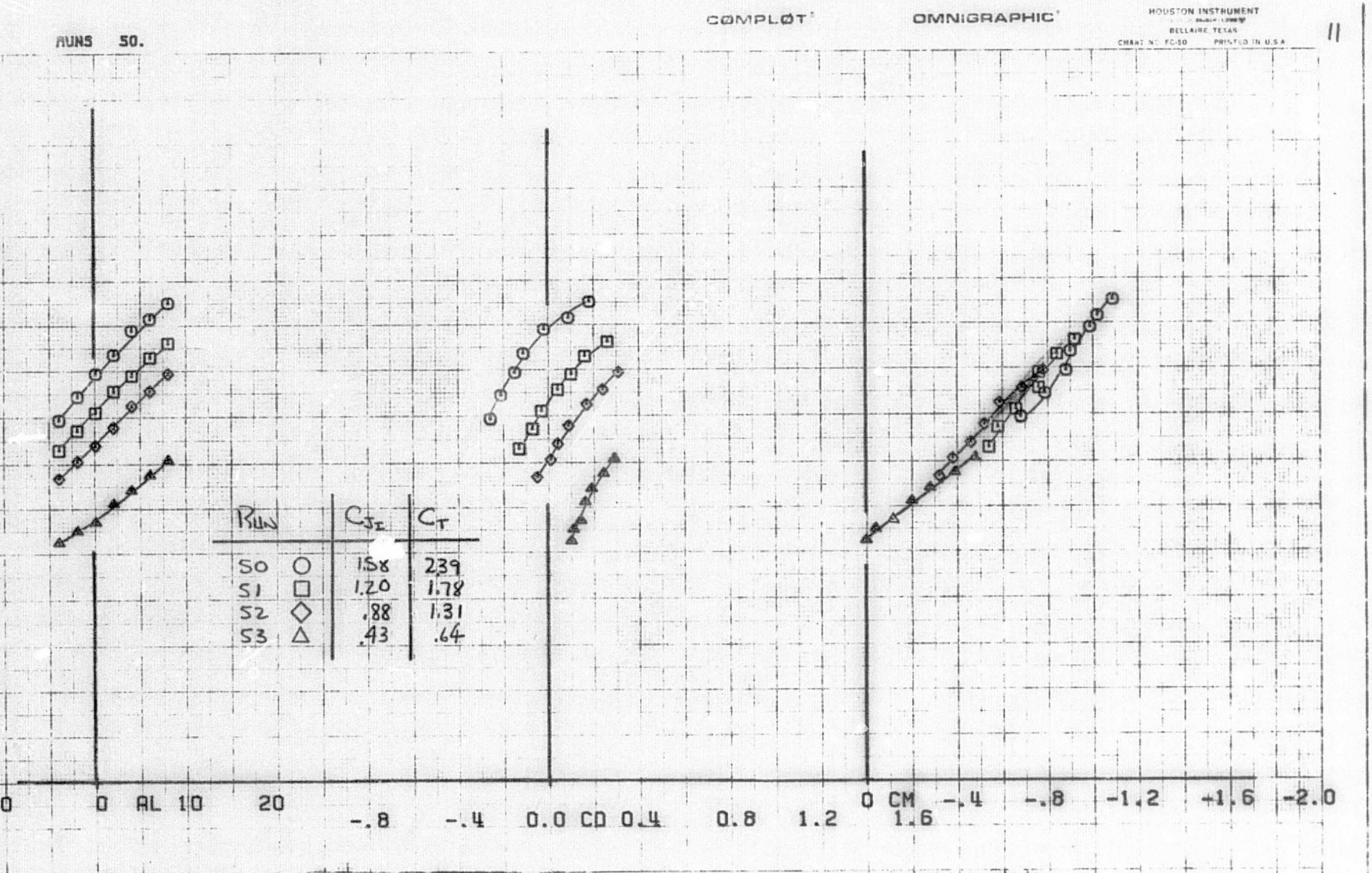

(d) T. S. = 40:60, tail on

Figure 21.- Continued.

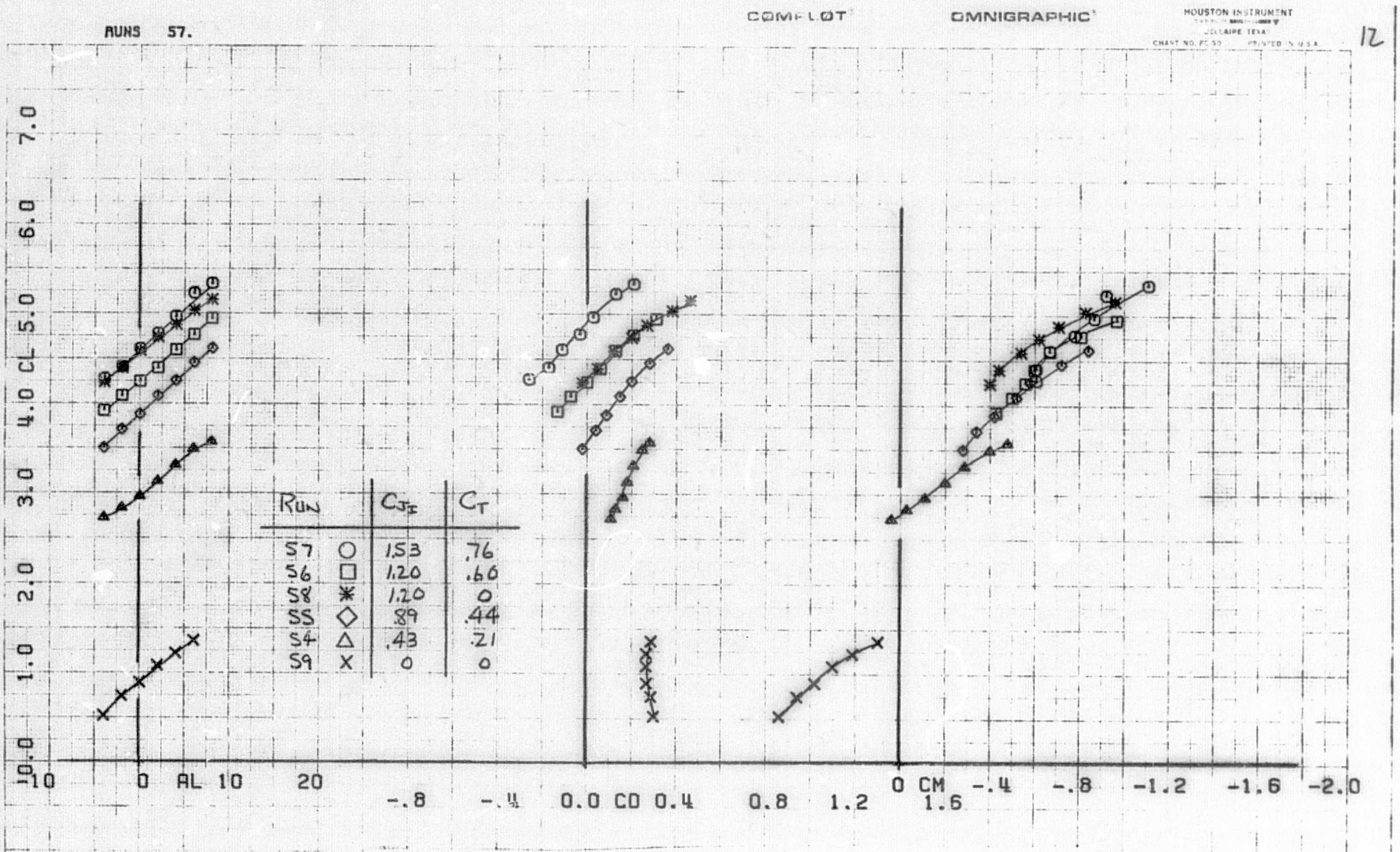

(e) T. S. = 67:33, tail on

Figure 21.- Concluded.

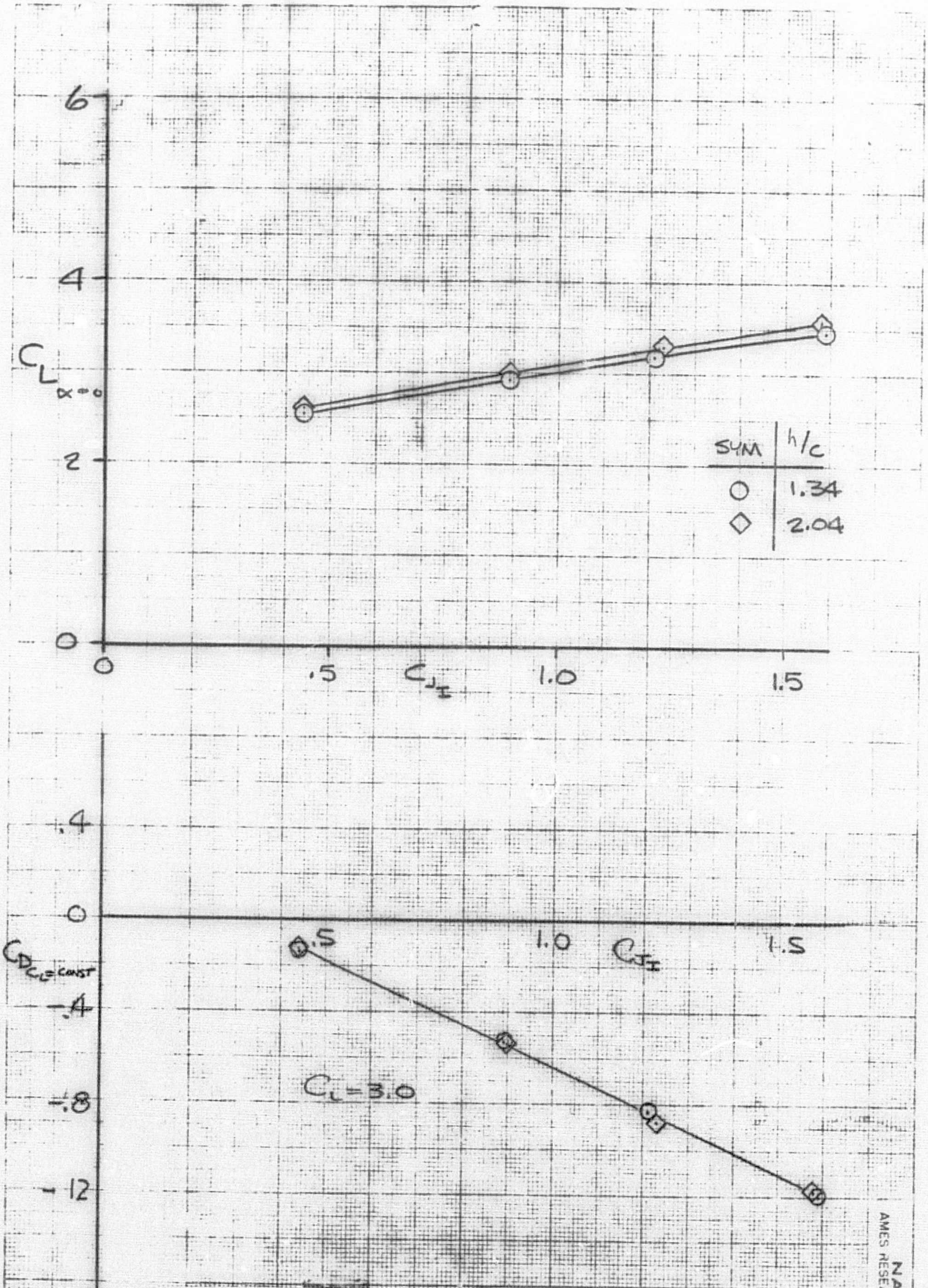

(a) Effect of h/c , T. S. = 40:60

Figure 22.- Summary of longitudinal aerodynamic characteristics with four JT-15 underwing engines; δ_f = 40°, tail off.

NASA AMES RESEARCH CENTER

27a

116

XP3

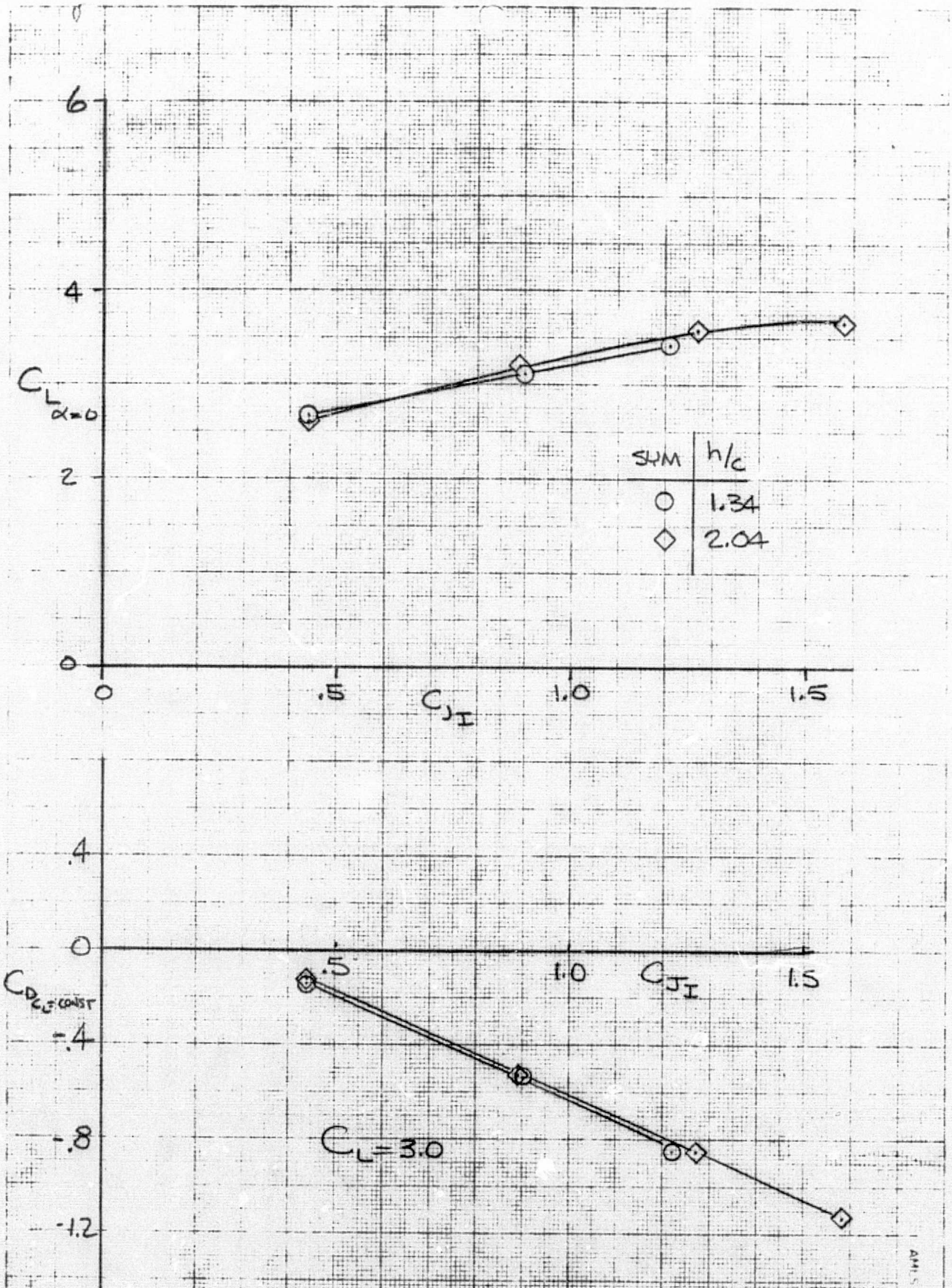

(b) Effect of h/c, T. S. = 67:33

Figure 22.- Continued.

NASA
AMES RESEARCH CENTER

922

XP4

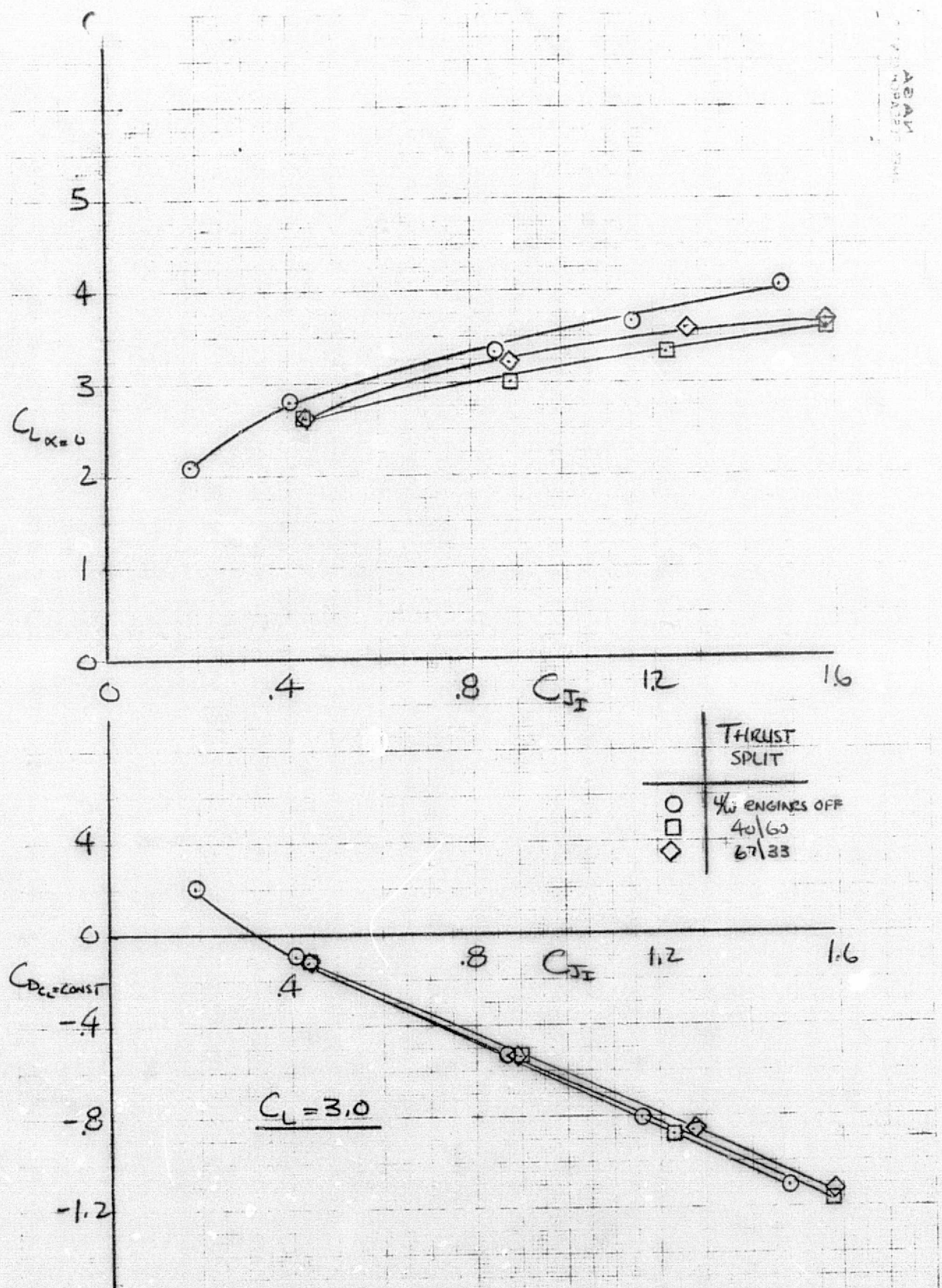

(c) Effect of T. S., h/c = 2.04

Figure 22.- Continued.

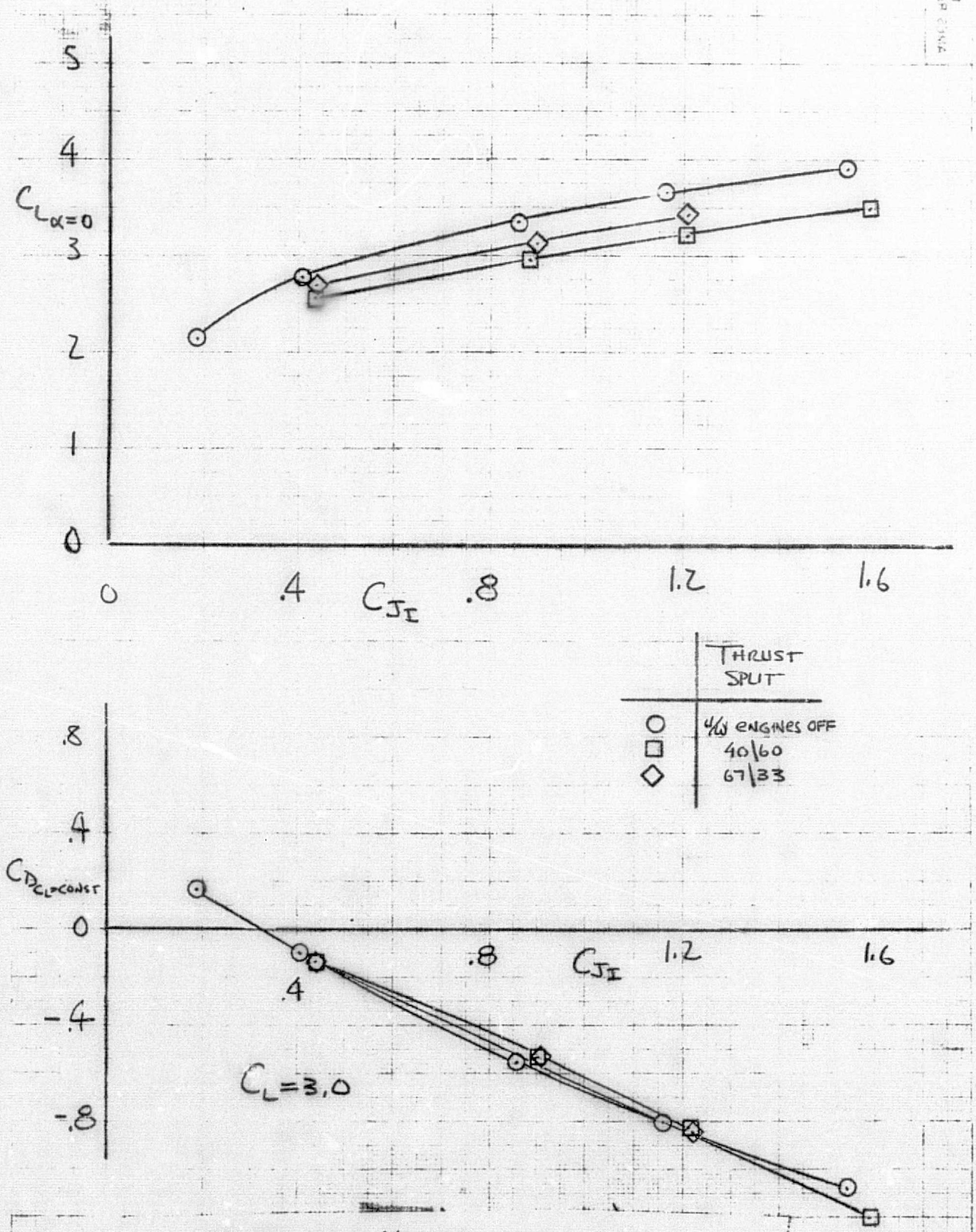

(d) Effect of T. S., h/c = 1.34

Figure 22.- Concluded.

22d

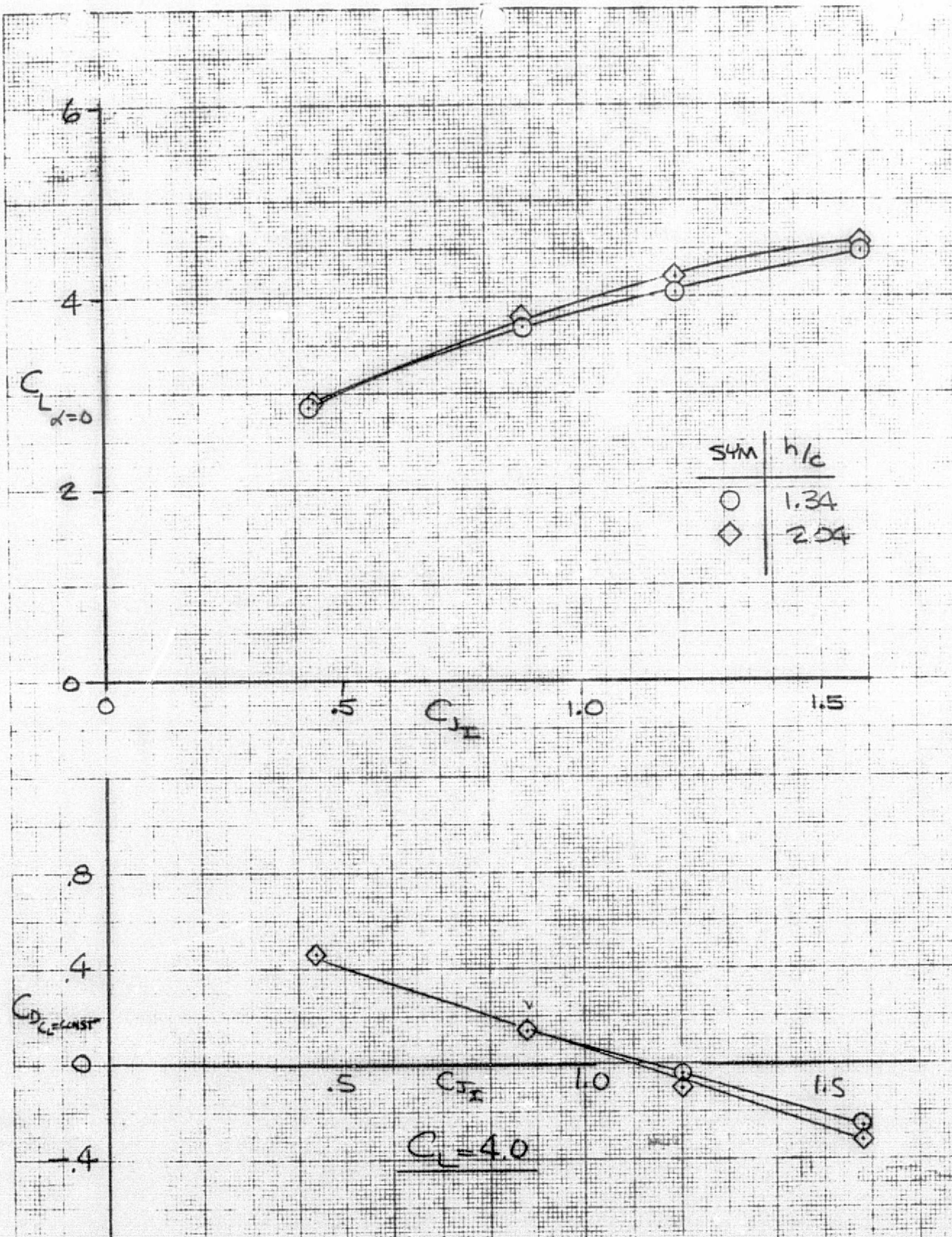

(a) Effect of h/c, T. S. = 40:60

Figure 23.- Summary of longitudinal aerodynamic characteristics with four JT-15 underwing engines; $\delta_f = 70^\circ$, tail on.

NASA AMES RESEARCH CENTER

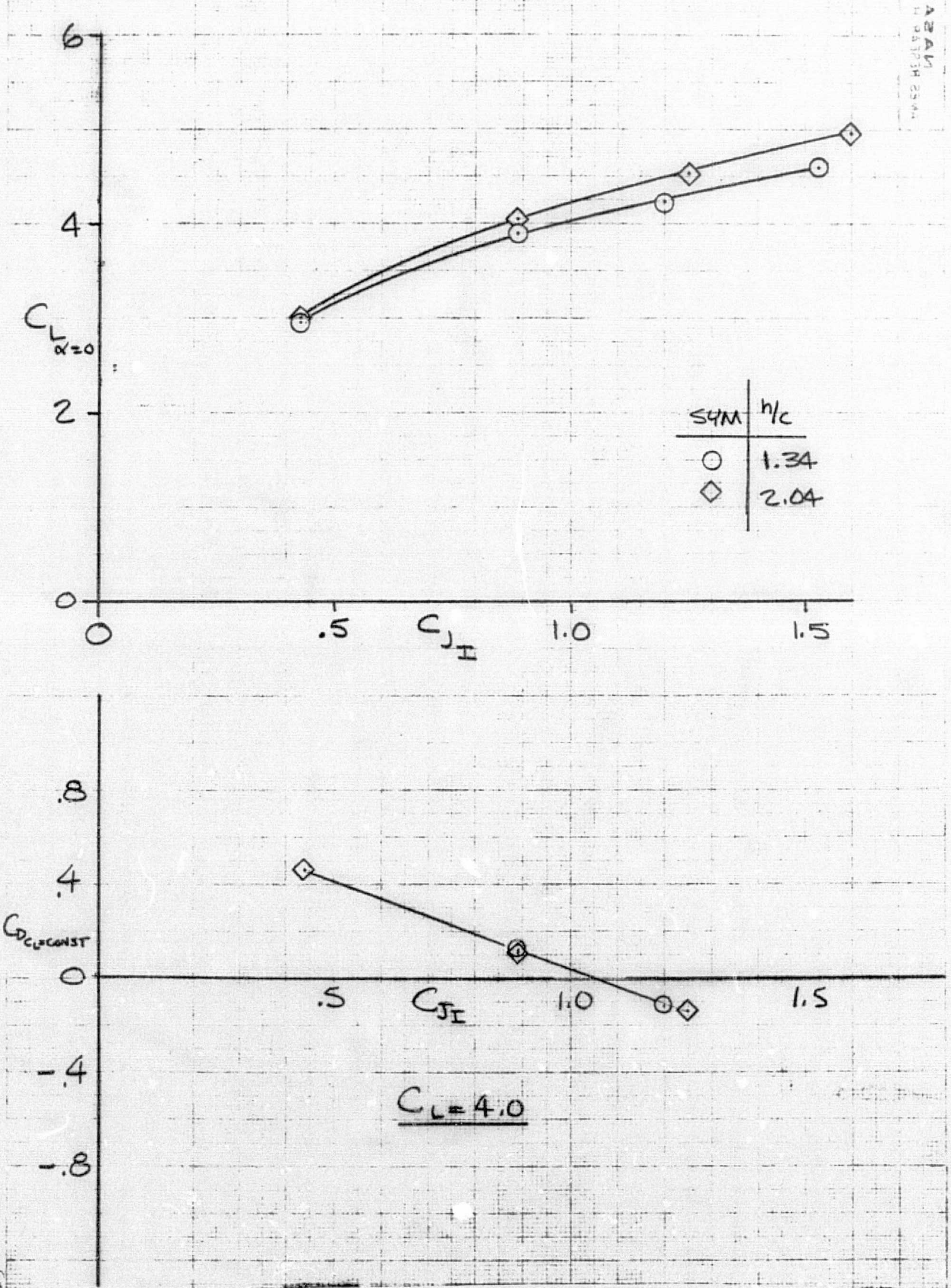

(b) Effect of h/c, T. S. = 67:33

Figure 23.- Continued.

236

XP6

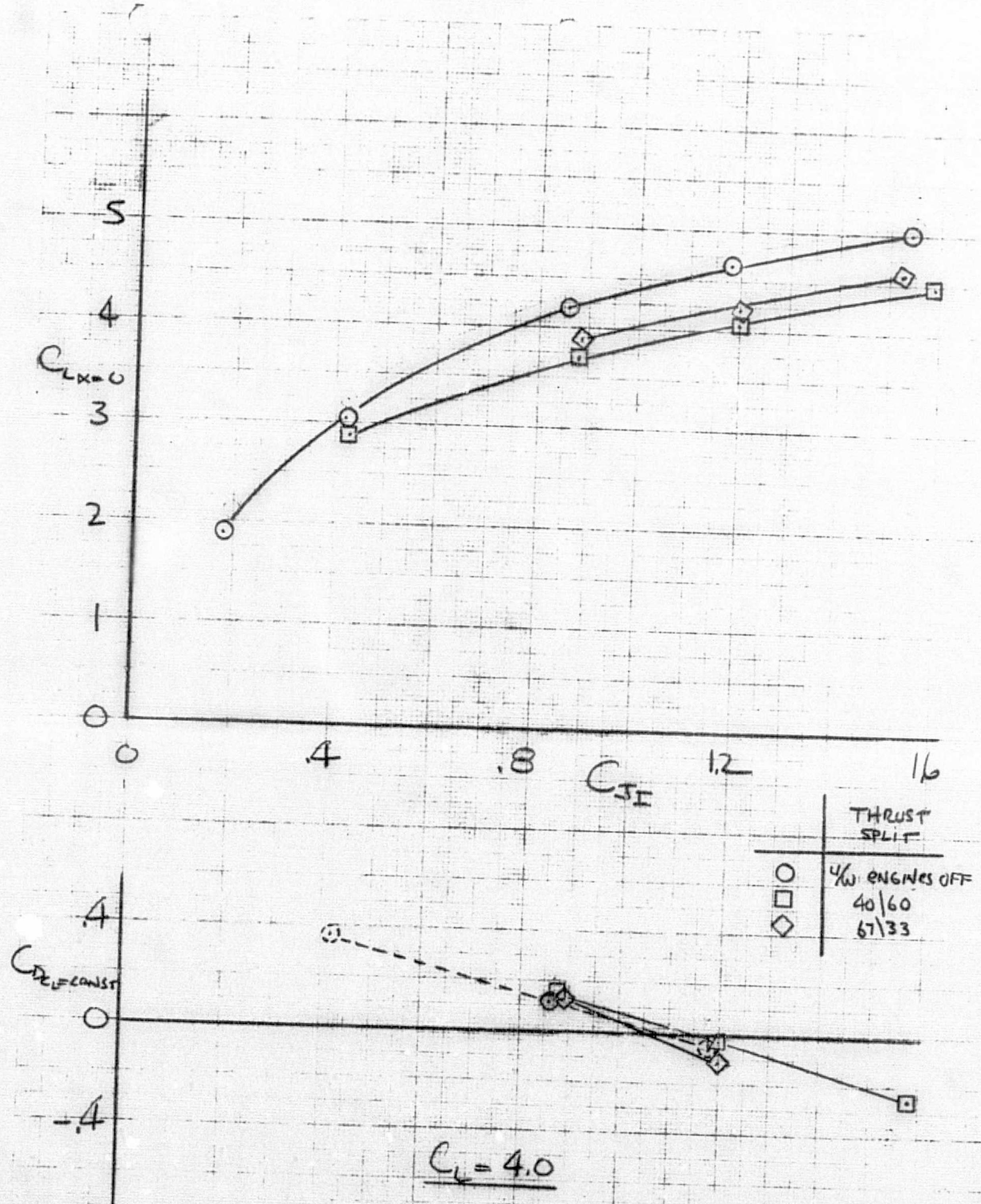

(c) Effect of T. S., h/c = 1.34

Figure 23.- Concluded.

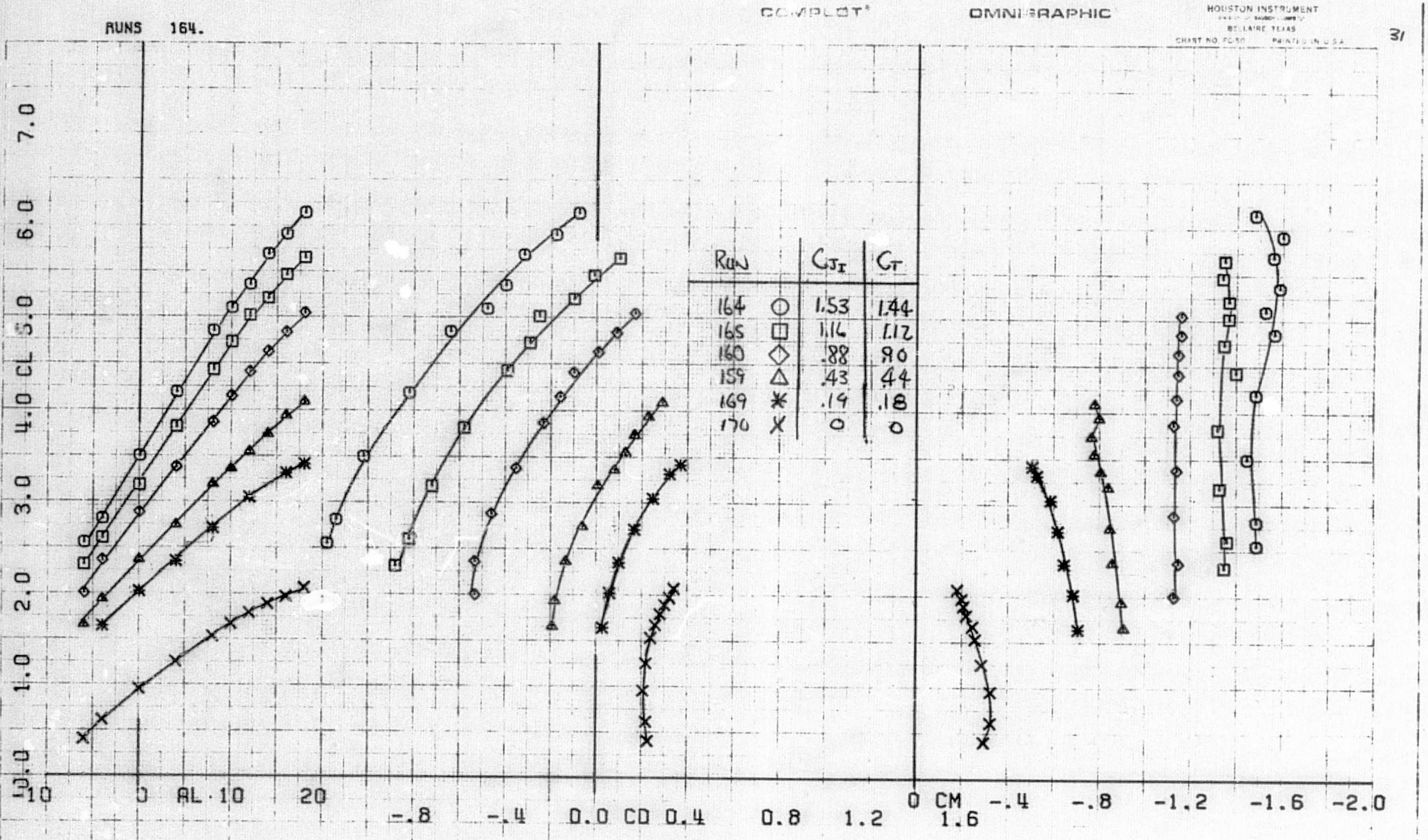

(a) T. S. = 50:50, tail off

Figure 24.- Longitudinal aerodynamic characteristics with two J-85 underwing engines; h/c = 2.04, $\delta_f = 40^\circ$, $\delta_{TH} = 0^\circ$.

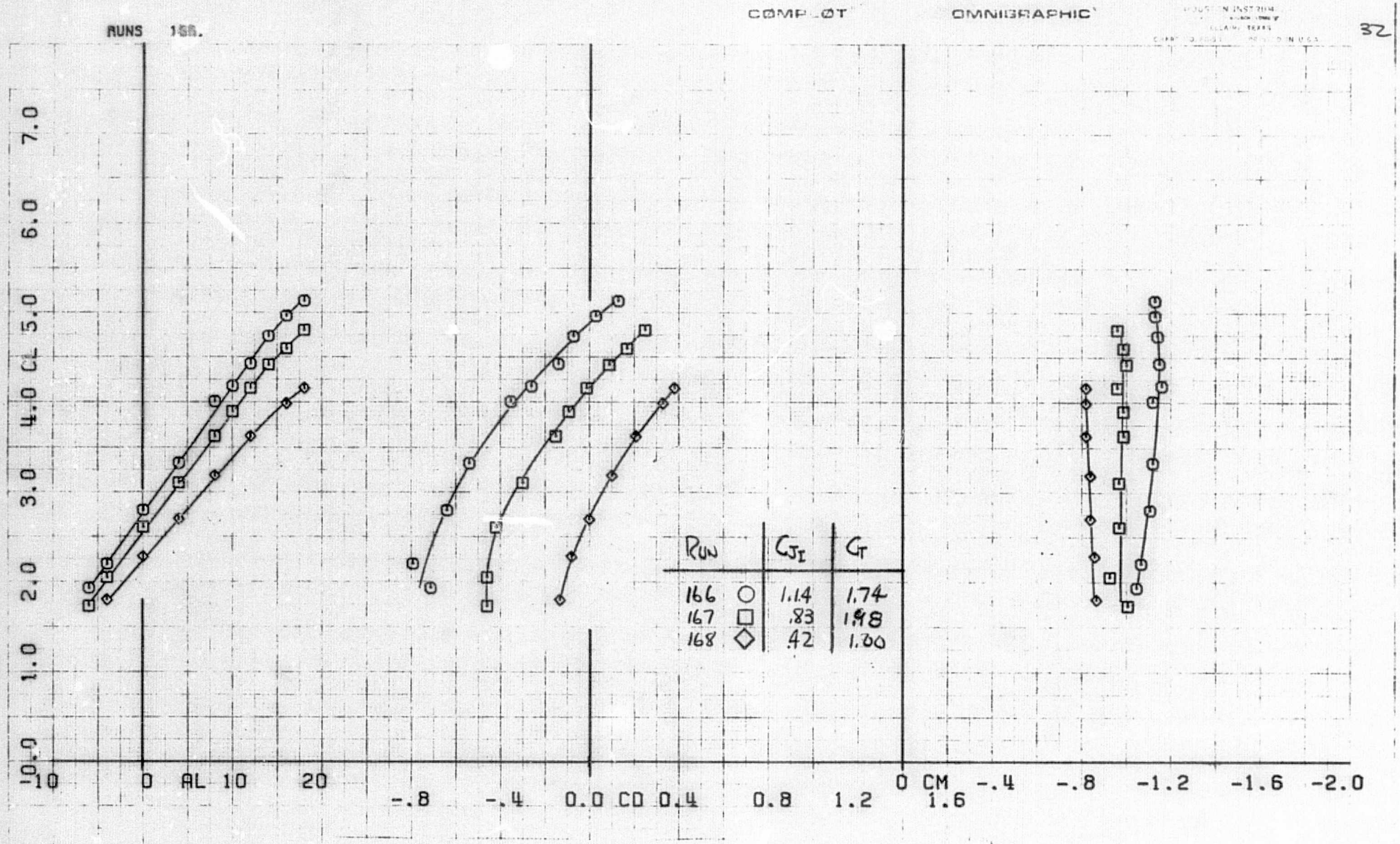

(b) T. S. = 30:70, tail off

Figure 24.- Continued.

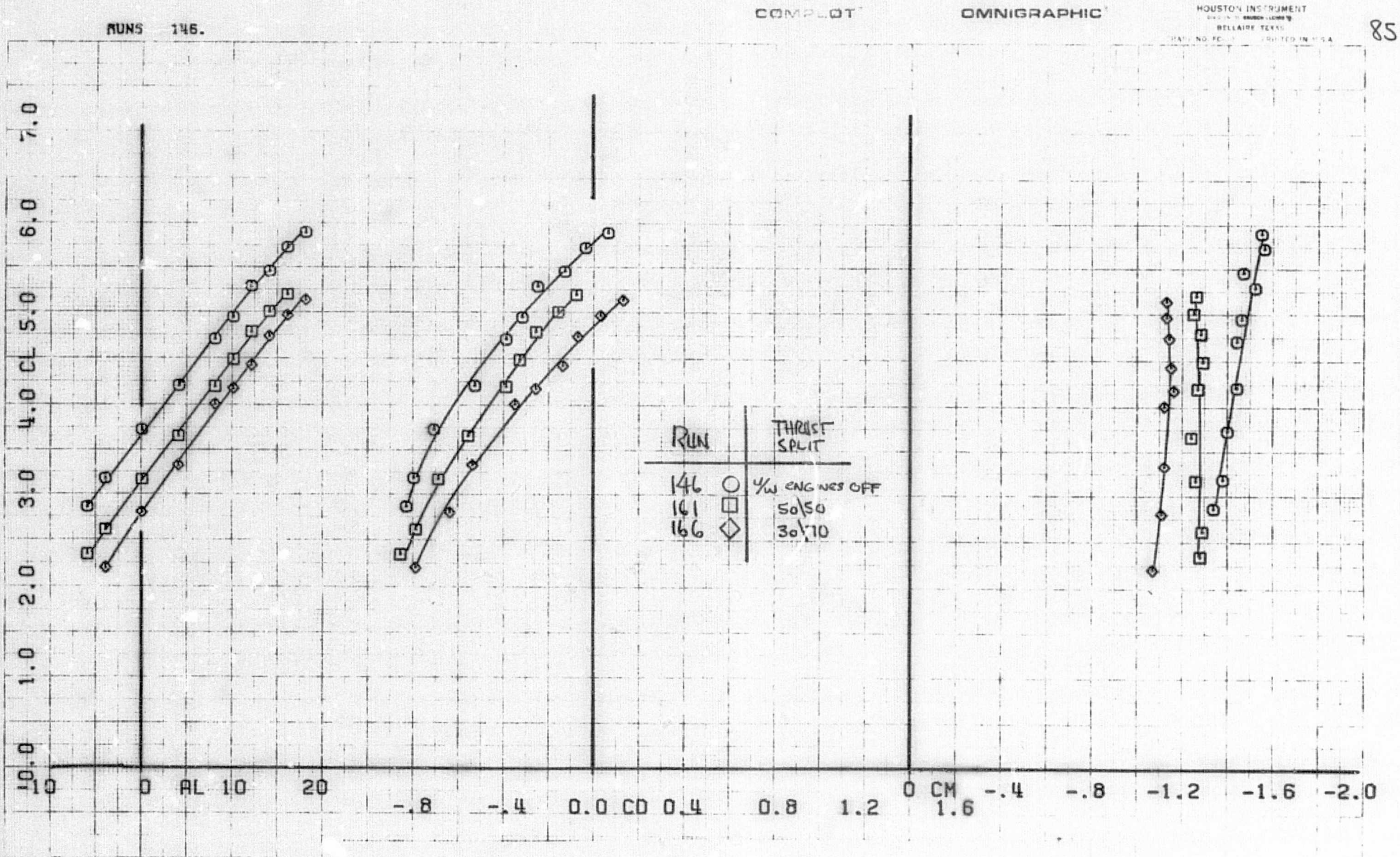

(c) Effect of T. S., $C_{J_I} = 1.2$, tail off

Figure 24.- Continued.

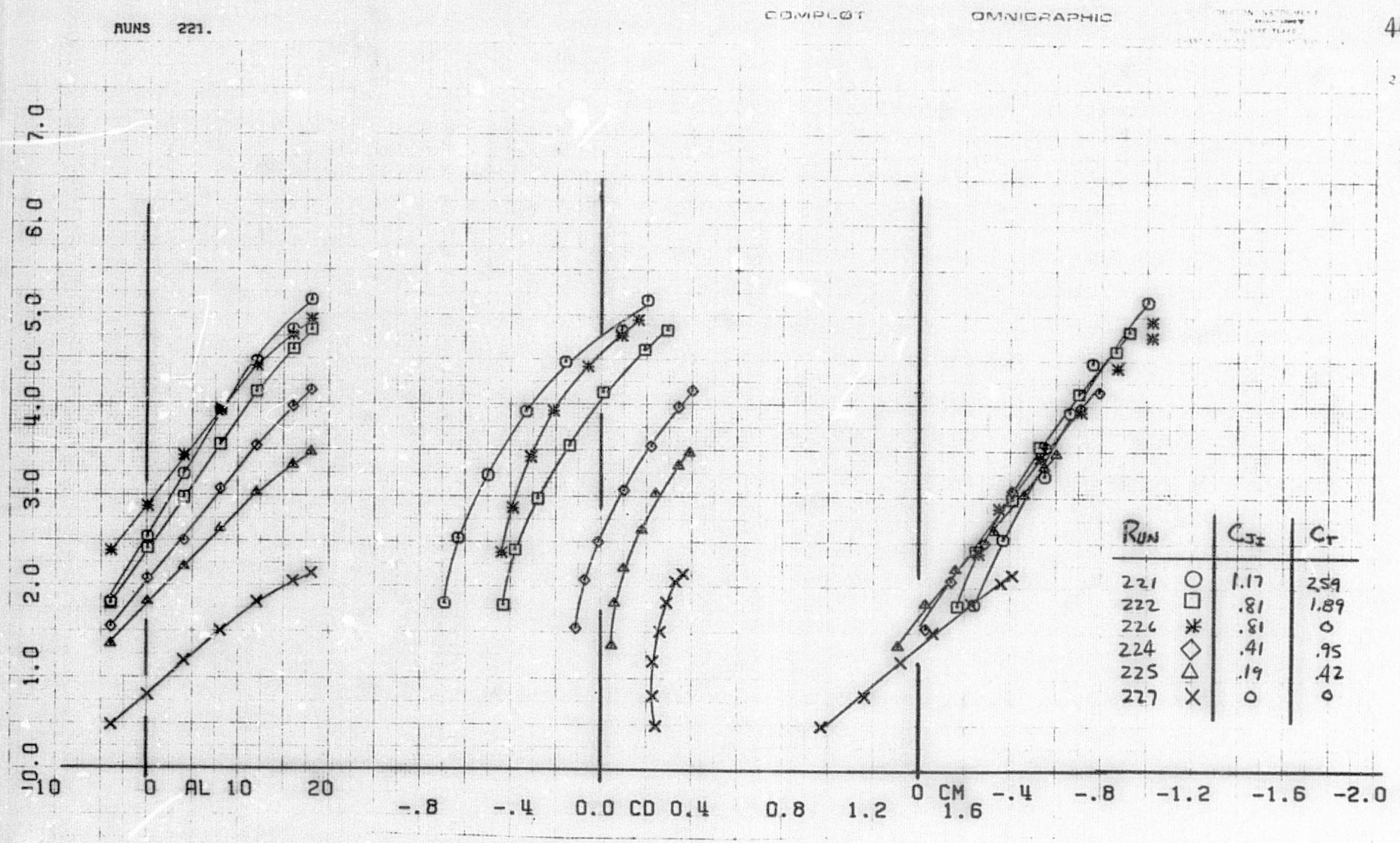

(d) T. S. = 30:70, tail on

Figure 24.- Concluded.

24d

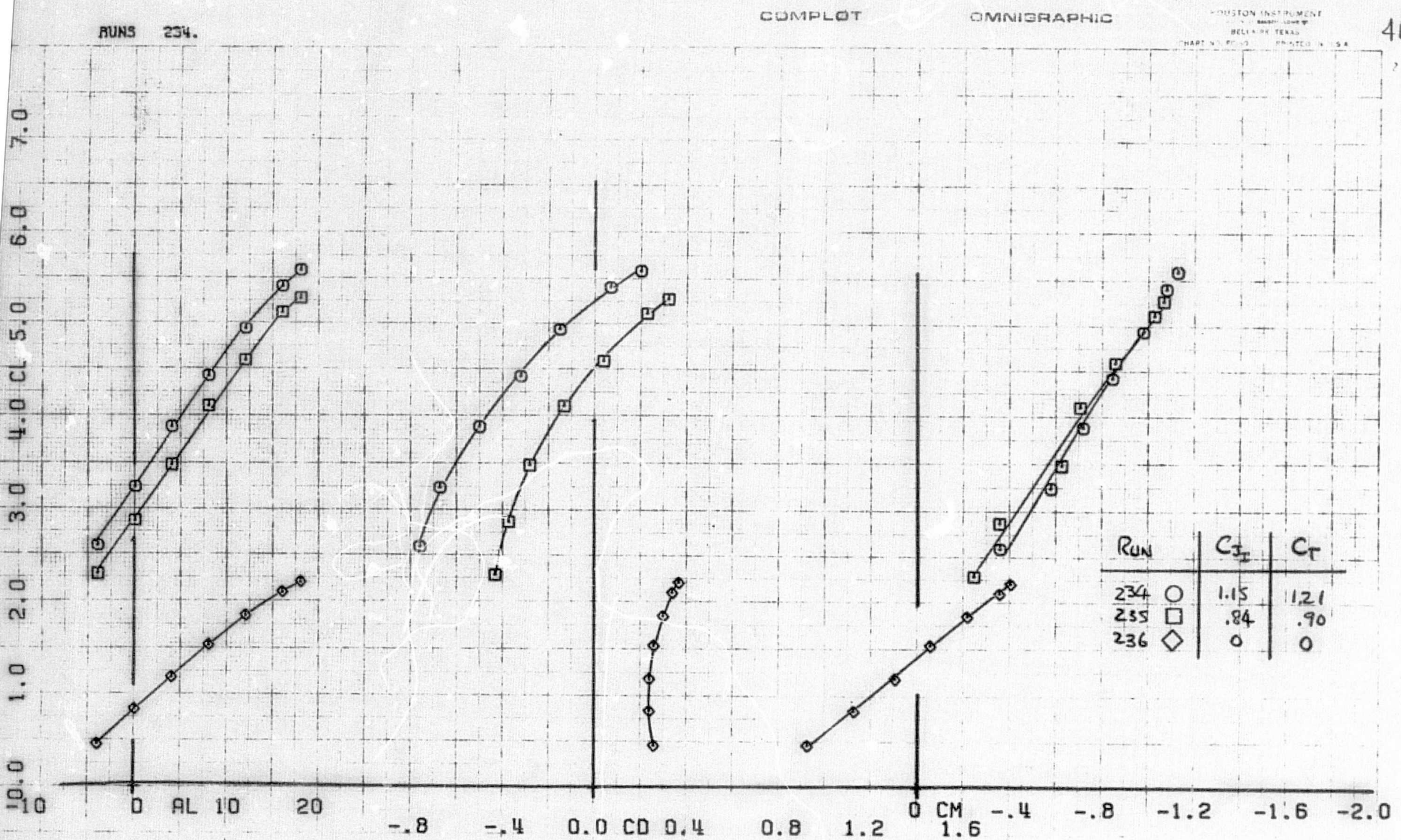

(a) T. S. = 50:50, tail off

Figure 25.- Longitudinal aerodynamic characteristics with two J-85 underwing engines; h/c = 2.04, $\delta_f = 40^{\circ}$, $\delta_{TH} = 30^{\circ}$.

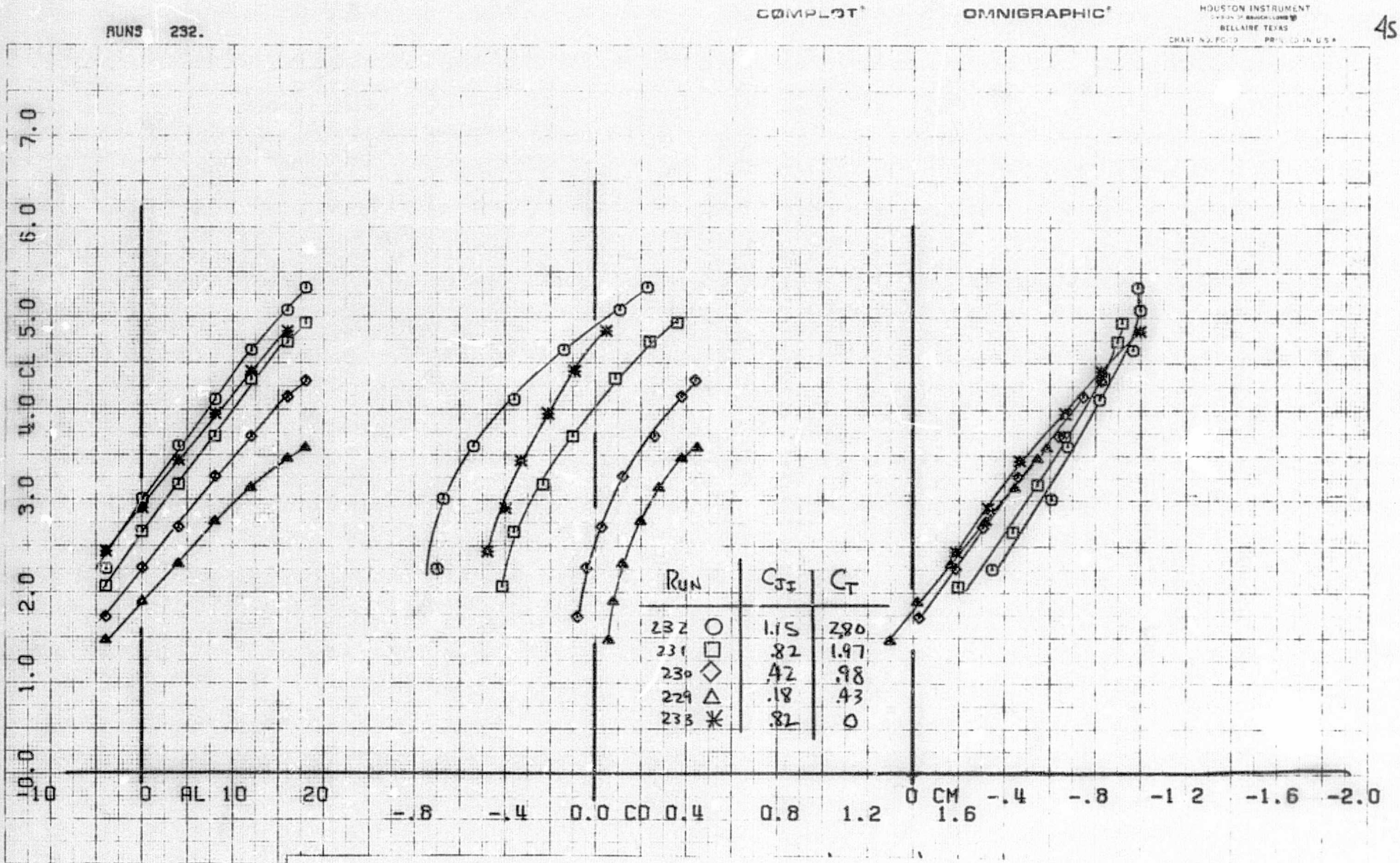

(b) T. S. = 30:70, tail on

Figure 25.- Continued.

256

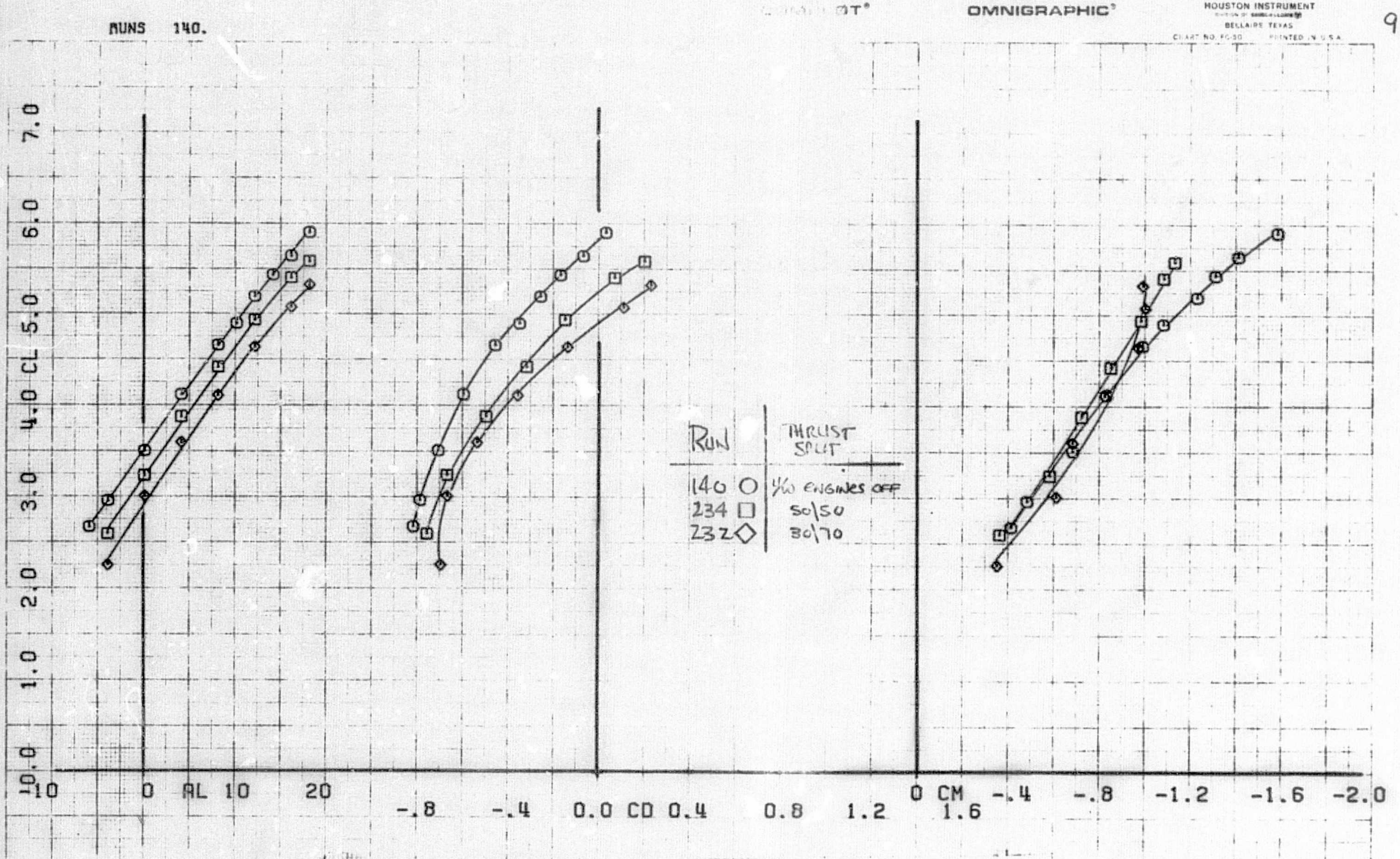

(c) Effect of T. S., C_{J_I} = 1.2, tail on.

Figure 25.- Concluded.

25c 100

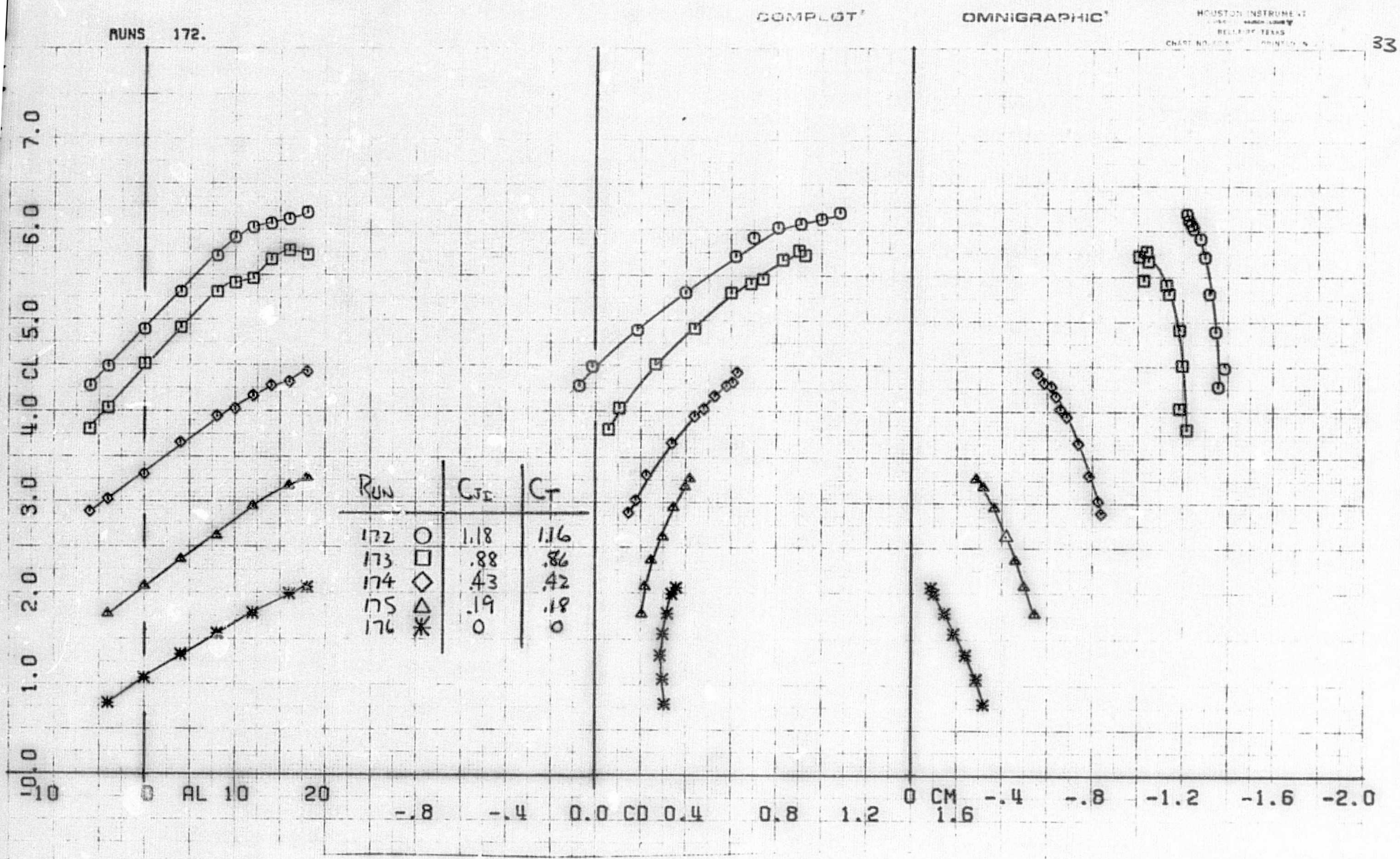

(a) T. S. = 50:50 tail off

Figure 26.- Longitudinal aerodynamic characteristics with two J-85 underwing engines; h/c = 2.04, $\delta_f = 70^o$, $\delta_{TH} = 60^o$.

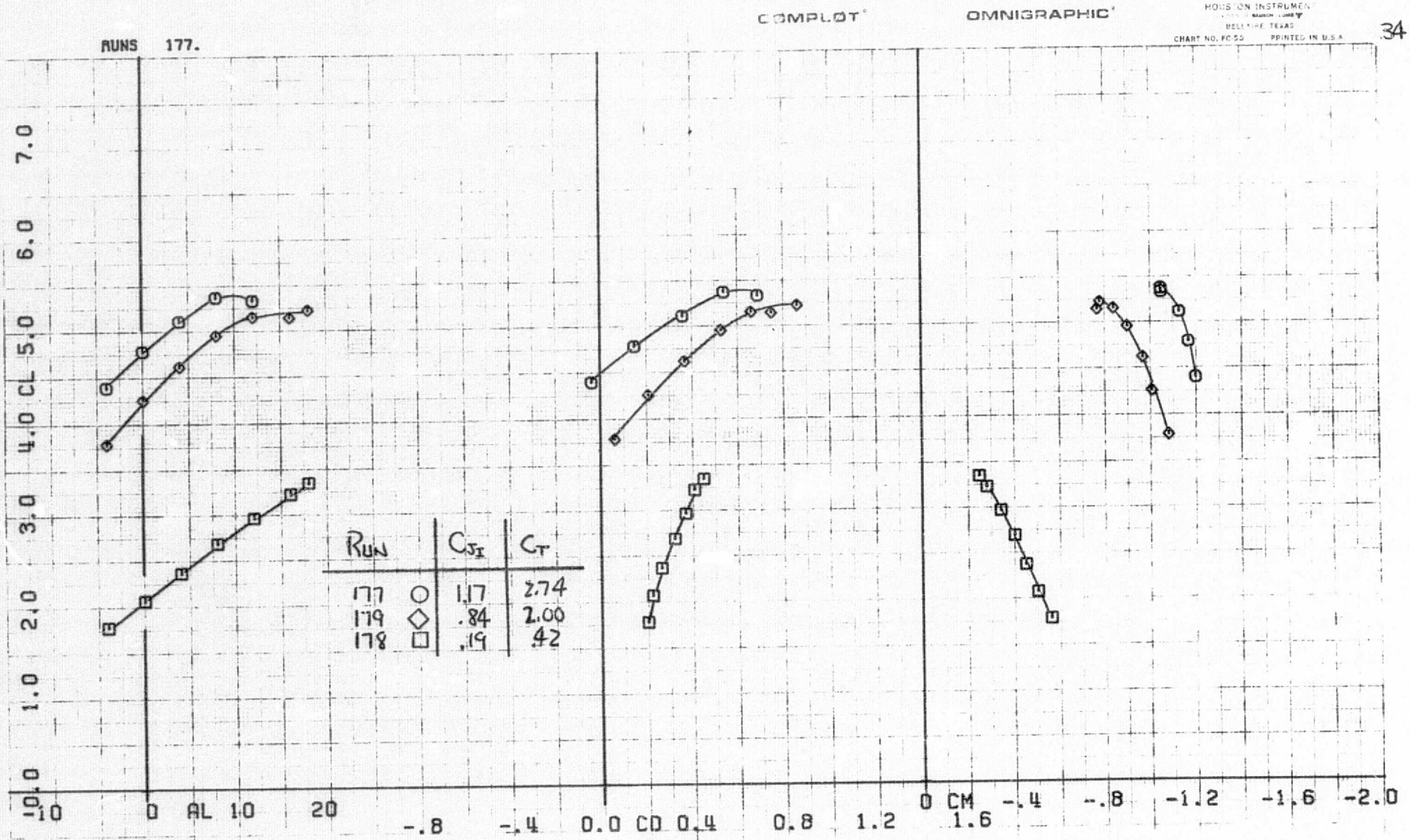

(b) T. S. = 30:70, tail off

Figure 26.- Continued.

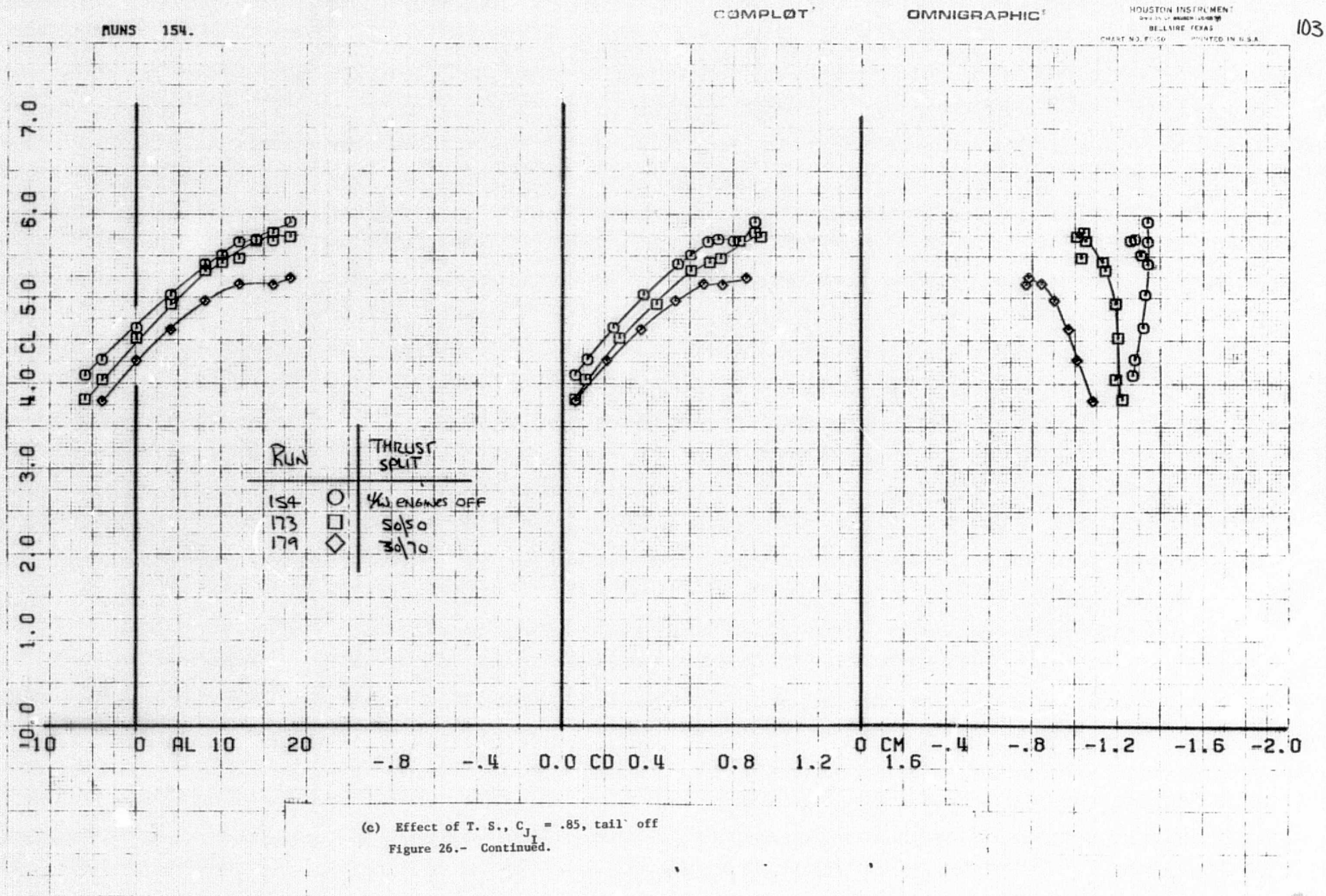

(c) Effect of T. S., C_{J_I} = .85, tail off

Figure 26.- Continued.

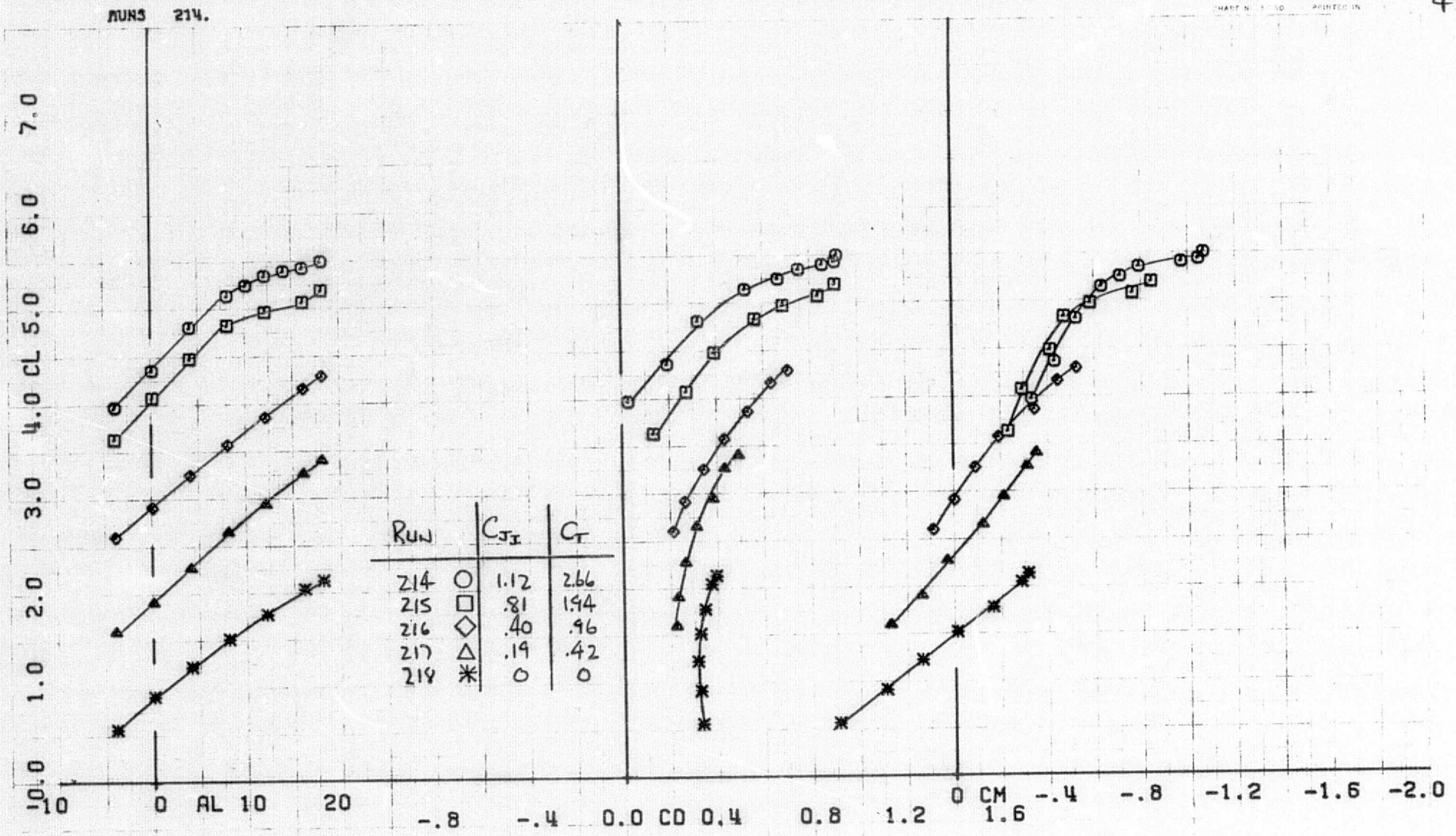

(d) T. S. = 30:70, tail on

Figure 26.- Concluded.

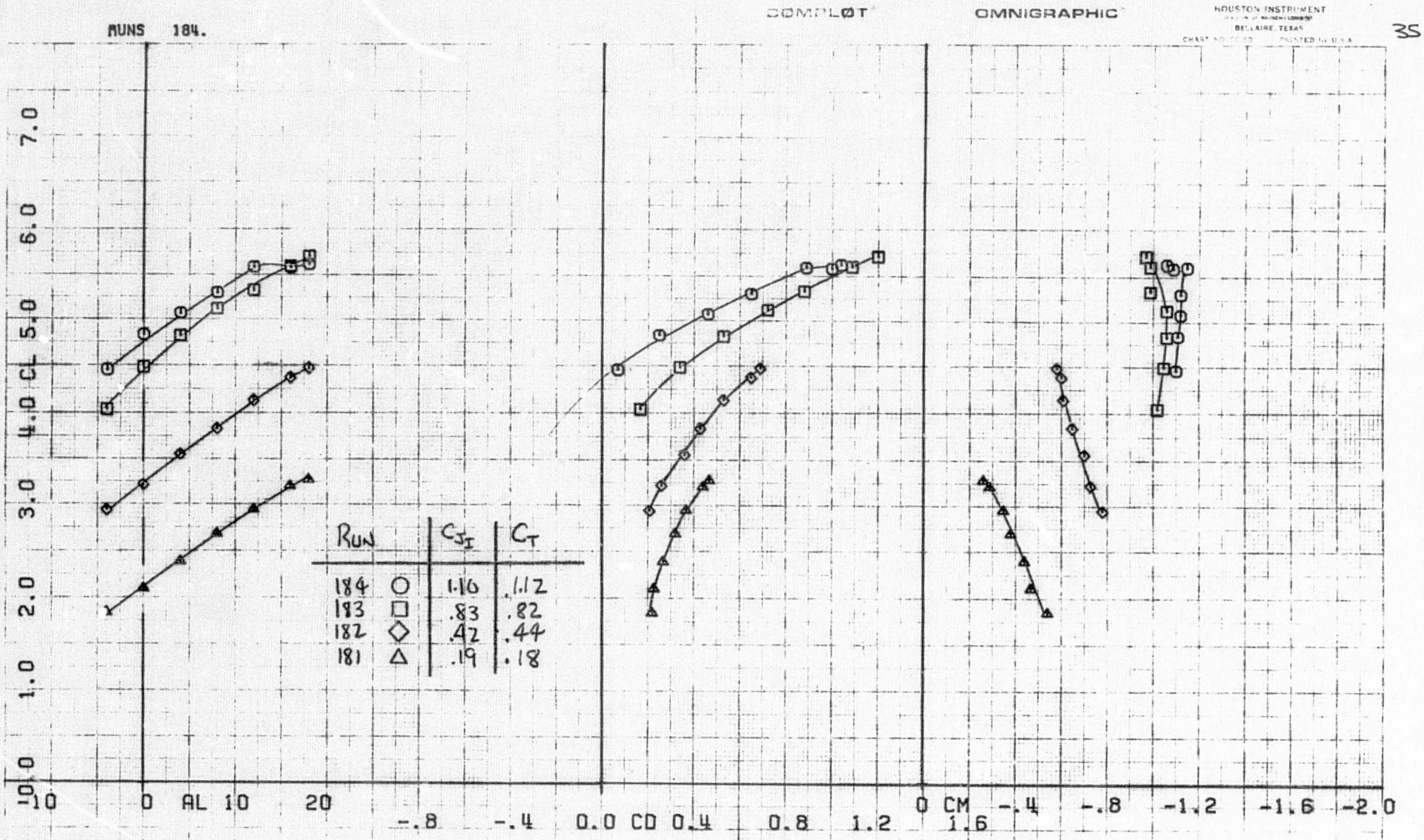

(a) T. S. = 50:50, tail off

Figure 27.- Longitudinal aerodynamic characteristics with two J-85 underwing engines; $h/c = 2.04$, $\delta_f = 70^{\circ}$, $\delta_{TH} = 90^{\circ}$.

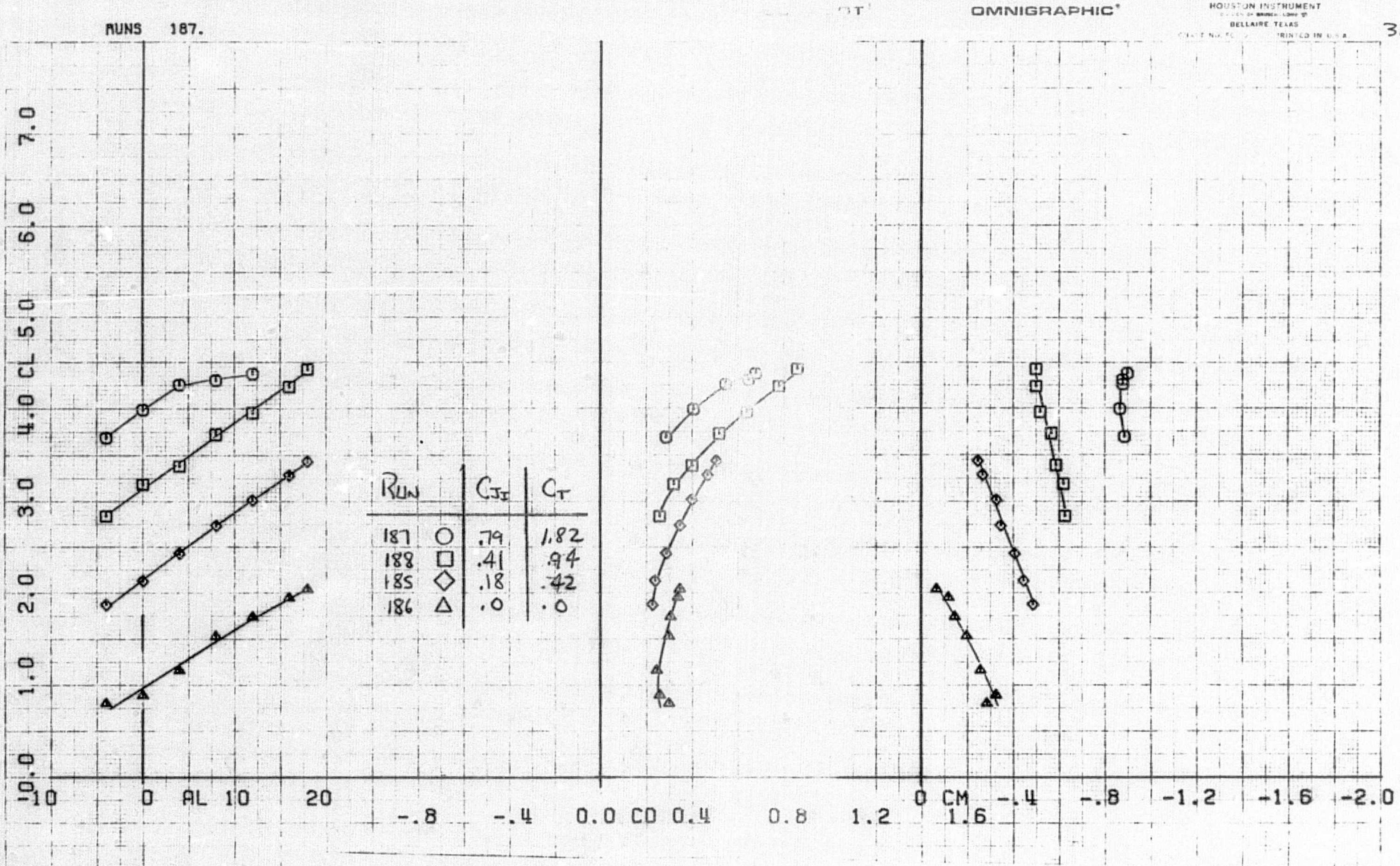

(b) T. S. = 30:70, tail off

Figure 27.- Continued.

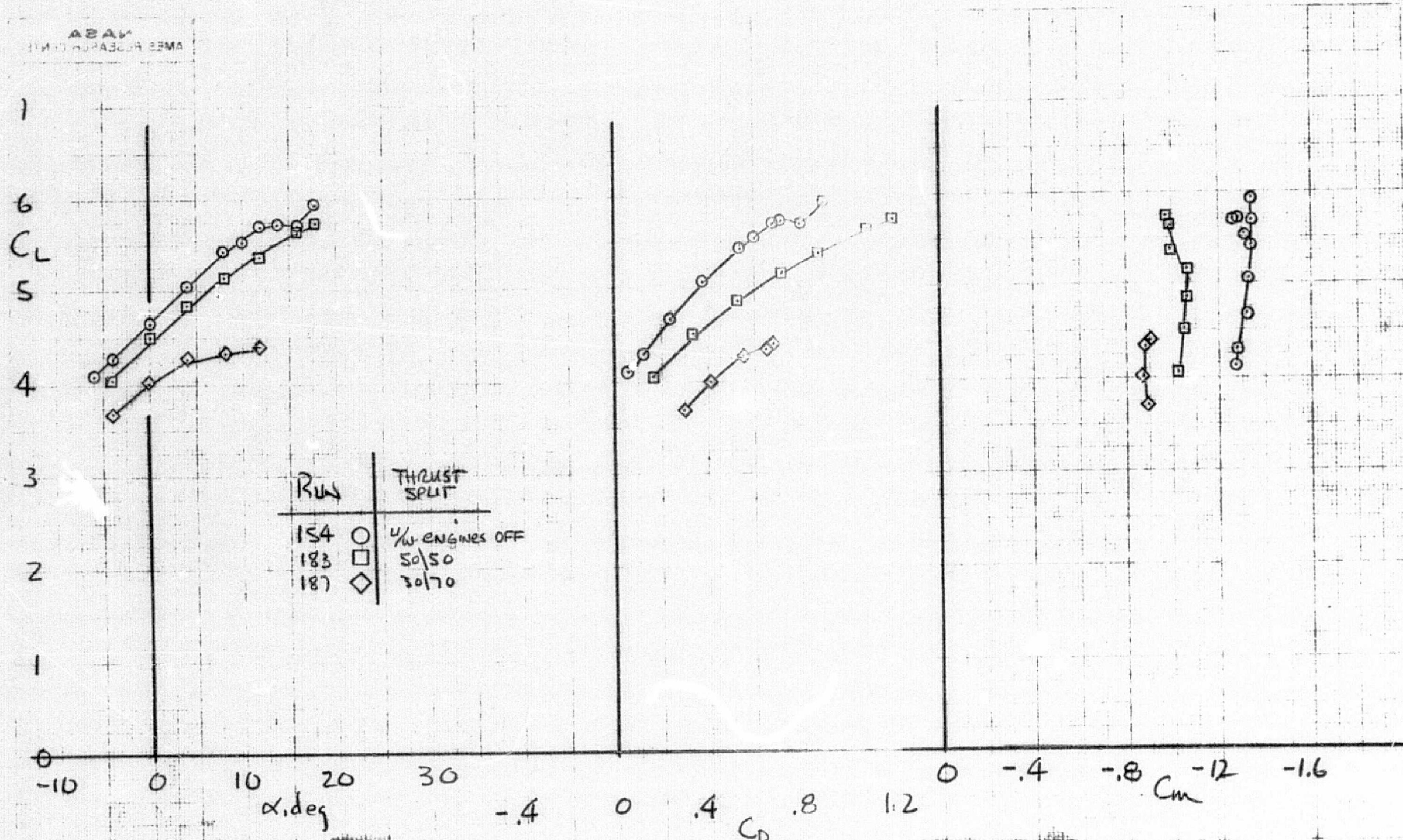

(c) Effect of T. S., tail off

Figure 27.- Continued.

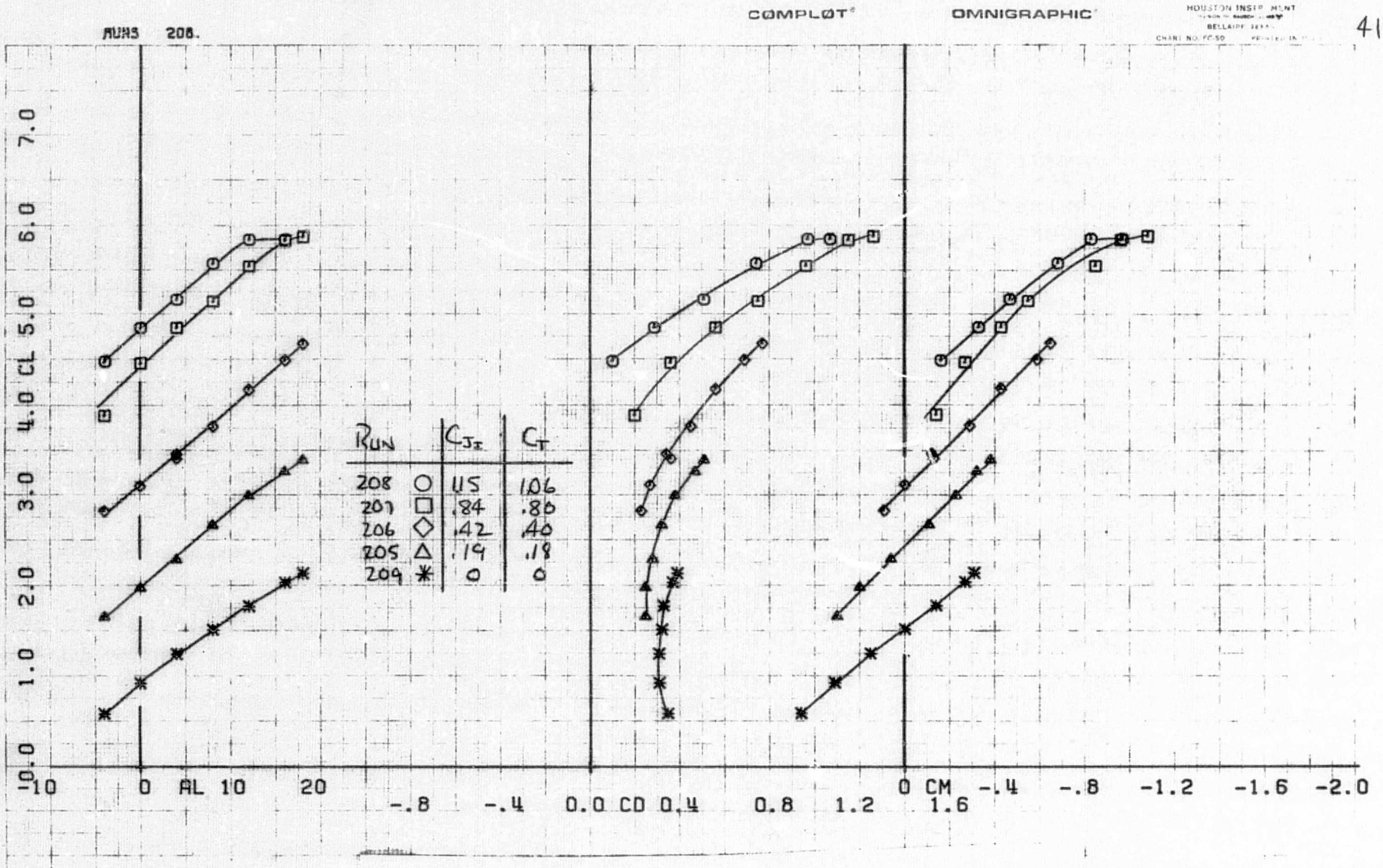

(d) T. S. = 50:50, tail on

Figure 27.- Continued.

27d

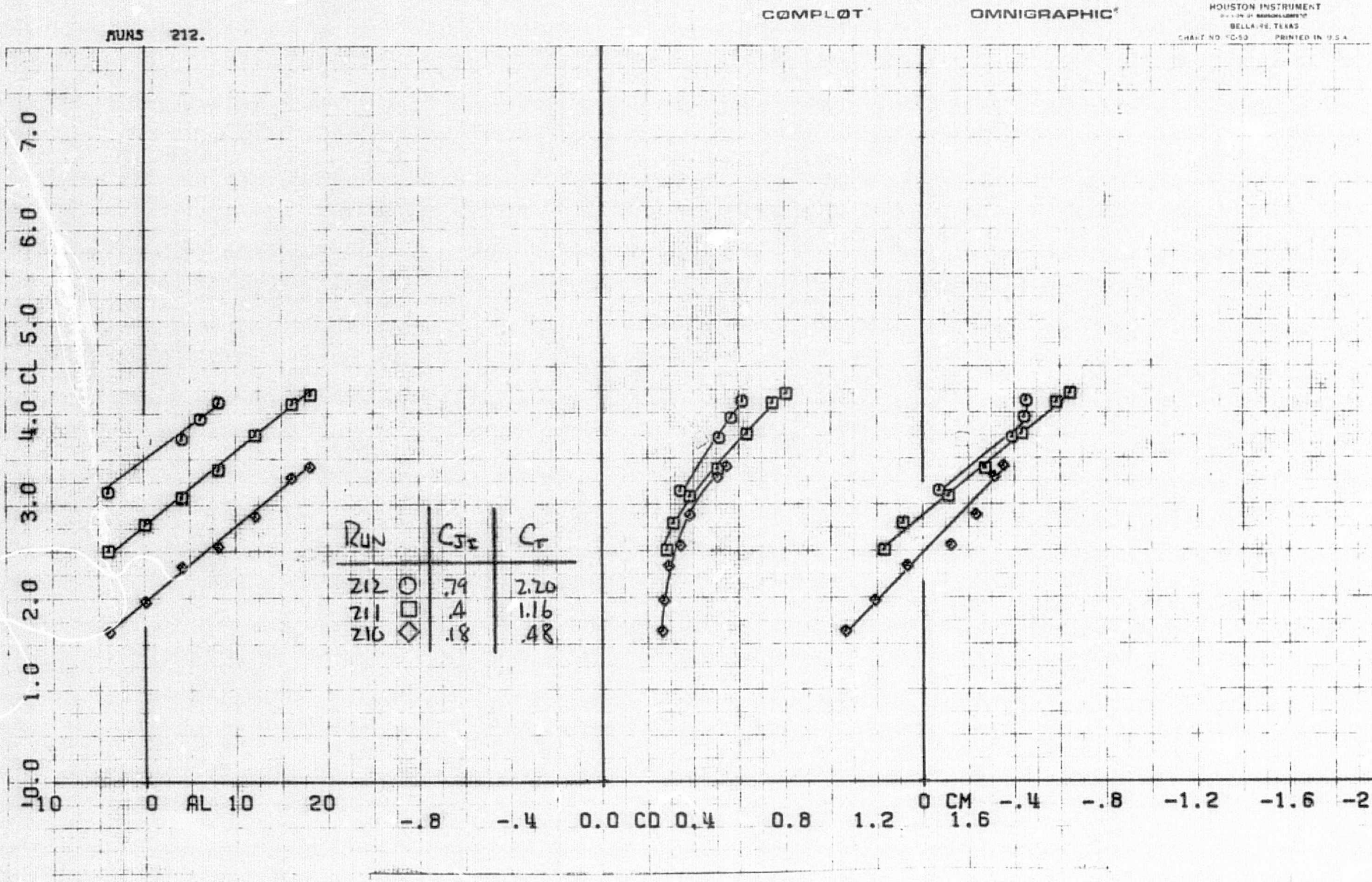

(e) T. S. = 30:70, tail on

Figure 27.- Concluded.

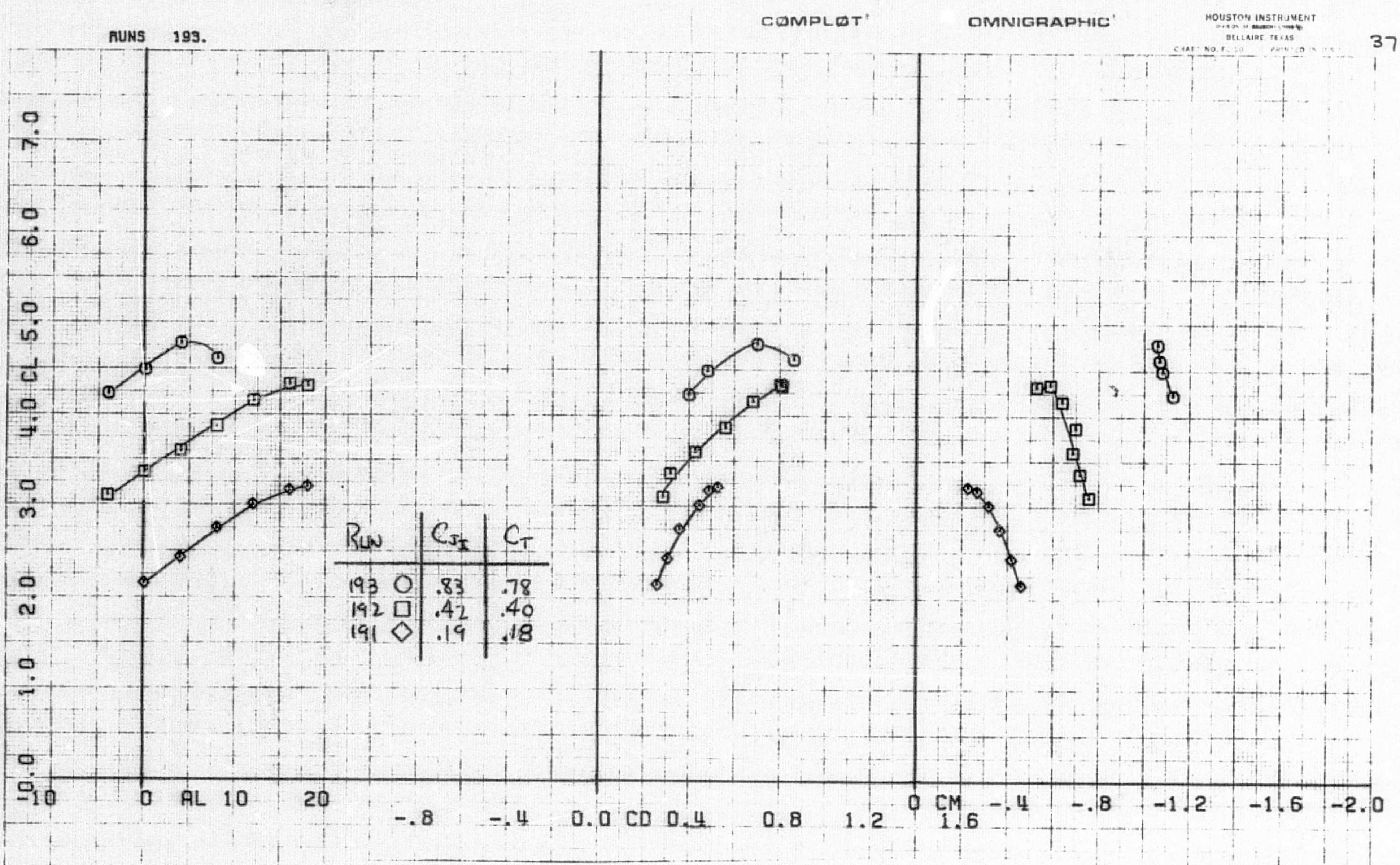

(a) T. S. = 50:50, tail off

Figure 28.- Longitudinal aerodynamic characteristics with two J-85 underwing engines; $h/c = 2.04$, $\delta_f = 70^\circ$, $\delta_{TH} = 120^\circ$.

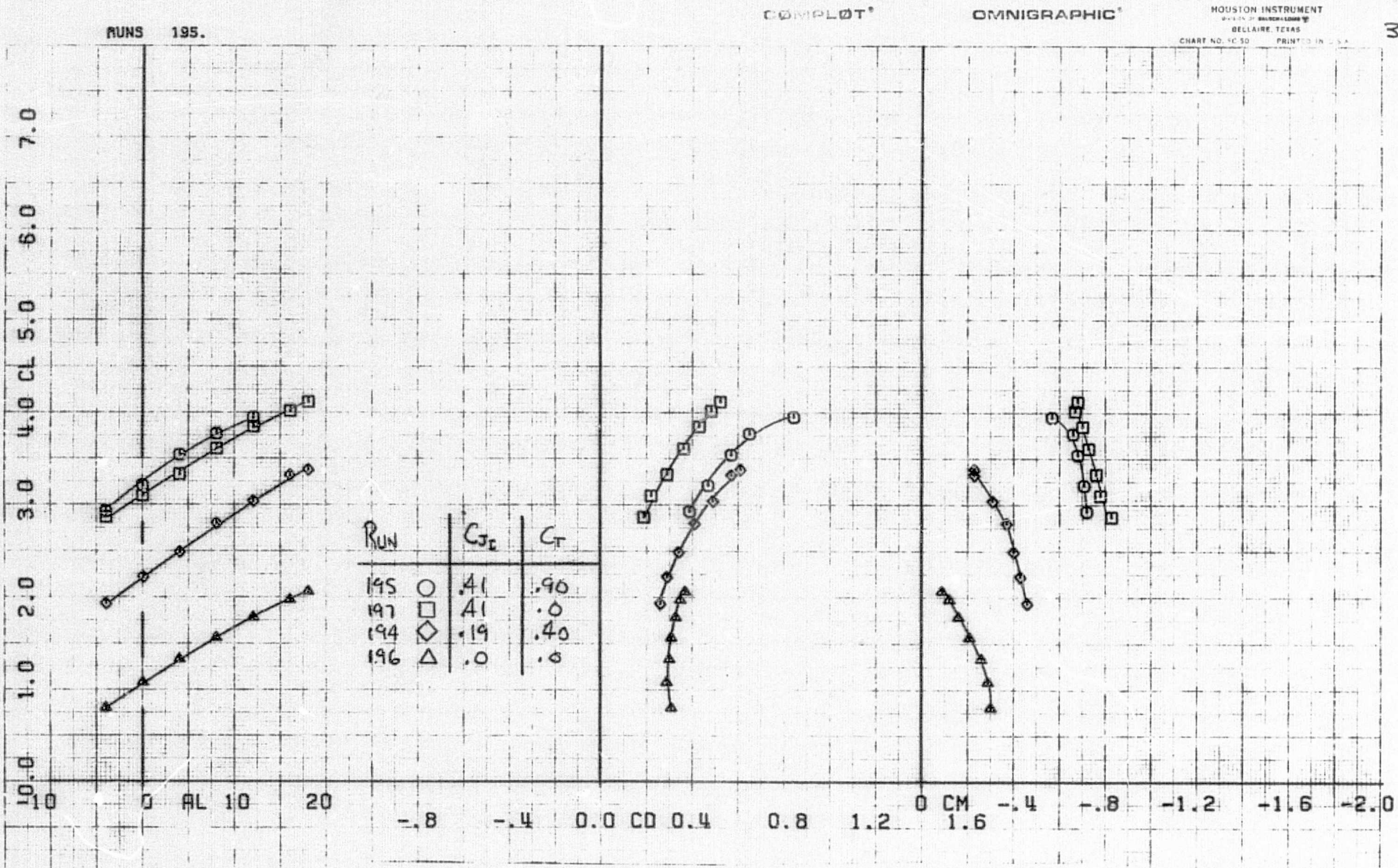

(b) T. S. = 30:70, tail off

Figure 28.- Continued.

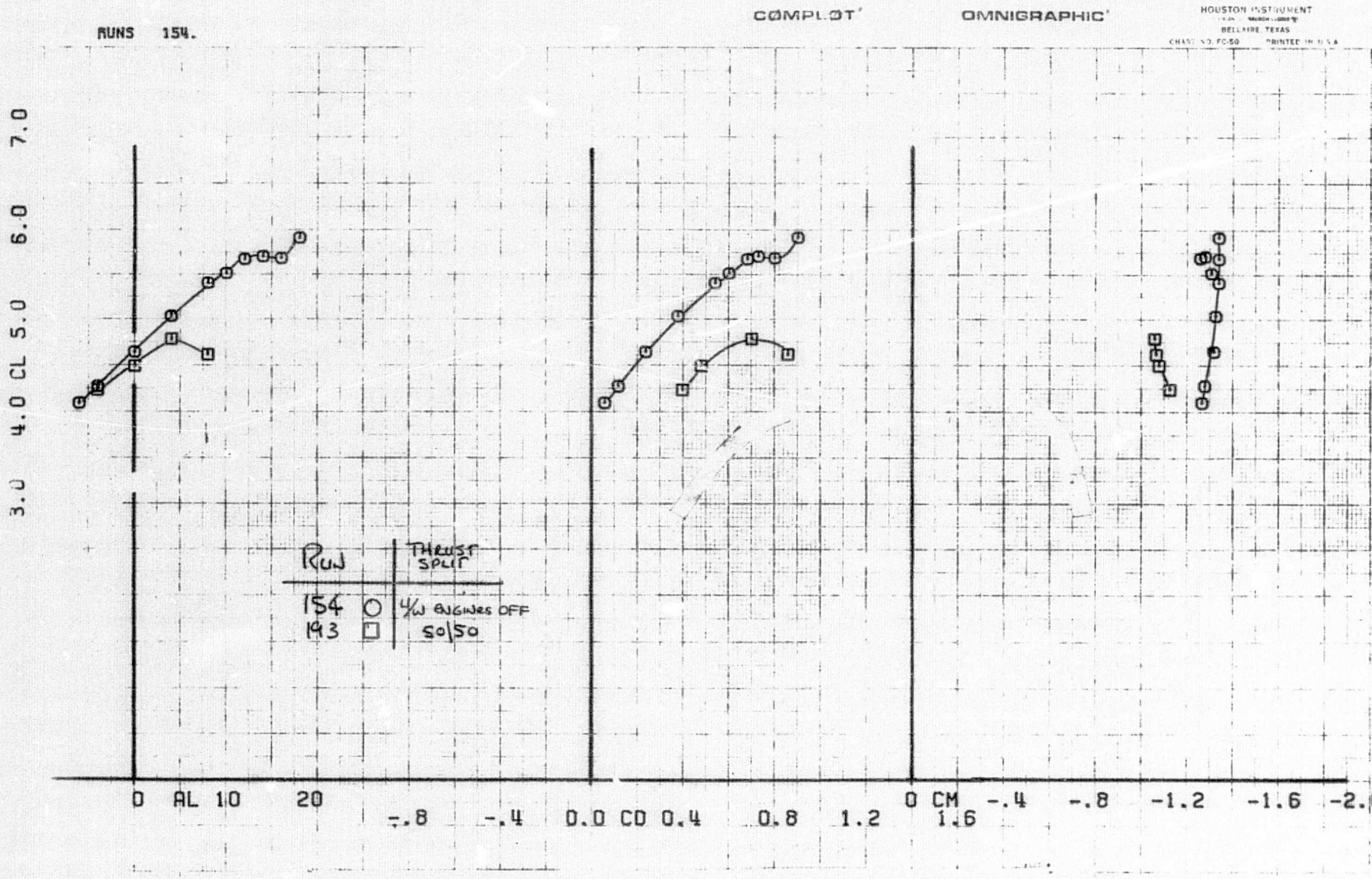

(c) Effect of T. S., C_{J_I} = .85, tail off

Figure 28.- Continued.

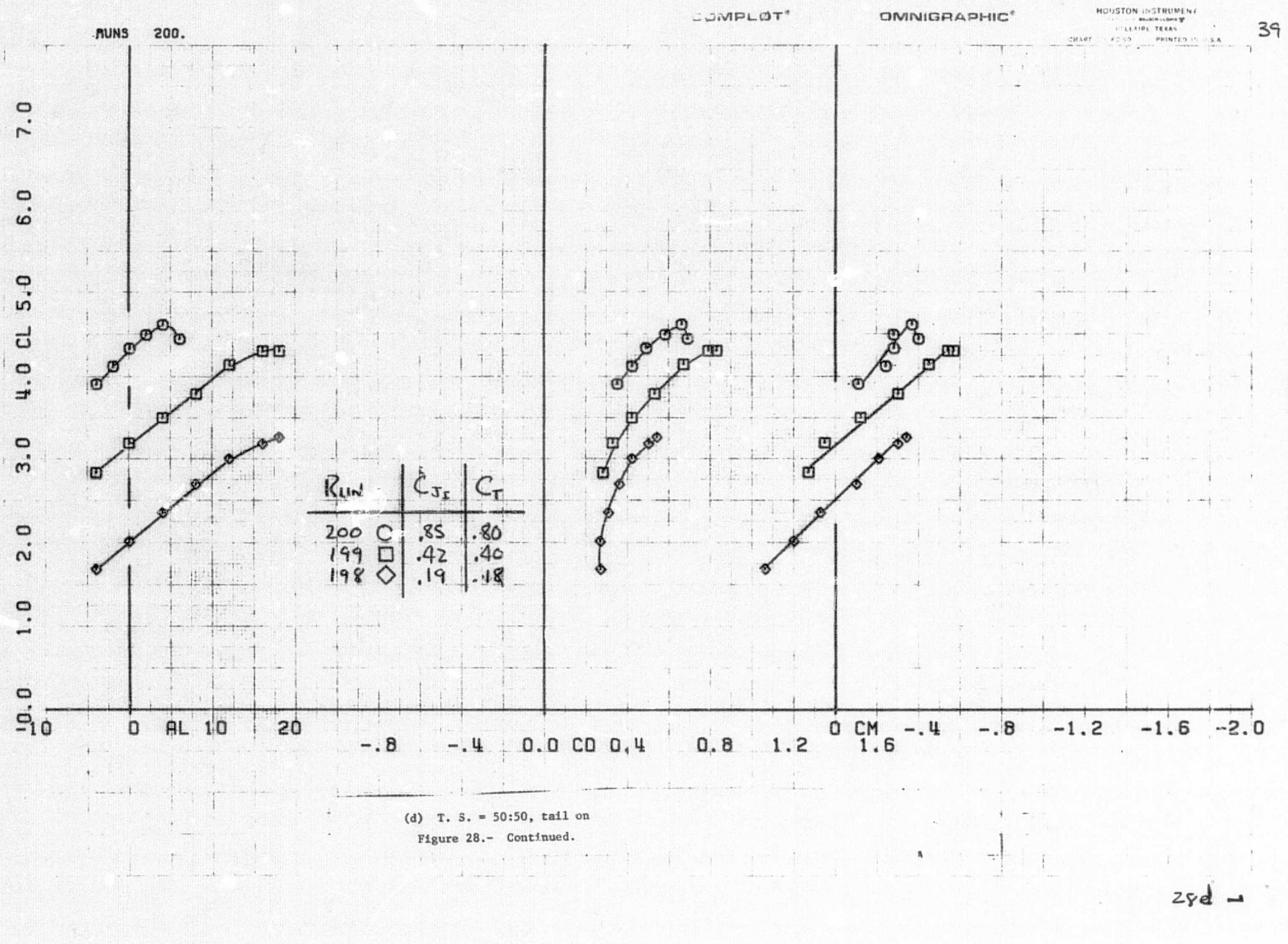

(d) T. S. = 50:50, tail on

Figure 28.- Continued.

28d

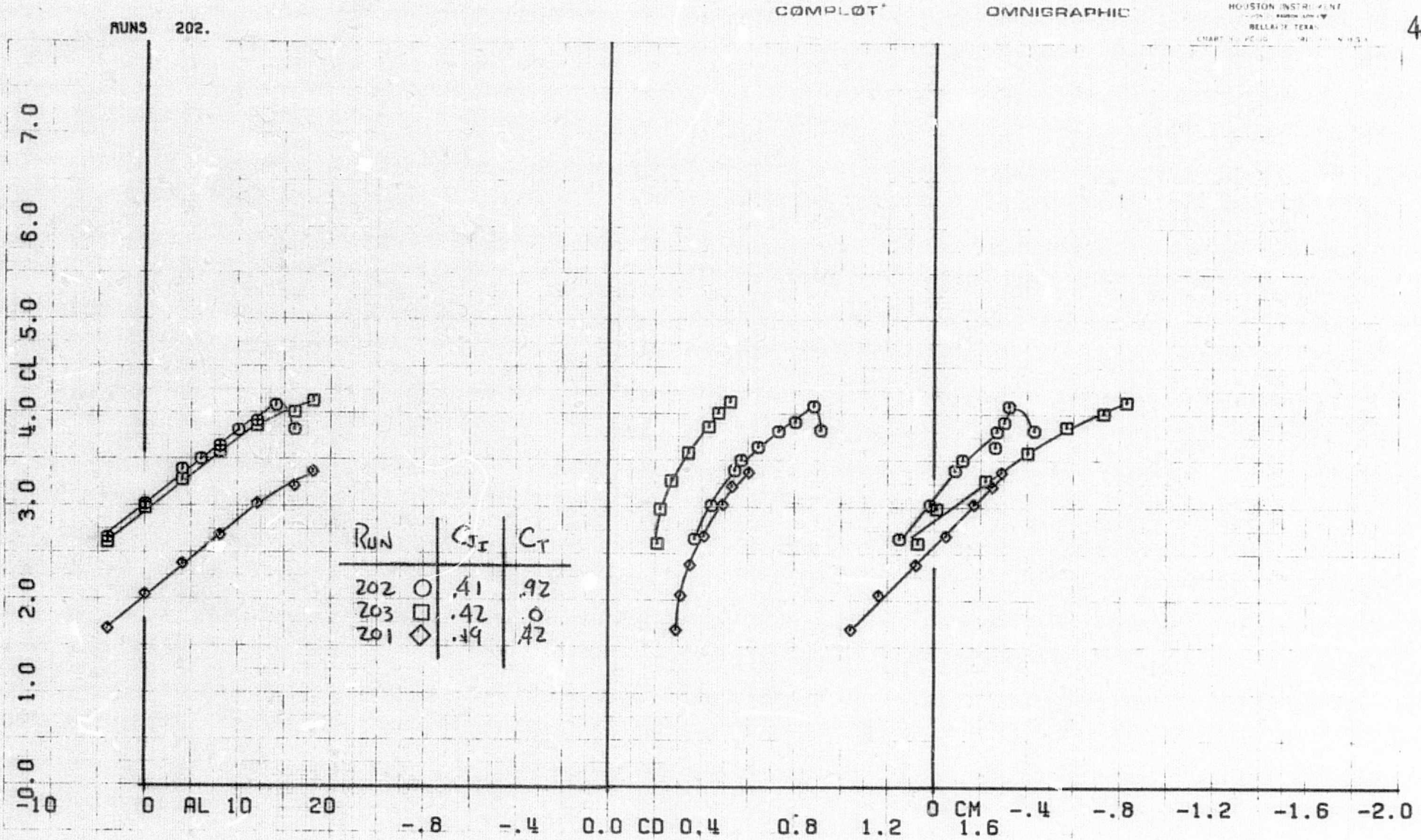

(e) T. S. = 30:70, tail on

Figure 28.- Concluded.

28e

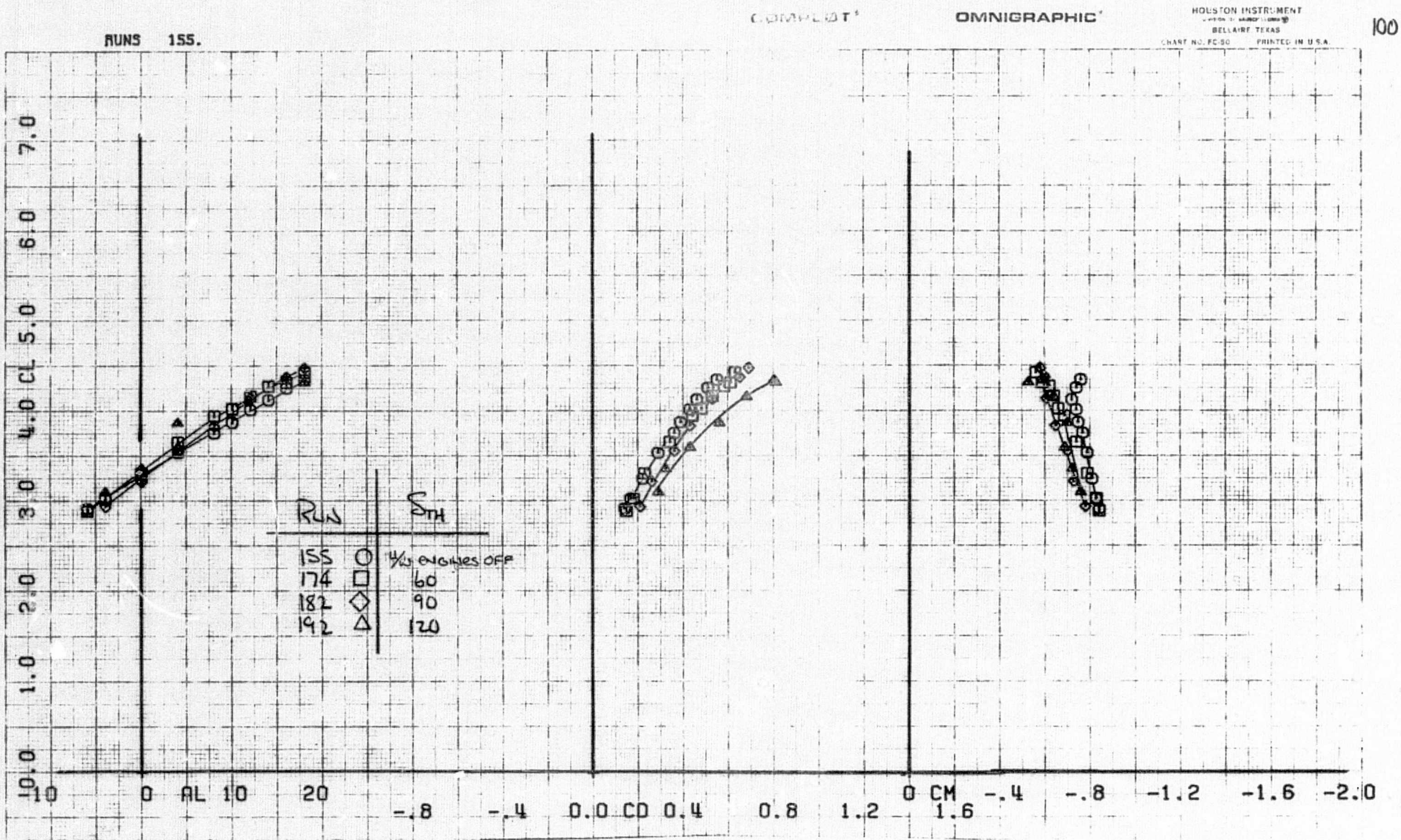

(a) $C_{J_I} = .42$

Figure 29.- Effect of δ_{TH} on longitudinal aerodynamic characteristics with two J-85 underwing engines; $h/c = 2.04$, $\delta_f = 70^\circ$, tail off, T. S. = 50:50.

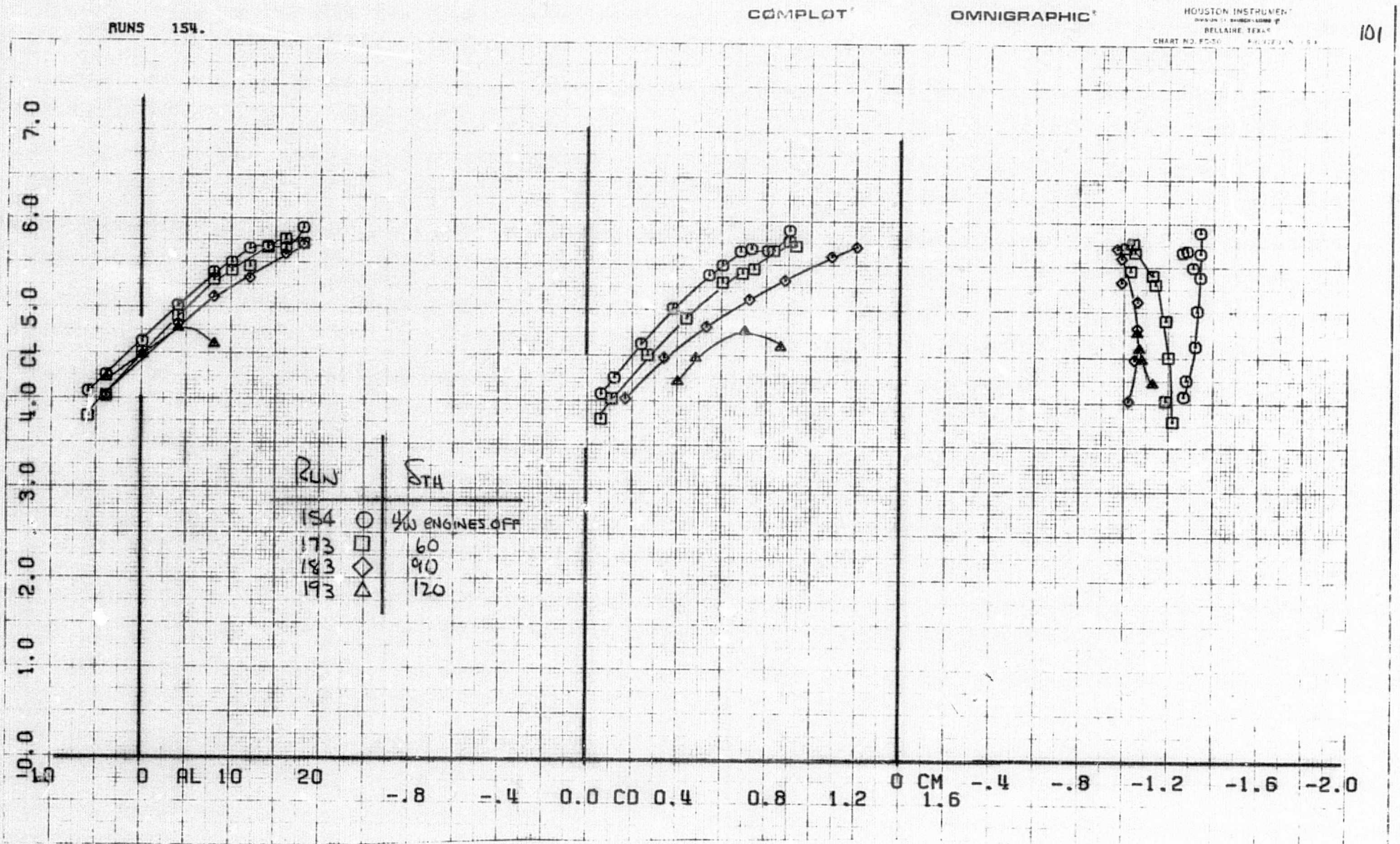

(b) C_{J_I} = .85

Figure 29.- Concluded.

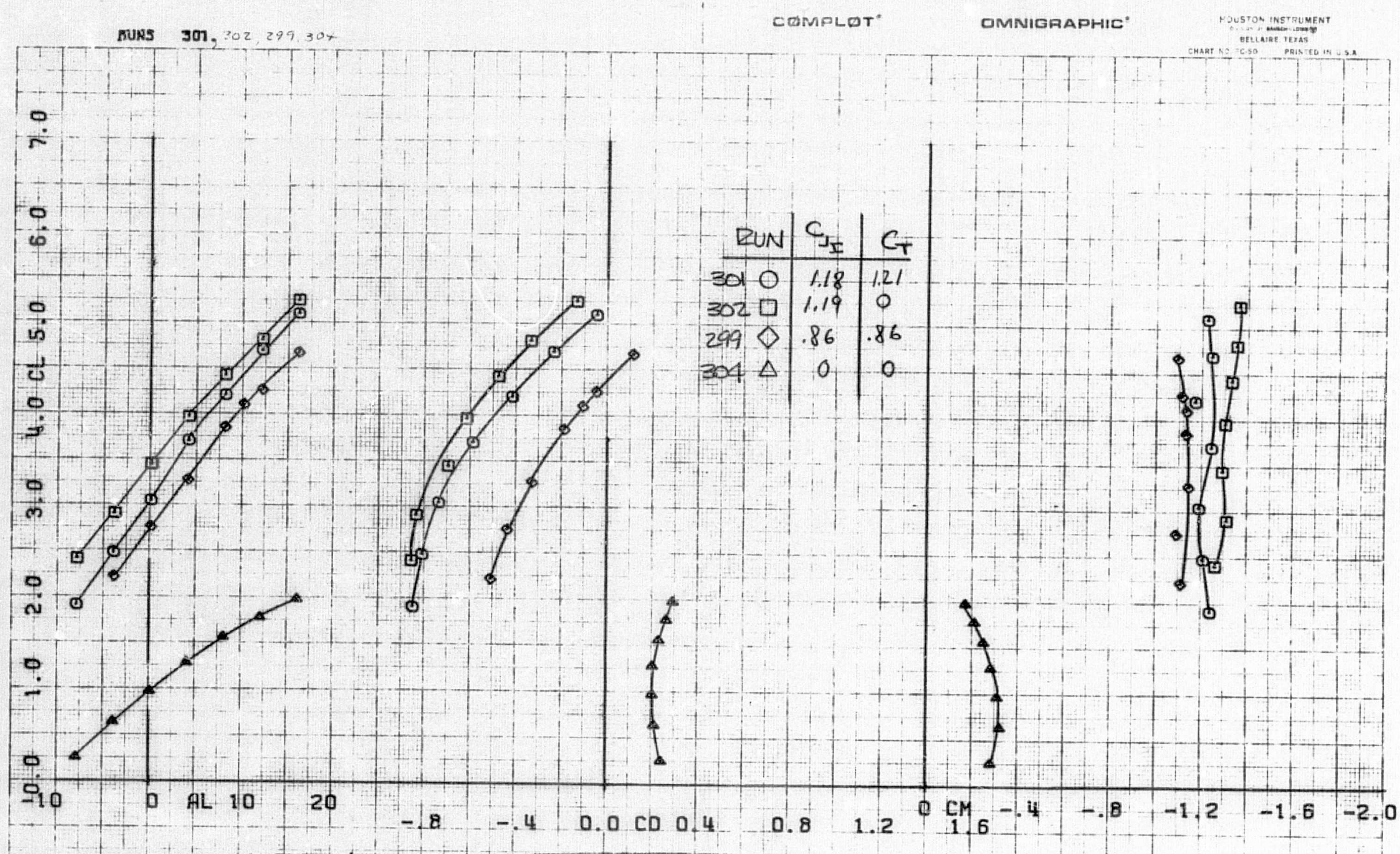

(a) T. S. = 50:50

Figure 30.- Longitudinal aerodynamic characteristics with two J-85 underwing engines; h/c = 1.61, $\delta_f = 40^\circ$, $\delta_{TH} = 0^\circ$, tail off.

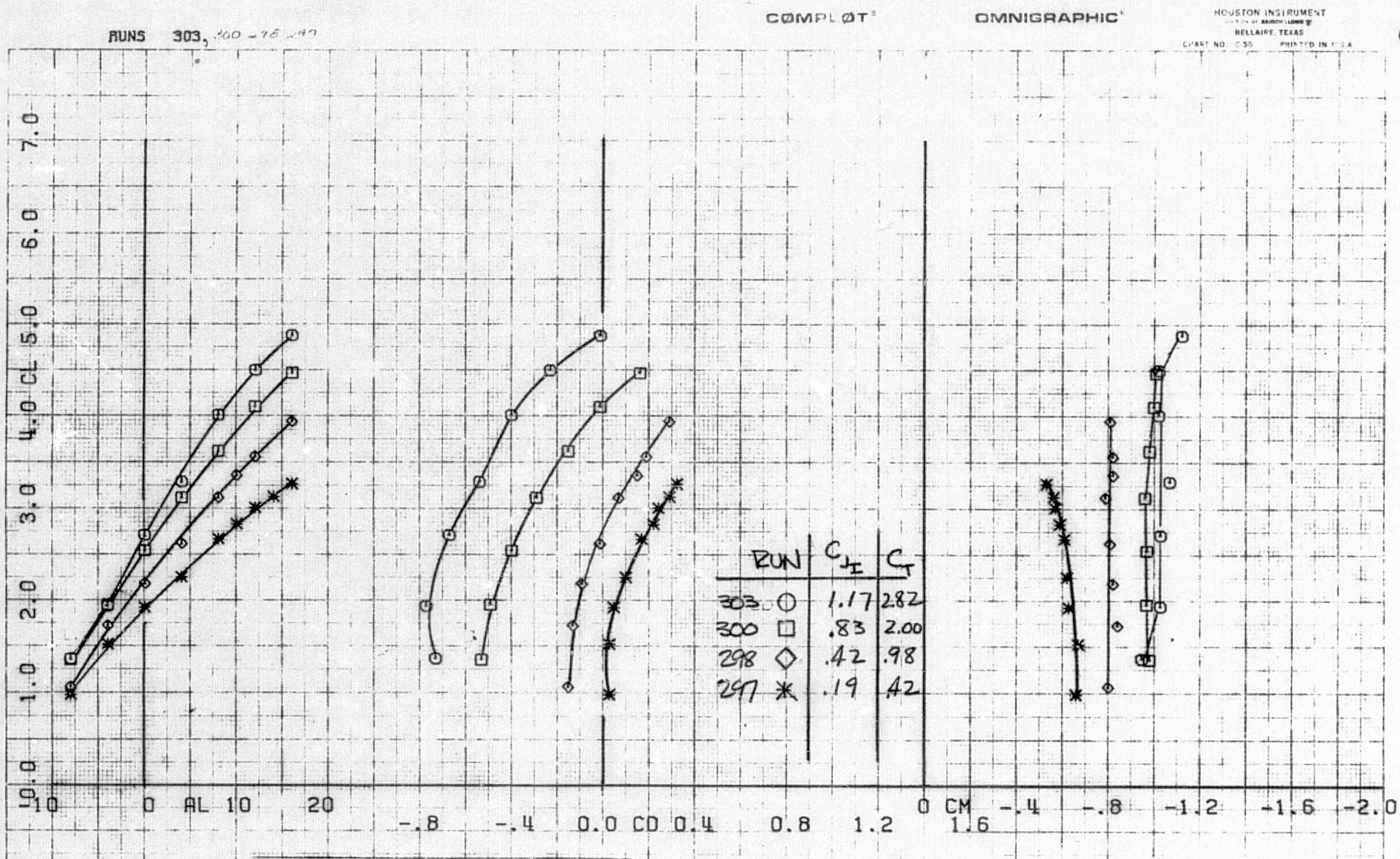

(b) T. S. = 30:70

Figure 30.- Continued.

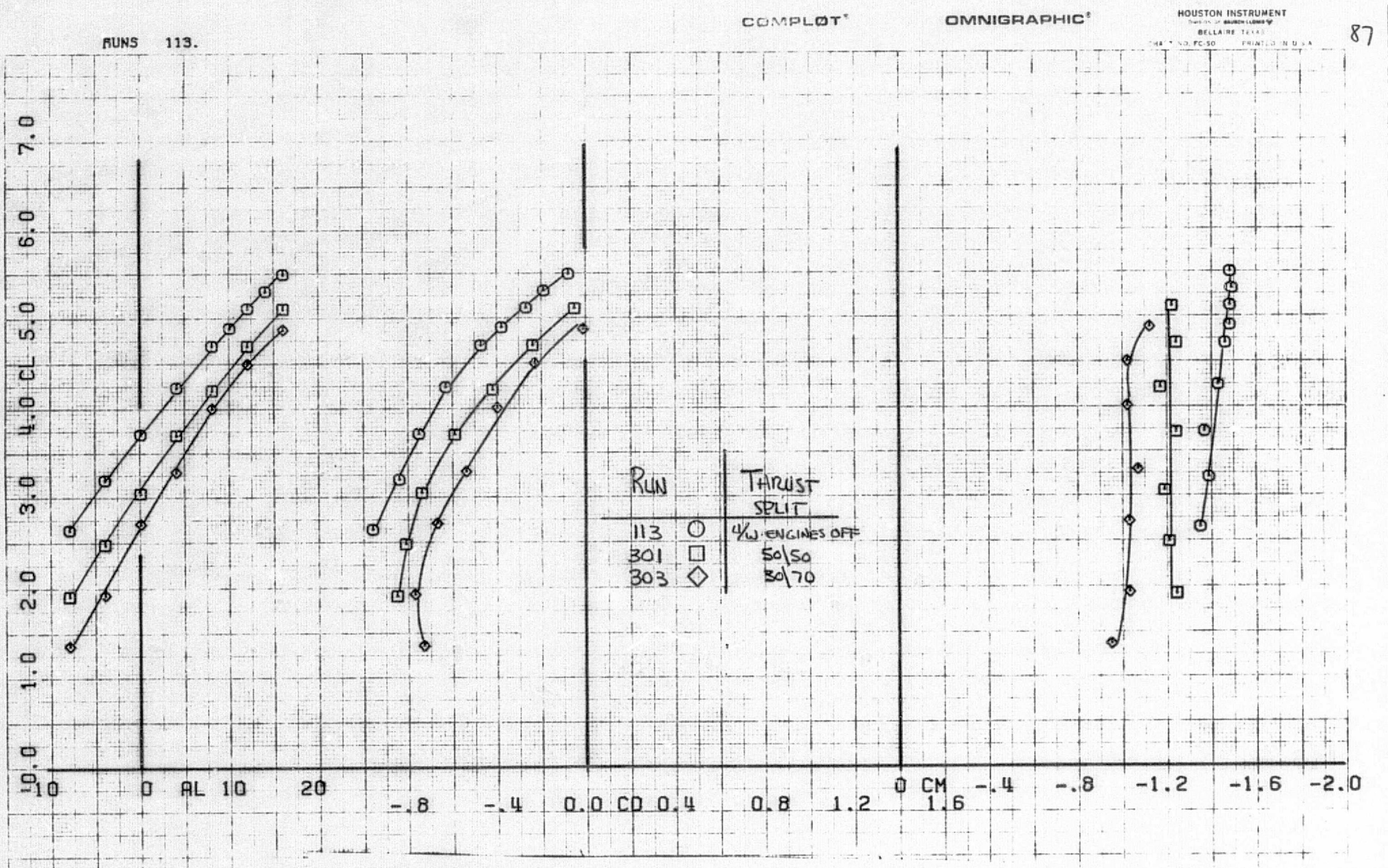

(c) Effect of T. S., $C_{J_I} = 1.2$

Figure 30.- Concluded.

30c

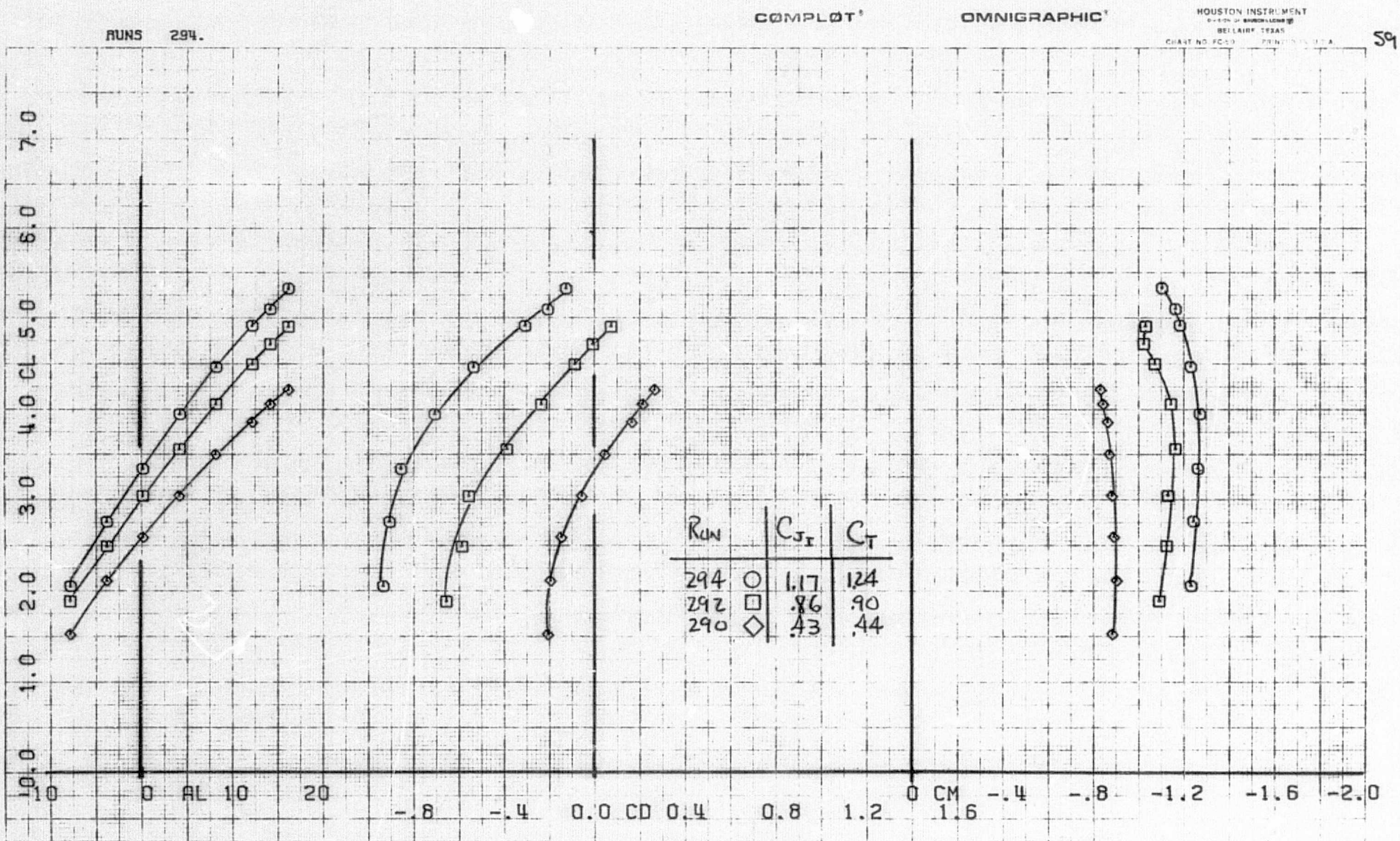

(a) T. S. = 50:50

Figure 31.- Longitudinal aerodynamic characteristics with two J-85 underwing engines; h/c = 1.61, δ_f = 40°, δ_{TH} = 30°, tail off.

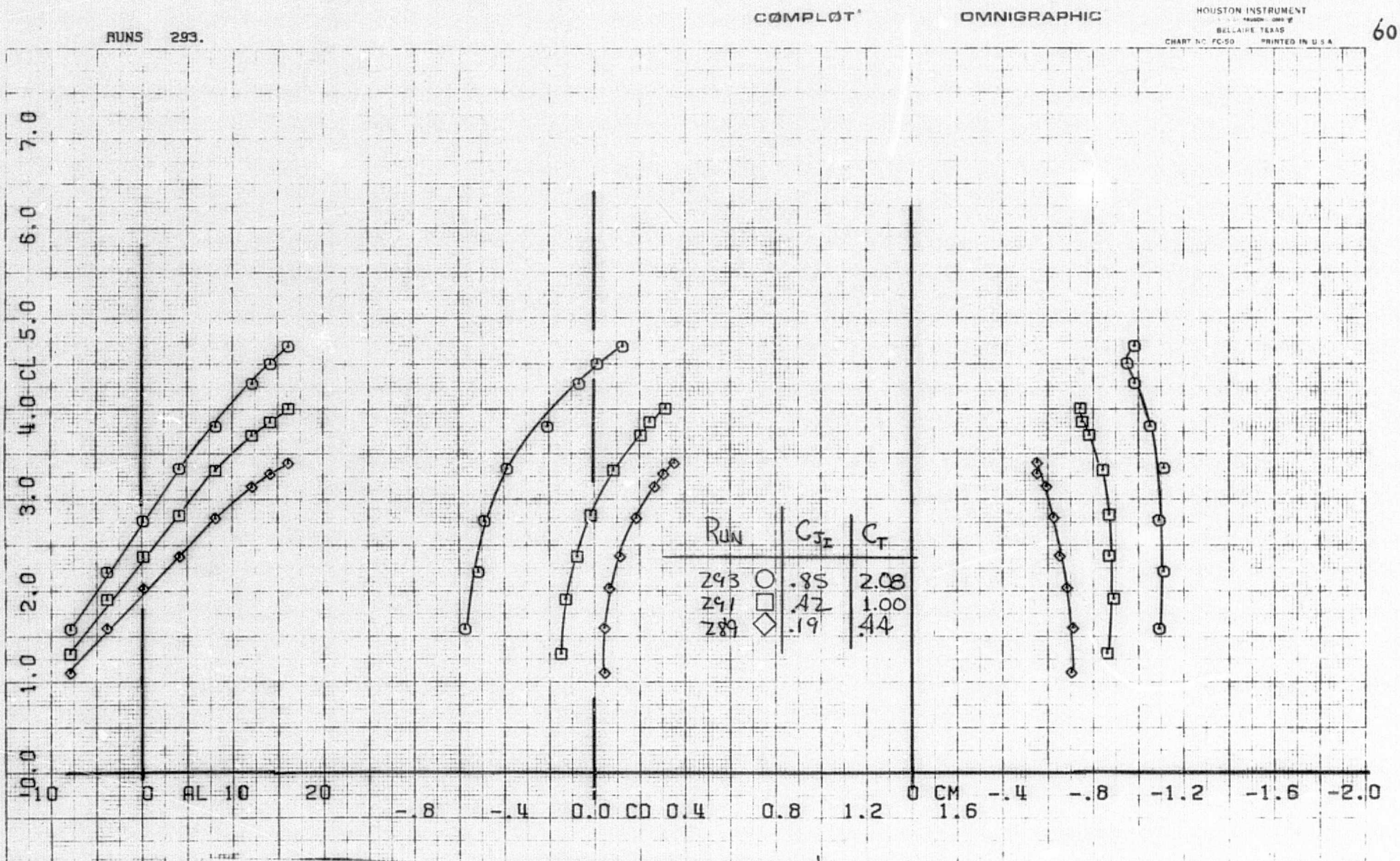

(b) T. S. = 30:70

Figure 31.- Continued.

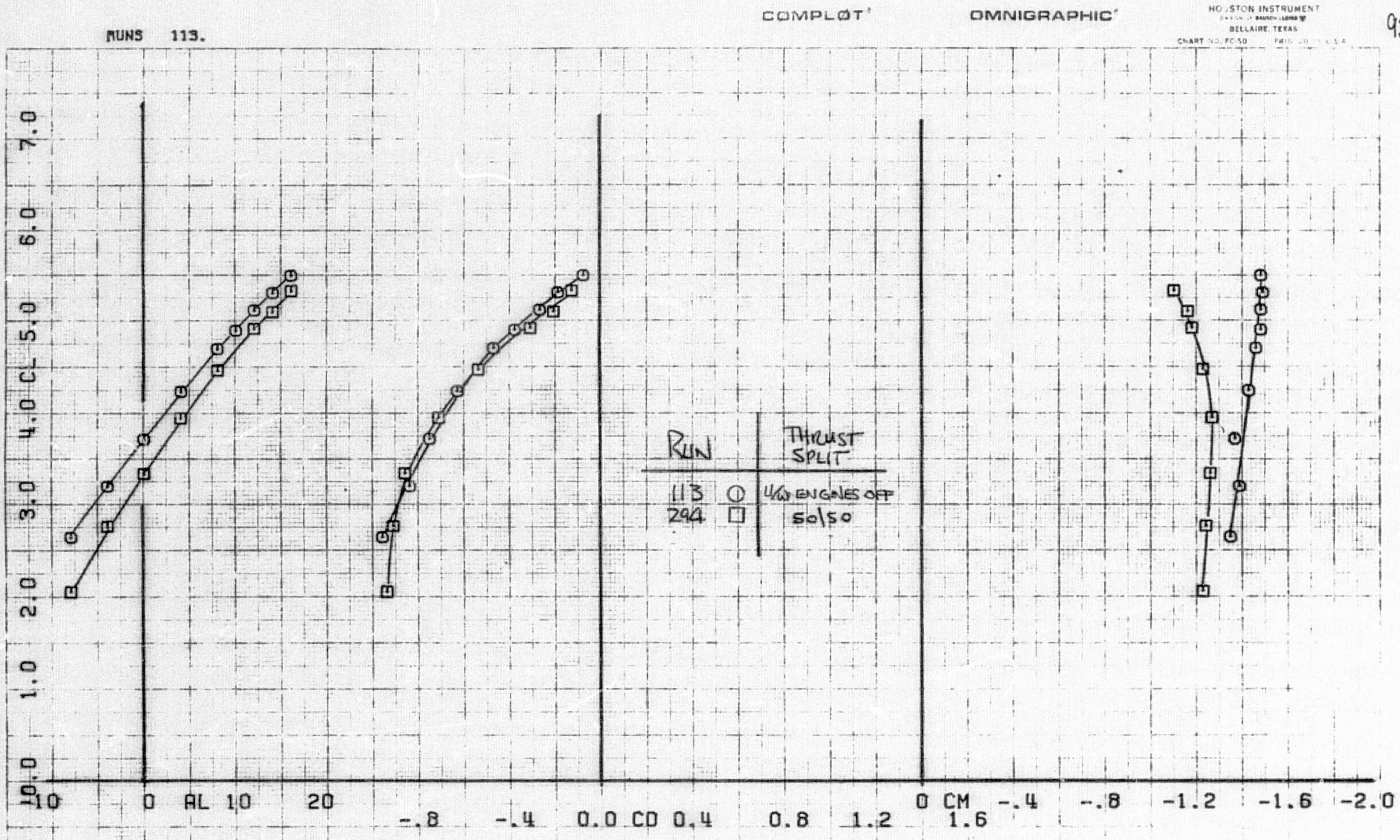

(c) Effect of T. S., C_{J_I} = 1.2

Figure 31.- Concluded.

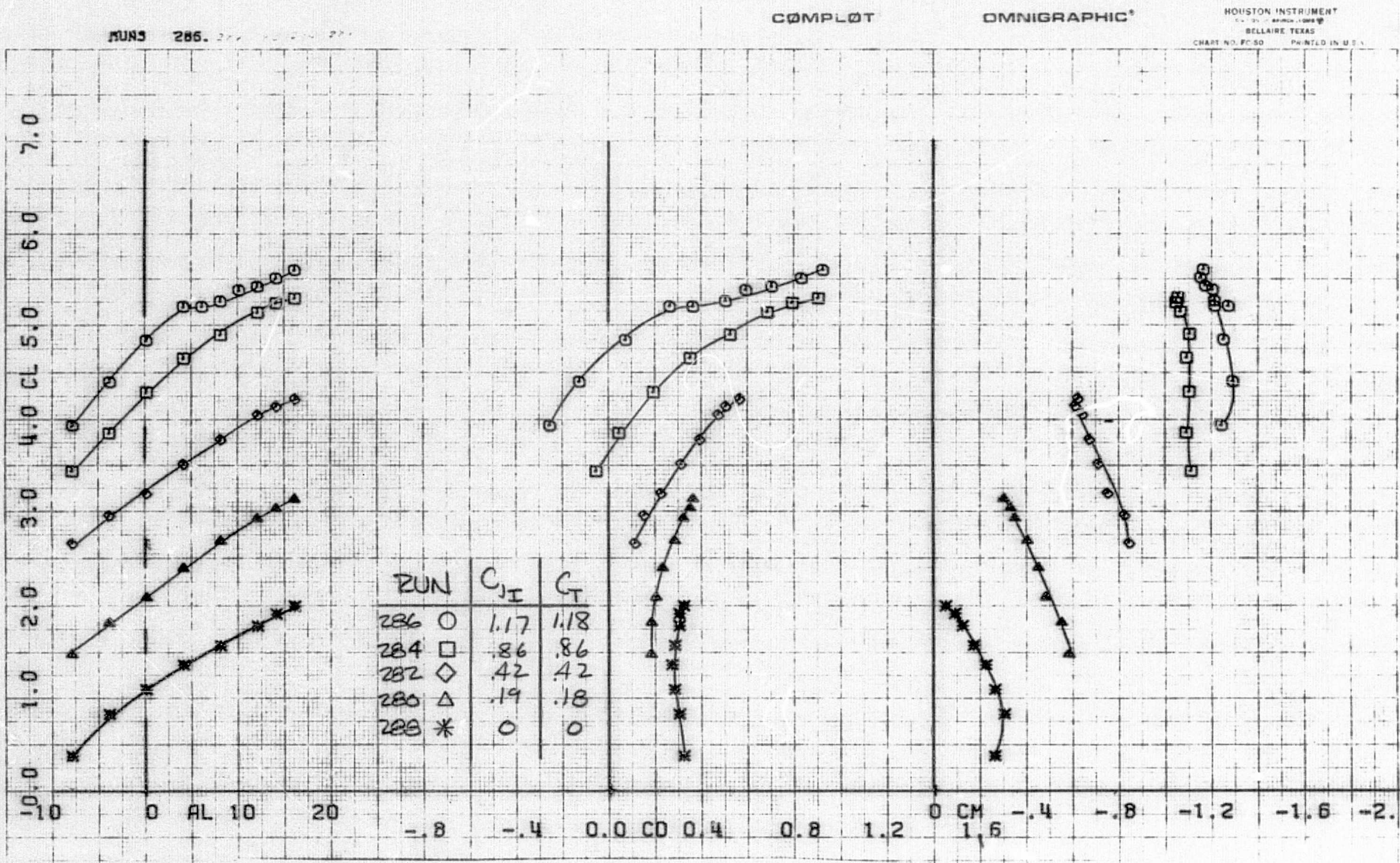

(a) T. S. = 50:50

Figure 32.- Longitudinal aerodynamic characteristics with two J-85 underwing engines; h/c = 1.61, $\delta_f = 70^{\circ}$, $\delta_{TH} = 60^{\circ}$, tail off.

32a

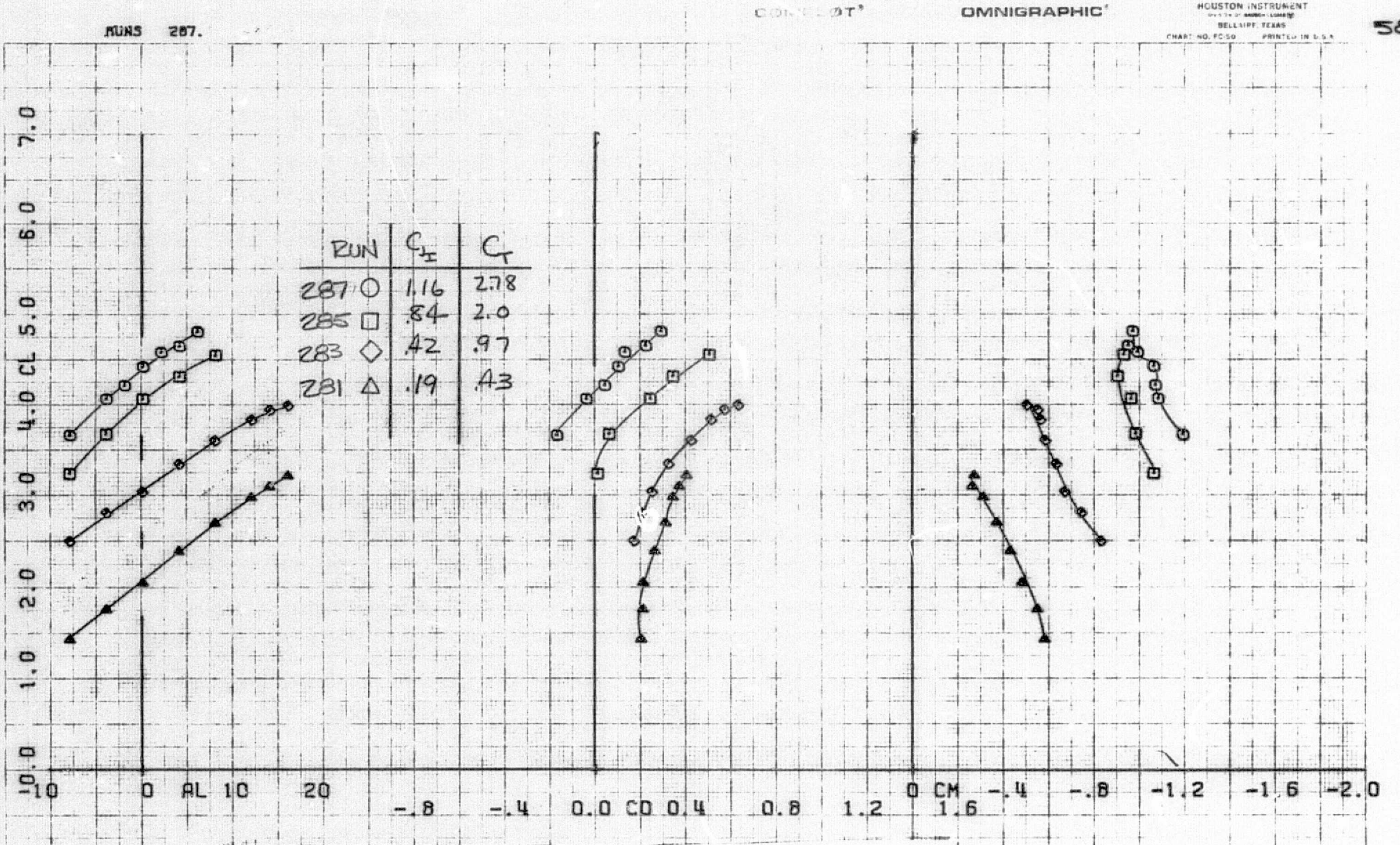

(b) T. S. = 30:70

Figure 32.- Continued.

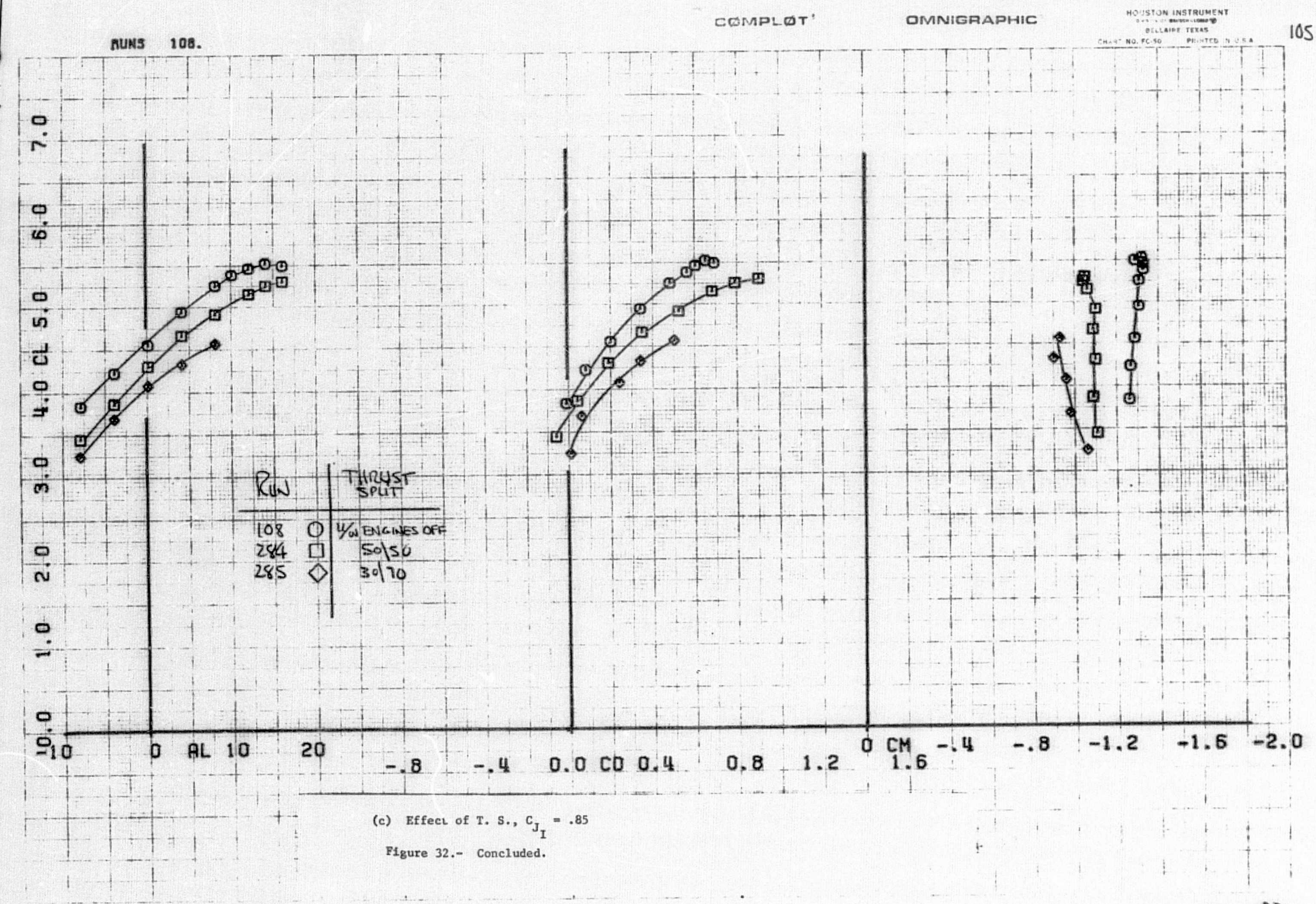

(c) Effect of T. S., C_{J_I} = .85

Figure 32.- Concluded.

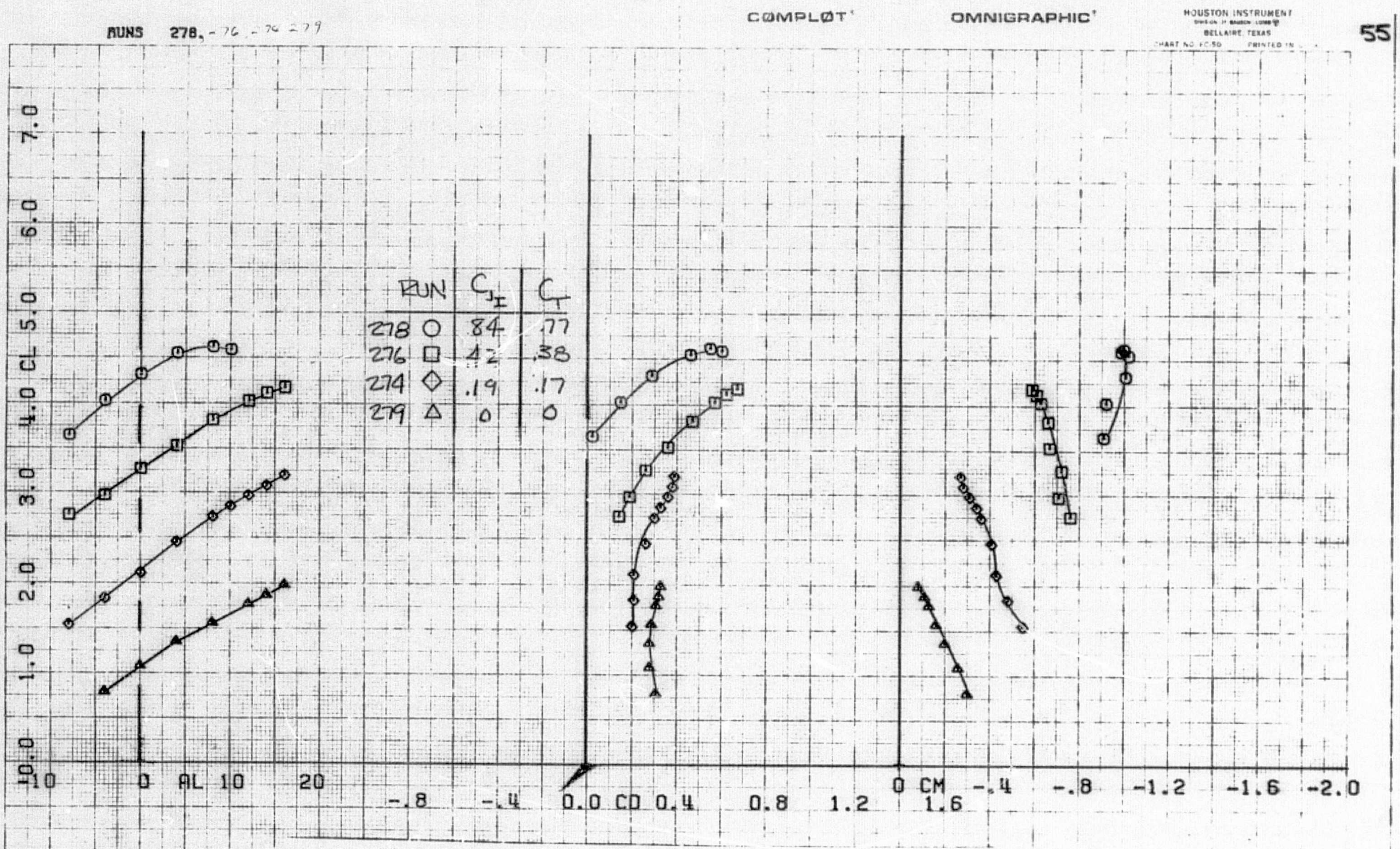

(a) T. S. = 50:50

Figure 33.- Longitudinal aerodynamic characteristics with two J-85 underwing engines; h/c = 1.61, $\delta_f = 70^\circ$, $\delta_{TH} = 60^\circ$, tail off.

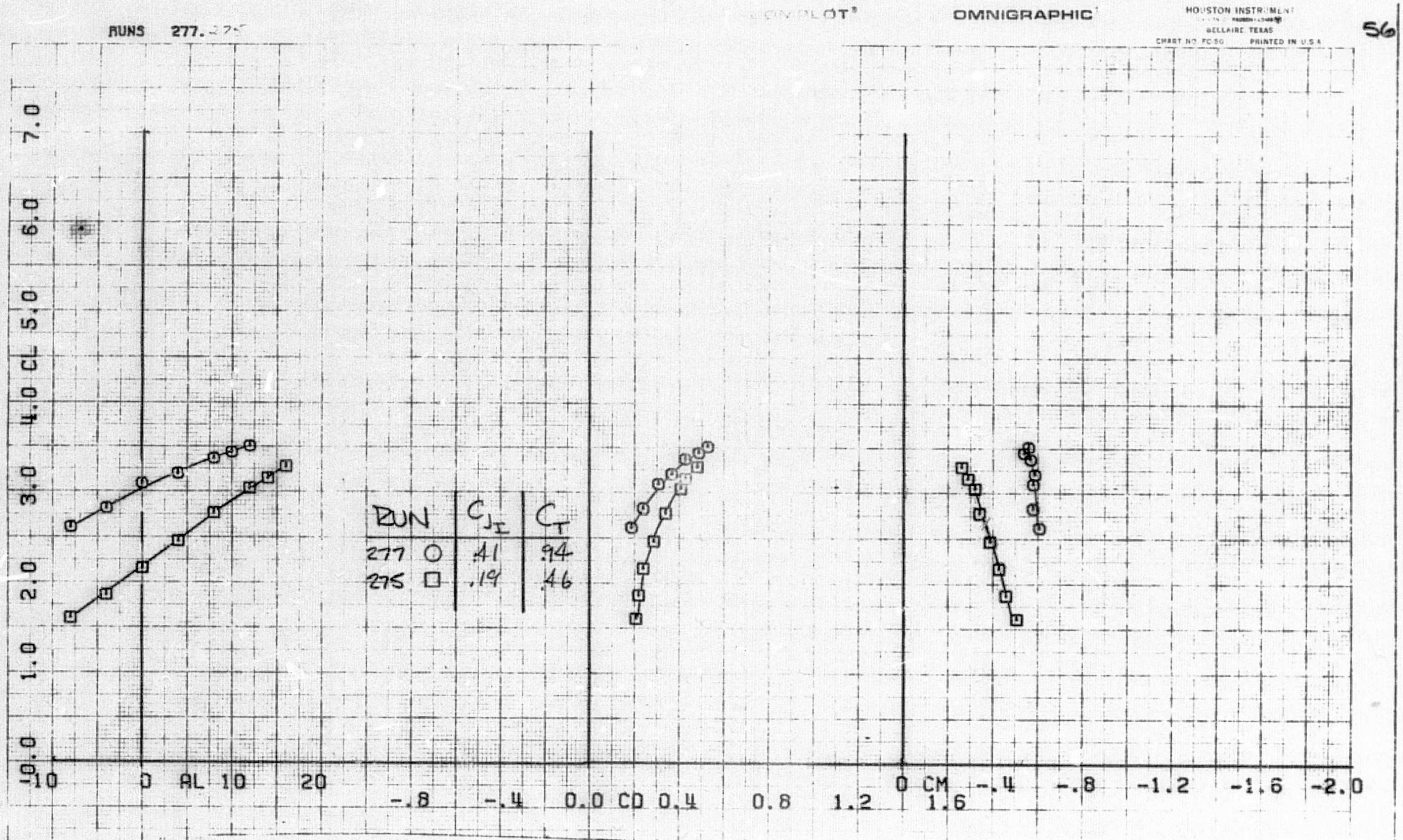

(b) T. S. = 30:70

Figure 33.- Continued.

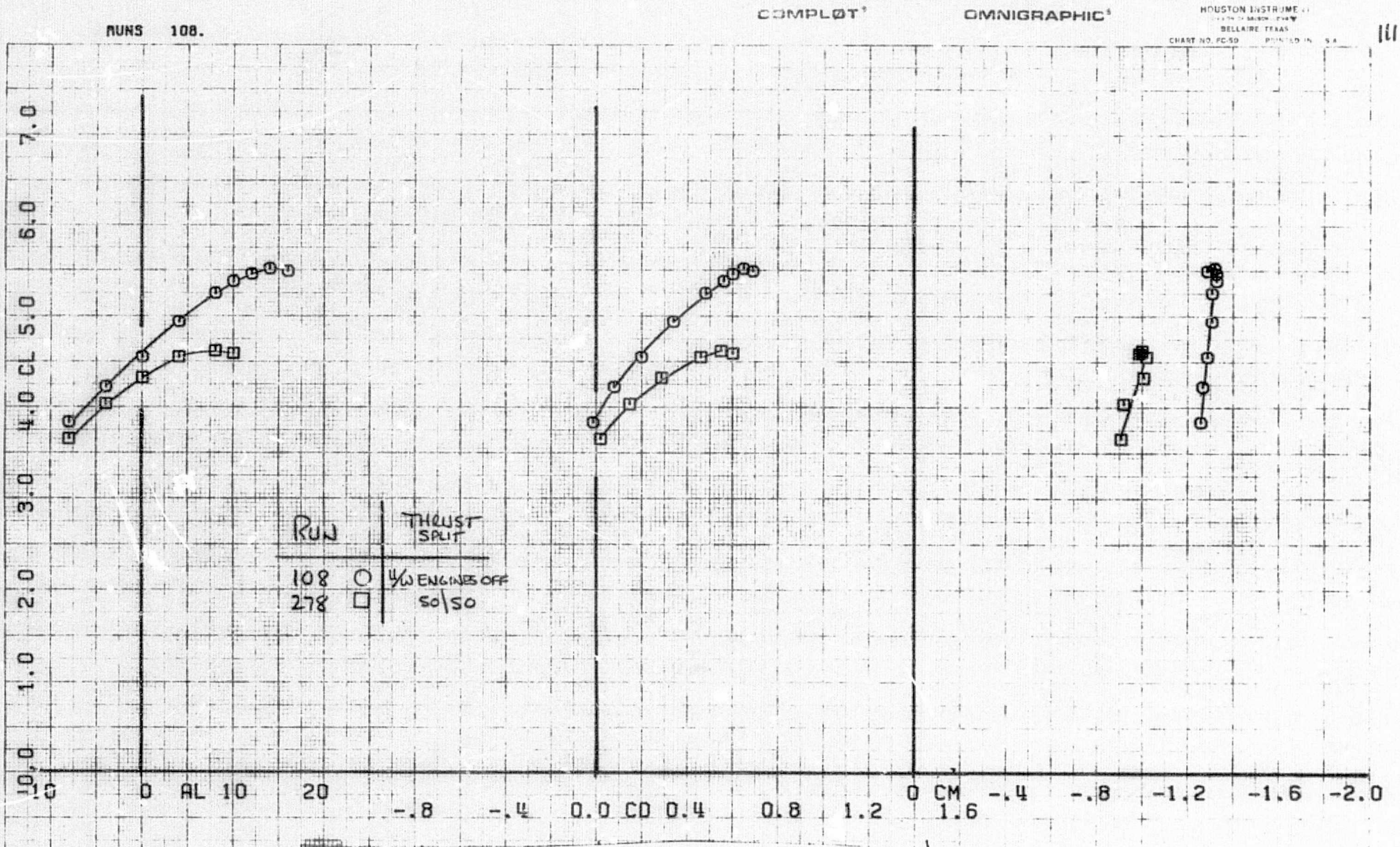

(c) Effect of T. S., C_{J_I} = .85

Figure 33.- Concluded.

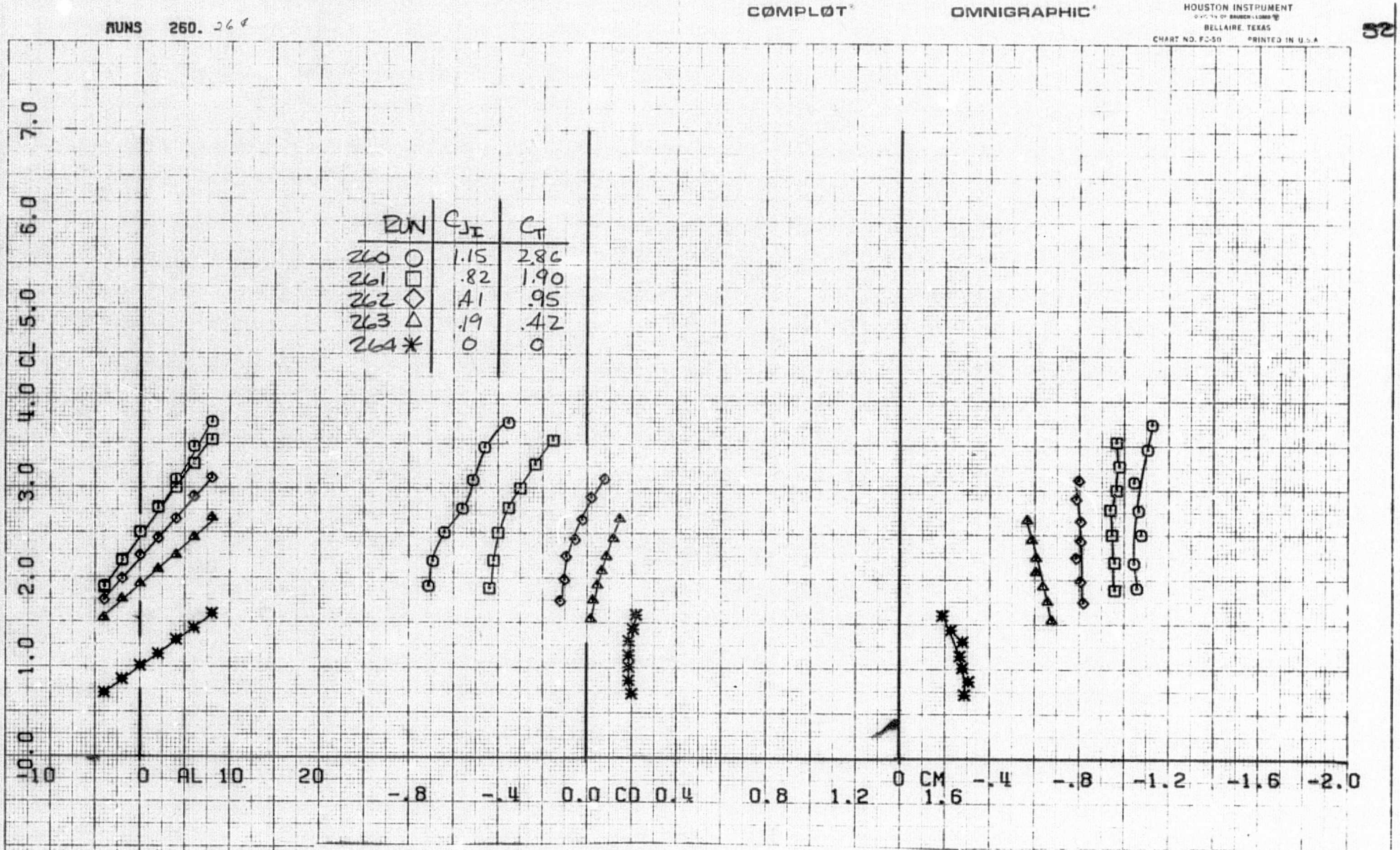

(a) T. S. = 30:70, tail off

Figure 34.- Longitudinal aerodynamic characteristics with two J-85 underwing engines; $h/c = 1.34$, $\delta_f = 40^o$, $\delta_{TH} = 0^o$.

34a

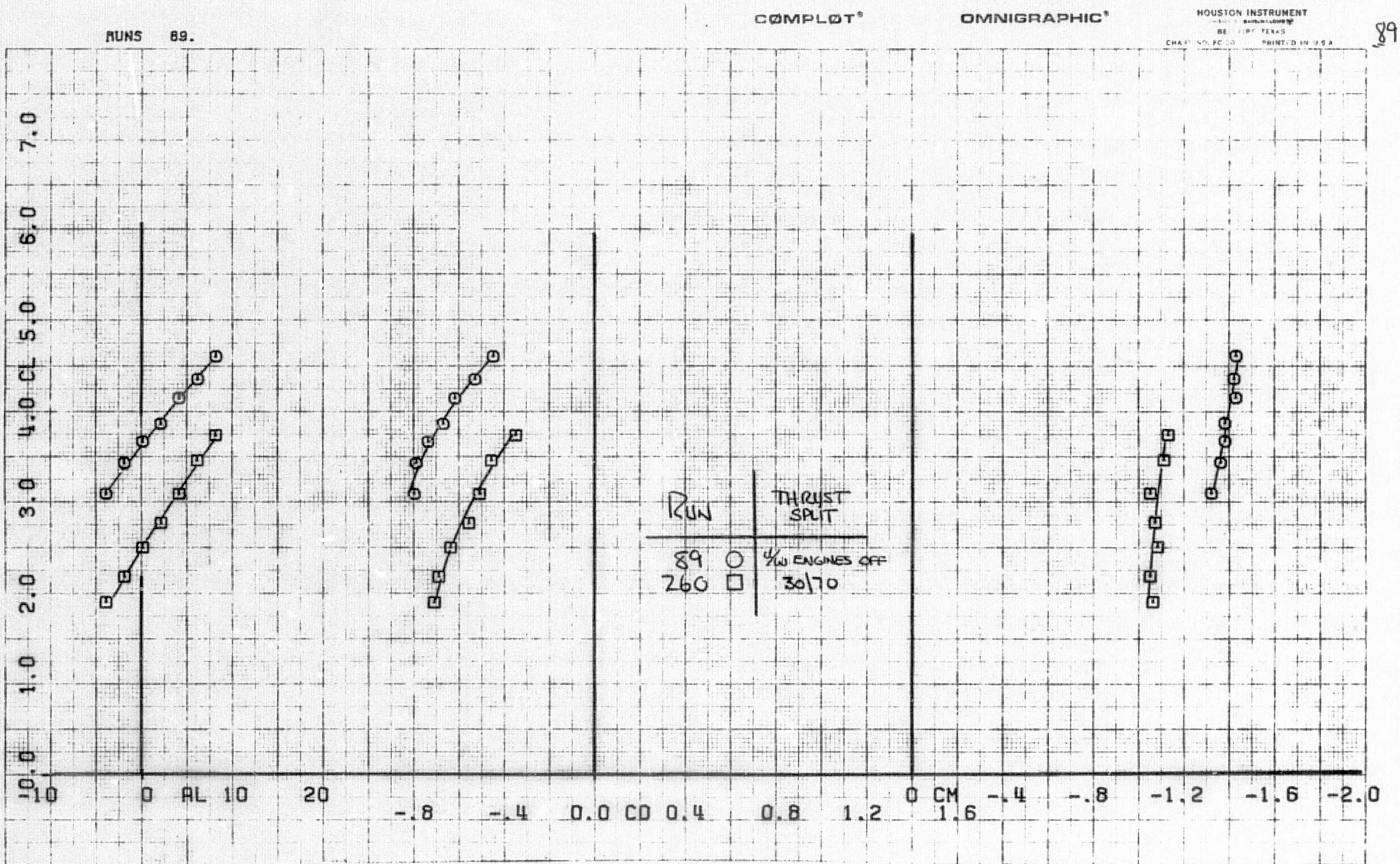

(b) Effect of T. S., C_{J_I} = 1.2, tail off

Figure 34.- Continued.

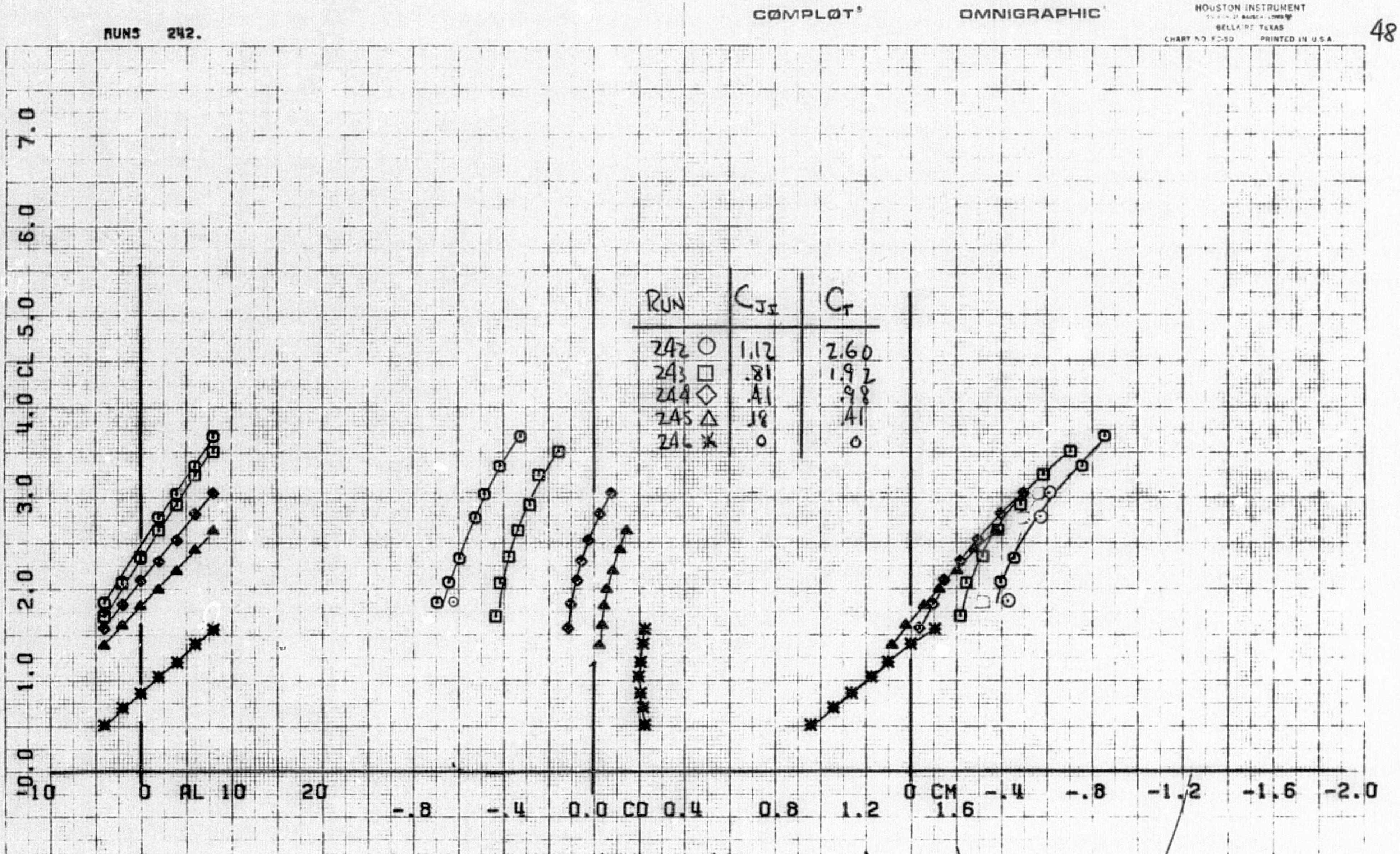

(c) T. S. = 30:70, tail on

Figure 34.- Concluded.

48

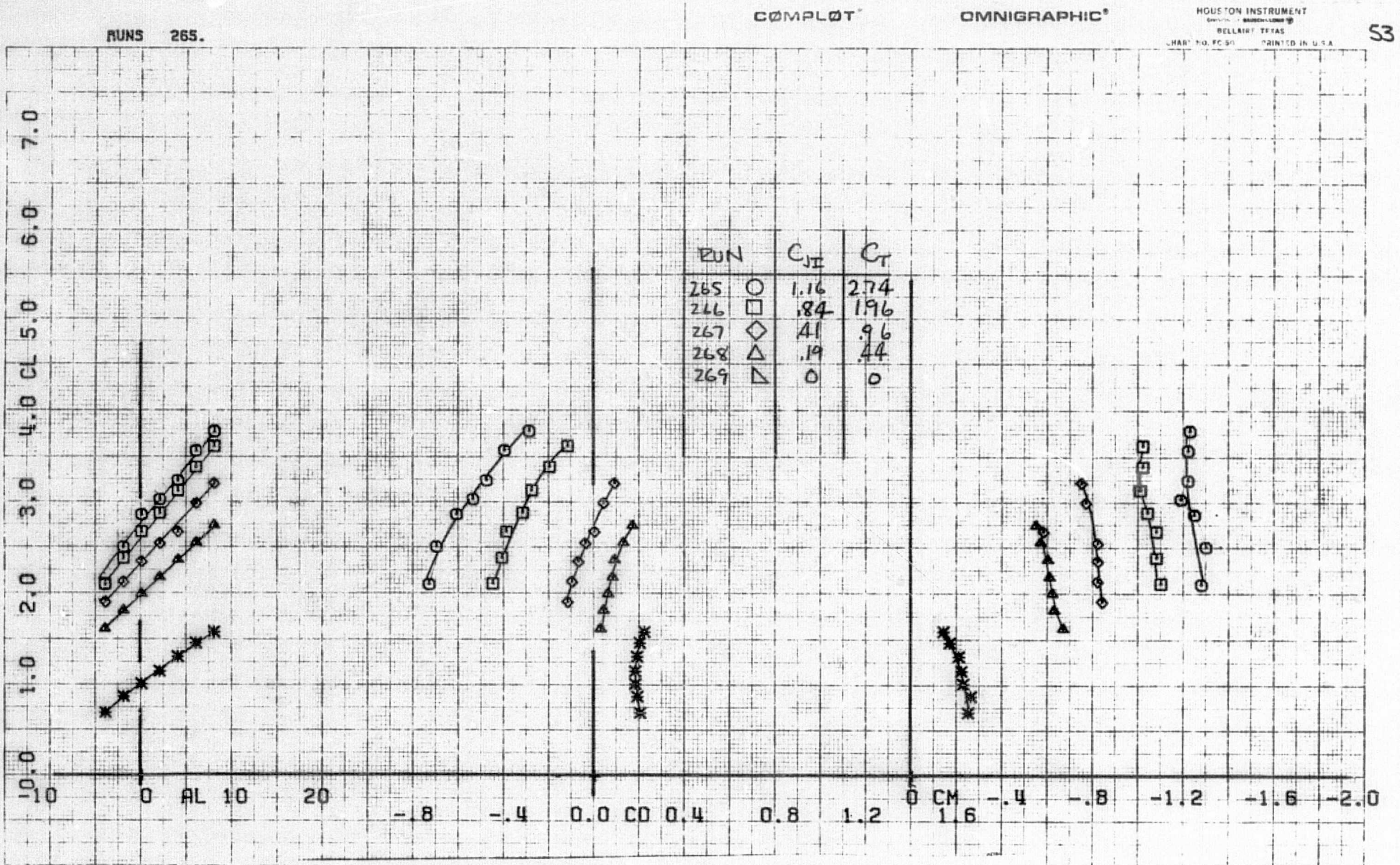

(a) T. S. = 30:70, tail off

Figure 35.- Longitudinal aerodynamic characteristics with two J-85 underwing engines; h/c = 1.34, $\delta_f = 40^{\circ}$, $\delta_{TH} = 30^{\circ}$.

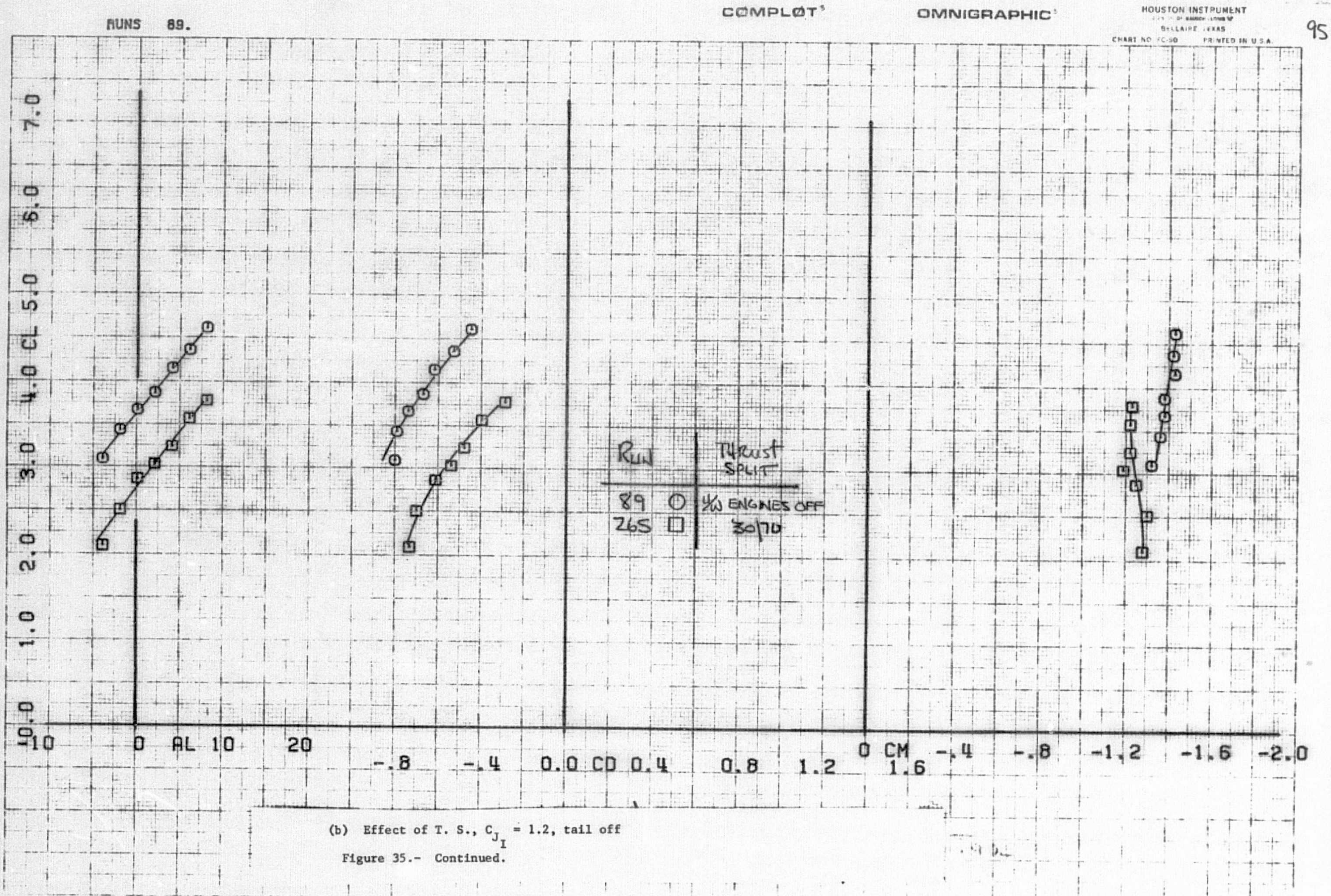

(b) Effect of T. S., C_{J_I} = 1.2, tail off

Figure 35.- Continued.

47

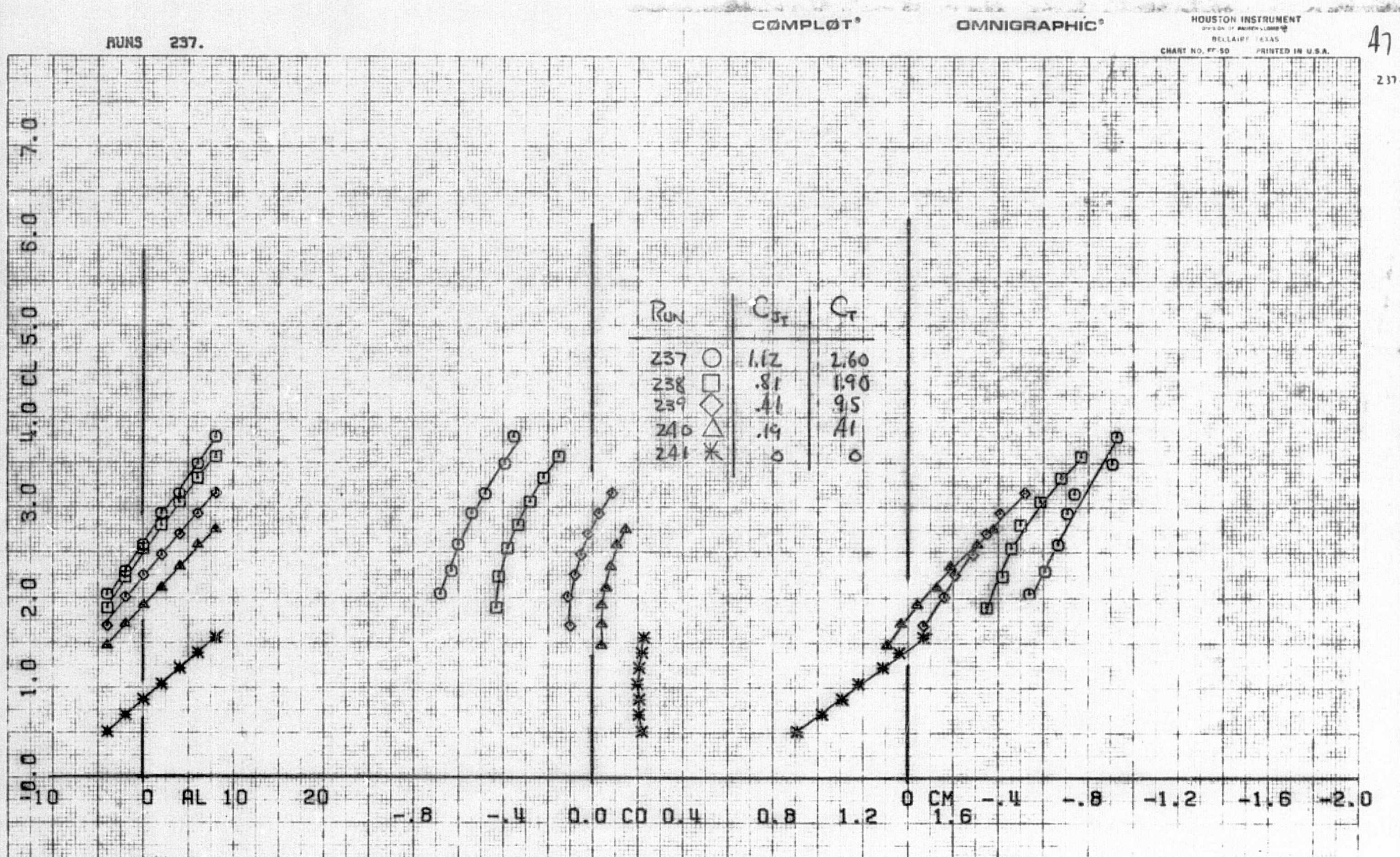

(c) T. S. = 30:70, tail on

Figure 35.- Concluded.

35c

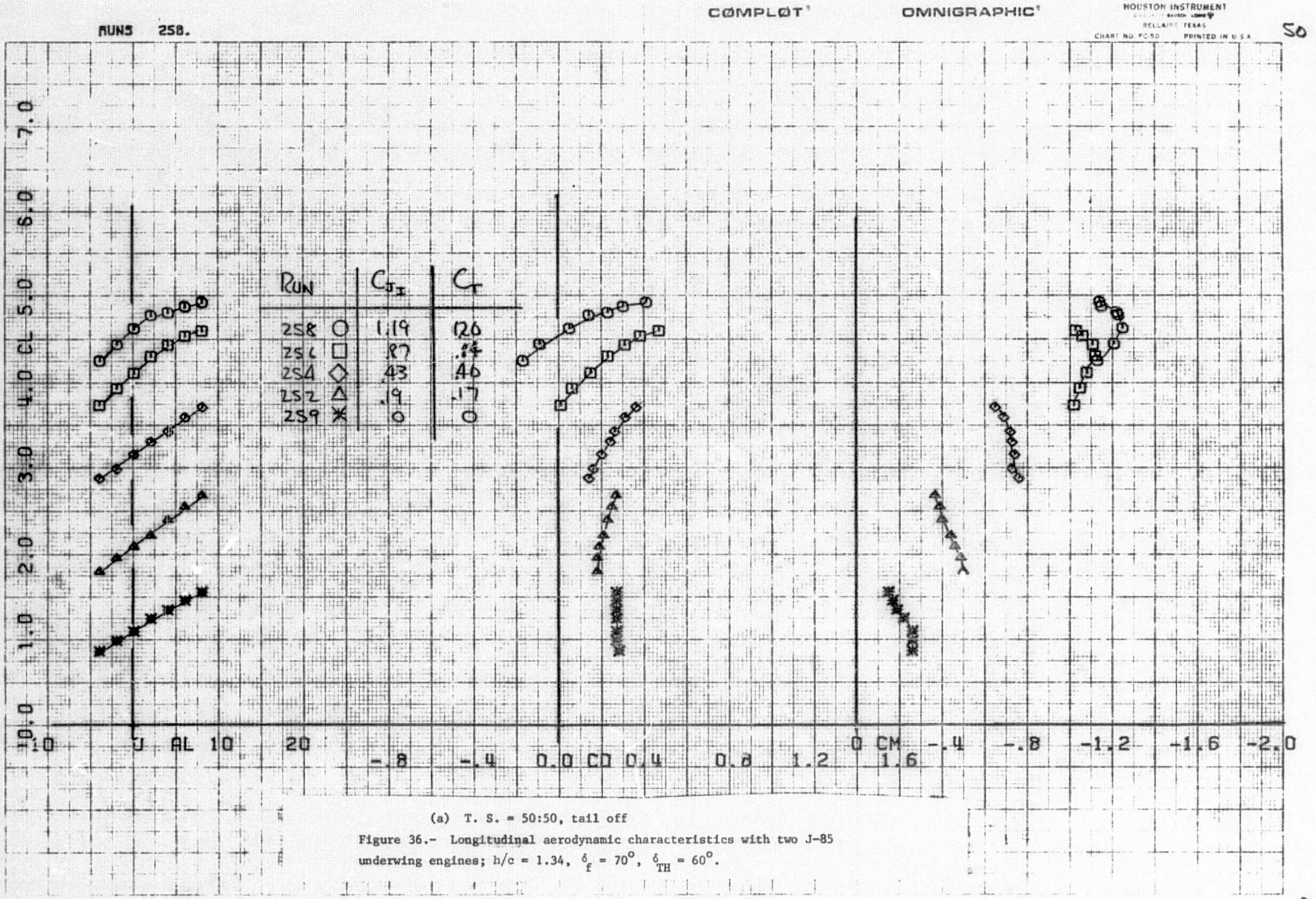

(a) T. S. = 50:50, tail off

Figure 36.- Longitudinal aerodynamic characteristics with two J-85 underwing engines; h/c = 1.34, $\delta_f = 70^\circ$, $\delta_{TH} = 60^\circ$.

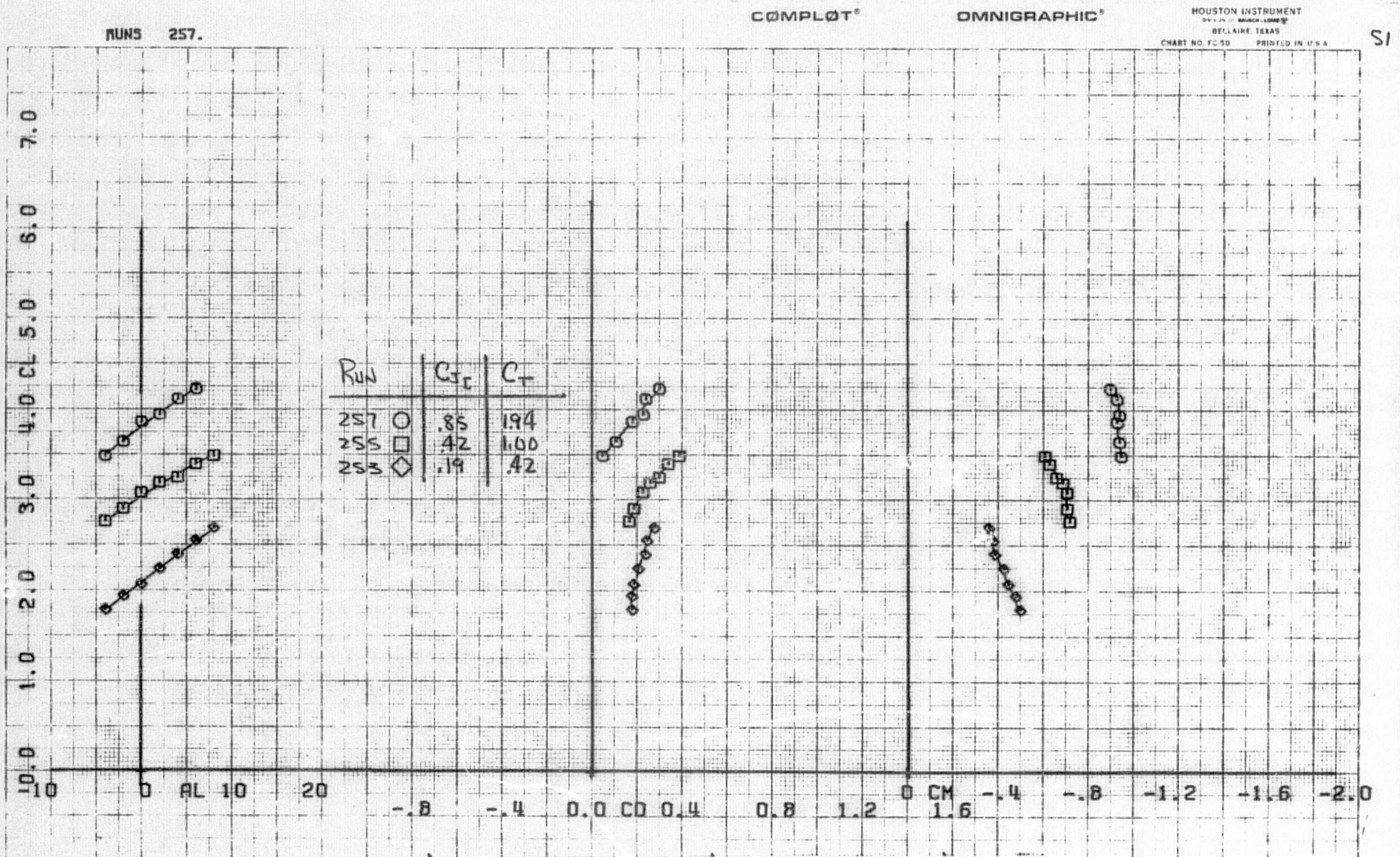

(b) T. S. = 30:70, tail off

Figure 36.- Continued.

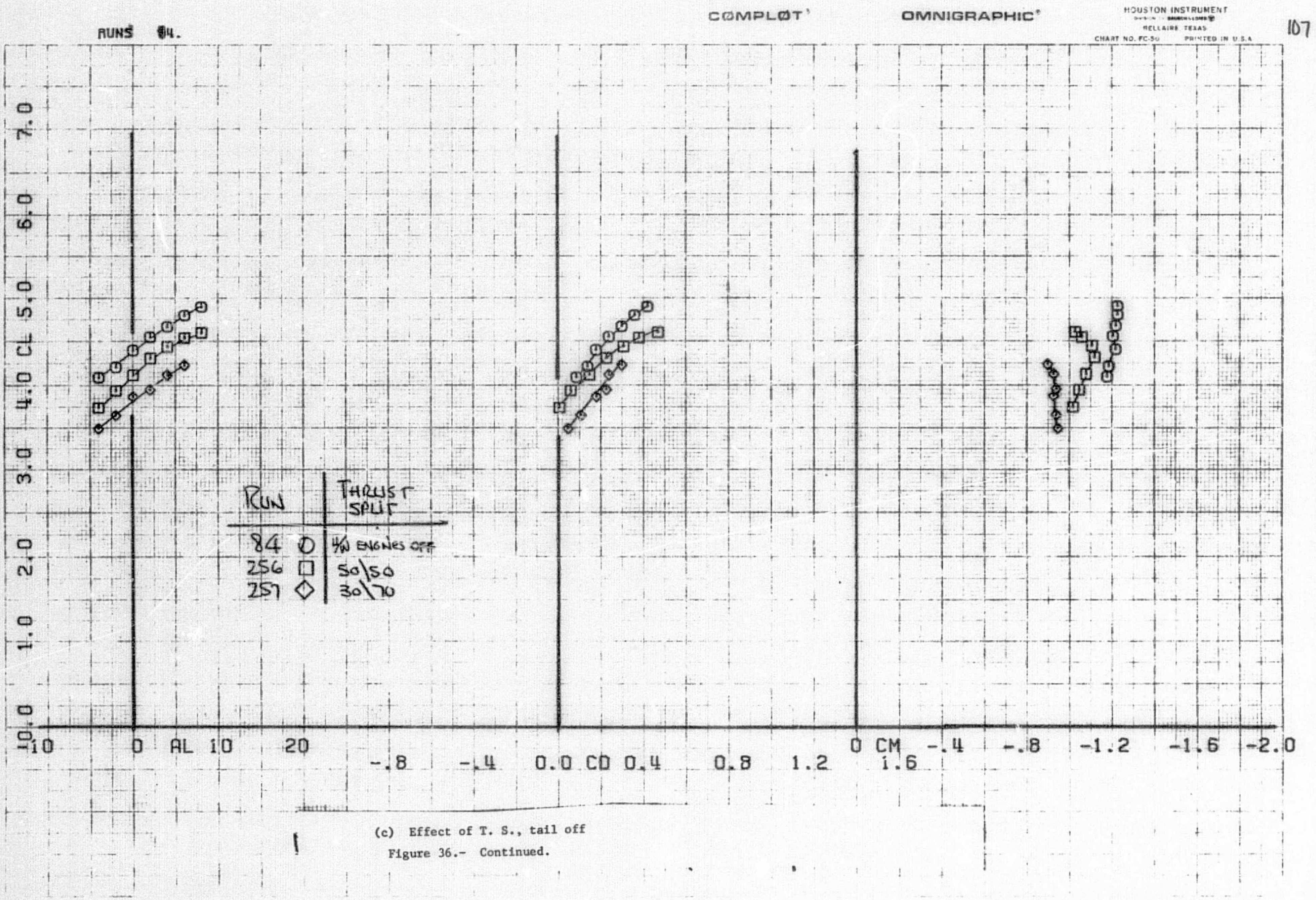

(c) Effect of T. S., tail off

Figure 36.- Continued.

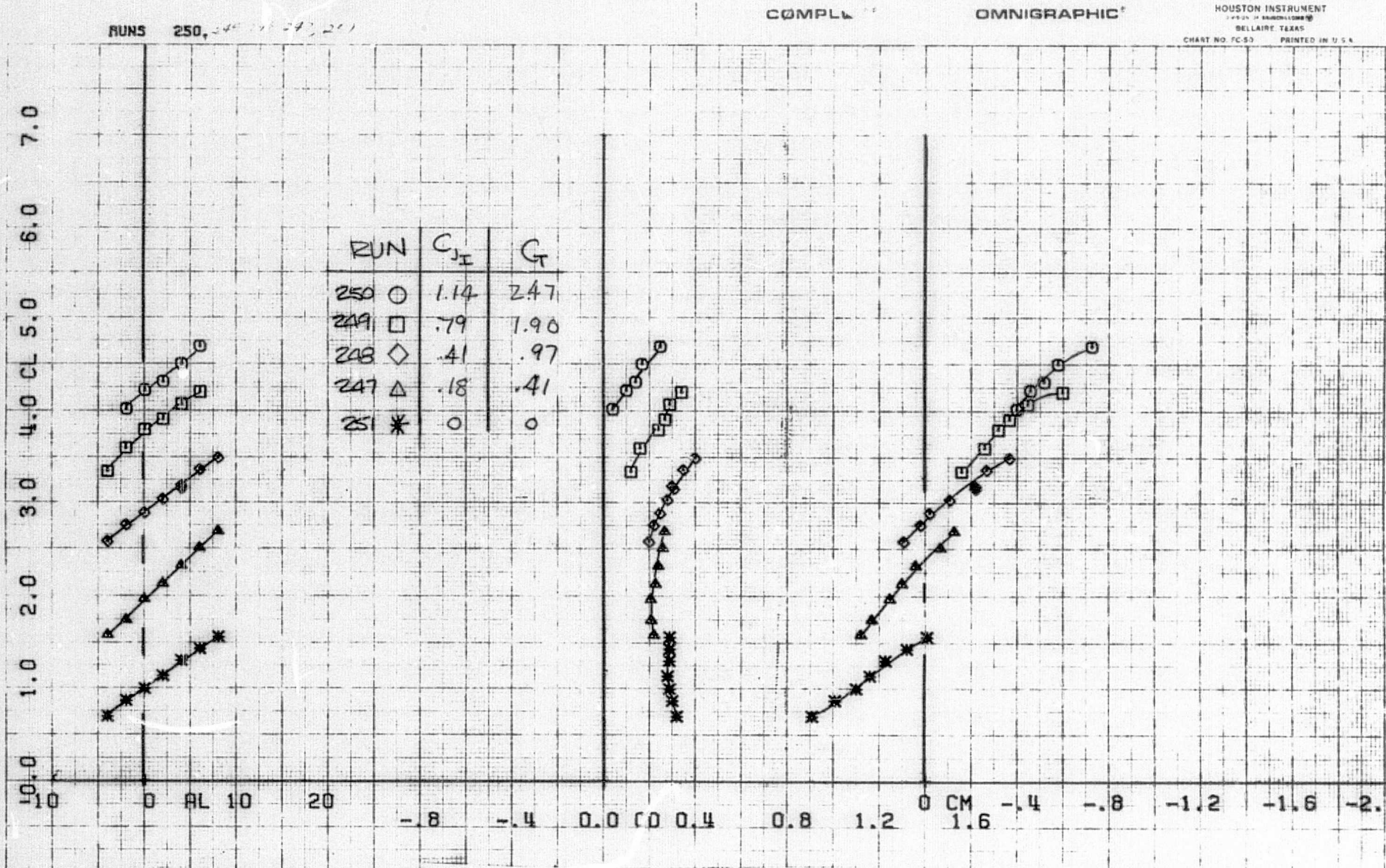

(d) T. S. = 50:50, tail on

Figure 36.- Concluded.

36d

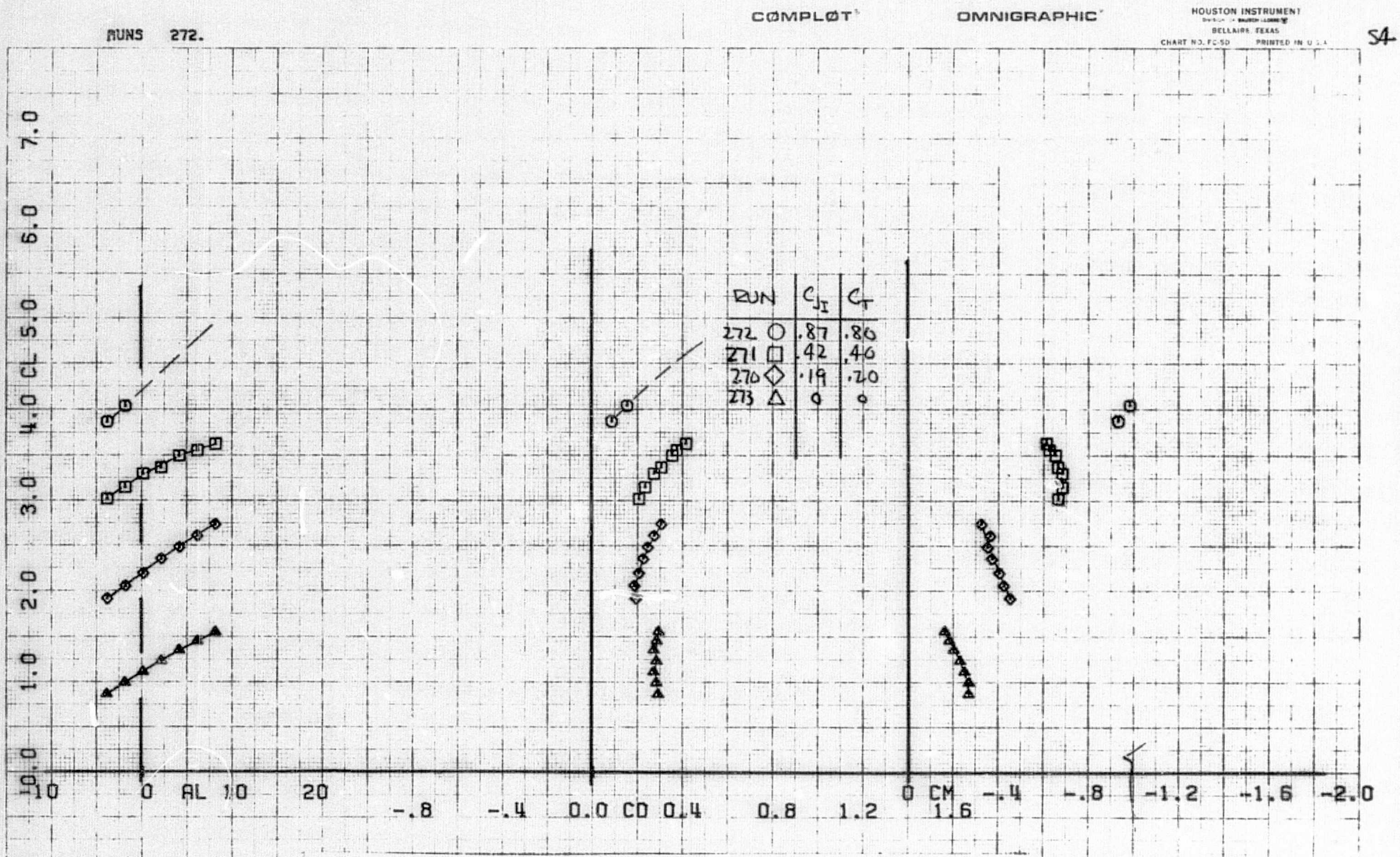

Figure 37.- Longitudinal aerodynamic characteristics with two J-85 underwing engines; $h/c = 1.34$, $\delta_f = 70^\circ$, $\delta_{TH} = 90^\circ$, tail off.

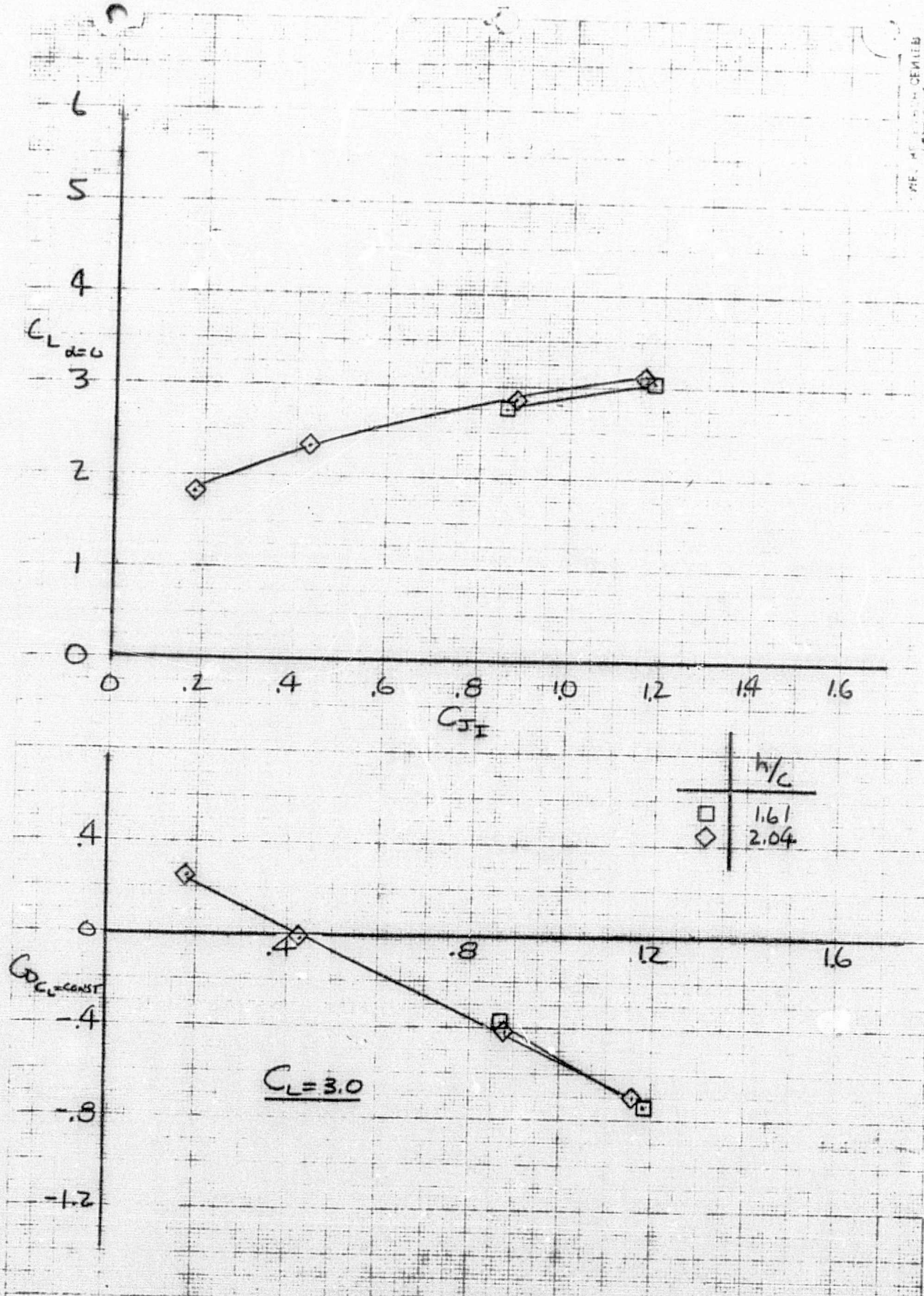

(a) T. S. = 50:50, $\delta_{TH} = 0^{\circ}$

Figure 38.- Effect of h/c on longitudinal aerodynamic characteristics wtih two J-85 underwing engines; $\delta_f = 40^{\circ}$, tail off.

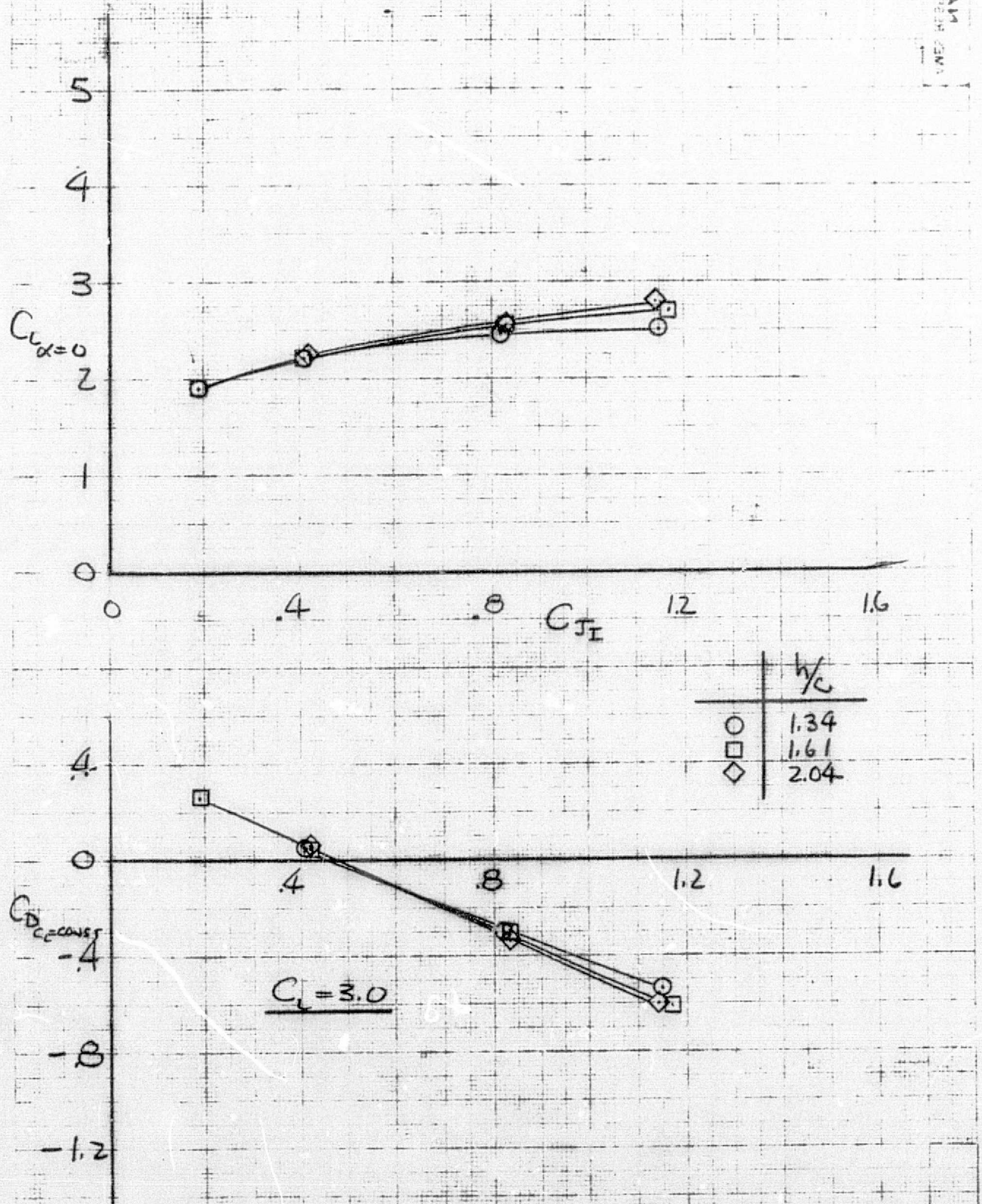

(b) T.S. = 30:70, δ_{TH} = 0°.

Figure 38.- Continued.

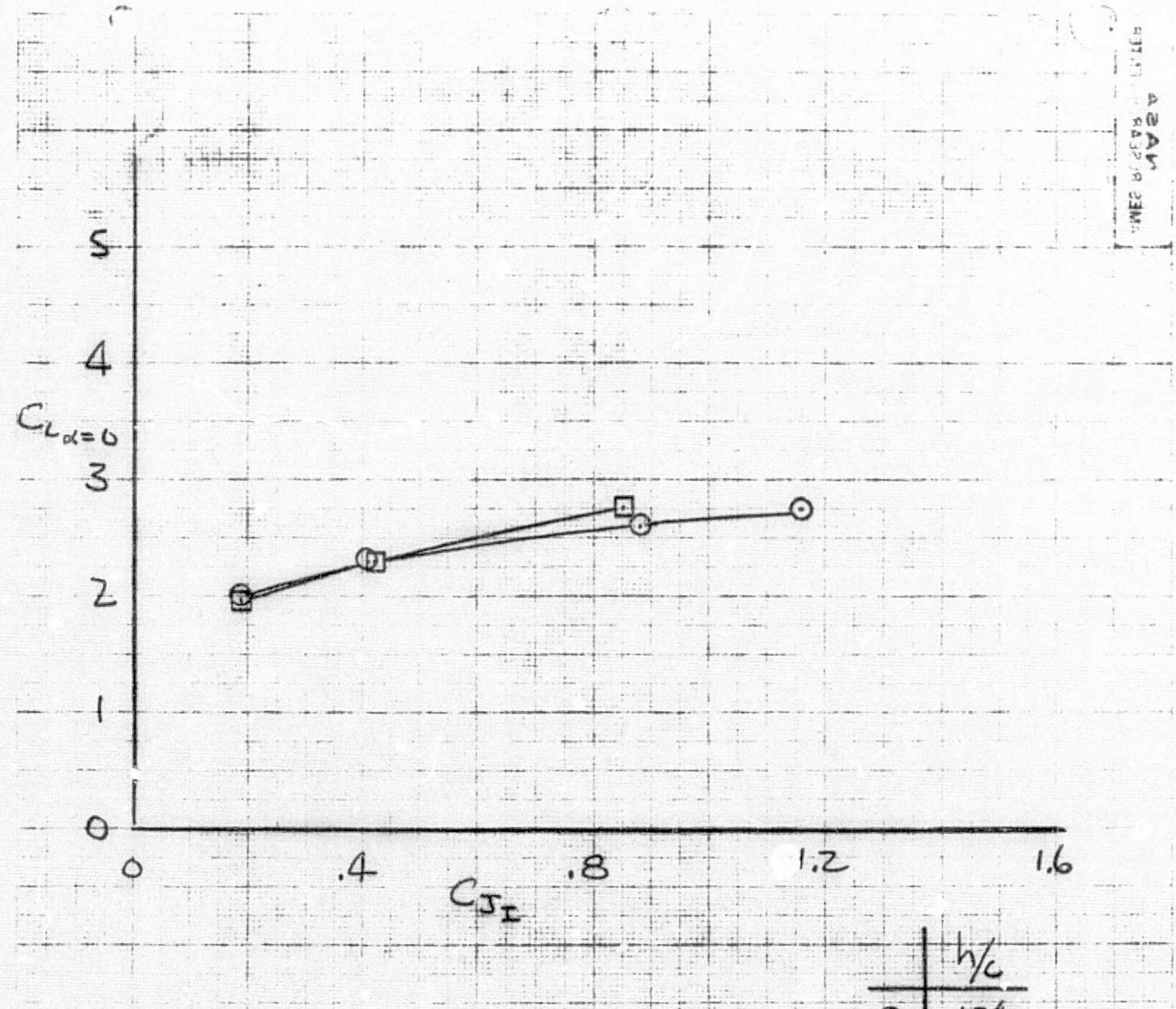

(c) T. S. = 30:70, δ_{TU} = 30°.

Figure 38.- Concluded.

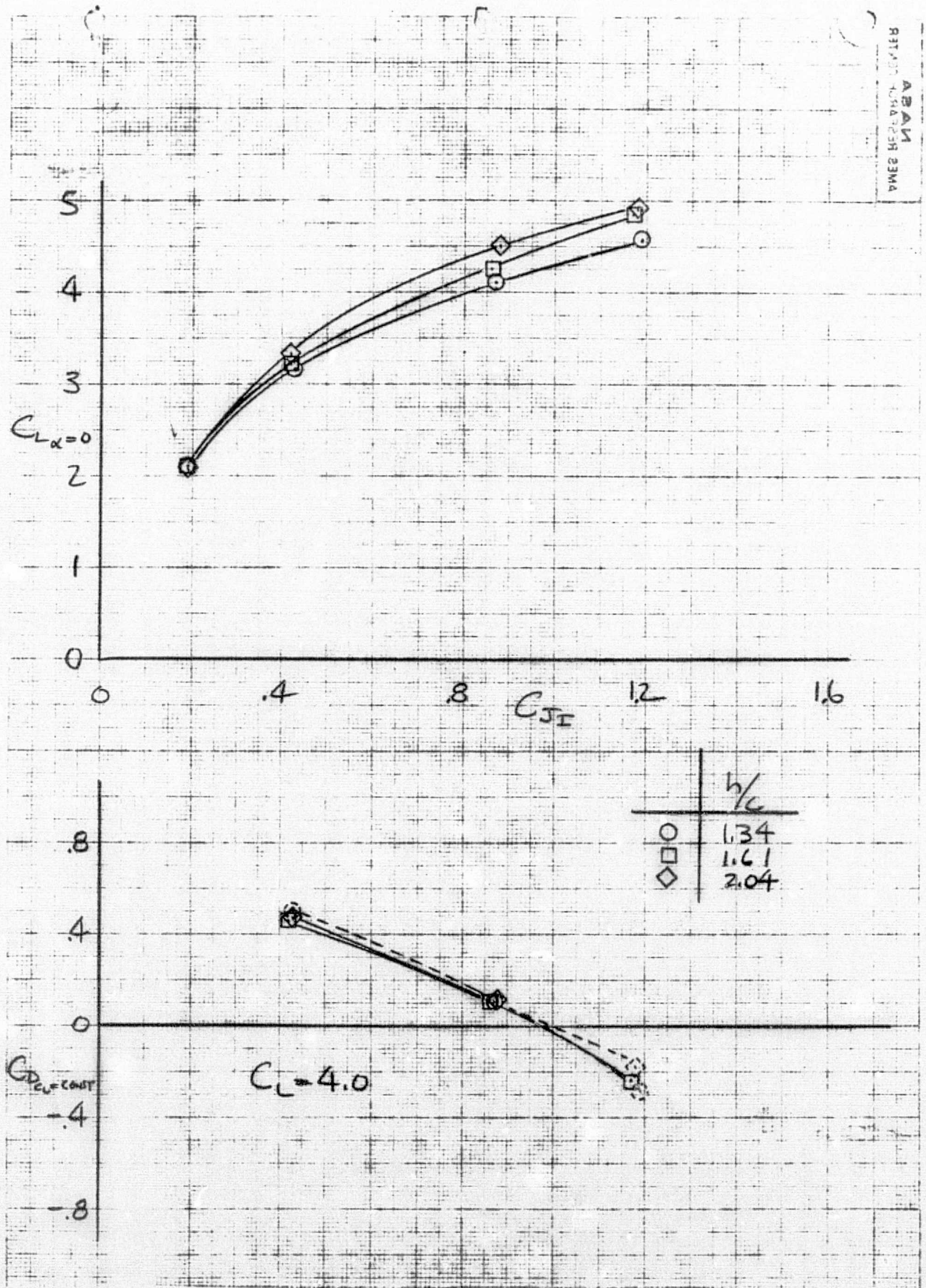

(a) T. S. = 50:50, δ_{TH} = 60°.

Figure 39.- Effect of h/c on longitudinal aerodynamic characteristics with two J-85 underwing engines; δ_f = 70°, tail off.

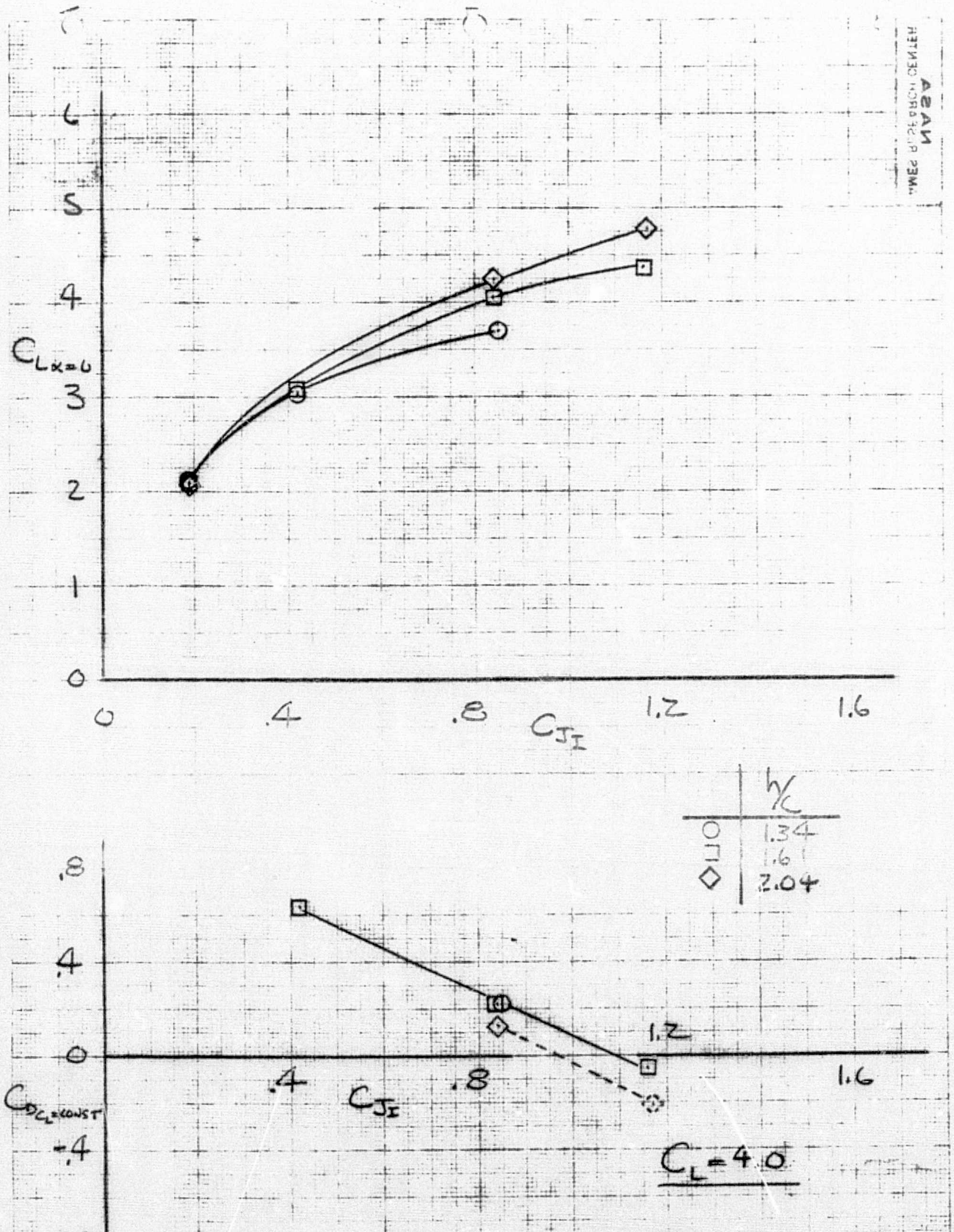

(b) T. S. = 30:70, δ_{TH} = 60°.

Figure 39.- Continued.

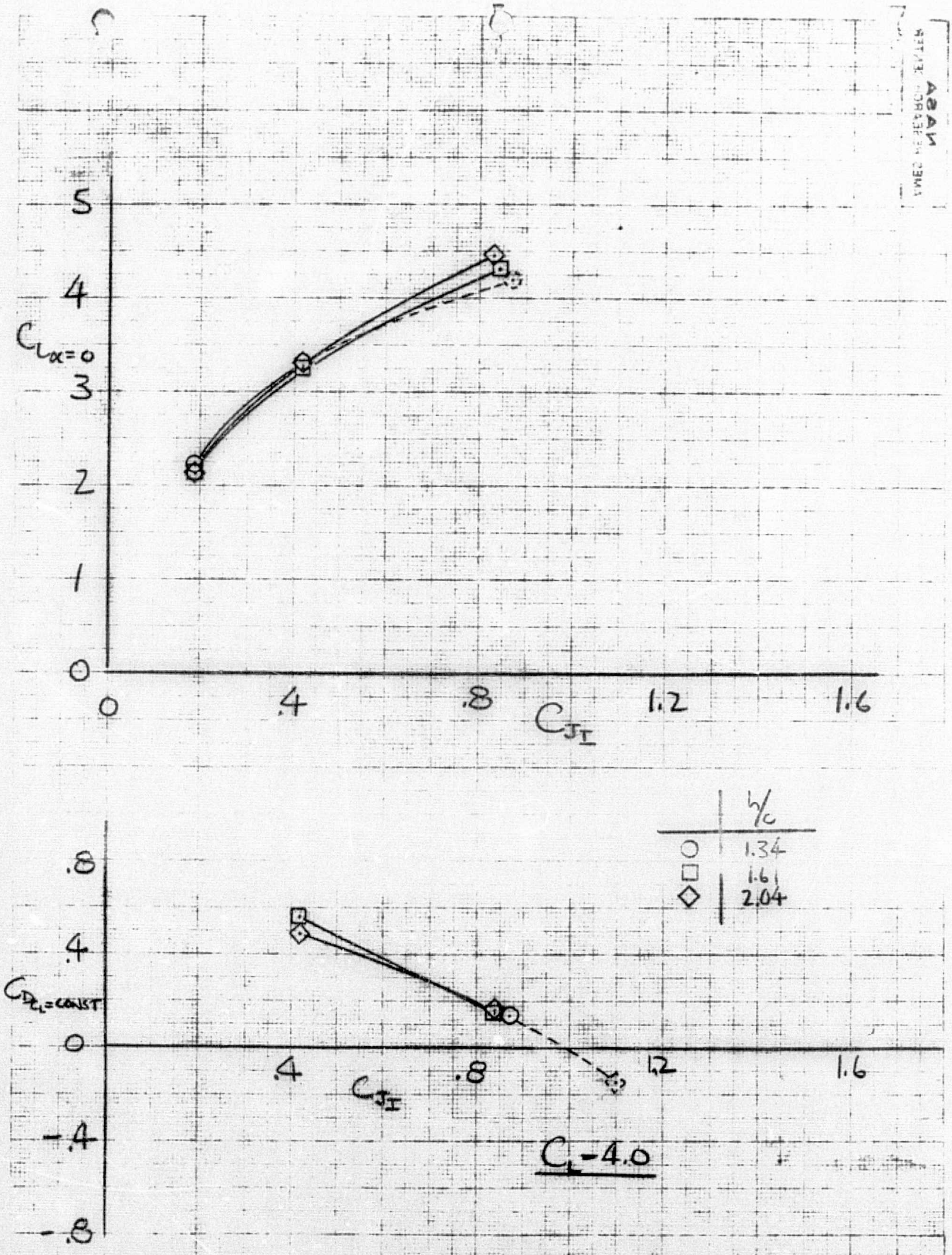

(c) T. S. = 50:50, δ_{TH} = 90°.

Figure 39.- Continued.

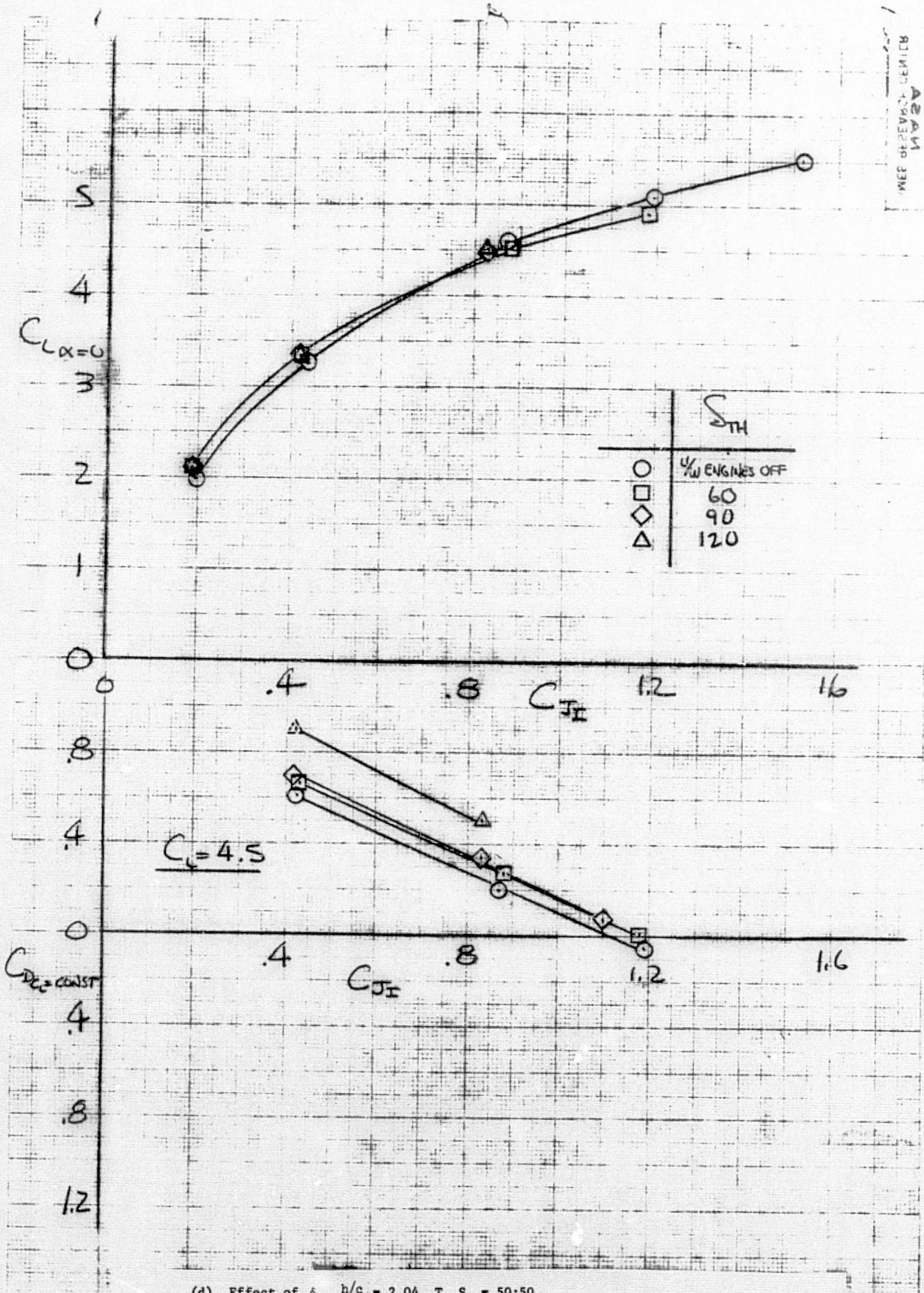

(d) Effect of δ_{TH}, h/c = 2.04, T. S. = 50:50

Figure 39.- Concluded.